Universidade do Minho
I3Bs - Instituto de Investigação em Biomateriais, Biodegradáveis e Biomiméticos

Gabriela Soares Diogo Carlos

Marine inspired composite biomaterials envisaging the engineering of hard tissues

Julho de 2020

Marine inspired composite biomaterials envisaging the engineering of hard tissues
Gabriela Soares Diogo Carlos
UMinho | 2020

Universidade do Minho

I3Bs - Instituto de Investigação em Biomateriais, Biodegradáveis e Biomiméticos

Gabriela Soares Diogo Carlos

Marine inspired composite biomaterials envisaging the engineering of hard tissues

Tese de Doutoramento

Doutoramento em Engenharia de Tecidos, Medicina Regenerativa e Células Estaminais

Trabalho efetuado sob a orientação de

Doutor Tiago José Quinteiros Lopes Henriques da Silva

Professor Doutor Rui Luís Gonçalves dos Reis

Julho de 2020

ACKNOWLEDGMENTS

Firstly, I am deeply grateful to Professor Rui for the opportunity to develop and realize my PhD at an institute of excellence like 3B's. In 3B's, I had the opportunity to learn and share knowledge with the best and, today, I am very happy and proud for having this opportunity. Thank you, Professor Rui, for your supervision and leadership that is for me an inspiration and reference in the scientific World.

To Doctor Tiago, who opened the 3B's door to me which was the trigger step to perform this PhD project many thanks. Tiago, this thesis is today real thanks to your insights, comments and guidance that encouraged me to learn more and more day by day. Thank you for your generosity, selfless support and especially for the excellent example and patience that you provided to me in the last four years, you have always a word to say.

A special thanks to Doctor Rogério for providing me guidance and feedback throughout the thesis. Rogério, you are for me an example of what a scientist must be.

I express my sincere gratitude to those who have contributed to this thesis and supported me in one way or the other during this amazing journey. Without any of them, this research work would not have been possible. Thank you to all work partners, particularly Catarina F. Marques.

To my friends, I would like to thank you for all patience, understanding and friendship. Catarina, I will always be there, as you have always been to me, it was wonderful to share with you these past four years that really cemented our friendship. Cláudia, with you nobody can stay down, thank you for always trying to lift me up, thank you for your friendship.

Thanks to my wonderful family for being with me in all moments of my life. My family is always there! Words cannot express the feelings that I have for all of you. You are a constant source of strength and inspiration to me, I love you. Paulo, I am lucky to have you by my side, you are the family I chose.

Finally, I would like to acknowledge all the funding that allowed me to perform all this work, Norte 2020, for financing my PhD scholarship "NORTE-08-5369-FSE-000044''.

STATEMENT OF INTEGRITY

I hereby declare having conducted this academic work with integrity. I confirm that I have not used plagiarism or any form of undue use of information or falsification of results along the process leading to its elaboration.

I further declare that I have fully acknowledged the Code of Ethical Conduct of the University of Minho.

ABSTRACT

The growing life expectancy pays the price of ageing-related musculoskeletal system diseases, compelling the urgent need for development of novel therapeutic strategies. Collagen-based solutions have been widely employed, but the primary sources for obtaining collagen, bovine and porcine, are not enough to keep up with needs. On the one hand, they conflict with certain religious beliefs, while on the other hand restrictive rules have been limiting their use, namely concerning the problems associated with the non-negligible risk of diseases transmission to humans, like bovine spongiform encephalopathy (BSE). Furthermore, we are facing the problem of terrestrial animals' overexploitation, that even so, does not meet the crescent collagen demands (**Chapter I**).

With this background, the work developed under the scope of this thesis focuses on the use of marine biomass, particularly blue shark (*Prionace glauca*) skin, as a promising source of collagen for production of safe, eco-sustainable and versatile composite biomaterials envisaging the engineering of hard tissues. The potential of blue shark collagen was tested after processing it in combination with marine-origin bioapatite, by freeze-dry technique, rendering 3D composite scaffolds. These 3D microporous scaffolds were suitable for Saos-2 cell line culture (**Chapter III**) and revealed capacity to promote *in vivo* bone regeneration in critical-size bone defects created in New Zealand rabbit models, 12 weeks post-implantation, similar to the performance observed with bovine collagen-based composite scaffolds (**Chapter IV**). Freeze-dry was also employed to produce blue shark collagen and blue shark collagen:hyaluronic acid scaffolds, with the former being able to trigger early-stage chondrogenic differentiation of human adipose stem cells (hASC), with hyaluronic acid being needed to support later stage chondrocyte phenotype (**Chapter V**). Inspired on the composite nano structural organization of mineralized tissues, a co-precipitation approach was followed to *in situ* mineralize blue shark collagen to ultimately produce stable bioinks to enable bioprinting approaches (**Chapter VI** and **VII**). Mouse fibroblast cell line (encapsulated) survival during and after printing was favored by the presence of mineralized collagen as exhibited by the biological performance of the hydrogels (**Chapter VI**). The osteogenic potential of the ink on encapsulated hASC, without exogeneous stimulations, was confirmed by immunodetection of RUNX2 and Osteopontin 21 days after hydrogels culture (**Chapter VII**). Based on a strategy of blue shark by-products valorization, highly promising tissue engineering approaches were developed envisioning the regeneration of bone and cartilage.

Keywords: Blue shark collagen, Bioprinting, Composite scaffolds, Freeze-dry, Hard tissues.

RESUMO

O aumento da esperança média de vida e, consequentemente, das doenças do sistema músculo-esquelético relacionadas com o envelhecimento, forçam a necessidade do desenvolvimento urgente de novas estratégias terapêuticas. Soluções baseadas em colagénio têm sido amplamente aplicadas; no entanto, as principais fontes de obtenção de colagénio, bovinas e porcinas, não são suficientes para suprir as necessidades. Por um lado, estas soluções entram em conflito com certas crenças religiosas, por outro lado, o seu uso tem sido limitado pelo risco de transmissão de doenças a humanos, como a encefalopatia bovina espongiforme. Para além disso, enfrentamos o problema da sobre-exploração de animais terrestes, que ainda assim não seria suficiente para acompanhar a crescente procura por colagénio (**Capítulo I**). Nesta perspetiva, o trabalho desenvolvido no âmbito desta tese foca-se no uso de subprodutos marinhos, particularmente pele de tubarão azul (*Prionace glauca*), como uma fonte promissora de colagénio para a produção de biomateriais compósitos, ambientalmente sustentáveis e versáteis para a aplicação na engenharia de tecidos duros. O potencial do colagénio foi testado, após processamento, em estruturas 3D preparadas pela técnica de liofilização. As estruturas mostraram-se adequadas para cultura com a linha celular Saos-2 (**Capítulo III**). *In vivo*, o potencial destas estruturas foi avaliado, 12 semanas após implantação em defeitos ósseos críticos criados em coelhos. Os resultados não mostraram diferenças significativas em comparação com estruturas de colagénio de origem bovina (**Capítulo IV**). No **Capítulo V**, a técnica de liofilização foi aplicada para produzir estruturas de colagénio e estruturas de colagénio:ácido hialurónico para estudar o potencial condrogénico de células estaminais do tecido adiposo humano, com e sem estimulação exógena. As estruturas de colagénio desencadearam a condrogénese no seu estágio inicial, enquanto o ácido hialurónico suportou o fenótipo de condrócitos num estágio posterior. Atendendo à nano-organização estrutural de tecidos mineralizados, foi explorada, nos **Capítulos VI** e **VII**, a mineralização *in situ* do colagénio para preparação de pastas para impressão. Fibroblastos incorporados na pasta revelaram uma maior sobrevivência, durante e após impressão, com o aumento da quantidade de colagénio. O potencial osteogénico da pasta, sem qualquer estímulo exógeno, foi confirmado através da imunodeteção da RUNX2 e Osteopontina 21 após cultura de células estaminais do tecido adiposo dos hidrogéis. A valorização de subprodutos de tubarão resultou em abordagens terapêuticas altamente promissoras para aplicação em Engenharia de Tecido.

Palavras-chave: Colagénio de tubarão azul, Impressão com células, Estruturas 3D, Liofilização, Tecidos Duros.

TABLE OF CONTENTS

LIST OF ABBREVIATIONS AND SYMBOLS

A

Abs - Absorbance

ACAN – Aggrecan

ACI - Autologous chondrocyte implant

ALP – Alkaline phosphatase

ASC – Acid solubilized collagen

Ap - Apatite

ATR - Attenuated total reflectance

ATR-FTIR - Attenuated total reflectance Fourier transform infrared spectroscopy

AM - Calcein

Au – Gold

α - Alpha

B

BAp - Bioapatite

bColl- Bovine collagen

BMP2 - Bone morphogenetic protein 2

BSA - Bone serum albumin

BSE - Spongiform encephalopathy

β - Beta

C

CaP – Calcium phosphates

CAM - Computer-aided-manufacturing

COMP - Cartilage oligomeric matrix protein

cm - Centimeter

Coll - Collagen

Col2A1 – Collagen type II gene

CLSM - Confocal laser scanning microscopy

CT – Computerized tomography

vCJD - Creutzfeldt-Jakob disease

CETC - Electrospun tilapia collagen membranes

cm^{-1} - Reciprocal wavelength centimeter

D

d - Day

Da – Dalton

DAPI - Diamidino-2-phenylindole

°C - Celsius Degree

DHT – Dehydrothermal

DNA - Deoxyribonucleic acid

DMSO – Dimethylsulfoxide

dsDNA - Double strained DNA

DMEM - Dulbecco's modified Eagle's medium.

DSC - Circular dichroism spectroscopy

E

ECM - Extracellular matrix

EDTA - ethylenediaminetetraacetic acid

EDC - 1-Ethyl-3-(3-dimethylaminopropyl) carbodiimide hydrochloride

et al. - And others

EU – European Union

Ex/Em – Excitation/emission

e.g. – "for example", form latin *exempli gratia*

3D – 3-dimensional

F

FBS - Fetal bovine serum

FCT - Foundation for Science and Technology

FTIR - Fourier Transform Infrared

FDM - Fused deposition modeling

FDA - U.S. Food and Drug Administration

G

GAGs – Glycosaminoglycans

GAG - Glycosaminoglycan

Gly- Glycine

G' – Elastic modulus

G'' – Plastic component

H

HAp - Hydroxyapatite

hASC - Human adipose stem cells

H&E - Hematoxylin and Eosin

HMDI - Hexamethylene diisocyanate

HMWHya - High molecular weight hyaluronic acid

Hya – Hyaluronic acid

h - Hour

Hz – Hertz

hB2M - β2-microglobulin

hMSC – Human mesenchymal stem cells

I

ICP-OES - Inductively coupled plasma optical emission spectrometry and Ion chromatography

ITS - Insulin-transferrin-selenium-G supplement

i.e. - "in other words", form latin *id est*

IFFT - Inverse Fast Fourier Transform

K

kD - Kilodalton

Kg - Kilogram

kN - Kilonewton

kPa – Kilopascal

kV – Kilovolt

L

L - Liter

LMWHya - Low molecular weight hyaluronic acid

M

MACI - Matrix-induced autologous chondrocyte implantation

mBAp – Marine bioapatite

mColl – Marine collagen

MT - Masson's trichrome

m/v - Mass/volume

MRI - Magnetic resonance imaging

MPa - Megapascal

MSCs - Mesenchymal stem cells

m - Meter

MHz - Megahertz

Micro-CT - Micro-computed tomography

min - Minute

mL - Milliliter

mm - Millimeter

mM - Millimolar

µg - Microgram

µg.DNA - Microgram of Deoxyribonucleic acid

µm - Micrometer

M - Molar

mg - Milligram

MWCO - Molecular weight cut off

Minimum essential medium alpha – MEM (α)

MTS - 3-(4,5-dimethylthiazol-2-yl)-5-(3 carbox- ymethoxyphenyl) 2-(4-sulphofenyl)-2*H*-tetrazolium

N

NSC - neutral salt solubilized collagen

NHS - N-Hydroxysuccinimide

N - Newton

n - Number of samples

nm - Nanometers

O

OHPro – Hydroxyproline

OP – Osteopontin

P

p - Statistical level of significance

Pa - Pascal

PBS - Phosphate-buffered saline

pDNA - Plasmid Deoxyribonucleic acid

pH - Potential hydrogenionic

PI - Propidium iodide

PG – *Prionace* glauca

PSC – Pepsin solubilized collagen

PS – Pepsin

Pro- Proline

Ph – Phalloidin

R

Ref. - Reference

RGD - Arginine-glycine-aspartic acid

RPM - Rotations per minute

RT - Room temperature

RUNX2 - Runt-related transcription factor 2

S

s - Seconds

SBF - Simulated body fluid

SD - Standard deviation

SEM - Scanning electron microscopy

SP - Sodium pyruvate

SLA - Stereolithography

SLS - Selective laser sintering

SOX9 - SRY-box transcription factor9

SDS-PAGE - Sodium dodecyl sulfate polyacrylamide

SVF - Stromal vascular fraction

T

TSE - Transmissible spongiform encephalopathies

TEM – Transmission electron microscopy

TE - Tissue engineering

TGF-β3 - Transforming growth factor-β3

Tm - melting temperature

TGA - Thermogravimetric analysis

U

U – Units

V

v/v - Volume/volume

X

XRD - X-ray diffraction

W

Wt – weight

Wp - water uptake

W0 - initial dry weight

λ - Wavelength

w/v - Weight/volume

w/w - Weight/weight

wt% - Percentage of weight

LIST OF FIGURES

LIST OF TABLES

SHORT *CURRICULUM VITAE*

Gabriela Soares Diogo Carlos was born in 1990 in Guarda, Portugal. Nowadays, she works as a researcher in 3B's Research Group, I3Bs – Research Institute on Biomaterials, Biodegradables and Biomimetics, University of Minho, under the supervision of Doctor Tiago H. Silva and Professor Rui L. Reis.

She graduated in Biomedical Sciences at Universidade da Beira Interior, Covilhã, Portugal in 2013. During her master she had the opportunity to be involved in research activities and from her work resulted two scientific publications within the biomaterials field, one of them as first author "*Manufacture of β-TCP/alginate scaffolds through a rapid prototyping technique for application in bone tissue engineering*", published in Biofabrication.

In 2013, she joined 3B's Research Group, after being awarded with a grant under the scope of Atlantic Area Transnational Cooperation Programme Project MARMED (2011-1/164) where she had the opportunity to work on the exploration of marine organisms as a promising source of bioactive compounds, for applications in Tissue Engineering. As a result of her research work, she was co-author of 3 papers in international journals.

In 2016 she started her PhD studies, supported by a PhD scholarship funded by NORTE2020, under the scope of Doctoral Programme in Tissue Engineering, Regenerative Medicine and Stem Cells. She has been working with marine-origin polymers, particularly collagen from blue shark *Prionace glauca*, envisioning hard tissue regenerative applications, under the supervision of Doctor Tiago H. Silva and Professor Rui L. Reis.

As a result of her PhD work, she has contributed with 6 publications as first author in international journals, two of them already accepted and the other four under revision. Furthermore, she participated in international conferences with 2 oral communications and 6 poster communications.

LIST OF PUBLICATIONS

The work performed during the PhD period resulted in the publications listed below.

INTERNATIONAL PUBLICATIONS IN SCIENTIFIC PEER-REVIEWED JOURNALS

Diogo G. S. López-Senra E. L., Pirraco R. P., Canadas R. F., Fernandes E. M., Serra J., Pérez-Martín R. I., Sotelo, C. G., Marques A. P., González P., Moreira-Silva J., Silva T. H., Rui L. R., *Marine collagen:apatite composite scaffolds envisaging hard tissue applications.* Marine Drugs, 2018. 16 (8): p. 269.

Diogo G. S., Marques C. F.; Sotelo C. G., Perez-Martín R. I., Pirraco R. P., Reis R. L., Silva T. H., *Cell-Laden Biomimetically Mineralized Shark-Skin-Collagen-Based 3D Printed Hydrogels for the Engineering of Hard Tissues*. ACS Biomaterials Science& Engineering, 2020. 6: p. 3664–3672.

Diogo G.S, Carneiro F., Freitas-Ribeiro S., Sotelo C. G., Pérez-Martín R. I., Pirraco R. P., Reis R. L., Silva T. H., *Prionace glauca skin collagen bioengineered constructs as a promising approach to trigger cartilage regeneration*, (Submitted).

Diogo G.S., Permuy M., Marques C. F, Sotelo C. G., Pérez-Martín R. I., Serra J., González P., López-Peña M., Pirraco R. P., Reis R. L., Silva T. H., *In vivo assessment of marine vs bovine origin collagen-based composite scaffolds promoting bone regeneration in a New Zealand rabbit model,* (Submitted).

Diogo G.S., Marques C. F., Freitas-Ribeiro S., Sotelo C. G., Pérez-Martín R. I., Pirraco R. P., Reis R. L., Silva T. H., *Next generation bioink based on mineralized shark collagen with intrinsic osteogenic properties: a step towards the future of bone regeneration*, (Submitted).

Diogo G.S., Pirraco R. P., Reis R. L., Silva T. H., *From its nature to its function: marine collagen-based biomaterials for the engineering of hard tissues*, (Submitted).

INTERNATIONAL PUBLICATIONS IN SCIENTIFIC PEER-REVIEWED JOURNALS (AS CO-AUTHOR)

Marques C. F., **Diogo G. S.**, Pina S., Oliveira J. M., Silva T. H., Reis R. L., *Collagen-based bioinks for hard tissue engineering applications: a comprehensive review*. Journal of Materials Science. Materials in Medicine. 2019. 30: p. 32.

Backes E., Fernandes E. M., **Diogo G.S.,** Silva T. H., Costa L., Passador F., Reis R. L., Pessan L., *Engineering 3D printed bioactive composite scaffolds based on the combination of aliphatic polyester and calcium phosphates for bone tissue regeneration*, (Submitted).

CONFERENCE ABSTRACTS PUBLISHED IN INTERNATIONAL SCIENTIFIC JOURNAL

Diogo G. S., Marques C. F.; Sotelo C. G., Perez-Martín R. I., Pirraco R. P., Reis R. L., Silva T. H., *Cell-laden Prionace glauca skin collagen-based 3d printed scaffolds for the engineering of mineralized tissues.* Transactions of the Annual Meeting of the Society for Biomaterials and the Annual International Biomaterials Symposium 40. 2019. pp. 884.

CONFERENCE ORAL PRESENTATIONS

Diogo G. S., Sotelo C. G., Perez-Martín R. I., Pirraco R. P., Reis R. L., Silva T. H., *Marine-Derived Collagen:hyaluronic acid biopolymer scaffolds envisioning cartilage lesions regeneration,* 29th Conference of the European Society for Biomaterials, Maastricht, The Netherlands, 2018.

Diogo G. S., Marques C. F.; Sotelo C. G., Perez-Martín R. I., Pirraco R. P., Reis R. L., Silva T. H., *Cell-laden Biomimetically Mineralized Shark Skin Collagen-based 3D Printed Scaffolds for the Engineering of Hard Tissues.* TERMIS-EU Chapter Meeting, Rhodes, Greece, 2019.

CONFERENCE ORAL PRESENTATIONS AS CO-AUTHOR

Martins E., **Diogo G. S**, Pires R. A., Reis R. L., Silva T. H., Marine demosponges skeletal elements as inspiration on the fabrication of 3D Collagen-Silica composites envisaging. 30th Conference of the European Society for Biomaterials, Dresden, Germany, 2019.

CONFERENCE POSTERS

Diogo G. S., López-Senra E., Pirraco R. P., Canadas R. F., Fernandes E. M., Serra J., Pérez-Martín R. I., Sotelo C. G., Marques A. P., González P., Moreira-Silva J., Silva T. H., Reis R. L., 2016. *Marine collagen/apatite scaffolds envisaging tissue engineering applications*. Chem2Nature First School, Porto, Portugal, 2016.

Diogo G. S.; Sotelo C. G., Pérez-Martín R. I., Silva T. H., Reis R. L., *Shark collagen mineralized scaffolds for engineering of bone tissue: Co-precipitation method*. TERMSTEM 2017, Porto, Portugal, 2017.

Diogo G. S., Pirraco R. P., Pérez-Martín R. I. Sotelo C. G., Silva T. H., Reis R. L., *Natural-derived composite scaffolds envisioning regeneration in cartilage lesions.* 29th Conference of the European Society for Biomaterials, Maastricht, The Netherlands, 2018.

Diogo G. S., Pérez-Martín R. I., Sotelo C. G., Pirraco R. P., Silva T. H., Reis R. L., 2018. *Marine derived collagen:hyaluronic acid biopolymer scaffolds envisioning cartilage lesions regeneration*. CHEM2NATURE Summer School. Porto, Portugal, 2018.

Diogo G. S., Marques C. F., Pérez-Martín R. I., Pirraco R. P., Sotelo C. G., Reis R. L., Silva T. H, *Cell-laden Prionace Glauca Skin Collagen-based 3D Printed Scaffolds for the Engineering of Mineralized Tissues*. Society For Biomaterials Annual Meeting and Exposition, Seattle, USA, 2019.

Diogo G. S., Marques C. F., Sotelo C. G., Pérez-Martín R. I., Pirraco R. P., Reis R. L., Silva T. H. *Hard tissues regeneration based on a strategy of 3D printed mineralized marine-collagen hydrogels*. 1st Discoveries Forum on Regenerative and Precision Medicine, Porto, Portugal, 2019.

CONFERENCE POSTERS (AS CO-AUTHOR)

Martins E., **Diogo G. S**., Pires R. A., Reis R. L., Silva T. H., *3D Collagen-silica composites inspired by body architecture of marine sponges.* FoReCast, Porto, Portugal, 2017.

Martins E., **Diogo G. S**., Duarte A. R. C., Pires R. A., Reis R. L., Silva T. H., *Bio inspiration in body architecture of North Atlantic deep-sea sponges for the development of 3D composite structures of marine collagen and silica*. Chem2Nature First School, Porto, Portugal, 2017.

Dudik O., **Diogo G. S.**, Pires R. A., Silva T. H., Reis R. L., *Potential of sponge-derived biosilica for the development of biomaterials for bone tissue engineering*. TERMSTEM, Porto, Portugal, 2017.

Martins E., **Diogo G. S.**, Pires R. A., Reis R. L., Silva T. H., *3D structures tailor-made by resemblance of the composition of the Demosponges skeleton envisaging bone tissue engineering application*. Chem2Nature Second, Guimarães, Portugal, 2018.

Martins E., **Diogo G. S.**, Pires R. A., Reis R. L., Silva T. H., *Collagen and silica-based materials with key biological properties for prompting bone regeneration*. 1st Discoveries Forum on Regenerative and Precision Medicine. Porto, Portugal, 2019.

Martins E., **Diogo G. S.**, Pires R. A., Reis R. L., Silva T. H., *Marine Collagen-Silica Composites for Bone Tissue Applications*. First Achilles Conference, Porto, Portugal, 2019.

Martins E., **Diogo G. S.**, Pires R. A., Reis R. L., Silva T. H., 3D composite scaffolds inspired by the skeleton architecture of the deep-sea marine sponges. Chem2Nature Second School, Porto, Portugal, 2018.

AWARDED GRANT: Horizonte Norte2020 PhD scholarship (NORTE-08-5369-FSE-000044)

OTHER PUBLICATIONS (work not directly related with the PhD):

Torres A. L., Gaspar V. M., Serra I. R., **Diogo G. S.**, Fradique R., Silva A. P., Correia I. J. *Bioactive polymeric-ceramic hybrid 3D scaffold for application in bone tissue regeneration,* Materials Science and Engineering C. 2013, Vol (33): p. 4460-4469.

Diogo G.S., Gaspar V.M., Serra I.R., Fradique R., Correia I.J., *Manufacture of β-TCP/alginate scaffolds through a Fab@home model for application in bone tissue engineering*, Biofabrication. 2014. 6: 025001.

Marques A. L. P., Sotelo C. G.; **Diogo G. S**., Moreira-Silva J., Blanco M., Silva T. H., R. I. Pérez-Martín; R. L. Reis. *Colagénio Marinho: valorização de subprodutos marinhos com vista à regeneração de tecidos,* In Valorización de Recursos Marinos: Biomateriales en Regeneración de Tejidos y Liberación de fármacos, edited by C. G. Sotelo et al, 2015. p: 49-77.

Moreira-Silva J., **Diogo G. S**., Marques A. L. P., Silva T. H., Reis R. L., *Marine Collagen Isolation and Processing Envisaging Biomedical Applications*. Biomaterials from Nature for Advanced Devices and Therapies. 2016. p 16-36.

Coelho R. C. G., Marques A. L. P., Oliveira S. M., **Diogo G. S.**, Pirraco R. P., Moreira-Silva J., Xavier J. C., Reis R. L., Silva T. H., Mano J. F., *Extraction and characterization of collagen from Antarctic and Sub-Antarctic squid and its potential application in hybrid scaffolds for tissue engineering*. Materials Science and Engineering C, 2017. 78: p 787-795.

Carvalho F. R., Calado S. M., Silva G. A. , **Diogo, G. S.**, Moreira-Silva J., Reis R. L., Cancela M. L., Gavaia P.J. *Altered bone microarchitecture in a type 1 diabetes mouse model Ins2Akita*. Journal of Cellular Physiology, 2019. 234: p 9338-9350.

INTRODUCTION TO THE THESIS FORMAT

This thesis reports the work developed under the scope of the doctoral programme in Tissue Engineering, Regenerative Medicine and Stem Cells, addressing the development of shark collagen-based biomaterials for the engineering of bone and cartilage tissues, envisaging the achievement of the doctoral degree. With this framework, the thesis is divided into four main **Sections** (**1** to **4**) comprising a total of eight **Chapters** (**I** to **VIII**). **Section 1** addresses a general introduction to the thesis theme, focusing on the use of marine collagens as a strategy for hard tissue applications (**Chapter I**). The overview of the overall materials and methods used in the thesis is addressed in **Section 2** (**Chapter II**). In **Section 3**, the experimental data are presented and discussed, focusing on the works developed envisioning the engineering of hard tissue (**Chapters III** to **VII**). This corresponds to the main body of the thesis and is based on published or submitted manuscripts in international journals. Each of these chapters follow a research paper format, *i.e.* abstract, introduction, experimental section, results and discussion, conclusion, acknowledgments, and references. Final Conclusions and Future Perspectives can be found in the last section of this thesis, Section 4 (**Chapter VIII**). Following, the contents of each chapter are briefly explained.

Section 1– General introduction

Chapter I – Introduction: This chapter displays a comprehensive overview on biomaterials engineered with marine origin collagens envisaging hard tissue regenerative applications, namely assessing drawbacks related with the use of collagen from mammalian sources that might be surpassed by the use of marine organisms as an alternative raw-materials for collagen production.

Section 2 – Materials and methods

Chapter II – Materials and Methods: This chapter provides a detailed description of the materials used in the work reported along the different experimental chapters of this thesis, as well as the processing methodologies used to process the collagen into different biomaterials, their characterization techniques and the strategies used to assess performance in hard tissue engineering strategies.

Section 3 – Experimental work regarding the use of blue shark collagen as a strategy for the development of 3D biomaterials for hard tissue applications.

Chapter III – Marine Collagen:Apatite Composite Scaffolds Envisaging Hard Tissue Applications: Blue shark *Prionace glauca* collagen was processed by freeze-dry into 3D composite scaffolds envisioning the engineering of hard tissues. Collagen from *Prionace glauca* was combined with bioapatite particles obtained from *Prionace glauca* and *Iurus oxyrinchus* and the resulting scaffolds were characterized, showing the capability to support the culture of Saos-2 cell line, depending on the formulation, namely materials ratios and crosslinking agent.

Chapter IV – *In vivo* Assessment of Marine vs Bovine Origin Composite Scaffolds Promoting Bone Regeneration in a New Zealand rabbit model: A comparative study between an entire marine-based composite scaffold with another composed by well-established counterparts was implemented. Blue shark skin collagen was combined with bioapatite particles obtained from teeth of blue shark *Prionace glauca* and mako shark *Iurus oxyrinchus*, while bovine collagen was combined with synthetic apatite particles commercially available. To validate the potential of the developed scaffolds, the scaffolds were implanted in critical-size bone defects created in White New Zealand rabbits and the regeneration of the defects was evaluated 12 weeks post-implantation, with marine and reference composite scaffolds exhibiting similar performance.

Chapter V – *Prionace glauca* Skin Collagen Bioengineered Constructs as a Promising Approach to Trigger Cartilage Regeneration: Collagen from blue shark (*Prionace glauca*) was used as building block for production of microporous 3D collagenous structures for cartilage applications. Collagen and collagen:hyaluronic acid scaffolds resulted from the coupling of the chemical reaction with EDC and the cryogelation method followed by freeze-drying technique. Blue shark collagen scaffolds triggered early-stage chondrogenesis, while hyaluronic acid supported later stage chondrocyte phenotype.

Chapter VI – Cell-Laden Biomimetically Mineralized Shark-Skin-Collagen-Based 3D Printed Hydrogels for the Engineering of Hard Tissues: The *in situ* mineralization of blue shark *Prionace glauca* collagen that was for the first time attempted for 3D printing with incorporated living cells (bioprinting). Alginate was used as support material to increase inks viscosity, enabling printability. The ions used to mineralize the blue shark collagen could have a synergistic effect through the ionic gelation of alginate,

making stable inks that supported L929 cell line survival during and after printing used as model to demonstrate bioprinting feasibility.

Chapter VII - Next Generation Bioink Based on Mineralized Shark Collagen With Intrinsic Osteogenic Properties: a Step Towards the Future of Bone Regeneration: To explore the osteogenic potential of the ink prepared with the mineralized collagen, human adipose stem cells were encapsulated at different densities, aiming to achieve the best cell density for an optimized bioink. A stable mineralized blue shark collagen:alginate bioink which supported high cell (hASC) viability was obtained, enabling the printing of hydrogels that, after 21 days of cell culture, maintained their structural properties while promoting differentiation towards osteogenic lineage..

Section 4 – Concluding remarks

Chapter VIII - Conclusions and Future Perspectives: The final section describes the main outcomes achieved within the different works and how these correlate into a scientific thesis on the potential of shark collagen-based biomaterials for the engineering of hard tissues, the current limitations and the future forecast.

"*Trying is the First Step Towards Failure and Failure is the First Step Towards Success.*"

SECTION 1

GENERAL INTRODUCTION

Chapter I

From its Nature to its Function: Marine Collagen-based Biomaterials for the Engineering of Hard Tissues

Chapter I

From its Nature to its Function: Marine Collagen-based Biomaterials for the Engineering of Hard Tissues[1]

I-1. ABSTRACT

Rapidly growing demand for collagen-based therapeutic applications requires a great amount of collagen stock. Mammals have been largely explored to extract collagen but problems like bovine spongiform encephalopathy (BSE) or religious constrains have been hampered its use.

Marine origin organisms, including vertebrates and invertebrates, have been explored as a safe source of a huge array of bioactive molecules, including collagen. In comparison with mammals' collagen, collagen extracted from marine organisms has a similar amino acidic composition and the possibility of using marine origin by-products as an economic, environmental, and social sustainable strategy for collagen extraction makes it highly attractive. The present review focuses on getting a comprehensive overview of the global drawbacks related with the use of mammalian sources and the main advantages of using marine organisms as an alternative for collagen-based products development. In general, marine-derived collagen is characterized by lower denaturation temperatures than its terrestrial counterpart, which compels the use of different processing procedures for the development of biomedical applications. In this regard, this review also discusses the use of novel technologies based on marine collagen processes for the design and development of sustainable and functional (bio)materials, specially focusing on therapies for hard tissues pathologies.

[1]This chapter is based on the following publication:

G.S. Diogo, R. P. Pirraco, R. L. Reis, T. H. Silva. From its nature to its function: marine collagen-based biomaterials for the engineering of hard tissues. (*submitted*).

I-2. INTRODUCTION

Collagen is a structural and the most abundant protein present in the extracellular matrix of all vertebrate animals. In invertebrates, its presence is distributed in the body walls and cuticles, wherein in unicellular organisms and plants it's absent, being its support function developed by polysaccharides and cellulose [1]. In general, collagen in mammals covers one-fourth of the whole-body protein, three quarters of dry weight skin, 90% of human tendon and corneal tissues, and it comprises most of the organic content in bones (80%) [2, 3]. In lesser amounts, it can be found in cartilage, teeth, vessels, and others.

Since collagen is the major component of all tissues, collagen-based materials have been extensively applied in the Tissue Engineering (TE) field [4]. It is known that collagen is biocompatible, provides natural biological cues for cells and induces its migration and proliferation, and can be remodeled *in vivo,* being thus recognized by its good biological performance, proper degradation properties and stability [5, 6].

Mammals have been used as the primary source of the whole industrially used collagen with particular emphases in bovine and porcine animals [7]. However, the risk of diseases transmission to humans (zoonosis) such as transmissible spongiform encephalopathies (TSE) and bovine spongiform encephalopathy (BSE), a fatal neurological disorder of cattle characterized by a long incubation period (2 to 8 years), limits its use particularly on medical context [7, 8]. Moreover, cultural and religious beliefs limit the usage of bovine and porcine derived products. In 2025, Muslims are expected to represent 30% of the world population [9] and they, together with Jews, refrain from consumption of porcine products [10]. On the other hand, consumption of bovine products is seriously hampered in Hinduism, a religion followed by about 1000 million people [11]. These disadvantages represents significant drawbacks for manufacturing biomaterials containing mammalian origin collagen, motivating the investigation of other potential sources of collagen [8, 12].

The marine ecosystem has attracted scientific attention in this regard, characterized by having high biodiversity and availability, with different species being studied as potential source of collagen, offering high quality product with few regulatory and quality control problems [4].

The main purpose of the present review was to understand the biomedical applications using marine origin collagen, especially focusing on the ones targeting hard tissues, described so

far. After blood, bone is the most transplanted tissue and despite the advances in the TE field, the most commonly used approaches (autografts) lack efficiency, cause a high degree of morbidity and lack donor sites. Marine collagen emerges as a promising approach to promote and enhance hard tissues regeneration. Different works already reported the potential of using collagen from marine species to induce human mesenchymal stem cells (hMSC) chondrogenic and osteogenic differentiation and suggested the faster formation and orientation of collagen fibrils with impact on the performance of derived biomaterials regarding both mechanic and cellular perspectives [13]. These and other studies will be discussed in the following sections, considering pros and cons in comparison to mammals collagen, building a forecast of their use in regenerative medicine in the coming years.

I-3. COLLAGEN PROTEIN

To date, almost thirty different types of collagen composed by distinct polypeptide chains were identified in humans and divided into fibrillar and non-fibrillar collagens [6]. Collagen type I, II and III form collagen fibrils with an axial periodicity of 67 nm and are the most abundant ones. Wherein type I collagen is a heterotrimer mostly present in bone, skin, tendon and cornea composed by three polypeptides chains (two $\alpha 1$ and one $\alpha 2$ chains), type II and III collagens are homotrimer molecules composed by the same polypeptide chains mostly present in cartilage and more flexible tissues, respectively. Non-fibrillar collagens are membrane-associated, including type IV collagen present in basement membrane [2, 6].

The collagen triple-helix structure stable form was described in the 1950s. It was proposed that a common axis is supercoiled by three polyproline II-like polypeptides. The three chains near the central axis must have glycine (Gly) as every third residue due to its smaller size enabling a close packing, creating this way the characteristic collagen $(Gly\text{-}Xaa\text{-}Yaa)_n$ repeating sequence, with and without interruptions. The Gly residues are located well inside the central core of the triple-helix, while residues in the Xaa and Yaa positions are well accessible to solvents, enabling intermolecular interactions. Collagen has a wide amino acids content, including proline (Pro) and the post-translationally modified hydroxyproline (OHPro), that often occupies the X and Y positions, respectively. These amino acids are responsible for the stability of the polyproline II conformation of individual chains, increasing the stabilization of the triple-helix. Collagen triplex

helix tertiary structure has a molecular weight of around 300 000 g.mol^{-1}, 280 nm in length and 1.4 nm in diameter. Triplex helix stability increases with intramolecular hydrogen bonds between glycines in adjacent chains as well as between the hydroxyl groups of the OHPro residues (**Figure I-1**). Type I collagen is the most common type and it is represented by elongated fibrils with a size average of around 500 µm in length and 500 nm in diameter [2]. The rearrangement varies according to the collagen type.

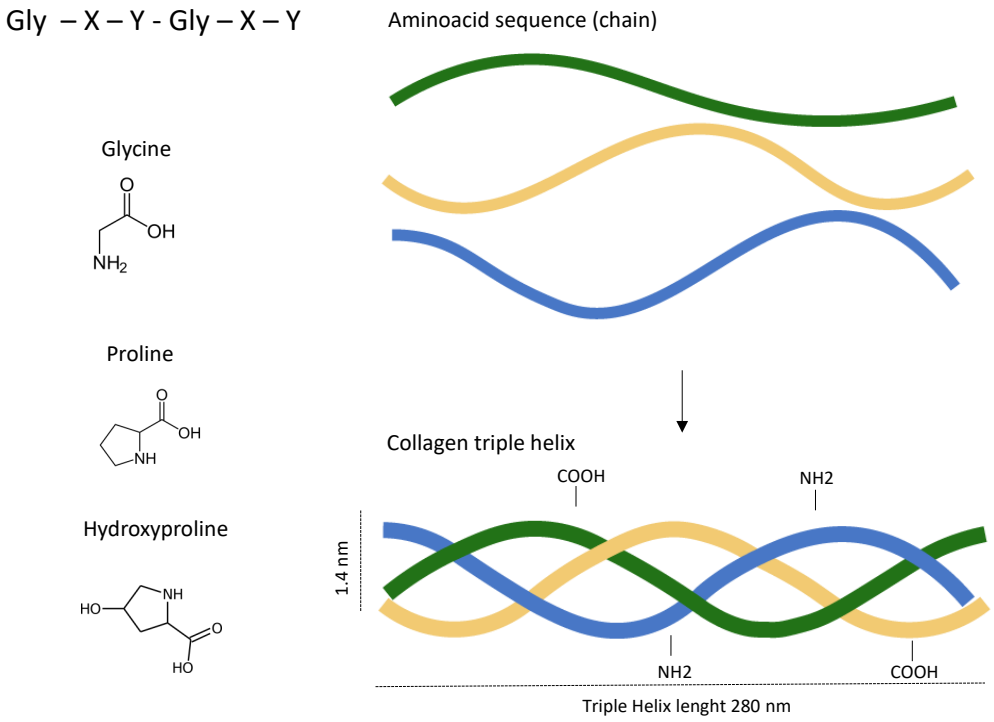

Figure I-1 - Schematic representation of amino acid composition of the repeating sequence (Gly-X-Y), generally proline and hydroxyproline occupies the X and Y position to stabilize the triplex helix.

I-3.1. Collagen sources

I-3.1.1. Mammals sources

Due to the structural and organizational similarity with humans, porcine and bovine sources are the most commonly used for the extraction of collagen together with rat tail and chicken also used in biotechnology research [2]. Collagen from porcine is mostly obtained from its skin, bones and small intestinal mucosa. Collagen from bovine is mainly obtained from achilles tendon (type I collagen), placental villi (type IV) and articular cartilage (type II) [3]. Other tissues like bones and hides have been also explored [3]. However, the risk of diseases transmission to humans such as

BSE, has been raising concerns, particularly considering biomedical context. Scientific studies have shown that the exposure to the BSE agent is related to the fatal Creutzfeldt-Jakob disease (vCJD) in humans. BSE is a progressive and mortal neurological disorder of cattle, transmitted by infectious agents that can be present in cattle food, especially in protein meal, has a long incubation period (2 to 8 years) and belongs to the family of TSEs. The individuals affected by the disease are normally separated from the rest of the animals and show signs of neurological and behavior modifications. They overreact to touch and sound and start to stumble, fall and have seizures until coma and death. Until 2014, 229 persons in 12 countries were identified with vCJD. Taking this in account, the European Union (EU) defined specific criteria for the sourcing and processing of collagen and its derivates used in the manufacture of biomedical products for human applications. The collagen manufacturing process, including alkaline and sodium sulfate treatment, calcium hydroxide and sodium hydroxide treatments or enzyme treatment, have similar steps from those of gelatin. However, the steps of collagen and gelatin isolation can vary in several parameters such as duration and pH which can result in significant differences of BSE inactivation capacity. Lower inactivation efficiency is thus expected for the collagen manufacturing process, requiring a special attention for the source origin to support the safety of the product. Risk assessment should be thus considered by the manufacturers. Collagen produced from tissues such as hides, skins, tendons and sinews do not usually have a significant TSE risk, since that contamination with probable infected materials, for instance spillage of blood and/or central nervous tissues, is avoided during procurement. The safest source of collagen is therefore the hides of the animals. Nevertheless, it is still possible that cross-contamination with brain material can occur during the slaughtering process.

I-3.1.2. Legislative and safety considerations of mammalian origin collagen

To regulate the use of cattle derived parts with possible contamination with BSE in human and veterinary products, the EU published several directives related to the subject. On March 11 2016, the European Commission published Regulation (EU) 2016/355, amending Annex III to Regulation (EC) No 853/2004, concerning the specific requirements for gelatin, collagen and highly refined products of animal origin intended for human consumption. In general, they define that all animal parts used for the production of medical products must be Category 3 (safe for humans) unless properly justified otherwise.

To minimise the risks of contamination, the EU advises the manufacturers to have in consideration three major parameters: the source and geographical origin of the animals, the nature of the animal part and the possible cross-contamination in the production process. In the specific case of collagen, the EU recommends additional attention to all the process. If the collagen is produced using bone as source, the conditions applied to gelatin (strict control of the starting materials and manufacturing process) should be considered, taking into account that the BSE inactivation capacity is lower in the case of collagen. Considering collagen extracted from hides, skins, tendons and sinews, the risk of contamination is usually lower. However, direct and cross-contamination can occur, so it is recommended the control of the process in every step to keep it safe. Overall, the additional care represents and increment on complexity of the production costs, resulting in failure to cope with regulations or higher costs.

Regarding the origin of the animals, currently, only New Zealand and Australia have received designation as not subject to certain Food and Drug Administration (FDA) restrictions on cattle-derived materials. Based on those constraints, the concern to find safe sources of collagens free of mammalian diseases amenable to be transmitted to humans is a key factor driving the batch for alternatives, as the use of marine collagen in the biomedical applications. In fact, regulatory agencies periodically enquire companies using mammals-origin materials on the absolute need of using them and if alternatives are available.

I-3.2. Marine environment

The human population is constantly growing, and the predictions are that this growing will be consistent in the years to come, putting more pressure in the global resources, including fish. The demand for fish is increasing exponentially with global fisheries production of 37 million tons in 1961 exploding to up to 200 million tons in 2016, with a tendency of rising [14]. The increase in fish production augments also fish waste, with reports showing that 20 up to 80% of fish is composed of heads, skin, bones, thorns and guts, depending on the species and processing method and generally discarded as waste [15].

This waste creates an increasing and severe environmental problem since its solid part is frequently deposited in landfills, and its liquid part often ends in the marine ecosystem, without any potential utilization and valorisation that can also improve profits for the fish industry.

Although being challenging, the valorisation of fish by-products is crucial for the future of fish industries.

These by-products are constituted by 15 to 30% of protein, 0 to 25% of fat and 50 to 80% of moisture and can nowadays be reused for several applications such as the fishmeal and oil industries, used for the production of silage, fertilizers and animal feed. They can also be applied in food for moisture maintenance (hydrolysates), source of proteins, amino acids, minerals, bioactive peptides and natural pigments.

Some industries also use them to biofuel production, dietic products, enzyme isolation (proteases) and gelation production and as an important source of collagen from the cosmetic to the pharmaceutical industries [16]. Collagen extraction emerges as a promising application for the maximization of uses for the fish by-products industry. New uses of these by-products are of extreme importance, both in environmentally and economically terms, so there is an increasing search and demand for new forms of utilizing them by the industry. Marine collagen can be isolated not only from fish by-products, but also, from invertebrate animals that include cuttlefish, prawns, star fish, sea anemone, jellyfish [16-19], sponges [20], octopus, sea urchin and squid [21]. The ocean covers 70% of earth surface and are populated by a huge variety of species. This large amount of organisms makes the marine ecosystem an amazing source of collagen and bioactive molecules [8].

An important feature of collagen from marine sources, that increases its potential uses is the fact that fish killing is accepted by all major religions, including Muslims, Jews, Hindus, Buddhists and Christians, unlike the use and killing of other animals that are forbidden for a huge percentage of world population. In addition, the consumers' concern for BSE does not apply to collagen from marine by-products increasing the potential economic return for the fishing industry.

I-3.2.1. Collagen extraction from marine organisms

The extraction process of collagen from marine organisms is separated in two main steps, the pre-treatment of the raw materials and the extraction itself (**Figure I-2**). During the pre-treatment, the raw materials are submitted to various processes for the extraction preparation, including cleaning to remove contaminants and size reduction, which maximizes the contact with

solvents and thus the collagen extraction efficiency, improving the final product quality. Normally, the raw materials used for extraction have, in addition to collagen, other proteins, lipids, pigments and other components that can be considered contaminants and diminish the quality of the whole process. Calcium and inorganic materials are also found in potential raw materials, like bones [17]. To remove non-collagenous proteins and pigments from the marine by-products, alkaline pre-treatment with 0.1 M sodium hydroxide (NaOH) is a commonly used method [18-21]. As to the removal of the calcium and the inorganic materials, ethylenediaminetetraacetic acid (EDTA) is the normally applied substance for the demineralisation of the raw materials [22]. Because of its chelating function, EDTA is an effective decalcifying agent, but inorganic acids, especially hydrochloric acid, can also be used to achieve decalcification [18]. The fatty parts of the materials are removed with a butyl alcohol treatment [18].

Extracted collagen can be divided into three groups based on the extraction process, namely neutral salt solubilized collagen (SSC), acid solubilized collagen (ASC) and pepsin solubilized collagen (PSC). Salt solubilization method has been rarely used due to the poor extraction efficiency [7, 23]. To achieve better yields, the neutral salt solution can be replaced by dilute acid solvents like citrate buffer, 0.5 M acetic acid, or hydrochloric acid (pH 2 – 3). Collagen from bone, cartilage or older animals' material has a higher content of keto-imine bonds, making it less soluble in these dilute acid solvents [7]. To maximize the yields, and since collagen has a relatively protease-resistant triple-helix, various enzymes such as trypsin, pepsin, and collagenase have been used. Pepsin is the most commonly used enzyme and is a promising method for different reasons: ***i)*** improves collagen purity - non-collagenous proteins can be hydrolysated and further removed by salt precipitation; ***ii)*** enhances collagen extraction efficiency - solubilization in acidic conditions can be facilitated by collagen telopeptides hydrolysis; ***iii)*** reduces antigenicity – by elimination of telopeptides commonly associated with immunogenic reactions [7, 23] . Some studies also report ultrasonic treatments (20 kHz with amplitude of 20 – 80%) to improve the yield of collagen extraction. Basically, in ultrasound-assisted extraction processes, the by-products are soaked in acetic acid for 12 h followed by ultrasonic treatment. The yield of collagen is directly proportional to the amplitudes and duration of the ultrasonic treatment. It was reported that the yield of collagen extraction from sea bass skin was higher when ultrasonic treatment was applied comparing with the traditional method [24]. Kim *et al.* investigated the effects of ultrasonic wave treatment on the extraction yield of acid soluble collagen from sea bass

(*Lateolabrax japonicu*) skin, showing that the ultrasonic treatment increased the yield of collagen without affecting its structural integrity [24].

All extraction methods overlap the steps of dialysis, precipitation and centrifugation that are performed to purify the extracted material. Depending on the species, tissue, age, and extraction parameters, including acid concentration, the ratio of acid solution to raw materials, extraction temperature and time, different yields can be achieved. Collagen isolated from swim bladder of sea bass rendered an higher yield (28.5%) when compared with collagen extracted from its skin (15.8%) [25]. Collagen extracted from Catla (*Catla catla*) skin revealed an higher yield comparatively with Rohu (*Labeo rohita*) skin collagen [23]. The yield of ASC and PSC extracted from skin, scales and fins of *Cirrhinus mrigala*, was 4.7 and 6.5; 3.2 and 5.1; and 5.7 and 7.7%, respectively [26]. Skin, scales and bone of grass carp [27] were also used as raw materials for collagen isolation. All these marine origin collagens were classified as being equivalent to human type I collagen, but different production yields were achieved. Skin and scale of grass carp demonstrated a higher yield (45.3 and 32.8%, respectively) when compared with that of bone (4.2%).

In general, higher acid concentrations, extraction temperature and time, results in higher yield of collagen extraction. However, such parameters can compromise collagen properties and stability, by promoting protein hydrolysis. In general, low temperatures (4 °C), acid concentration (0.5 M acetic acid) and extraction time (48 h) have been applied when it is intended to obtain collagen with preserved triple-helix structure, particularly when envisaging applications in biomedicine.

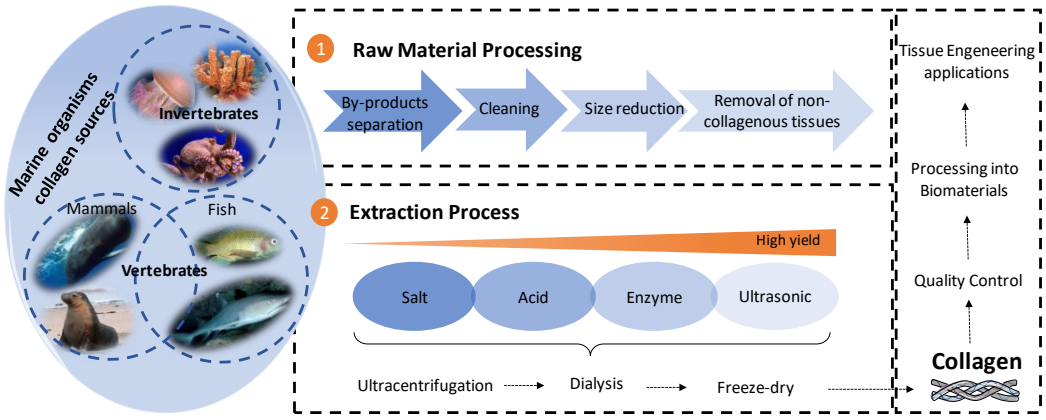

Figure I-2 - Representative image of collagen extraction processes from marine vertebrate and invertebrate organisms envisaging biomedical applications.

I-3.2.2. Marine collagen properties: characterization routes

I-3.2.2.1 Protein chains and amino acid composition

The amino acid composition is one of the most important features to characterize collagen. The high OHPro content of collagen makes it different from the other proteins and the specific sequence of these amino acids determines the type of collagen. In terms of amino acid composition, collagen derived from marine organisms has been mostly shown to be like bovine and porcine one and, naturally, as type I collagen in humans. Sodium dodecyl sulfate polyacrylamide (SDS-PAGE) is commonly used to characterized collagen through separation of proteins according to their molecular weight, charge, size and shape [28]. Most of fish collagens have been found to consist of two α - chains, designated as α-1 and α-2 with the former being present in the double amount of the latter, like type one in mammals [8]. In addition, the presence of β and γ components can be related to the higher molecular weight of collagen that increases with animal age due to its higher crosslinked form [29]. Generally, collagen from marine organisms results in less prominent bands when compared with mammals, due to its lower molecular weight. While similar, it is thought that the small differences in terms of biochemical composition affects its behavior. Collagen-specific helical structure and its stability is highly influenced by the amino acid composition. Glycine, for instance, is one of the most important and abundant amino acid in mammals collagen occupying more than 30% of all protein, also Pro and OHPro determines collagen properties [2]. Such amino acids have a key role for the stability of the polyproline II conformation of the individual chains, increasing the stability of the collagen triple-helix. Through intramolecular hydrogen bonds between glycines in adjacent chains, the triple helix stability increases [2]. In marine organisms, glycine is also the most common amino acid, but its ratio varies according to the species, tissue source and extraction method [8]. In a total of 1000 residues per gram of protein, ASC and PSC from the skin of brown banded bamboo shark have in its composition 318 (ASC) and 323 (PSC) residues of glycine [20], silver carp skin 329 (ASC), carp skin 332 (ASC), cod skin 342 (ASC) [21], blue shark (*Prionace glauca*) collagen 392 (ASC) and 387 (PSC), Nile tilapia (*Oreochromis niloticus*) 333 (ASC) and 338 (PSC) [30]. Such amounts are in the range of the ones obtained for mammals' collagen (**Table I-1**). However, marine sponges present a lower content of glycine. The amount of glycine in *Chondrosia reniformis* sponge was 189/1000, quite similar from those

obtained for grass sponge Spongia graminea 163/1000 [31, 32]. In a more recent study, it was found for *Axinella cannabina* and *Suberites carnosus* a content of glycine around 257/1000 and 295/1000, respectively [33]. Other marine invertebrate organisms like squid, present similar glycine content when compared with marine vertebrates or terrestrial mammals. For instance, collagen from skin and muscle of *Kondakovia longimana* was found to have 303/1000 (ASC), 323/1000 (PSC) and 315/1000 (ASC), 278/1000 (PSC), respectively. Skin of *Illex argentines*, another species of squid, was found to have 315/1000 (ASC) and 327/1000 (PSC) of glycine content [34].

Collagen triplex helix is also stabilized by intramolecular hydrogen bonds between the hydroxyl groups of OHPro residues [2]. Hydroxyproline content can be determined through amino acid composition by chromatography analysis or even through a simple method of OHPro content determination, like ninhydrin assay [35]. In terms of Pro and OHPro content, marine collagen has in general a lower content (**Table I-1**). The amount significantly varies among the different marine organisms and even within the different fish species. They are mostly dependent on the environmental temperature. It was reported that cold sea fishes have lower degrees of OHPro than those of fishes from warm or tropical seas. ASC collagen of salmon (Pro 73 and OHPro 48) and codfish (Pro 91 and OHPro 55), revealed a lower content of Pro and OhPro when compared with blue shark *Prionace glauca* (Pro 132 and OHPro 80) (**Table I-1**) [36] . *Prionace glauca* prefers higher water temperatures (between 12 - 20 °C) when compared with salmon or codfish that are considered cold water fishes. The degree of hydroxylation of Pro in marine organisms has been calculated to be 35 – 48%, similar, in some cases with the levels observed in mammalian tissues (approximately 45%).

Table I-1 – Summarized table of glycine (Gly), proline (Pro), and hydroxyproline (OHPro) of acid soluble (ASC) and pepsin soluble (PSC) collagen obtained from different tissues of diverse marine origin organisms. The amino acid content is represented in gram per 1000 residues of protein. Calf and porcine skin and human tendon collagen were used as a mammalian collagen as comparative control.

	By-product			Collagen characterization				Ref
	Marine organism	Species	Tissue	Extraction method	Gly	Pro	OHPro	
Vertebrates	Silver Carp	*Hypophthalmichthys*	skin	ASC	329	114	78	[21]
	Carp	*C. carpio*	skin	ASC	332	114	76	[21]
	Grass Carp	*Ctenopharyngodon idellus*	skin	ASC	380	71	77	
				PSC	398	79	76	

			bone	ASC	373	80	80	[27]
				PSC	390	70	77	
			scale	ASC	429	46	52	
				PSC	380	79	76	
	Bighead carps	*Hypophthalmichthys nobilis*	fin	PSC	339	107	60	[22]
			scale	PSC	350	100	56	
			skin	PSC	341	92	73	
			bone	PSC	332	100	74	
			bladders	PSC	331	95	81	
	Nile Tilapia	*O. niloticus*		ASC	338	110	79	[30]
				PSC	333	119	86	
	Brownbanded bamboo shark	*C. punctatum*	skin	ASC	318	111	93	[20]
				PSC	323	113	94	
	Blue shark	*P. glauca*	skin	ASC	332	121	64	[37]
	Blue shark		skin	ASC	392	132	80	[38]
				PSC	387	124	98	
	Cod fish	*G. morhua*	skin	ASC	342	103	51	[21]
	Cod fish		skin	ASC	332	91	55	[36]
	Salmon	*Salmo salar*	skin	ASC	365	73	48	[36]
Invertebrates	Star fish	*A. amurensis*	all tissue	PSC	338	97	61	[39]
	Squid	*K. longimana*	skin	ASC	303	56	63	[34]
				PSC	323	55	50	
			muscle	ASC	315	74	63	
				PSC	278	54	37	
		I. argentinus	skin	ASC	315	59	60	
				PSC	327	60	62	
	Jellyfish	*Catostylus tagi*	umbrella	PSC	269	78	65	[40]
	Sponge	*C. Reniformis*	all tissue	PSC	189	54	24	[31]
		A. cannabina	all tissue	PSC	257	58	38	
		S. carnosus	all tissue	PSC	295	56	47	
		Hyalonema	all tissue	PSC	245	65	69	
Calf			skin	PSC	330	121	94	[21]
Porcine			skin	PSC	341	123	97	[41]
Human			tendon	ASC	337	121	92	[42]

I-3.2.2.2 Thermal stability

Collagen triple-helix stability is highly dependent on the amino acid composition, as previously reported. The melting temperature of human type I and type III collagen has been shown to be 41.5 °C and 39.5 °, respectively [43].

Circular dichroism spectroscopy (DSC) is traditionally used to assess the denaturation temperature of pure or treated collagen, together with differential scanning calorimetry (micro DSC). Generally, body temperature of fishes is lower than the mammalian ones, being the denaturation temperature of marine organisms also lower. When placed at human physiological temperatures, marine collagens melts faster when compared with mammalian collagen which compromises its use in terms of clinical applications [44].

Collagen denaturation temperature derived from different marine organisms has been tested. The higher OHPro content of *Prionace glauca* significantly influences its higher denaturation temperature (28 - 30 °C) when compared with Chum salmon (*Oncorhynchus keta*) that has a lower denaturation temperature, of around 19 °C. Another parameter that influences marine collagen thermal stability is the collagen pH of the solution wherein the collagen is disperse. Collagen melting temperature from jellyfish varied from 29 to 33 ° C when pH was changed from 3.0 to 7.5 [45]. Surprisingly, it was recently found that tilapia collagen has higher denaturation temperature when compared with sea bass and even porcine collagen. Since all samples were extracted and treated with the same method, the authors suggested that this result might be attributed to the high content of OHPro and cysteine in Tilapia collagen [46]. It was suggested that the triple-helix stability did increase due to the disulfide bonds formed between cysteines intermolecular crosslinking [2].

In contrast to fish collagens, collagen extraction from marine mammals is not common. So far, there is just one scientific publication [47] reporting the extraction of collagen from marine mammals: the extraction of collagen from Minke Whale (*Balaenoptera acutorostra*) identified as type I collagen. Its denaturation temperature was found to be approximately 31.5 °C, 6 - 7 °C lower than porcine collagen but significantly higher than most of the fish species [47]. It could be a potential collagen source for biomedical applications in terms of collagen properties, but not suitable in terms of source sustainability. This and similar species are covered by generic regulations for the protection of cetaceans or marine mammals in several range states.

I-3.2.2.3 Crosslinking routes

Due to its relatively lower molecular weight, when compared with mammals' collagen, marine origin collagens are faster absorbed by the human body. Chemical and physical crosslinking agents have been widely employed to increase its stability. Since marine collagen has similar amino acid content and the same functional groups of mammals' collagen, the crosslinking routes are similar. Aldehydes (glutaraldeyide) [48],isocyanates (HMDI) [49] and carbodiimides (1-ethyl-3-(3-dimethylaminopropryl) carbodiimide (EDC) [50] have been by far the most widely used chemical crosslinking agents. Yamada *et al*, reported that the addition of the chemical compounds increased the denaturation temperature of chum salmon from 19 to 55 °C [51]. The crosslinking of collagen also transforms it in a functional material to make gels, scaffolds, films and membranes [2]. To study crosslinking efficiency, ninhydrin assay, which quantifies primary free amino groups, is customarily used [2]. Despite this, it should be taken into account that chemical crosslinking can potentially affect biocompatibility and be cytotoxic [2]. To avoid the adverse effects associated with the chemical crosslinkers, physical or biological methods, like dehydrothermal (DHT), ultraviolet irradiation and transglutaminase, have been assessed. Physical and biological methods are often weak and in the case of the physical methods there is a great association with collagen denaturation [2]. For instance, salmon collagen scaffolds crosslinked with DHT demonstrated poor stability when compared with salmon collagen scaffolds crosslinked with EDC [52] .

I-3.2.2.4 Biocompatibility and biodegradability

Collagen protein is recognized by its excellent biocompatible and low antigenic properties. The RGD (arginine (Arg)-glycine (Gly)-aspartic acid (Asp)) complex, present in collagen, has cell adhesion properties, making it an excellent building block for biomaterial development.

Biocompatibility assays are a key factor to determine how safety each material is. In Europe, for collagen commercialization a set of conditions should be in compliance with the essential requirements defined in the Annex I of the Council Directive 93/42/ EEC (replaced by the Medical Device Regulation (MDR) 2017/745).

Collagen processing methodology, from its native form to the final product, must be fully validated to ensure reproducibility and safety for human use [53]. In this regard, several research

studies have been focusing to investigate the biocompatibility of marine collagen and resulting devices, in agreement with which standard ISO 10993 already stablish for biocompatibility tests [30, 54].

The cytocompatibility evaluation of marine collagen-based materials have been thus assessed in different studies. *In vivo* cytokine responses and *in vivo* inflammatory potential of crosslinked electrospun tilapia collagen membranes (CETC) were recently evaluated and compared with the commercial membrane Bio-Gide® (collagen from porcine origin) for oral tissue regeneration. It was evidenced by histological analysis that the CETC membrane exhibited a lower tissue response from the host when compared to that of Bio-Gide® [55]. Also, Tilapia type I collagen, did shown high *in vitro* and *in vivo* biocompatibility [55]. Non-fibrillar collagen from the predominant Mediterranean Sea sponge *Chondrosia reniformis* has also been shown to be a sustainable source for safe collagen, due to its reduced toxic compounds [56]. The capacity of marine origin organisms to offer safe sources of collagen with biological cues, support its use as potential alternative to mammalian collagen, to produce medical products.

In terms of biodegradability, generally, collagen from marine organisms present a faster degradation due to its lower denaturation temperature, as aforementioned. However, it is described in the literature that its degradation occurs in the same way of collagen from mammalian origin. The cleavage by collagenase digestion of blue shark collagen occurred similarly to pig collagen, although in a much faster rate [37]. This can be overcome by applying crosslinking agents that results in more stable forms, as discussed above.

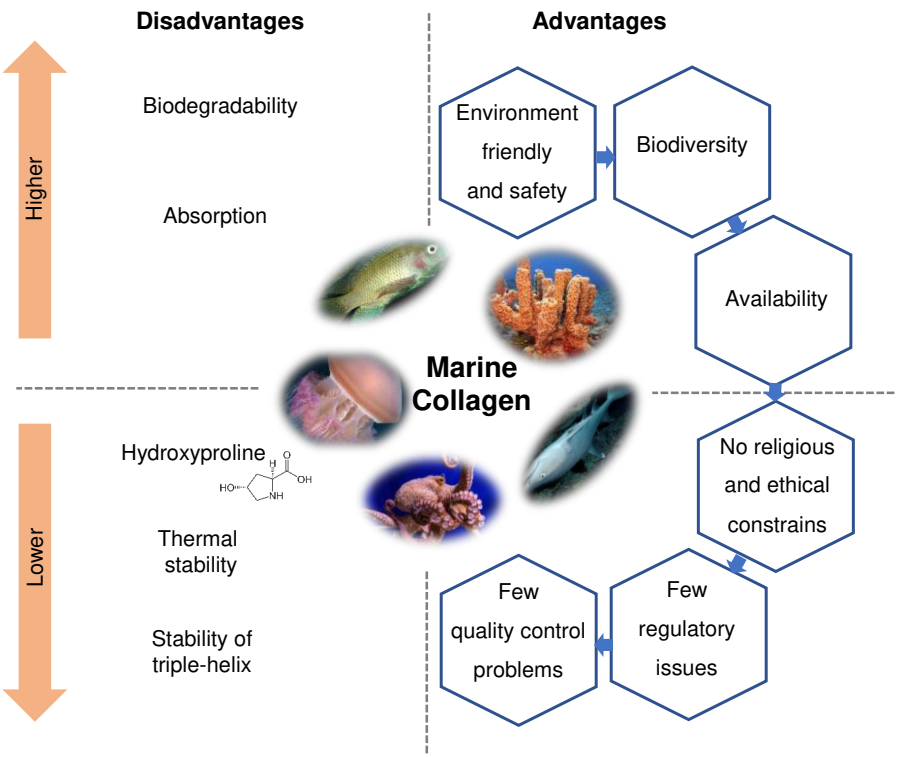

Figure I-3 - Marine collagen features highlighting its advantages and disadvantages.

I-4. MARINE COLLAGEN FOR THE ENGINEERING OF HARD TISSUES

The applicability of marine origin collagens in the healthcare-related field is in a transition state and under investigation. The use of marine collagen directly in the native, denatured (gelatine) or in peptide form, instead of processed systems based on this biopolymer, leads the global marine collagen market, however, currently, most of the target sectors involve the use of marine derivatives (gelatine and peptides), instead of native collagen [57]. As a first attempt to determine the suitability of their use in the engineering of hard tissues, many researches have been focusing on studying the activity of marine collagens as supplementary diet, since nutritional factors have been demonstrated to play an important role in skeletal development during growth [58, 59]. Other works have been directing to study the biological activity of marine collagen before its processing, for instance in coatings for cellular culture, as a first biological approach to assess its performance [59]. The use of marine collagen in the native, denatured or in peptide form, have been shown to promote absorption of calcium and other minerals contributing for bone homeostasis and growth. The use of marine collagen for development of medical devices is more challenging and still poorly explored, with only a few approaches of

collagen processing reported so far to use marine collagen in biomaterials [60]. The processing of collagen and particularly marine collagens demands a strict control of surrounding conditions, specially pH and temperature to maintain its intrinsic structural, chemical, and biological properties. Therefore, its processing, including solvent conditions to disperse collagen and the production techniques, is still very limited to the most conventional techniques of structures fabrication, like solvent casting and freeze-dry, mainly resulting in simple materials such as membranes, gels, sponges or other similar. It is worth noting that, nowadays, freeze-dry holds the lion's share in preparation of marine-based biomaterials for biomedical applications – as it seems to occur with mammals' collagens -, particularly for hard tissue applications. One reason is that this technique is straightforward, although time-consuming, using solvents that are rapidly cooled and gradually removed through vacuum sublimation resulting in highly porous structures with great interest for cells spread and nutrients diffusion. At the same time, the processing conditions can almost preserve the native structural form and the biological properties of collagen. Due to the its poor stability and mechanical properties, the use of marine collagen as biomaterial in TE is often only possible after physical or chemical crosslinking treatments or combination with other polymers or robust materials, like ceramics, specifically when applied to regeneration of bone tissue that must sustain higher compression forces. The usefulness of marine collagen for biomedical applications is determined by the type and source of collagen and the target application [8]. In bone, type I collagen stands out as the most abundant organic component; in cartilage, type II collagen assumes the lead.

Table I-2 represents an exhaustive list with all the known works published so far with marine origin collagen in the hard tissue engineering field, including bone, cartilage, and osteochondral tissues. Among the different marine organisms, collagen obtained from fish by-products shares the major part of all marine exploitation. This is likely because to the large availability of fish discards resulting from the fish processing industry, which ultimately results in a higher sustainability of the source, both in quantity and supply costs [57]. Type I collagen extracted from tilapia, salmon and sharks has been the most widely explored and applied in the biomedical field within the marine ones and will be particularly discussed.

I-4.1. Tilapia collagen for hard tissues-related applications

Tilapia is a globally cultured fish, with an important position in China, being therefore widely available [30, 61]. Collagen obtained from its skin has been tested for different biomedical applications, namely the fabrication of scaffolds for bone and [13, 62] cartilage TE approaches [63]. In contrast to other marine origin collagens, tilapia collagen has a high denaturation temperature (near 37 °C), which makes its use suitable for cell culture conditions. Matsumoto *et al.* studied the potential of using tilapia scales collagen for bone tissue regeneration [13]. Tilapia and porcine collagen fixed at 3 $mg.mL^{-1}$ were used to cover culture dishes, being then placed in contact with human mesenchymal stem cells. Firstly, they studied how fast the fibril formation was with tilapia collagen exhibiting better results. Then they investigated their potential to promote osteogenic differentiation and osteoblastic markers such as alkaline phosphatase activity (ALP), osteopontin, and bone morphogenetic protein 2 (BMP2) were quantified. Upregulation was observed when hMSCs were cultured on a tilapia collagen surface, specially in the early osteoblastic differentiation stage. These results suggest that the degree of fibril formation of tilapia collagen positively influenced the osteoblastic differentiation of hMSCs. Afterwards, they studied the potential of using tilapia scales for the engineering of cartilaginous tissue [63]. According to the obtained results, tilapia collagen formed thicker fibrils in comparison with porcine collagen. From quantitative RT-PCR results, chondrogenic-related markers like SOX9 and AGGRECAN expression in hMSCs cultured on tilapia collagen were significantly higher at an early stage, when compared with that of porcine collagen-coated and control dishes. In addition, collagen II expression was significantly higher on the tilapia collagen, 6 days after cell culture, compared with that of porcine and the control treatment. They hypothesized that the special fluctuations of tilapia scale collagen might make the binding of integrin and collagen easier to trigger not only osteoblastic differentiation, but also chondrogenic differentiation of hMSCs.

I-4.2. Salmon collagen for hard tissues-related applications

Salmon by-products are highly available, and collagen is easily isolated from its skin, being one of the most studied within the marine organisms. Nagai *et al.* studied its potential for different biomedical applications, including periodontal ligaments [52, 59]. In a pioneer work with porous *Oncorhynchus keta* salmon collagen EDC crosslinked scaffolds they demonstrated its

potential to induce proliferation and ALP activity of human periodontal ligament cells. Hoyer *et al.* demonstrated the feasibility of using porous scaffolds made of mineralized salmon collagen by freeze-dry technique. The resulting scaffolds exhibited interconnective porosities with stable mechanical properties. Human mesenchymal stem cells adhered abundantly to these scaffolds and the osteogenic differentiation was demonstrated by the alkaline phosphatase activity [64]. *In vivo*, the potential of using salmon-derived atelocollagen sponges was tested in osteochondral defects of femoral trochlea. Twelve weeks post-implantation, the regeneration of the critical-sized bone defect was evident when salmon collagen crosslinked sponges were used comparatively with the empty control group [65].

I-4.3. Shark collagen for hard tissues-related applications

Within the different marine collagen sources, sharks have been getting increasing attention, especially blue shark. According, to the International Union for Conservation of Nature (IUCN), the annual global catch of blue sharks is likely to be around 20 million individuals, being thus its by-products a promising source for collagen extraction. Currently, no species-specific catch limits or other protections in place in the Mediterranean sea. [66]. Many authors have been demonstrating its potential mainly for bone and cartilage through the fabrication of 3D structures [67]. *Prionace glauca* is one of the widest ranging shark specie. In 1997, Yoshihiro Nomura *et al*, published for the first time a comparative study between the biochemical features of *Prionace glauca* collagen in comparison with porcine collagen [37]. The results demonstrated a high similarity between the two collagens in terms of amino acid composition, although shark collagen has revealed a lower content of Pro. The collagenase-digestion pattern suggested that blue shark collagen cleavage occurred in the same way of porcine collagen, although being faster. Although similar, the detailed molecular structure showed small differences between them, which influenced the digestion sensibility. The authors considered two hypotheses: the lower denaturation temperature due to the lower content of Pro and the collapse of the helical structure after collagen cleavage, which makes the collagen fragments susceptible to be attacked by non-specific proteases [37]. The osteogenic effect of type-II collagen from blue shark cartilage comparatively with collagen from bovine origin was also studied after collagen processing into composite scaffolds by combination with chitosan or hydroxyapatite [68]. The marine-based composite scaffolds showed higher stiffness, lower biodegradation rate and better

biocompatibility when compared with those of bovine collagen. Additionally, they exhibited a higher ALP activity, suggesting its osteogenic potential.

Considering the relevance of collagen molecular composition and arrangement for osteogenic response, Elango *et al.* did investigate in a very recent work the potential of using *Prionace glauca* collagen (PSC and ASC) before its processing. Due to higher OHPro content, PSC had higher thermal stability than that obtained for ASC, with denaturation temperatures being 29.8 °C and 28.3 °C, respectively. Proliferation of differentiated mouse bone marrow-mesenchymal stem and of differentiated osteoblastic (dMC3T3E1) cells was enhanced in collagen treated groups rather than in the controls, with upregulation of Runx2 gene expression.

The potential of *Prionace glauca* collagen for scaffolds fabrication envisioning bone tissue regeneration was also studied by combining it with calcium phosphates extracted from the same source [67].The applied freeze-dry technique combined with the crosslinking methodology (EDC/NHS or HMDI) was useful to create scaffolds with different microporosities. From the 3D microarchitecture evaluation, it was observed that, in general, pore size decreased as the crosslinking concentration increase. In addition, for the used concentration of crosslinkers it could be observed that the EDC/NHS crosslinked scaffolds revealed, in general, a smaller pore size, which suggested a higher efficiency of crosslinking. *In vitro*, EDC/NHS crosslinked scaffolds revealed a less cytotoxic effect over Saos-2 cell line.

I-4.4. Marine invertebrates' collagen for hard tissues-related applications

Collagen extracted and processed from invertebrates is mainly obtained from jellyfish and squid.

Jellyfish from *Rhopilema esculentum* species has been used for the production of collagen, mainly type II collagen, being thus preferred for cartilage applications. In 2012, a new rat model for nasal cartilage replacement to evaluate the *in vivo* biocompatibility of jellyfish collagen (*Rhopilema esculentum*) was, for the first time, created. Due to the specificity of the immunological environment, subcutaneous animal models do not meet the requirements to study the nasal cartilage reconstruction. From the results, the freeze-dried porous jellyfish collagen scaffolds did provide good microenvironmental conditions to produce cartilaginous ECM (glycosaminoglycans, collagen type II and aggrecan). The results were improved when cell

seeded scaffolds were implanted [69]. Also, Pustlauk *et al.* studied the potential of combing *Rhopilema esculentum* type II collagen with alginate to make collagen scaffolds for chondrogenic differentiation of hMSC. To increase collagen stability, *N*-(3-dimethylaminopropyl)-*N*'-ethylcarbodiimide hydrochloride EDC was used as a crosslinking agent. *Rhopilema esculentum* collagen did shown a similar composition when compared with mammalian type II collagen supporting the chondrocytic phenotype [70]. Hoyer *et al*. also studied the potential of type II collagen from *Rhopilema esculentum* for cartilage repair, after its processing into 3D structures [71]. The freeze-drytechnique resulted in highly cytocompatible porous scaffolds with upregulation for chondrogenic-related markers (SRY-box transcription factor, aggrecan and Collagen II). Ribbon jellyfish (*Chrysaora sp. morphotype*) was also used to extract type II collagen with a maximum yield of 19%. The authors suggested its use to replace the land-based sources [72].

Type II collagen extracted from squids was also studied for cartilage repair in degenerative osteoarthritis cases by different authors [73, 74], being also demonstrated as a useful material for biofilm preparation in composites with chitosan [75] and hierarchical scaffolds production with improved mechanical properties and cell seeding efficiency [34].

Still within the invertebrates organisms, only a few works reported the extraction of sea urchin, star fish, cuttlefish, prawn, octopus collagen and their potential for biomedical applications [39, 76, 77].

Table I-2 – Marine origin collagens used on different strategies for the engineering of hard tissues applications (bone, cartilage and osteochondral) and main outcomes. (ND, non-identified).

Tissue	Collagen type and source	Extraction method	Targeted applications	Main outcomes	Ref.
Bone	Atelocollagen; chum salmon (*Oncorhynchus keta*) skin	ASC	Activity of human periodontal ligament cells in chum Salmon scaffolds	No differences in the thermal stability, porous structure, and cell proliferation rate between salmon and bovine collagen scaffolds were observed. But enhanced ALP activity of HPDL cells was observed in salmon scaffolds.	[52]
	Coll type I; skin of blue shark (*Prionace glauca*)	ASC	Osteoporosis animal model	Collagen administration in ovariectomized rats resulted in higher bone mineral density of the femur epiphysis than that of sham-operated rats.	[78]
	N.D; Marine collagen peptides (MCPs). skin of wild-caught chum salmon (*Oncorhynchus keta*)	Enzymatic hydrolysis	Femurs development in rats	Supplementation with MCPs improved physiologically and biomechanically bone development in growing rats, through the increased osteoblastic activity. The effect was greater in male rats than in female ones.	[58]
	Coll type I; skin of Atlantic salmon	ASC	Effect in mesenchymal stem cells differentiation	Scaffolds of type I salmon collagen have been shown to MSCs adhesion, proliferation, and differentiation into osteogenic linage.	[64]
	Mainly col type II; Jellyfish *(Rhopilema esculentum)*	ASC followed by Enzymatic digestion with pepsin	*In vitro* and *in vivo* nasal cartilage repair	Defects of septal cartilage treated with jellyfish scaffolds seed with autologous chondrocytes demonstrated significant reduction in the number of nasal septum perforations compared to no replacement.	[69]
	Hydrolyzed fish collagen (HFC); Tilapia scales	Enzymatic hydrolysis	Multidirectional differentiation potential of rBMSCs.	HFC (2, 0.2 and 0.02 $mg.mL^{-1}$) was tested. The findings described demonstrated that 0.2	[79]

			mg.mL^{-1} HFC was able to enhance and guides rBMSCs viability and differentiation toward osteogenic lineage in the absence of additional inducing factors.	
ND; Fish collagen peptide (FCP). Bone and skin of cods	PSC	Effect of FCP in human osteoblasts	FCP increased expression of osteocalcin, osteopontin and integrin β3 proteins in treated cells. Furthermore, accelerated matrix mineralization in the cultures. The results suggested the potential utility of FCP on biomaterials	[80]
Coll type I; Tilapia scales (Oreochromis niloticus)	ND	*In* vitro responses of MDPC-23 to type I collagen coatings	Enhanced ALP activity, upregulated gene expression of BSP and accelerated matrix mineralization was observed for Tilapia collagen when compared with porcine collagen, suggesting its use for oral-maxillofacial area.	[54]
ND; Collagen from bovine (BC) and Jellyfish *(C. reniformis)*	ND	*In vitro* evaluation of different composites using hBMSCs	*C. reniformis* collagen-calcium-phosphate bone cements (CPC) demonstrated a significant, but clinically irrelevant, increase in terms of cytotoxicity when compared with bovine collagen (BC)-CPC. However, the ALP activity was higher when compared with BC-CPC composites.	[56]
Coll type II; Cartilage of blue shark (*Prionace glauca)*	ASC and PSC	Comparative study of marine collagen-based scaffolds with mammalian ones	Composite scaffolds prepared from fish collagen did present better osteogenic properties when compared with the mammalian ones	[68]
ND; Silver carp (*Hypophthalmichthys molitrix)*	ND	Bone defect healing in a rat model	Bone formation was significantly increased in treated bone lesions comparing to untreated bone tissue. No significant	[81]

			differences were noted between the healing of the defects filled with bovine or marine-based substitutes.	
Hydrolized collagen; Scales of tilapia	Enzymatic hydrolysis	*In vitro* periodontal tissue regeneration	The upregulation of osteogenic markers ALP, COL I, RUNX2, and OCN at the gene level and the production of osteogenic-related proteins (alkaline phosphatase and osteocalcin) evidenced the success of osteogenic differentiation of hPDL cells treated with HFC.	[62]
Coll type I;Skin of tilapia (*Oreochromis niloticus*)	ASC	Bone tissue regeneration	It was evident by histological analysis that the tilapia collagen membranes elicited a lower tissue response from the host when compared to that of Bio-Gide®	[55]
Mainly Coll type I; skin of blue shark *(Prionace glauca)*	ASC	Scaffolds for bone regeneration	Mineralization occured preferentially in the apatite-based composite scaffolds. Despite scaffolds' properties being affected by different parameters, scaffolds crosslinked with 12.5% EDC/NHS appear to be better. High-quality and low-cost bioactive compounds from fish waste were produced.	[67]
Coll type I; Cartilage of blue shark *(Prionace glauca)*	ASC and PSC	Osteogenic response of type I ASC and PSC	Cells treated with PSC showed higher osteogenic regulatory protein expressions than ASC treated cells.	[38]
Fish collagen (FC); Skin and scales	ND	BMSCs and human gingival fibroblasts cells (HGF) behaviour	The addition of n-HAp (nano-hydroxyapatite) and FC improved the cytocompatibility of the lactide-co-glycolide membrane to BMSCs and HGFs	[82]
Coll type I; Salmon skin	ASC	For bone applications	The mineralization of fish-Coll solution with hydroxyapatite resulted in scaffolds with better mechanical properties that	[83]

				the ones achieved for the mineralized porcine collagen	
	ND; Marine sponge *(Aplysina fulva)*	Tris-HCL	Bone defect healing in Wistar rats	*Aplysina fulva* collagen into hydroxiapatite scaffolds did improved the biological performance of the composite and would have a positive stimulus into bone formation	[84]
	Coll type I; Blue shar (*Prionace glauca*)	ASC	Bone applications	*Prionace glauca* collagen was successfully *in situ* mineralize to prepare bioactive inks for 3D bioprinting.	[85]
Cartilage	Mainly type II; Jellyfish *(R. esculentum)*	ASC	Cartilage applications	Cytocompatible scaffolds with potential to support and maintain chondrogenic stimulation of human mesenchymal stem cells were successfully produced.	[86]
	Coll type I; Chum Salmon skin	PSC	*In vivo* efficacy of salmon sponges incorporated with osteogenic protein (OP) 1- to induce cartilage regeneration	Salmon sponges incorporated with OP-1 up regulated chondrocytes metabolism enhanced cartilage repair in rat models.	[87]
	Coll type I; Shark skin *Scyliorhinus canicular*	ASC	Collagen scaffolds for cartilage repair	High porous scaffolds were achieved by crosslinking with low genipin concentrations. No cytotoxic effect to the chondrocyte-like cell line was observed. Cell adhesion, growth, and proliferation was demonstrated.	[88]
	ND; Jellyfish (*Rhopilema esculentum*)	PSC	Collagen matrix for chondrocytes phenotype maintenance	Jellyfish collagen scaffolds demonstrated the potential to maintain the conservation of chondrocytes phenotype and matrix reproduction when compared with collagen type I and II of vertebrates.	[89]
	Mainly type II; Jellyfish *(Rhopilema esculentum)*	ASC	Scaffolds for cartilage repair	hMSC chondrogenic differentiation was confirmed through expression of SOX9 and aggrecan.	[70]

	Mainly Coll type I; Tilapia	ND	Comparative study of tilapia and porcine collagen on cultures with hMSCs on collagen-coated dish surfaces	hMSCs adhesion on tilapia collagen was faster and higher when compared with that of porcine or non-coated surfaces. Tilapia scale collagen fibrils provided an appropriate ECM scaffold for hMSC chondrogenesis by inducing the binding efficiency of integrins, fibronectins, and their receptors.	[63]
Osteochondral	Atelocollagen; Chum Salmon (*Oncorhynchus keta*) skin	ASC and PSC	*In vivo* study in osteochondral defects	By SOX9 expression, type II collagen and aggrecan demonstrated the potential of salmon collagen for cartilage and osteochondral repair.	[65]
	Col type I; from jellyfish and Col type II from salmon	ASC and PSC	Biphasic scaffolds for osteochondral defects	A sequential seeding of the biphasic scaffolds and a pre-differentiation of the cells into both osteogenic and chondrogenic lineage was enough to obtain functional osteochondral constructs.	[90]
	Coll type I; swim bladder of bester sturgeon fish	ASC and PSC	Collagen fibril-based double network (DN) hydrogels for osteochondral defect of rabbit knee	The *In vivo* experiments suggested that the produced hydrogels demonstrated good biomechanical performance and strong bonding ability with bone.	[91]

I-5. CONCLUSIONS AND FUTURE REMARKS

Collagen products from different sources are widely commercially available and used for different clinical applications. The demand for collagen is growing fast and it is expected that the market continues to expand with the exponential augment of the human population in the next decades and the arising of new biomaterial-based therapeutic solutions, as a result of a societal pressure for better quality of life and healthier ageing. To date, primary sources of collagen have bovine and porcine origin, but non-negligible risk of disease transfer and religious constraints, is questioning their use.

Marine collagen emerges as an attractive alternative: it is represented by a high biodiversity and availability of organisms from which it can be obtained, it is safe of disease transmission, being environmentally friendly, when produced from fish by-products, and has less regulatory and quality control constrains. The marine environment and the huge variety of species that populate it represent thus an extensive source for collagen extraction, with potential applications in several areas of the healthcare field.

Considering, in particular, biomaterials for the engineering of hard tissues, marine collagen is being processed using conventional techniques like freeze-dry and solvent casting. However, these are limited to the creation of simple structures such as membranes, gels, powders and sponges, unlike the need described by physicians of more complex structures, that better mimic human native tissues, with great capacity of revascularization and replacement of the implanted tissue, and particularly for application in hard tissue engineering, to sustain higher compression forces. To overcome these obstacles, combination of physical or chemical crosslinking treatments with processing by more advanced techniques, such as 3D bioprinting, must be further developed and explored. In addition, further knowledge is needed with regards to the underlaying mechanisms of action and biological and mechanical behavior, to design and develop safe, yet functional materials providing right structural and biological cues to guide good cellular responses.

To date, only a few works regarding the exploration of marine collagen, as biomaterials for hard tissues, as an alternative to mammals collagen have been published, so its fully potential is yet to explore, but so far good outcomes have been demonstrated. The higher and faster orientation of collagen fibrils from certain marine species like tilapia when compared with porcine collagen positively contributes to the tensile and bending strength of bone and induced human mesenchymal stem cells chondrogenic and osteogenic differentiation.

It is thus clear the necessity of further works and investigations to deepen knowledge and better understand marine collagen, and its behavior in the years to come. This can be achieved by exploring other potential marine sources of collagen or/and with the application of better and more advanced processing techniques to create more and more complex structures to fulfill the market demand. In addition, it is also necessary more exhaustive and deep studies with, including for instance the *in-vivo* application of marine collagens, to reach the clinical trials phase and to finally develop a product for the market. This product would stand out as an illustrative

example of the potential of marine collagen materials in clinics and serve as benchmarking for other developments in the field, but there is still a long way to go before a real clinical application. To our knowledge there is still not a single marine collagen derived product applied to hard tissues in the market.

The expansion and democratization of marine collagen use in the biomedical field will represent a leap for the healthcare collagen industry with positive impacts both economically and environmentally with potential benefits for our world.

I-6. ACKNOWLEDGMENTS

This study was funded by the Portuguese Foundation for Science and Technology (FCT) under the scope of the BiogenInk project (M-ERA-NET2/0022/2016), by European Regional Development Fund through INTERREG Atlantic Area Program, under the scope of BLUEHUMAN (EAPA_151/2016) project and through Norte de Portugal Regional Operational Program (NORTE 2020), under the scope of Structured project NORTE-01-0145-FEDER-000021. The Doctoral Program NORTE-08-5369-FSE-000044 supported by NORTE 2020, under the PORTUGAL 2020 Partnership Agreement, through the European Social Fund, is also greatly acknowledge by the PhD fellowship of GSD. RP thanks FCT for the contract IF/00347/2015.

I-7. REFERENCES

1. Müller, W.E., *The origin of metazoan complexity: Porifera as integrated animals.* Integrative and Comparative Biology, 2003. **43**(1): p. 3-10.
2. Sorushanova, A., et al., *The collagen suprafamily: from biosynthesis to advanced biomaterial development.* Advanced Materials, 2019. **31**(1): p. 1801651.
3. Silvipriya, K., et al., *Collagen: Animal sources and biomedical application.* Journal of Applied Pharmaceutical Science, 2015. **5**(3): p. 123-127.
4. Rahman, M.A., *Collagen of Extracellular Matrix from Marine Invertebrates and Its Medical Applications.* Marine Drugs, 2019. **17**(2): p. 118.

5. Park, S.-H., et al., *Comparative analysis of collagens extracted from different animal sources for application of cartilage tissue engineering.* International Journal of Precision Engineering and Manufacturing, 2012. **13**(11): p. 2059-2066.

6. An, B., Y.-S. Lin, and B. Brodsky, *Collagen interactions: Drug design and delivery.* Advanced Drug Delivery Reviews, 2016. **97**: p. 69-84.

7. Berillis, P., *Marine collagen: Extraction and applications*. Research Trends in Biochemistry, Molecular Biology and Microbiology;. 2015, SMGroup. 1-13.

8. Felician, F.F., et al., *Collagen from marine biological sources and medical applications.* Chemistry & Biodiversity, 2018. **15**(5): p. e1700557.

9. Karim, A. and R. Bhat, *Gelatin alternatives for the food industry: recent developments, challenges and prospects.* Trends in Food Science & Technology, 2008. **19**(12): p. 644-656.

10. Almarzouqi, F., et al., *Porcine-derived biomaterials in tissue engineering and reconstructive surgery: Considerations and alternatives in Muslim patients.* Journal of Tissue Engineering and Regenerative Medicine, 2019. **13**(2): p. 253-260.

11. Eriksson, A., J. Burcharth, and J. Rosenberg, *Animal derived products may conflict with religious patients' beliefs.* BMC medical ethics, 2013. **14**(1): p. 48.

12. Ehrlich, H., et al., *Collagens of poriferan origin.* Marine Drugs, 2018. **16**(3): p. 79.

13. Matsumoto, R., et al., *Rapid oriented fibril formation of fish scale collagen facilitates early osteoblastic differentiation of human mesenchymal stem cells.* Journal of Biomedical Materials Research Part A, 2015. **103**(8): p. 2531-2539.

14. Nawaz, A., et al., *Valorization of fisheries by-products: Challenges and technical concerns to food industry.* Trends in Food Science & Technology, 2020. **99**: p. 34-43.

15. Kratky, L. and P. Zamazal, *Economic feasibility and sensitivity analysis of fish waste processing biorefinery.* Journal of Cleaner Production, 2020. **243**: p. 118677.

16. Marti-Quijal, F.J., et al., *Fermentation in fish and by-products processing: An overview of current research and future prospects.* Current Opinion in Food Science, 2020. **31**: p. 9-16.

17. Regenstein, J. and P. Zhou, *Collagen and gelatin from marine by-products*, in *Maximising the value of marine by-products*. 2007, Elsevier. p. 279-303.

18. Benjakul, S., S. Nalinanon, and F. Shahidi, *Fish collagen.* Food biochemistry and food processing, 2012: p. 365-387.

19. Nagai, T., Y. Araki, and N. Suzuki, *Collagen of the skin of ocellate puffer fish (Takifugu rubripes).* Food Chemistry, 2002. **78**(2): p. 173-177.

20. Kittiphattanabawon, P., et al., *Isolation and characterisation of collagen from the skin of brownbanded bamboo shark (Chiloscyllium punctatum).* Food Chemistry, 2010. **119**(4): p. 1519-1526.

21. Zhang, J., et al., *Characterisation of acid-soluble collagen from skin of silver carp (Hypophthalmichthys molitrix).* Food Chemistry, 2009. **116**(1): p. 318-322.

22. Liu, D., et al., *Extraction and characterisation of pepsin-solubilised collagen from fins, scales, skins, bones and swim bladders of bighead carp (Hypophthalmichthys nobilis).* Food Chemistry, 2012. **133**(4): p. 1441-1448.

23. Pal, G.K., T. Nidheesh, and P. Suresh, *Comparative study on characteristics and in vitro fibril formation ability of acid and pepsin soluble collagen from the skin of catla (Catla catla) and rohu (Labeo rohita).* Food Research International, 2015. **76**: p. 804-812.

24. Kim, H.K., et al., *Effects of ultrasonic treatment on collagen extraction from skins of the sea bass Lateolabrax japonicus.* Fisheries Science, 2012. **78**(2): p. 485-490.

25. Sinthusamran, S., S. Benjakul, and H. Kishimura, *Comparative study on molecular characteristics of acid soluble collagens from skin and swim bladder of seabass (Lates calcarifer).* Food Chemistry, 2013. **138**(4): p. 2435-2441.

26. Mahboob, S., *Isolation and characterization of collagen from fish waste material- skin, scales and fins of Catla catla and Cirrhinus mrigala.* Journal of Food Science and Technology, 2015. **52**(7): p. 4296-305.

27. Wang, H., et al., *Physical-chemical properties of collagens from skin, scale, and bone of grass carp (Ctenopharyngodon idellus).* Journal of Aquatic Food Product Technology, 2014. **23**(3): p. 264-277.

28. Bürck, J., et al., *Observation of triple helix motif on electrospun collagen nanofibers and its effect on the physical and structural properties.* Journal of Molecular Structure, 2018. **1151**: p. 73-80.

29. Veeruraj, A., M. Arumugam, and T. Balasubramanian, *Isolation and characterization of thermostable collagen from the marine eel-fish (Evenchelys macrura).* Process Biochemistry, 2013. **48**(10): p. 1592-1602.

30. Sun, L., et al., *Characterization of acid-and pepsin-soluble collagen extracted from the skin of Nile tilapia (Oreochromis niloticus).* International Journal of Biological Macromolecules, 2017. **99**: p. 8-14.

31. Swatschek, D., et al., *Marine sponge collagen: isolation, characterization and effects on the skin parameters surface-pH, moisture and sebum.* European Journal of Pharmaceutics and Biopharmaceutics, 2002. **53**(1): p. 107-13.

32. Gross, J., Z. Sokal, and M. Rougvie, *Structural and chemical studies on the connective tissue of marine sponges.* Journal Histochemistry & Cytochemistry, 1956. **4**(3): p. 227-46.

33. Tziveleka, L.A., et al., *Collagen from the Marine Sponges Axinella cannabina and Suberites carnosus: Isolation and Morphological, Biochemical, and Biophysical Characterization.* Marine Drugs, 2017. **15**(6).

34. Coelho, R.C., et al., *Extraction and characterization of collagen from Antarctic and Sub-Antarctic squid and its potential application in hybrid scaffolds for tissue engineering.* Materials Science and Engineering: C, 2017. **78**: p. 787-795.

35. Zeugolis, D.I., R.G. Paul, and G. Attenburrow, *Factors influencing the properties of reconstituted collagen fibers prior to self-assembly: animal species and collagen extraction method.* J Biomed Mater Res A, 2008. **86**(4): p. 892-904.

36. Alves, A., et al., *Cosmetic Potential of Marine Fish Skin Collagen.* Cosmetics, 2017. **4**: p. 39.

37. Nomura, Y., et al., *Structural property and in vitro self-assembly of shark type I collagen.* Bioscience, Biotechnology, and Biochemistry, 1997. **61**(11): p. 1919-1923.

38. Elango, J., et al., *Evaluation of Differentiated Bone Cells Proliferation by Blue Shark Skin Collagen via Biochemical for Bone Tissue Engineering.* Marine Drugs, 2018. **16**(10).

39. Lee, K.-j., et al., *Biochemical characterization of collagen from the starfish Asterias amurensis.* Journal of the Korean Society for Applied Biological Chemistry, 2009. **52**(3): p. 221-226.

40. Calejo, M., Z. Morais, and A. Fernandes, *Isolation and biochemical characterisation of a novel collagen from Catostylus tagi.* Journal of Biomaterials Science, Polymer Edition, 2009. **20**(14): p. 2073-2087.

41. Ikoma, T., et al., *Physical properties of type I collagen extracted from fish scales of Pagrus major and Oreochromis niloticas.* International journal of biological macromolecules, 2003. **32**(3-5): p. 199-204.

42. Steven, F. and D. Jackson, *Purification and amino acid composition of monomeric and polymeric collagens.* Biochemical Journal, 1967. **104**(2): p. 534-536.

43. Raghunath, M., P. Bruckner, and B. Steinmann, *Delayed triple helix formation of mutant collagen from patients with osteogenesis imperfecta.* Journal of Molecular Biology, 1994. **236**(3): p. 940-9.

44. Subhan, F., et al., *Marine Collagen: An Emerging Player in Biomedical applications.* Journal of Food Science and Technology, 2015. **52**(8): p. 4703-7.

45. Miki, A., et al., *Structural and physical properties of collagen extracted from moon jellyfish under neutral pH conditions.* Biochemistry & Molecular Biology 2015. **79**(10): p. 1603-7.

46. Bao, Z., et al., *The promising indicators of the thermal and mechanical properties of collagen from bass and tilapia: synergistic effects of hydroxyproline and cysteine.* Biomaterials Science, 2018. **6**(11): p. 3042-3052.

47. Nagai, T., N. Suzuki, and T. Nagashima, *Collagen from common minke whale (Balaenoptera acutorostrata) unesu.* Food Chemistry, 2008. **111**(2): p. 296-301.

48. McDade, J.K., et al., *Interactions of U937 macrophage-like cells with decellularized pericardial matrix materials: influence of crosslinking treatment.* Acta Biomaterialia, 2013. **9**(7): p. 7191-9.

49. Bryan, N., et al., *The innate oxygen dependant immune pathway as a sensitive parameter to predict the performance of biological graft materials.* Biomaterials, 2012. **33**(27): p. 6380-92.

50. Olde Damink, L.H., et al., *Cross-linking of dermal sheep collagen using a water-soluble carbodiimide.* Biomaterials, 1996. **17**(8): p. 765-73.

51. Yamada, S., et al., *Potency of fish collagen as a scaffold for regenerative medicine.* BioMed Research International 2014. **2014**: p. 302932.

52. Nagai, N., et al., *Application of cross-linked salmon atelocollagen to the scaffold of human periodontal ligament cells.* Journal of Bioscience and Bioengineering, 2004. **97**(6): p. 389-94.

53. Silva, T.H., et al., *Marine origin collagens and its potential applications.* Marine Drugs, 2014. **12**(12): p. 5881-5901.

54. Tang, J. and T. Saito, *Biocompatibility of Novel Type I Collagen Purified from Tilapia Fish Scale: An In Vitro Comparative Study.* BioMed Research International, 2015. **2015**: p. 139476.

55. Hassanbhai, A.M., et al., *In Vivo Immune Responses of Cross-Linked Electrospun Tilapia Collagen Membrane.* Tissue Engineering Part A, 2017. **23**(19-20): p. 1110-1119.

56. Palmer, I., et al., *Biocompatibility of calcium phosphate bone cement with optimized mechanical properties.* Journal of Biomedical Materials Research, 2016. **104**(2): p. 308-15.

57. Luca, S., et al., *Marine collagen and its derivatives: Versatile and sustainable bio-resources for healthcare.* Materials Science and Engineering: C, 2020: p. 110963.

58. Xu, Y., X. Han, and Y. Li, *Effect of marine collagen peptides on long bone development in growing rats.* Journal of the Science of Food and Agriculture, 2010. **90**(9): p. 1485-91.

59. Nagai, N., et al., *In vitro growth and differentiated activities of human periodontal ligament fibroblasts cultured on salmon collagen gel.* Journal of Biomedical Materials Research PART A, 2007. **82**(2): p. 395-402.

60. Claverie, M., et al., *Marine-Derived Polymeric Materials and Biomimetics: An Overview.* Polymers, 2020. **12**(5): p. 1002.

61. Song, W.-K., et al., *Physicochemical and Biocompatibility Properties of Type I Collagen from the Skin of Nile Tilapia (Oreochromis niloticus) for Biomedical Applications.* Marine Drugs, 2019. **17**(3): p. 137.

62. Liu, C. and J. Sun, *Hydrolyzed tilapia fish collagen induces osteogenic differentiation of human periodontal ligament cells.* Biomedical Materials, 2015. **10**(6): p. 065020.

63. Hsu, H.-H., et al., *Chondrogenic differentiation of human mesenchymal stem cells on fish scale collagen.* Journal of Bioscience and Bioengineering, 2016. **122**(2): p. 219-225.

64. Hoyer, B., et al., *Biomimetically mineralized salmon collagen scaffolds for application in bone tissue engineering.* Biomacromolecules, 2012. **13**(4): p. 1059-66.

65. Kawaguchi, Y., et al., *In vivo effects of isolated implantation of salmon-derived crosslinked atelocollagen sponge into an osteochondral defect.* Journal of Materials Science: Materials in Medicine, 2011. **22**(2): p. 397-404.

66. Stevens, J., *The IUCN Red List of Threatened Species 2009: e.T39381A10222811* 2009.

67. Diogo, G.S., et al., *Marine Collagen/Apatite Composite Scaffolds Envisaging Hard Tissue Applications.* Marine Drugs, 2018. **16**(8): p. 269.

68. Elango, J., et al., *Rheological, biocompatibility and osteogenesis assessment of fish collagen scaffold for bone tissue engineering.* International Journal of Biological Macromolecules, 2016. **91**: p. 51-59.

69. Bermueller, C., et al., *Marine collagen scaffolds for nasal cartilage repair: prevention of nasal septal perforations in a new orthotopic rat model using tissue engineering techniques.* Tissue Engineering Part A, 2013. **19**(19-20): p. 2201-2214.

70. Pustlauk, W., et al., *Jellyfish collagen and alginate: Combined marine materials for superior chondrogenesis of hMSC.* Materials Science and Engineering: C, 2016. **64**: p. 190-198.

71. Hoyer, B., et al., *Jellyfish collagen scaffolds for cartilage tissue engineering.* Acta Biomaterialia, 2014. **10**(2): p. 883-892.

72. Barzideh, Z., et al., *Isolation and characterisation of collagen from the ribbon jellyfish (C hrysaora sp.).* International Journal of Food Science & Technology, 2014. **49**(6): p. 1490-1499.

73. Dai, M., et al., *Cartilage repair in degenerative osteoarthritis mediated by squid type II collagen via immunomodulating activation of M2 macrophages, inhibiting apoptosis and hypertrophy of chondrocytes.* Biomaterials, 2018. **180**: p. 91-103.

74. Dai, M., et al., *Squid type ii collagen as a novel biomaterial: Isolation, characterization, immunogenicity and relieving effect on degenerative osteoarthritis via inhibiting stat1 signaling in pro-inflammatory macrophages.* Materials Science and Engineering: C, 2018. **89**: p. 283-294.

75. Uriarte-Montoya, M.H., et al., *Jumbo squid (Dosidicus gigas) mantle collagen: Extraction, characterization, and potential application in the preparation of chitosan–collagen biofilms.* Bioresource Technology, 2010. **101**(11): p. 4212-4219.

76. Benedetto, C.D., et al., *Production, characterization and biocompatibility of marine collagen matrices from an alternative and sustainable source: the sea urchin Paracentrotus lividus.* Marine Drugs, 2014. **12**(9): p. 4912-33.

77. Bama, P., et al., *Extraction of collagen from cat fish (Tachysurus maculatus) by pepsin digestion and preparation and characterization of collagen chitosan sheet.* International Journal of Pharmacy and Pharmaceutical Sciences, 2010. **2**(4): p. 133-137.

78. Nomura, Y., et al., *Increase in bone mineral density through oral administration of shark gelatin to ovariectomized rats.* Nutrition, 2005. **21**(11-12): p. 1120-1126.

79. Liu, C. and J. Sun, *Potential application of hydrolyzed fish collagen for inducing the multidirectional differentiation of rat bone marrow mesenchymal stem cells.* Biomacromolecules, 2014. **15**(1): p. 436-43.

80. Yamada, S., et al., *Early gene and protein expression associated with osteoblast differentiation in response to fish collagen peptides powder.* Dental Materials Journal, 2013. **32**(2): p. 233-40.

81. Hadzik, J., et al., *A silver carp skin derived collagen in bone defect treatment-A histological study in a rat model.* Annals of Anatomy - Anatomischer Anzeiger, 2016. **208**: p. 123-128.

82. Jin, S., et al., *Fish Collagen and Hydroxyapatite Reinforced Poly(lactide- co-glycolide) Fibrous Membrane for Guided Bone Regeneration.* Biomacromolecules, 2019.

83. Chang, M.C., B.-G. Kim, and J.-H. Whang, *Compressive strength enhancement of artificial bone using hydroxyapatite/fish-collagen nanocomposite.* Journal of the Korean Ceramic Society, 2020: p. 1-10.

84. Parisi, J.R., et al., *Evaluation of the In Vivo Biological Effects of Marine Collagen and Hydroxyapatite Composite in a Tibial Bone Defect Model in Rats.* Marine Biotechnology (New York, NY), 2020.

85. Diogo, G.S., et al., *Cell-Laden Biomimetically Mineralized Shark-Skin-Collagen-Based 3D Printed Hydrogels for the Engineering of Hard Tissues.* ACS Biomaterials Science & Engineering, 2020. **6**(6): p. 3664-3672.

86. Hoyer, B., et al., *Jellyfish collagen scaffolds for cartilage tissue engineering.* Acta Biomaterialia, 2014. **10**(2): p. 883-92.

87. Mori, H., et al., *Development of a salmon-derived crosslinked atelocollagen sponge disc containing osteogenic protein-1 for articular cartilage regeneration: In vivo evaluations with rabbits*. Vol. 14. 2013. 174.

88. Fernandes-Silva, S., et al., *Porous hydrogels from shark skin collagen crosslinked under dense carbon dioxide atmosphere.* Macromolecular Bioscience, 2013. **13**(11): p. 1621-31.

89. Sewing, J., M. Klinger, and H. Notbohm, *Jellyfish collagen matrices conserve the chondrogenic phenotype in two- and three-dimensional collagen matrices.* Journal of Tissue Engineering and Regenerative Medicine, 2017. **11**(3): p. 916-925.

90. Bernhardt, A., B. Paul, and M. Gelinsky, *Biphasic scaffolds from marine collagens for regeneration of osteochondral defects.* Marine Drugs, 2018. **16**(3): p. 91.

91. Mredha, M.T.I., et al., *Anisotropic tough double network hydrogel from fish collagen and its spontaneous in vivo bonding to bone.* Biomaterials, 2017. **132**: p. 85-95.

SECTION 2

EXPERIMENTAL DESIGN

Chapter II

Materials and Methods

Chapter II

Materials and methods

II-1. Overview

This Chapter describes all the materials, reagents, and processing methodologies of 3-dimensional (3D) structures production, complementing the information provided in "Materials and Methods" in **Chapters III**, **IV**, **V**, **VI** and **VII**. In a first part the different polymer (marine and bovine collagen, hyaluronic acid and alginate) and ceramic materials (marine apatite and synthetic apatite particles) used to develop the 3D structures are detailed. In a second part, it can be found a comprehensive overview of the selected techniques to fabricate the structures and the required equipments and techniques to finally assess the general properties of all produced structures.

II-2. MATERIALS

II-2.1. Collagen

Collagen is by far the oldest protein discovered to date; it was found for the first time in soft tissue of fossilized bones of *Tyrannosaurus rex* fossil at 68 million-year-old ago [1]. Collagen is a human body natural protein with remarkable biological and mechanical properties. It is naturally synthesized by cells and degraded by collagenase enzyme. Collagen is ample distributed in connective tissues, occupying about 25% to 35% of the total body's protein content [2].

Up to now, more than 29 forms of collagen with distinctive compositions and organizations were reported, being type I collagen the most abundant [3]. Type I collagen is typically characterized by its intrinsic fibrillar building form which naturally provides structural resistance to tensile, shear and compression forces. It is composed by three polypeptides chains (two $\alpha 1$ and one $\beta 2$) with a characteristic sequence of aminoacids, Gly-X-Y (X, proline and Y, hydroxyproline) that ultimately forms the triple helix collagen molecule (**Figure II-1**). It is mainly present in skin, tendons, ligaments, blood vessels, cartilage, bone, and teeth. In bones, it comprises around 80% of the organic matter [3]. The RGD (Arginine-Glycine-Aspartate) domains of collagen and the high aminoacid content, makes it a natural polymer with excellent biocompatibility for use in advanced Tissue Engineering (TE) approaches.

Collagen is found as the protein with the highest commercial value [4]. Its exploitation is mainly attributed to overcome the trending behavior of plastic disposal, taking advantage of its biodegradable properties [5]. In addition, its processing can result in different types of materials, such as films, sheets, beads, meshes, fibers, and sponges with tissues regeneration capabilities [6]. In the biomedical field it has been largely applied in skin, cartilage, bone, tendon among others. *In vitro* it has been demonstrated to promote cell adhesion, proliferation, and differentiation. *In vivo* it offers attractive biological cues that hopefully supports cell and tissue integration with a reduced inflammatory response. Animal tissues rich in type I collagen are thus preferred to extract type I collagen.

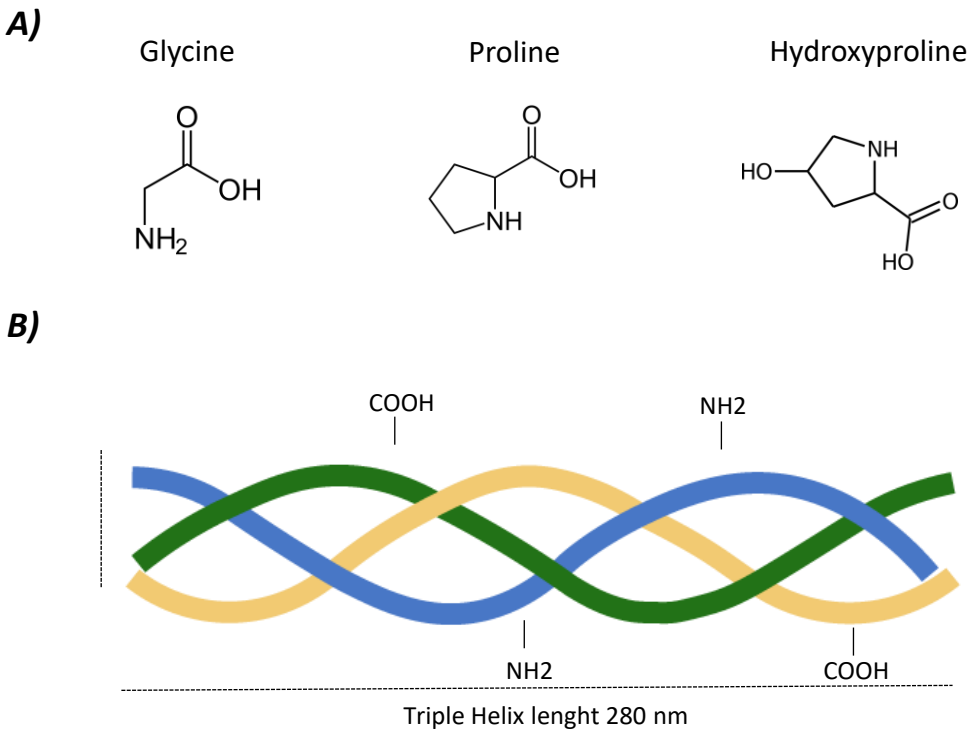

Figure II-1– Collagen structure.

II-2.1.1. Bovine Collagen

Mammalian origin sources like, bovine and porcine, are still the first option to extract collagen [1]. The majority of the commercially available scaffolds made of collagen have bovine and porcine-origin [4]. The potential of using bovine collagen (bColl) as a biomaterial was recognized and approved by Food and Drug Administration (FDA) within certain rules (discussed in Chapter I). Bovine sources are commonly used to extract collagen due to the structural and organizational resemblance with humans [3]. The extraction of type I collagen from bovine is mainly obtained from achilles tendon, bones and hides, discards resulting from meat production.

Three different methods of collagen extraction: neutral salt-soluble collagen (SSC), acid-soluble collagen (ASC) and pepsin- soluble collagen (PSC) have been described. Collagen properties are highly dependent on the source and on the extraction procedure [5]. In general, PSC presents an higher yield, while ASC better retains the native features of the triple helix.

In this thesis, bovine collagen was extracted from hides through an ASC method, as depicted in **Figure II-2,** by Centro de Investigaciones Marinas in Vigo. The process was divided in three main steps:

Processing of raw materials: During this process, hides from cow were cut in small pieces and cleaned for hair removal. After that, the raw materials were soaked in an alkaline solution (0.1 M NaOH (1:10 (w:v)) for 24 h ate 4 °C to remove the non-collagenous proteins. This step was followed by centrifugation to separate the non-collagenous proteins from the collagenous ones.

Collagen extraction: For collagen extraction, an acetic acid solution of 1:10 (w:v) was added for 72 h, at 4 °C. The extracted collagen was precipitated (overnight) with 2 M NaCl and separated by centrifugation.

Collagen purification: For purification, the separated collagen was once again solubilized in acetic acid and subjected to a dialysis process with successive decreasing concentrations of acetic acid, for 8 days, to remove any residual contaminations. The final collagen was then freeze-dried.

The extracted collagen was characterized and used in **Chapter IV** to prepare 3D collagen-based composite scaffolds by freeze-dry technique.

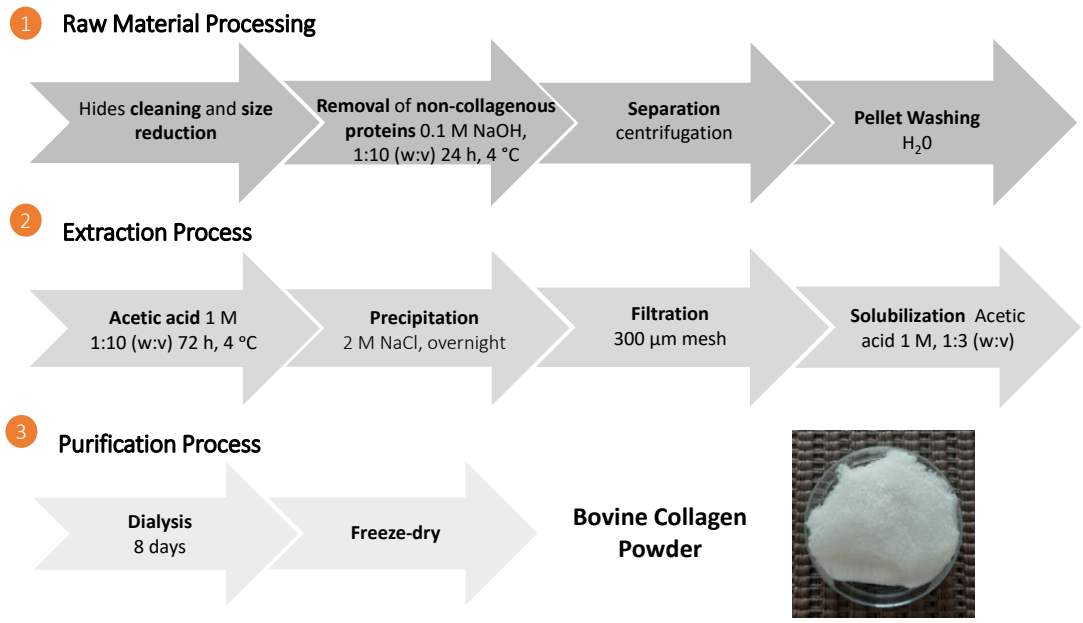

Figure II-2 - Process of bovine collagen extraction.

II-2.1.2. Marine Collagen

Marine origin collagens have gain special attention in the last years. Aquatic organisms, vertebrates and non-vertebrates, poses the advantage of avoidance the risk of mammalian origin diseases like, bovine spongiform encephalopathy (BSE), being an attractive alternative to mammalian

origin collagens [7-9]. Marine ecosystem offers diverse forms of collagen, with appropriated mechanical and biological properties, that can be applied in a wide range of applications, as before described in **Chapter I**.

Collagen from marine sources are mostly obtained from fishing by-products, considered waste for the fishing transformation industry [10, 11]. Inspired on a concept of marine by-products valorization, blue shark (*Prionace glauca (PG)*) collagen was used in **All Chapters** of this thesis. The final aim was the processing of this by-product into biomaterials proposing tissue regeneration approaches, in a strategy for sustainable valorisation of marine resources. The three main reasons that motivated the exploration of this specie were:

i) *Prionace glauca*, a oceanic pelagic species in tropical and temperate waters, among all pelagic sharks, it represents the highest known population growth rate, being thus a sustainable source, ***ii)*** it is a major bycatch in commercial fishing, ***iii)*** in addition there is an increased demand for its consume, which will increases its by-products [12, 13].

Collagen from blue shark (**Figure II-3**) was extracted by using the previously reported methodology (**section II-1.1.1**). Its potential was tested for bone and cartilage applications.

Figure II-3 - Blue shark (*Prionace glauca*) collagen.

II-2.2. Hyaluronic acid

Hyaluronic acid (Hya) is a natural non-sulphated glycosaminoglycan found in the extracellular matrix (ECM) of several human tissues, like in the vitreous fluid, joint fluid, and derma [14]. It is

recognized as a linear and anionic polymer with a D-glucuronic acid and N-acetyl-D-glucosamine bound with β-glycosidic linkages β (1–4) and β (1–3) (**Figure II-4**) [14]. Cell membrane-bound enzymes (Hya synthases) are responsible to synthesize hyaluronic acid, in contrast to hyaluronidases that are responsible by its natural degradation [15].

In the human body, Hya is responsible for the maintenance of the elastoviscosity of liquid connective tissues, for the regulation of water transport and tissue hydration, for the supramolecular assembly of ECM proteoglycans like aggrecan, and for different cell-mediated receptors with crucial roles in cell detachment, migration, mitosis, tumor development and metastasis, and inflammation [16]. But different molecular weights (MW) display different physicochemical and biological properties, sometimes opposite properties [14]. High molecular weight hyaluronic acid (HMWHya) unveil anti-inflammatory, anti-angiogenic, and immunosuppressive properties, while low molecular weight hyaluronic acid (LMWHya) is highly associated with pro-inflammatory responses.

Due to its unique biocompatible, bioactive and, viscoelastic properties, the introduction of Hya in several clinical applications has been demonstrated of great interest. In TE approaches, particularly in cartilage regeneration, Hya has been used to fabricate 2D and 3D structures to stimulate chondrogenic differentiation of mesenchymal stem cells (MSCs) [17]. Past studies report that, Hya with MW ranging between 700 to 6000 kDa is highly recommendable for cartilage repair, avoiding the inflammatory properties of the LMWHya [18].

Thus, envisioning cartilage tissue regeneration, high molecular weight (≈1500-1800 kDa) bacterial Hya (Sigma-Aldrich, Portugal) was used in this thesis, in **Chapter V**, to produced 3D scaffolds in combination with blue shark PG collagen.

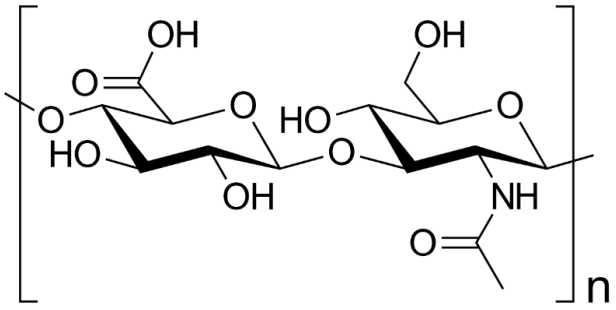

Figure II-4 - Chemical structure of hyaluronic acid.

II-2.3. Alginate

Alginate is the most abundant polysaccharide in brown seaweeds. The most commercially exploited brown seaweed are: *Laminaria hyperborea*, *Macrocystis pyrifera* and *Ascophyllum* [19]. This natural polysaccharide constitutes a family of linear copolymers 1,4-linked β-D-mannuronic acid (M) and α-L-guluronic acid (G) and its final chemical composition relies on the biological source, growth, and stationary conditions [19]. It has high affinity for divalent cations such as, Ca^{2+}, Sr^{2+} and Ba^{2+} and through ionic interaction with the carboxyl functional groups of the G units forms stable gels, which makes alginate a hopeful candidate for different TE engineering approaches. Fibers, nanofibers, microparticles and 3D structures have been thus explored [20].

Alginate is represented by good mechanical properties, which are highly sensitive to the species and concentrations of ions present in solution [21]. While, alginate with high content of G residues results in stiff and stable gels, alginate with low contents of G residues gives more elastic and less stable gels [22]. Physiologically, alginate is biocompatible and represents low cytotoxic effects. However, it is deprived of cell-adhesion sites, which compromises its biological functions. In alternative, cell-adhesive peptides are frequently combined. In mammals, the lack of alginase, the enzyme responsible to cleave alginate chains, makes alginate a non-degradable polymer [23]. However, ionically crosslinked gels are easily dissolved through the release of the divalent ions into the surrounding media due to the exchange reactions with monovalent cations, such as sodium ions [24].

In this thesis, alginate (Sigma-Aldrich, Portugal) was used in **Chapter VI** and **VII** to produce stable inks for 3D bioprinting (printing with incorporated living cells), by one side it could offer mechanical support due to its high viscosity, by other side it could serve as binding spots for mineralized collagen due to the presence of Ca^{+2} ions in the collagen. This effect will be better detailed in section **II-3.3**.

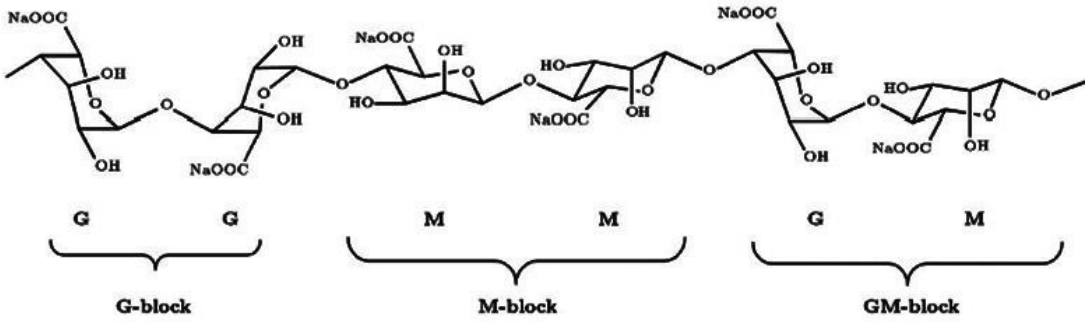

Figure II-5 - Chemical structure of sodium alginate.

II-2.4. Calcium phosphates

Calcium phosphates are a family of materials containing calcium ions (Ca^{2+}) and phosphate anions PO_4^{3-}. They can be found in many living organisms, like bones and teeth [25].

In humans, apatite, particularly, hydroxyapatite (HAp) is the most common form of calcium phosphate present in mineralized tissues. Biological apatite particles are mainly present in the form of nanocrystalline solid with a carbonated chemical composition called, carbonate-hydroxy-apatite [26]. Its formation occurs naturally in the human body as a result of a highly regulated and complex process. It comprises up to 65% of the total bones weight and up to 90% of enamel teeth, being responsible by different biological and mechanical rules [27].

As a major component of mineralized tissues, calcium phosphates-based materials are of special interest for TE applications, mostly in orthopedic and dental field, due to their close resemblance with the native inorganic compounds [28]. Calcium phosphates are bioactive inorganic materials with good biocompatibility, osteoconductivity, and bioresorbability properties being a hopeful alternative to autografts, the gold standard treatment in critical-size bone defects. As bioactive material, HAp has the ability to induce its biological integration in living tissues, by chemically interacting with the host tissue, being thus the most used ceramic.

II-2.4.1. Synthetic apatite

The term apatite (Ap) is used to refer a family of compounds that have the same structure, but do not necessarily have the same composition [29]. Synthetic apatite can be made by applying different production techniques including: precipitation, sol-gel methods, hydrothermal technique, microemulsion

technique, microwave and other. Different processing conditions results in materials with different properties [30].

At present, there are many manufacturers of hydroxyapatite: Bio-Rad, Sigma Graft, Zimmer Biomet, Nano Interface Technology, Plasma Biotal, among others.

In this thesis, Captal ® 'R' powder was purchased from Plasma Biotal and was used in **Chapter IV** to develop bovine collagen-apatite 3D structures. The aim was to have a synthetic commercially available source of Ap to compare with biologic apatite (bioapatite (BAp)) obtained from blue shark teeth.

II-2.4.2. Biological apatite

Biologic apatite is an Ap form obtained from biological origin (e.g. bone and teeth). Biologic apatites have similar chemical and structure compositions from that of native bone [31]. Due to its outstanding bioactivity and biocompatibility they are attractive bone substitutes for the reconstruction of bone defects in oral implantology, periodontology, oral, and maxillofacial surgery as well as orthopedics [32]. Given the significant role of biological apatite in the structure and function of biological tissues and its clinical applications, numerous studies have been carried out focusing on its use.

Marine ecosystem is represented by a rich source of different bioactive molecules of great interest for biomedical applications. Some of these compounds can be found in rare or unexploited organisms, but most of them can have origin from commonly fished species [33]. This is the case of mako shark *Isurus oxyrinchus* and blue shark *Prionace glauca*, two wide-ranging oceanic pelagic dispersed specie.

These species represent a relatively abundant source of fish by-products, mostly heads and skeletons, amenable to be processed to obtain valuable compounds.

In this thesis, BAp particles were used in **Chapter III** and **IV** to prepare collagen-BAp composite scaffolds. Shark teeth of *Isurus oxyrinchus* and *Prionace glauca*, provided by the Centro Tecnológico del Mar (CETMAR, Vigo, Spain) and by the fishing company COPEMAR S.A. (Porto de Vigo, Spain) were used for bioapatite extraction. The process was divided in three main steps (**Figure II-6**):

Teeth isolation and preparation: Heads of mako shark *Isurus oxyrinchus* and blue shark *Prionace glauca* were boiled in water for 3 h for teeth removal. After that, teeth were cleaned and washed being followed by dried at 60 °C for 24 h.

Grinding: For particle size homogeneity, the teeth were grinded in a ball mill (Retsch MM2000) for 5 min with an oscillation frequency between 90 to 100 Hz for powder of 100 to 0.1 µm.

Thermal treatment: Thermal treatment is one of the most straightforward methods used to eliminate the organic components of biological materials. The selected processing conditions including time, temperature, and atmosphere varies according to the study. Here, grinded teeth were pyrolyzed at 950 °C for 12 h with a heating ramp of 2 °C/min and a cooling ramp of 20 °C/min to remove the organic material of teeth. The resulting granules of apatite were separated by sieves below 63 µm of particle size.

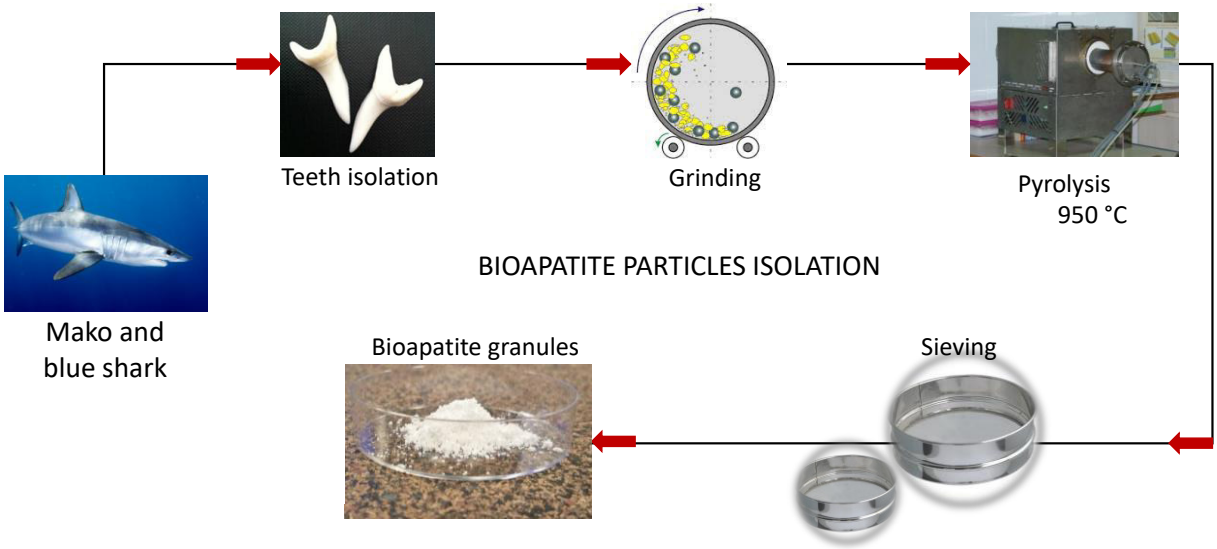

Figure II-6 - Bioapatite extraction from shark teeth.

II-3. REAGENTS

Unless addressed otherwise, all the reagents used in this thesis were purchased from Sigma-Aldrich.

II-4. TECHNIQUES OF 3-DIMENSIONAL STRUCTURES PRODUCTION

II-4.1. Freeze-dry

3-dimensional TE approaches should involve a set of conditions to meet tissues specific functionalities [34]. Several techniques of structures production have been employed to recreate the 3-

dimensional spatial microenvironment of the target tissues, functioning as anchor platforms for cell adhesion, allowing their growth and new tissue integration, both *in vitro* and *in vivo* [35].

Within all scaffolding production techniques, salt-leaching, gas foaming, electrospinning, freeze-drying and rapid prototyping are the most common ones [36]. Different techniques give different advantages, yet there is not a perfect and universal methodology capable to reproduce exactly the target tissue, there is still a long way to go. But, it is well described that, the best scaffold for an engineered tissue should support cell adhesion and growth, working as the extracellular matrix (ECM) of the target tissue in its native state.

Freeze-drying is an widespread technique of great interest for porous polymeric scaffolds production. This technique involves three main steps (**Figure II-7**): ***i)*** solubilization of a polymer in an appropriated solvent and concentration ***ii)*** freezing of the polymer-solvent mixture into a mold. The final shape can be modulated by using different types of molds. Also, the internal structure (pore size and pore interconnectivity) is manageable by controlling and changing the freezing method, namely the freezing rate and, the temperature range and time. ***iii)*** finally, the solvent is gradually removed through vacuum sublimation [36, 37].

The physical accumulation of polymer around the crystals formed during the freezing, results in 3D solid structures. The macroporosities arises from the slow release of the solvent, which corresponds to the empty spaces initially occupied by ice crystals [38]. Ice crystals growth are greatly influenced by the rate of freezing, slower freezing rates lead to the formation of higher crystals, which ultimately results in higher pores. In general, lower temperatures (i.e, -80 °C) and lower freezing periods are associated with smaller pores [39]. When the technique is used to freeze solutions with different phases, hoping to get more complex structures, the redistribution of the different phases and the homogeneity mainly depends on the nature of the compounds. If one of the compounds is particle-based, the particle size, density, conductivity and surface charge are important, being the particle size the most critical parameter to get a final homogeneity [39].

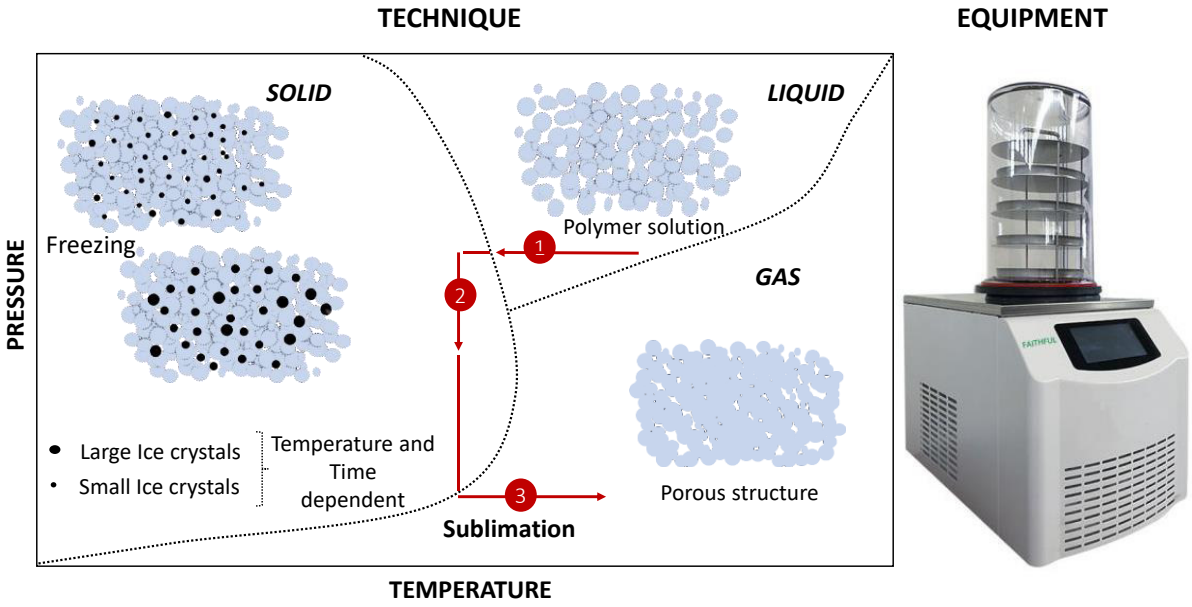

Figure II-7 - Schematic representation of freeze-dry technique for scaffolds production.

In biomedical field, this technique is widely applied to develop a variety of porous structures for different applications, being particularly interesting for collagen-based scaffolding production since it can almost preserve the native structural form and the biological properties of collagen [40].

Freeze-drying, was used in this thesis to produce scaffolds for bone in **Chapter III** and **IV**, and scaffolds for cartilage in **Chapter V**.

Due to its resemblance with the extracellular matrix, specific degradation properties to the action of enzymes, and improved recognition by the living body, *Prionace glauca* collagen was used as standard material.

II-4.1.1. Freeze-dry for bone

II-4.1.1.1 Marine collagen-bioapatite based composite scaffolds'

In Chapter III, marine collagen (mColl) was extracted from *Prionace glauca* skin and marine BAp was extracted from teeth of *Isurus oxyrinchus* and *Prionace glauca*, according to the protocol described in the beginning of this **Chapter**. For scaffolds production marine collagen was solubilized in 0.5 M of an acetic acid solution at 1.5% (w:v). After that, marine BAp was combined with collagen in different proportions: mColl:BAp ratios of 100:0, 70:30, 50:50, 30:70 (w:w). To increase collagen stability two

different crosslinking agents were tested, 1-ethyl-3-(3-(dimethylaminopropyl) carbodiimide/ N-hydroxysuccinimide (EDC/NHS) (Mw: 191,70 g/mol, Sigma-Aldrich, Portugal) or hexamethylene diisocyanate (HMDI) at 12.5% and 25% and, 1% and 5%, respectively. After allowing the crosslinker to react (24 h, RT), the solutions were poured into a desired round shape mold and freeze-dried for at least 5 days. To wash out any harmful residual compound all scaffolds were thoroughly rinsed with distilled water immediately before using in cell culture experiments.

Inspired on a marine-based approach, reusing marine by-products, it was aimed in this first work to test the *in vitro* performance of the collagen-bioapatite composite scaffolds when cultured with Saos-2 cell line.

EDC/NHS

1-ethyl-3-(3-(dimethylaminopropyl) carbodiimide is a water-soluble carbodiimide able to react with carboxyl groups to form an active ester intermediate. This reaction is firstly used to couple carboxyl groups to primary amines. N-hydroxysuccinimide (NHS) is simultaneously used to increase the reaction efficiency, since it stabilizes the amine-reactive intermediate by converting it into an amine-reactive sulfo-NHS ester. It is called a 'zero-length' crosslinker once the amide linkages are formed without leaving any residual spacer molecule. This is a non-cytotoxic reaction as the remained products and by-products (isourea) can be easily removed with washing steps [41]. For this reason, and due to the high amino acid content of collagen, enriched with primary amines, EDC/NHS was selected to increase *Prionace glauca* skin collagen stability.

HMDI

Hexamethylene diisocyanate (HMDI) is an organic compound with isocyanate functional groups, that readily react with compounds containing active hydrogen atoms, like amines, alcohols, water, and carboxylic acids. Crosslinking of collagen-based biomaterials with HMDI mostly comprises the formation of stable urea groups resulting from the reaction of isocyanate groups with amine groups [42].

In addition, isocyanate groups can react with surface hydroxyl groups of hydroxyapatite resulting in urethane linkages [43]. Based on the proposed composite formulations (collagen-bioapatite particles) it was tested HMDI as crosslinking agent with dual effect, linking both collagen and bioapatite.

II-4.1.1.2 Marine collagen-bioapatite vs Bovine collagen-apatite composite scaffolds'

In Chapter IV, the core idea was to compare an entire marine-based material with a "commercial" (it was not used a commercial available material but, the source of collagen (bovine) and the source of apatite (synthetic) are the most found in the market) one. The best scaffolding condition (mColl:BAp, 30:70% (w:w) 12.5% EDC/NHS) resulting from **Chapter III** was reproduced with bovine collagen (bColl) and synthetic apatite (Ap), only a few optimizations were done.

For scaffolds production both origin collagens were solubilized at 1.5% (w/v) in a 0.5 M acetic acid solution. After that, marine BAp from teeth of *Isurus oxyrinchus* and *Prionace glauca* and commercial Ap from biotal were added to the mColl and bColl, respectively (30:70, collagen:apatite particles). To increase scaffolds stability, EDC at 12.5% (w:w) was added. Here, the crosslinking reaction was carried out for 4 h at 6 °C, the solutions were poured into a round shape mold and freeze-dried. Water washes were performed to remove any harmful compound before cell culture experiments.

Scaffold matrices with cylindrical shape (5 x 5 mm) were used for structural characterization and *in vivo* assessment in critical-size bone defects created in condyles of New Zealand rabbits.

II-4.1.2. Freeze-dry for cartilage

II-4.1.2.1 Marine collagen and marine collagen:hyaluronic acid scaffolds'

Freeze-dry is a highly versatile technique of porous scaffolding production [44]. After showing the success of freeze-drying technique for developing scaffolds for bone, it was applied the same methodology envisioning cartilage applications.

Collagen, chondrocytes, proteoglycans, and other residual proteins are the main constituents of the solid phase of cartilage. Each component holds a specific role to maintain cartilage healthy. While collagen fibrils form a dense and highly interconnected matrix with biological and mechanical functions. Glycosaminoglycans (GAGs) chains, like hyaluronic acid, are responsible to form proteoglycan aggregates which offer hydroscopic properties (absorb water) and contributes for the resilience of cartilage [45, 46].

In line with this, *Prionace glauca* collagen and hyaluronic acid were used to prepare porous structures for cartilage repair.

Prionace glauca collagen was solubilized in a 10 mM hydrochloric acid (HCl, Sigma-Aldrich, Portugal) solution at 1% (w/v) of concentration. Hyaluronic acid was solubilized at 0.5% (w/v) in distillated water and added to the collagen solution with a final concentration of 0.05% (ratio of collagen-to-hyaluronic acid, 1:20). To increase scaffolds stability 60 mM EDC crosslinking reaction was carried out (- 20 °C, 4 h). The cryogelation method was used to increase scaffolds porosity. To ensure scaffolds non-cytotoxicity, the formed gels were washed before freeze-drying.

The mail goal of this work was to test the potential of PG collagen to be used as 3D matrices in cartilage regeneration approaches when seeded with human adipose stem cells (hASC).

II-4.2. Rapid Prototyping

Conventional techniques of scaffolding production, including gas foaming, salt leaching and freeze-dry are still the golden standard in tissue engineering applications [35]. However, the lack of efficient solutions, demands the exploration of new therapeutic approaches. Rapid prototyping (RP) technology emerges as a promising alternative to build up 3D structures with more complex geometries. In contrast to the most conventional techniques of scaffolds production, RP allows the production of scaffolds with controllable porosity, well-defined microstructures and great producibility [47]. Controlling these parameters allow the production of scaffolds with improved mechanical and biological properties. In addition, RP, when combined with imaging techniques like computerized tomography (CT) scans, allows the creation of patient specific anatomical parts [48]. Based on the data collected in daily routine clinic examinations and computer-aided-manufacturing (CAM) programs, a 3D volume of the tissue can be rendered and then used in the production of a patient specific physical model through RP techniques.

RP involves different techniques like stereolithography (SLA), selective laser sintering (SLS), fused deposition modeling (FDM), and 3D plotting [49]. SLA uses the photo polymerization capacity of a polymer to convert its liquid state into a solid, when exposed to a ultraviolet light. In SLS, a laser beam is focused on a polymer powder and raises its temperature, causing the fusion of the particle. FDM uses a small temperature-controlled extruded material and deposit simultaneously polymer onto a platform and constructs a 3D structure through a layer-by-layer process. 3D Plotting, also called 3D extrusion-based systems, was described for the first time by Landers *et al*, is a system based on a dispenser solution that is forced to pass through a syringe onto a platform to generally form a hydrogel

[50]. 3D extrusion-based printing can be used with incorporated living cells (bioprinting), which provides an improved biomimetic cell/material rearrangement (**Figure II-8**) [47].

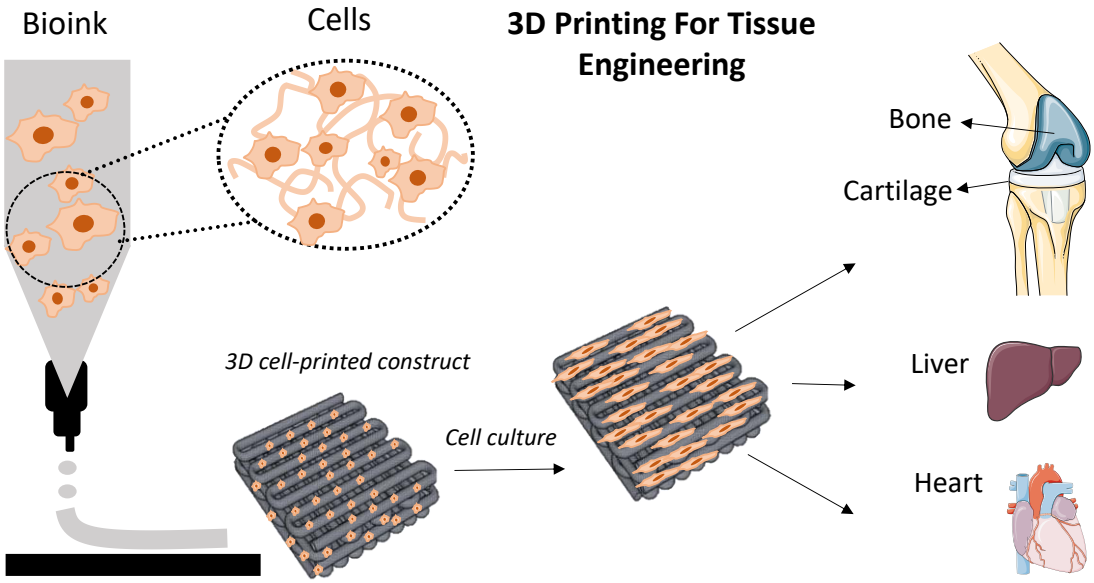

Figure II-8 - Schematic representation of 3D printing with incorporated living cells for Tissue Engineering.

Printing with living cells is very attractive but, also very challenging. The successful of the cell-laden inks relies on three main parameters: ***i)*** the unique physical and chemical properties of the material ***ii)*** the viscoelastic properties to allow printing and ***iii)*** the capability to ensure cell viability during printing and post-printing.

The selection of the fabrication technique depends on the material of interest, equipment limitations, and the specific requirements of the final scaffold.

In this thesis, 3D printing of *Prionace glauca* collagen with incorporated living cells was allowed in **Chapter VI** and **VII** by using a REGEMAT3D PRINTER dispensing system (**Figure II-9**) (Granada, Spain). The used materials in combination with the cells justifies the technique selection.

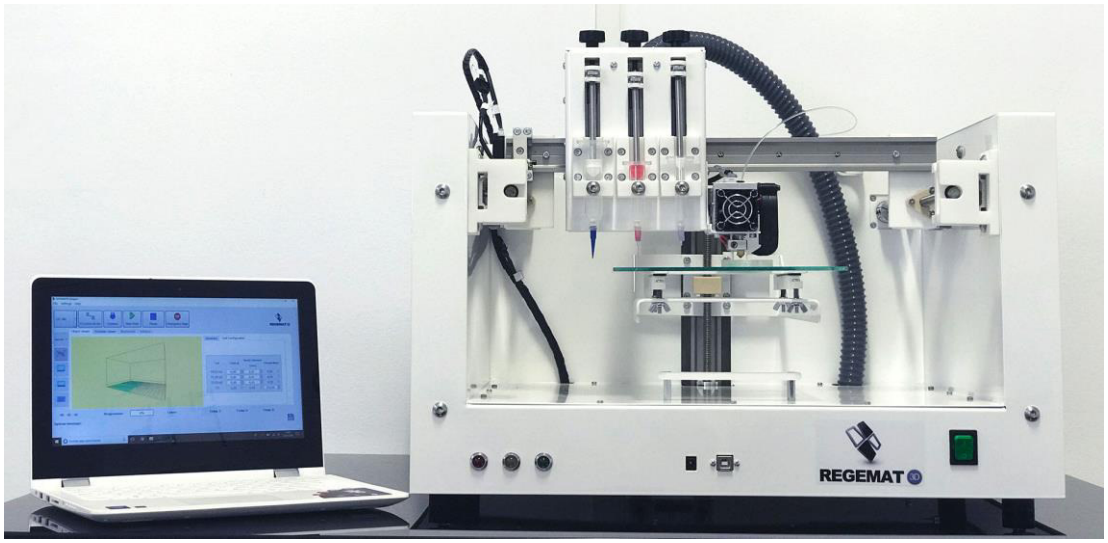

Figure II-9 - REGEMAT 3D Printer dispensing system.

II-4.2.1. Marine-based 3D printable hydrogels with incorporated L929 living cells – Optimization of inks properties

In **Chapter VI**, such methodology was for the first time used to manufacture 3D printable cell-laden hydrogels. The manufacturing process comprised the following four main steps:

Collagen mineralization: Blue shark collagen was solubilized at (20 $mg.mL^{-1}$) in 10 mM hydrochloric acid. To induce collagen mineralization. Calcium chloride ($CaCl_2$, VWR, Portugal) was added followed by neutralization with sodium hydroxide (NaOH, Enzymatic, SA, Portugal) at 15 mM. After that, $(NH_4)_2HPO_4$ was added as a phosphate supplier of the reaction considering a 1.67 calcium-to-phosphorous ratio. To promote hydroxyapatite formation, the process was carried out for 2 h at low temperatures (6 °C) under magnetic stirrer at controlled pH (8). All the process was maintained under sterile conditions.

Ink preparation: For inks preparation sodium alginate (Sigma-Aldrich, Portugal) solubilized in 0.9% (w:v) of a sodium chloride (NaCl, Mw:58.44 $g.mol^{-1}$, Laborspirit, Portugal) solution at 12% (w:v), was combined in different proportions with mineralized collagen (1:1, 1:2 and 1:3 of mineralized collagen:alginate (v:v), resulting in stable inks. This effect is related with the synergistic effect of calcium ions used in the process. On the one hand, they are important to induce the collagen mineralization, on the other, they are useful to ionically crosslink the collagen, making stable inks.

Cell-laden ink preparation: The different cell-laden inks were prepared by encapsulating $1.2x10^6$ cells.mL^{-1} of mouse fibroblast cell line (L929 from Thermo Fisher, Portugal). Briefly, 250 µL of culture medium containing the respective number of cells, were transferred by pipetting into the middle of each bioink blend, and manually carefully stirred to create an homogenous distribution of the cells.

3D printing: Each cartridge was filled with 2.5 mL of biomaterial/cells. The printing process was carried out at room temperature (25 °C) using sterile material. A printing nozzle of 410 µm of inner diameter, at a printing speed of 10 mms^{-1} was used to print the 3D mesh structures: 12 x 12 x 2.8 mm (width x length x height) with a total of 6 layers and a pore size of 1000 µm. To reinforce the structures stability, the 3D printed structures were ionically crosslinked during 3 min with a 10% (w/v) $CaCl_2$ solution dissolved in DMEM. After that, the hydrogels were maintained in cultutre conditions until use.

II-4.2.2. Marine-based 3D printable hydrogels with incorporated hASC – Optimization of cell densities and osteogenic differentiation studies

Taking in consideration the results obtained in **Chapter VI**, in **Chapter VII** it was applied the same methodology to produce 3D-printable hydrogels with incorporation of hASC at different cell densities aiming at the end to study its osteogenic potential.

Blue shark collagen was mineralized, as previously described, and combined with alginate to prepare the final ink. The cell-laden inks were prepared by encapsulating three different cell densities $2.5x10^6$, $5x10^6$, $7.5x10^6$ cells.mL^{-1} of human adipose stem cells (hASC). Briefly, 150 µL of culture medium containing the respective number of cells, were transferred by pipetting into the middle of each ink blend, and manually carefully stirred to create an homogenous distribution of the cells. For printing, each cartridge was filled with 2.5 mL of biomaterial/cells. Squares with 8 mm in length and 2 mm in height with 750 µm of pore size (considered as the distance between the parallel struts) were printed with 90 ° orientation at 10 mms^{-1} with a printing nozzle of 410 µm of inner diameter. The printing was carried out at 20 °C and the resulting 3D structures were maintained in culture medium at 37 °C and 5% CO_2 until characterization 21 Days.

II-5. CHARACTERIZATION TECHNIQUES OF THE DEVELOPED SCAFFOLDS

II-5.1. Physico-chemical characterization of scaffolds

II-5.1.1. Fourier transform infrared spectroscopy

Attenuated total reflectance–Fourier transform infrared (ATR–FTIR) spectroscopy is a powerful technique to measure infrared spectra of solids and liquid compounds [51].

Infrared spectroscopy is a method for the analysis of molecular vibrations. Analysis based on the absorption at different wavelengths of an infrared beam by a sample. When a frequency of light corresponds to a molecular vibration it is absorbed by the sample. The fraction of light transmitted by the sample compared with the light incident as a function of frequency gives the infrared spectrum of the sample. Fourier transformation algorithm allied to IR spectroscopy gives a spectrum of IR absorption per frequency/wavelength. The major advantages of this technique are: the high spectral resolution, signal-to-noise balance, and the reduced cost-effectiveness, since it measures a broad region of the spectrum in a short period of time [52]. Regarding that each compound has a specific IR spectrum and that similar chemical groups absorb in the IR at similar frequencies, FTIR analysis enables to identify the chemical structure of a compound and subsequent chemical modifications.

An IR Prestige-21 FTIR spectrometer (Shimadzu, Japan) with the attenuated total reflectance (ATR) technique was used in **Chapter IV** and **VI**, to identify different chemical structures. A transmittance spectrum was obtained by performing 32 scans in each spectrum over a range of 400-4000 cm^{-1} at a 2 cm^{-1} resolution by the KBr disk method.

FTIR was used in **Chapter IV** to study the chemical composition of both (marine and bovine) extracted collagens.

In **Chapter VI** it was used to study the efficiency of the method used to mineralize the collagen through the identification of phosphate bonds.

II-5.1.2. X-ray powder diffraction

X-ray diffraction (XRD) is a useful technique to distinguish a crystalline material from an amorphous one [53]. Crystalline materials are characterized by the long range orderly periodic arrangements of atoms. This atoms can diffract light and the wavelength of x-rays are similar to the distance between

atoms.The scattering of x-rays from atoms produces a diffraction pattern, which contains information about the atomic arrangement within the crystal. By measuring the intensity and angles of these signals, it is possible to know the crystallinity and arrangement of the atoms in the crystals. Amorphous materials do not have a periodic array with long-range order, so they do not produce a diffraction pattern.

In this thesis XRD analysis was carried out in **Chapter IV**, **VI** and **VII** to evaluate materials crystallinity and to determine the crystalline phases.

II-5.1.3. Inductively coupled plasma optical emission spectrometry (ICP-OES) and ion chromatography

ICP-OES comprises a light source unit, a spectrophotometer, a detector and a data processing unit [54]. When plasma energy is given to a sample, the atoms are excited. When the excited atoms return to low energy position, emission rays (spectrum rays) are released and the emission rays that correspond to the photon wavelength are measured. This technique is highly sensitive and promotes sequential analysis of multiple elements. The element type is determined based on the position of the photon rays, and the content of each element is determined based on the rays' intensity.

Ion chromatography (or ion-exchange chromatography) is a chromatography process that separates ions and polar molecules based on their affinity to the ion exchanger.

ICP-OES and Ion chromatography were used in **Chapter III** to evaluate the elementary composition of BAp particles and the presence of Fluorine. Four measurements per condition were taken and data are represented as mean value in weight percentage (wt.%) and with standard deviation.

II-5.1.4. Amino acid pattern

The amino acid composition is of particular interest to determine the biochemical composition of a compound [55]. Proteins like collagen have high aminoacid content, being one of the most important features to characterize collagen [1]. The amino acid composition develops a crucial role in collagen triple helix stability. Different sources and extraction methods results in different amino acid profiles. In general, marine origin collagen has low proline and hydroxyproline content when compared with mammalian origin collagens, which results in lower denaturation temperatures [5].

To characterize the extracted blue shark *Prionace glauca* and Bovine collagen, the amino acid pattern was analyzed in **Chapter IV** and **VI** by using a quantitative amino acid Biochrom 30 (Biochrom

Ltd, U.K) in Centro de Investigaciones Biológicas of the Spanish National Research Council (CSIC), in Madrid (Spain). Briefly, after all extraction and purification process the collagen was hydrolyzed and separated through a cation-exchange resin column accordingly to a procedure developed by Spackman, More and Stein in 1958. The column eluent was mixed with ninhydrin reagent to react with the aminoacids. The reaction formed colored compounds that were analyzed at two different wavelengths, 440 and 570 nm. Norleucine was used as an internal standard for the quantitative analysis. The results are the mean of three independent measurements.

II-5.1.5. Sodium dodecyl sulfate polyacrylamide (SDS-PAGE)

SDS-PAGE is a electrophoretic system commonly used as a method to separate proteins according to their MW, charge, size and shape. It is hopefully used to help identify and isolate protein molecules [56]. Separation of proteins by electrophoresis frequently uses a discontinuous polyacrylamide gel as a support medium and sodium dodecyl sulfate (SDS) to denature the proteins. SDS is an anionic detergent, that when binds the polypeptides chain confers negative charge within a wide pH range that is proportional to its relative molecular mass. The negative charges on SDS destroy most of the complex structure of proteins and are strongly attracted toward an anode (positively-charged electrode) in an electric field.

Polyacrylamide gels restrain larger molecules from migrating as fast as smaller molecules. Because the charge-to-mass ratio is nearly the same among SDS-denatured polypeptides, the final separation of proteins is dependent almost entirely on the differences in relative molecular mass of polypeptides. The greater the acrylamide percentage in the gel, the greater the frictional coefficient and slower the migration rate will be. If the proteins of interest are of a high molecular mass, and if the % gel is high, the proteins may not even enter the gel (due to overwhelming friction). Thus, it is essential to match the % gel to the mass of the proteins being separated.

To fully characterized and determine the type of collagen that were extracted, SDS-PAGE was performed in **Chapter VI and VII**.

SDS-PAGE (7% running gel and 4% of stacking gel) was prepared by using reagents from sigma and casted on a Biorad Mini Protean II System. Solubilized collagen was mixed with a buffer heated at 95°C for 5 min into a digital thermo block TD150P3 (FALC) until proteins denaturation. After that, 15 µL sample loading volume (10 µg per lane) was used. Also, 4 µL of protein marker was loaded with the samples. Electrophoresis was carried out at 75 V for 15 min followed by 150 V until the frontline

reached the lower part of the gel. After running, gel was stained with Coomassie blue R-250 in methanol (50%) and acetic acid (10%) for 30 min followed by destaining with methanol (5%) and acetic acid (7%).

In **Chapter IV** the polyacrylamide was performed at 7% in **Chapter VII** at 10%.

II-5.2. Morphology and microstructure characterization

II-5.2.1. Scanning electron microscopy

Scanning electron microscopy (SEM) is a image technique useful to characterized materials surface through the acquisition of 2D high-resolution images [57]. An incident beam of electrons focuses and scans the samples' surface by interacting with its atoms, resulting in a set of signals containing the collected information. This information is transmitted and detected by the SEM equipment and transformed into a 2D image. The successful of the technique is highly dependent on the sample preparation and constitution. Since the electron beam requires conductivity for scattering, SEM samples requires special preparation to increase their conductivity and to stabilize them. Thus, non-conductive samples are usually coated with a thin layer of conductive materials, such as gold, platinum or carbon.

SEM analysis was performed by using a Leica microscope (JSM-6010LV, JEOL, Japan) in **Chapters III**, **IV**, **VI** and **VII**. Prior to the analysis, samples were sputter coated with gold (Fisons Instruments, Sputter Coater SC502, United Kingdom) and the micrographs were taken at different magnifications.

In Chapter III, SEM analysis was used to qualitatively assess the crosslinking effects over the surface microarchitecture of the produced structures, complementing the micro-CT qualitative results. In addition, it was also used to evaluate the apatite formation onto the scaffolds after immersion in simulated body fluid (SBF).

In Chapter IV, low magnification images provided composites surface morphology, while high magnification images were useful to morphologically characterize the different Ap and BAp particles (synthetic and marine-based).

In Chapter VII, low magnification SEM images were useful to assess the microarchitecture of the 3D printed structures, including the printing accuracy. Higher magnifications provided detailed information about the surface morphology.

II-5.2.2. Transmission electron microscopy

Transmission electron microscopy (TEM) is a imaging technique that provides 2D high-resolution images [58]. While SEM provides information of sample's surface and composition, TEM uses the electrons which are passing through the sample (transmitted electrons) and gives information of the inner structure and composition of the sample. Finally, high magnification and resolution images are obtained.

A JEOL 2200F TEM (Tokyo, Japan) was used to assess the efficacy of collagen *in situ* mineralization, **Chapter VI** and **VII**. The mineralized collagen solution was deposited on TEM grids, ultrathin 6 carbon film on lacey carbon support film, 400 mesh, copper (IESMAT).

For images acquisition, the equipment was operated at an acceleration voltage of 200 kV. For images processing (Digital Micrograph 3.3.1., Gatan) was used. The lattice spacing were measured based on the histogram analysis obtained from the Inverse Fast Fourier Transform (IFFT) of the HR-TEM micrographs.

II-5.2.3. Coulter

Coulter technique is a versatile, robust, and accurate non-optical method for particle counting and sizing [59]. The technique uses electrical impedance to measure the volume of particles as they individually pass through an aperture of defined size. One of the major advantages of this system is that its response is not affected by particle color, shape, composition or refractive index, being thus a useful technique to characterize a wide variety of particles.

Particle size and distribution are important factors determining the structural properties and mechanical behaviors of scaffolds fabricated thereof. Particle size distribution of biological (from a mixture of mako and blue shark tooth) and synthetic (from biotal) apatite powders were measured using a particle size analyser (COULTER LS230, UK) with Fraunhofer optical mode in **Chapter IV**. This technique was used to complement the powders characterization.

II-5.2.4. Micro-Computed tomography

Micro-CT analysis is a powerful and non-invasive technique highly attractive to analyze the internal microarchitecture of scaffolds [57]. This technique uses a x-ray diffraction source and a stationary

detector. While scanning, the sample rotates, and the final result is a serie of 2D cross-sections that can be processed and reconstructed in 3D images. This technique gives detailed information regarding sample density and microstructure, including porosity, pore size and pore wall thickness. CTvox software provides qualitative information wherein CTan offers qualitative information.

The microstructure and architecture of the structures produced in **Chapters III, IV, V and VII**, namely the porosity, mean pore size, and interconnectivity, as well as 3-D reconstructions were assessed by micro-CT analysis. At least three samples of each formulation were scanned using a high-resolution SkyScan 1072, (Skyscan, Belgium) and SkyScan 1272 (Bruker, USA).

In **Chapter III**, composite scaffolds were scanned by using a Skyscan 1072 with a voltage range and current source between 32 - 40 kV and 220 - 248 uA, respectively. Quantitative parameters were measured by CT-Analyzer software (version 1.12.0.0) from 3D model reconstruction of a representative selection of slices and a designed region of interest. A threshold between 30 - 60 and 120 - 255 was applied for the differentiation of soft (mColl) and hard (BAp particles) materials, respectively. 3D images were finally obtained by CTvox software resulting in a color scale directly related to the chosen threshold according to the material density/hardness.

In **Chapter IV**, micro-CT SkyScan 1272, an advanced edition of 1072, was used for two purposes, to study de microarchitecture of the produced composite scaffolds and to evaluated bone regeneration after scaffolds implantation.

For assessment of scaffolds microarchitecture, dried samples were scanned using a pixel size of 10 μm over a rotation angle of 360º. Porosity, mean pore size and interconnectivity were assessed after reconstruction of images stacks in a CTanalyzer program by defining a threshold from 30 - 255, to distinguish the composite structure from the pore voids. To understand if the Ap and BAp particles were homogenously distributed through the constructs it was applied a threshold from 65 - 255.

To evaluate the *in vivo* regeneration of the bone defects created in the rabbit femoral condyles, all samples were micro-CT scanned using the Skyscan micro-CT 1272. Fixed samples were scanned with an aluminum/copper filter at 13 μm pixel size resolution with an x-ray source voltage of 90 kV and current source of 111 μA, 0.4 rotation steps and 2 averaging frames during 0h:56m:36s of scanning. The micro-CT images were reconstructed with a NRecon program version 1.1.3 (Skyscan) and the reconstructed images were reoriented with a Dataviewer program version 1.17.0.0 (Skyscan) for subsequent analysis. To qualitatively assess the percentage of bone volume (new bone plus scaffold) it was applied a cylindrical region of interest (ROI) corresponding to the bone defect size filled with the different structures. Phantoms of 0.25 and 0.75 $g.cm^{-3}$ were scanned and reconstructed with the same

parameters for bone mineral density (BMD) calibration. All analysis was performed by trained staff who did not know what material was being analyzed.

In **Chapter V,** micro-CT analysis was used to evaluate the microarchitecture of the dried collagen-based networks produced by cryogelation followed by freeze-drying. Samples were scanned using a pixel size of 5 μm over a rotation angle of 360º, with a rotation step of 0.4º. Representative data sets of 300 slices were transformed into binary images using a dynamic threshold between 25 - 255 (grey values) to distinguish the polymeric material from pore voids. Such data were used to assess the morphometric analysis, namely structures porosity, pore size, trabecular thickness and pores interconnectivity (CT Analyser). 3D virtual models of representative regions in the bulk of the materials were created using an image processing CTvox software.

In **Chapter VII**, micro-CT it was specifically used to study the filaments microarchitecture of the 3D printed hydrogels. The samples were lyophilized and scanned using a SkyScan 1272, with a pixel size of 8 μm, voltage range of 50 kV and current source of 200 μA. Approximately 250 projections were acquired over a rotation angle of 360°, with a rotation step of 0.3°. Data sets were reconstructed using a standardized cone-beam reconstruction NRecon software. Representative data set of the slices was segmented into binary images with a dynamic threshold between 30 – 255. After that, the binary images were used for morphometric analysis and to build the 3-D models. Quantitative information of total porosity (%), pore size (μm), pore distribution (%) and interconnectivity (%) was assessed for the hydrogels' filaments.

II-5.3. Mechanical assays

3D porous matrices should act as temporary templates, allowing cell adhesion and proliferation, and providing mechanical support until new bone tissue formation [60]. *In vivo*, the scaffolds are subjected to a compressive forces thus, an ideal 3D structure should stand the hydrostatic pressures and, at same time, maintain the spaces needed for cell growth and new matrix formation [61].

Since native tissues present characteristic stiffness, when addressing an *in vitro* tissue model, it is important to understand the mechanical behavior of the produced constructs to select the best scaffold for the desire application.

To assess the mechanical behavior of the different composite scaffolds, uniaxial compression tests were carried out to measure materials deformation under compressive forces.

In **Chapters III** and **IV**, compressive tests were performed by using an Instron 5540 Universal

Machine (Instron Corporation, USA). This equipment is useful to perform tensile, compression, bend, peel, tear, and other mechanical tests on materials. The selected test depends on the application, in this thesis five replicates of each condition were tested with a crosshead speed of 2mm /min and a load cell of 1 kN under compression mode until 60% of compression. The elastic modulus was defined by the slope of the initial linear section of the stress–strain curve.

II-5.4. Rheology assays

Rheometry is an experimental technique used to determine the rheological properties of materials [62]. A vast number of rheometric tests can be performed to determine flow and viscoelastic properties of a material. This technique offers information about materials elasticity, viscosity and plastic behavior over the strain, frequency, time, or temperature. It can be a useful tool to evaluate materials properties in a wide range of applications, being particularly interesting when speaking about 3D printing with incorporated living cells. High-performance-bioinks should retain adequate rheological properties to allow ink flow, maintain shape fidelity during printing and, at same time, granting cell survival [63].

In this thesis, rheometry assays were performed by using a Kinexus pro+rheometer (Malvern Instruments, UK), with a specific acquisition software rSpace (Malvern Instruments, UK) for two different purposes.

In Chapter V, it was used to determine the viscoelastic properties of the produced scaffolds when hydrated. Oscillatory assays that involve the use of two plates (a stationary plate and an oscillatory plate), and a material set between the plates, in which a sinusoidal shear deformation was applied, and the resultant stress response was measured. The shear strain was achieved through frequency sweep curves, after LVER (linear viscoelastic region) determination. Then, frequency sweep curves were obtained from 0.1 Hz to 10 Hz of frequency, at a shear strain of 0.1% at 37 °C. All these experiments were repeated at least 3 times.

In Chapter VI and **VII**, this technique was used to determine inks printability.

In **Chapter VI**, the apparent viscosity was measured in viscometry mode using a cone and plate sensor system (4° / 40 mm). The viscoelastic properties were assessed with plate and plate sensor, with 1 mm gap size. In the oscillatory mode a solvent trap was used to prevent water evaporation from the samples during the tests and the temperature was maintained at 37 °C throughout the measurement period. The shear rate was swept from 0.01 to 10 and 0.01 to 100 s-2 to determine the

elastic modulus (G´) and viscosity, respectively, with records taken every 10 points per frequency sweep range.

In **Chapter VII**, rheology was used to study how temperature affects collagen rheological properties and also to study the influence of the mineralization process in the theological properties. For that, oscillatory temperature sweep experiments were carried out. The complex viscosity (n*), storage (G'), and tangent delta (tan δ = G''/G') were obtained by using a measuring system composed by an upper staineless steel parallel plate of 8 mm diameter (PU20 SR1740SS), with 1 mm gap size. A temperature sweep ranging between 4 °C and 45 °C with a ramping rate of 2 °C min^{-1} (1% strain and frequency = 1 Hz) was conducted within the range of the Linear Viscoelastic Region (LVER) previously determined. To study the final ink printability, the shear rate was swept from 0.01 to 100s^{-2} with the recordings taken every 10 points per frequency sweep range.

II-5.5. *In vitro* tests

II-5.5.1. Bioactivity assay with simulated body fluid

To *In vitro* assess the bioactive nature of the marine-collagen based composite scaffolds, simulated body fluid (SBF) bioactivity assay was carried out.

According to the pioneering definition of Hench *et al.,* "a bioactive material is one that elicits a specific biological response at the interface of the material which results in the formation of a bond between the tissues and the material" [64]. Biomaterial-host tissue interface plays a critical role in the therapeutic outcomes. Different origin materials can induce different responses. In general, calcium phosphates-based materials are highly bioactive due to their intrinsic osteoconductive properties and chemical/crystallographic resemblance with mineral phase of skeletal tissue.

In this thesis, SBF bioactivity assay was used in **Chapter III** to study the bioactive nature of the prepared composite scaffolds. For that, the 3D composite scaffolds were immersed in a simulated body fluid (SBF) solution, this solution has ion concentrations nearly equal to those of human blood plasma (Na^+ 142.0, K^+ 5.0, Mg^{2+} 1.5, Ca^{2+} 2.5, Cl^- 103.0, HCO^{3-} 27, HPO_4^{2-} 1.0 and SO_4^{2-} 0.5 mM) [65]. To better mimic the physiological conditions, the experiment was carried out at 37 °C and pH 7.4, for 14 days. The volume of SBF varied with scaffolds surface area. After each culture period (1,3,7 and 14), the samples were removed from the solution and washed with distilled water to avoid formation of salts during the drying process. To evaluate the apatite formation, samples before and after soaking in SBF

were coated with gold and analysed by scanning electron microscopy (SEM) (JSM-6010LV, JEOL, Japan) with an acceleration voltage of 15 kV at different magnifications.

SBF, is well accepted for the Technical Committee ISO/TC150 of International Organization for Standardization as a suitable approach for *in vitro* assess the apatite-forming ability of materials [66].

II-5.5.2. Biological tests

3D structures were biologically tested, *in vitro*, for their innocuity, safety, and efficacy. Biocompatibility tests are considered a prerequisite before undertaking *in vivo* performance. The main goal of doing *in vitro* assays is to determine the biocompatibility response of the different biomaterials. As a first screening, cytotoxicity assays are commonly used to evaluate the living cells reaction with the materials. It is not possible to change de the humans' body physiology but, it is yet possible to modulate materials properties to achieve an appropriate host response. Thus, the *in vivo* assays relies on the *in vitro* response, it does not make sense to follow with *in vivo* assays in case of cytotoxic materials [67].

The major advantages of using *in vitro* assays are the reduced costs, time, and the automation. However, they cannot replace animal tests.

In this thesis*, in vitro* studies were performed by using three different cell types, Saos-2 in **Chapter III**, L929 in **VI** and hASC in **Chapter V** and **VII**.

II-5.5.3. Cell sources

Immortalized cell lines are commonly used for cytotoxicity screening assays. According to the International Organization for Standardization, for cytotoxicity assays it is recommended the use of immortalized cells over primary cells. In contrast to primary cells, they exhibit less batch-to-batch variability, which results in more reproducible and accurate assays. Moreover, they are more robust, proliferates faster, and have much less nutritional requirements compared to primary explanted cells obtained from living tissues [68]. In this thesis, Saos-2 and L929 cell line were used in **Chapter III** and **V**.

II-5.5.3.1 Saos-2

Saos-2 is a cell line derived from the primary osteosarcoma. Saos-2 cell line possess several osteoblastic features, they have the ability to deposit mineralized extracellular matrix, which makes these cells a valuable model for studying events associated with osteoblastic differentiation [69].

For culture, Saos-2 cells were expanded in Dulbecco's modified Eagle's medium (DMEM) supplemented with 10% fetal bovine serum (ALFAGENE) and a 1% antibiotic–antimycotic (ALFAGENE) mixture.

Saos-2 cells were incubated in 5% CO_2 at 37 °C, and the medium changed every 2 - 3 days. Cells were routinely trypsinized (0.25% trypsin–EDTA solution; Life Technologies, USA), centrifuged at 300 g for 5 min (Eppendorf 5810R centrifuge equipped with an A-4-62 rotor), and re-suspended at a density of 5 x 10^5 cells in T150 cell culture flasks (BD Biosciences, Enzifarma, Porto, Portugal).

Saos-2 cells were used in **Chapter III** aiming to evaluate the potential cytotoxicity effect of the produced collagen:bioapatite composite scaffolds.

II-5.5.3.2 L929

L929 cell line from mouse connective tissue (purchased from ECACC, UK) were cultured in low Dulbecco's modified Eagle's medium (DMEM) supplemented with 10% fetal bovine serum (ALFAGENE) and a 1% antibiotic–antimycotic (ALFAGENE) mixture.

The L929 cells were incubated in 5% CO_2 at 37 °C, and the medium changed every 2 - 3 days. Cells were routinely tripsinized (0.25% trypsin–EDTA solution; Life Technologies, Carlsbad, CA, USA), centrifuged at 300 g for 5 minutes (Eppendorf 5810R centrifuge equipped with an A-4-62 rotor), and re-suspended at a density of 5 x 10^5 cells in T150 cell culture flasks (BD Biosciences, Enzifarma, Porto, Portugal).

These cells were used in **Chapter V** to evaluate cell viability within the different developed ink blends.

II-5.5.3.3 Human adipose stem cells (hASC)

The use of mesenchymal stem cells, particularly hASCs, are of special interest in musculoskeletal disorders due to its limited autoimmune response, potential cell expansion ex vivo, high capability to differentiate into several mesodermal cell lineages, and additional effects of therapeutic interest such as secretion of neurotrophic factors and anti-inflammatory properties [70].

Human adipose stem cells were isolated from the human adipose tissue with patient agreement following a very well optimized protocol approved by the Ethics Committee of University of Minho [71].

The isolation protocol was divided in four main steps:

i) collection of human adipose tissue by liposuction aspiration and washed in phosphate buffered saline (PBS) with 1% antibiotic ***ii)*** enzymatic digestion with 0.05% (w/v) of collagenase type II (Sigma, USA) under agitation for 45 min at 37°C ***iii)*** the resulting stromal vascular fraction (SVF) pellet (with hASC and other cells), obtained after filtration and centrifugation (800 g, 10 min, 4 °C) was re-suspended in red blood cell lysis buffer (155 mM of ammonium chloride, 12 mM of potassium bicarbonate and 0.1 mM of ethylenediaminetetraacetic acid, all from Sigma-Aldrich, Portugal) for 10 min at RT, ***iv***) after centrifugation (300 g, 5 min, RT), the supernatant was discarded and the cell pellet re-suspended and cultured in MEM alpha medium (α-MEM; GibcoR, Life Technologies, Carlsbad, CA, USA), supplemented with 2.2 g/L of sodium bicarbonate, 10% (v/v) of FBS and 1% (v/v) of antibiotic/antimycotic solution (complete **α**-MEM medium) and maintained at 37 °C in an incubator with 5% CO_2 atmosphere. Human ASCs were selected by plastic adherence and harvested (P0) 7 days after isolation at 90% confluence. The phenotype of hASCs has been extensively characterized using tissue samples obtained from the same anatomic region (abdominal subcutaneous adipose tissue), collected using similar techniques and isolated following the same procedure.

For cell culture, cells were maintained in culture conditions and routinely tripsinized until further use.

The isolated cells were used in this thesis in **Chapter V** and **IV** for chondrogenesis and osteogenesis differentiation.

II-5.5.4. Cryopreservation

For cryopreservation was used a Statebourne Biosystem 24 cryogenic tank (Statebourne Cryogenics Ltd., UK). Briefly, cell suspensions of 1×10^6 cells.mL^{-1} were prepared in a cryopreservation solution, consisting of 10% (v/v) Dimethyl sulfoxide - DMSO (VWR, USA) in FBS, and transferred into 1.5 mL cryovials (VWR, USA). Then, cell suspensions were gently cooled down, first at -20 °C for at least 2 h and then moved to -80 °C freezer for a minimum period of 12 h. The cryovials were subsequently stored at -176 °C in the gas nitrogen phase of the cryogenic tank.

II-5.5.5. Culture conditions

II-5.5.5.1 Cell-seeded approaches

In **Chapter III** and **V**, the cytocompatibility of the produced composites in contact with the different cell types was evaluated to guarantee that the processing method of scaffolding fabrication did not result in any harmful residual compound.

In **Chapter III**, Saos-2 cells were expanded in DMEM supplemented with 10% fetal bovine serum (ALFAGENE) and a 1% antibiotic–antimycotic (ALFAGENE) mixture. After achieving a confluent state, cells were seeded on top of the different mColl:BAp combinations in 48-well plates at a density of $2.5x10^4$ cells per scaffold. To assess scaffolds' cytotoxicity, metabolic activity at 1 and 3 days after seeding was determined using a 3-(4,5-dimethylthiazol-2-yl)-5-(3 carboxymethoxyphenyl) 2-(4-sulphofenyl)-2*H*-tetrazolium, inner salt (MTS) (VWR) assay. The results are the mean of three independent experiments (n=3) with three replicates for each condition and per experiment.

In **Chapter V**, hASC at $2x10^{*6}$ cell density were seeded by using a top down approach with 50 µL of droplet. After 1 hour a final volume of 500 µL was completed with α-MEM culture media supplemented with 2.2 g/L of sodium bicarbonate, 10% (v/v) of FBS and 1% (v/v) of antibiotic/antimycotic solution (basal conditions) and maintained at 37 ºC in an incubator with 5% CO_2 atmosphere. To assess scaffolds' cytotoxicity, cell seeded onto the scaffolds' were maintained in basal conditions at 37 ºC in an incubator with 5% CO_2 atmosphere. Metabolic activity at 1, 2 and 3 days after seeding was determined using a MTS assay. The results are the mean of three independent experiments (n=3) with three replicates for each condition and per experiment.

To study the potential of the structures to promote chondrogenesis, hASC at $2x10^{-6}$ cell density were seeded by using the same methodology, the cell seeded scaffolds were cultured in basal and chondrogenic conditions. The basal conditions were maintained with the same medium used for hASC cells expansion, as aforementioned. Chondrogenic conditions were treated with a supplemented α-MEM with Insulin-Transferrin-Selenium-G Supplement (ITS; Invitrogen), 1 mM dexamethasone (Sigma-Aldrich), 0.1 M sodium pyruvate (Invitrogen), 0.17 mM ascorbic acid-2-phosphate (Wako Pure Chemical Industries, Ltd.), 0.35 mM L-proline (Sigma-Aldrich) and 10 ng ml-1 TGF-3, without FBS. To study the differentiation state of the cells, real-time PCR was carried out 7, 14 and 21 days after cell seeding in both scaffold formulations maintained under basal and chondrogenic conditions. Complementary, the immunodetection of SOX-9 and ACAN in the 3D constructs was evaluated 21 days after cell seeding.

II-5.5.5.2 Cell-laden approaches

After assessing the potential of the marine-collagen to support seeded cells it was aimed in **Chapter VI** and **VII** to test its potential with incorporated living cells.

In **Chapter VI**, L929 cell-line were incorporated in the different developed ink blends (**section II-3.4.1.1**). For cells encapsulation, 250 µL of DMEM low glucose, supplemented with 10% fetal bovine serum (ALFAGENE, Carcavelos, Lisbon) and 1% Penicillin/Streptomycin (ALFAGENE, Carcavelos, Lisbon) containing $1.2x10^{6}$ cells/mL^{-1}, was transferred by pipetting into the middle of each ink blend, and manually carefully stirred to create an homogenous distribution of the cells. Cell viability within the printed constructs was quantitatively evaluated by DNA and MTS assays and qualitatively evaluated by live/dead viability assay 1 and 7 days after printing.

In **Chapter VII**, hASC were encapsulated in the prepared collagen-based ink blends (**section II-3.4.1.2**) at different cell density 2.5, 5 and $7.5x10^{6}$ cells.mL^{-1}. For cells encapsulation, 150 µL of culture medium containing the respective number of cells, were transferred by pipetting into the middle of each syringe, and carefully stirred to create an homogenous distribution of the cells.

To assess cell viability during printing, live/dead assay was performed. For quantification, the images were processed in the ImajeJ software by selecting an appropriated threshold encoding the green (live cells) and red (dead cells) colors. To assess cell viability in a long-term, live/deda assay and cell metabolic activity was determined at 1,7 and 14 days. The best condition was selected to evaluate the potential of the 3D printable hydrogels to induce osteogenic differentiation, for that immunodetection of bone-related proteins (RUNX2 and osteopontin) was assessed.

II-5.5.6. Biological activity - quantitative assessment

II-5.5.6.1 MTS assay

3-(4,5-dimethylthiazol-2-yl)-5-(3 carboxymethoxyphenyl) 2-(4-sulphofenyl)-2*H*-tetrazolium, inner salt (MTS) (VWR) assay quantifies cell metabolic by the reduction of tetrazolium salt reagent (yellow color) to formazan (brown color) after a period of 3 - 4 h of incubation at 37 °C in controlled atmosphere. Absorbance intensity, which is directly proportional to the metabolic activity, was measured at 492 nm using a microplate reader (SYNERGY HT, BIO-TEK). The results are the mean of three independent experiments (n=3) with 3 replicates for each condition and per experiment. Since MTS is a colorimetric assay that quantifies cell metabolic activity by using the reducing power of living cells, the color intensity reflects the number of viable cells, as dying cells lose the capacity to reduce MTS. MTS assay combines all features of a good measurement system, is user-friendly, fast, sensitive, precise, and specific to determine cytotoxicity [72].

In **Chapter III, IV**, **V** and **VII** the CellTiter 96 AQueous One Solution cell proliferation assay (Promega, USA) was performed according to the instructions of the manufacturer. At the defined time points, cells were washed twice with sterile PBS solution, and 500 µL of a mixture of culture medium (without FBS and phenol red) and MTS reagent (5:1 ratio) was added to each well. The culture plates were kept in the dark, at 37 °C in the CO_2 incubator for 3 h. The absorbance of the MTS reaction was read in a microplate reader (Synergy HT, BioTek, USA) using 100 µL supernatant per well, at 490 nm.

II-5.5.6.2 DNA quantification

DNA quantification is a useful method to evaluate cell proliferation by quantifying the total amount of double stranded DNA (dsDNA) of the samples [73]. DNA content can be determined by several fluorescence methods. Pico-Green® dsDNA quantification assay allows the accurately measure of DNA by detecting selectively as little as 25 pg.mL^{-1} of dsDNA in the presence of single-stranded DNA, RNA and free nucleotides. In contrary to other methods, contaminants do not interfere with the results. In this assay, the addition of the PicoGreen® fluorescent marker to the samples enables the emission of fluorescence through its specifically binding to the dsDNA. DNA content is further determined through a DNA standard curve, prepared using standard dsDNA solutions with concentrations ranging from 0 to 2 µg.mL^{-1}.

In this thesis, DNA quantification was performed in **Chapters V and VI,** the Quant-iT™, PicoGreen® dsDNA Assay Kit (Invitrogen, Molecular Probes, USA) was used according to the manufacturer instructions. At the defined time points, samples were collected and washed with PBS. After that, 1 mL of ultrapure water was added to each well material and maintained at 37 °C per 1 h and further kept at –80 °C. For analysis, the samples were thawed at RT and to complete the lysis of cell membrane all samples were sonicated for 15 min in a cold-water bath to avoid DNA degradation. Then, 28.7 μL of sample or standard were added to a 96-well opaque plate, mixed with 100 μL of 1X Tris-EDTA (TE) buffer and 71.3 μL of 1X Quant-iT™ PicoGreen® reagent, in a total volume of 200 μL. The plate was incubated at RT for 10 min, fluorescence was measured using an excitation/emission wavelength of 485/528 nm, respectively, in a microplate reader (Synergy HT, BioTek Instruments, USA). The quantification of DNA was calculated based on a standard curve for DNA prepared by using DNA standards between 0 and 2 μg/ml. The results are the mean of three independent experiments (n=3) with 3 replicates for each condition and per experiment.

Particularly, in **Chapter V**, prior to start DNA quantification all scaffolds' samples were digested with collagenase (Sigma, Lisbon, Portugal) at 0.05 % (w/v) concentration to ensure the complete removal of DNA from the collagen matrix.

II-5.5.6.3 Gene expression - RNA isolation and first-strand cDNA synthesis

Sample storage and treatment are highly important to define a reliable protocol for analysis of sample quality and quantity. RNA quantity is largely determined by the yield of rRNA, whereas the RNA quality is determined by the purity and the degradation status of the RNA molecules [74]. However, there is a significant connection between the two factors once it is difficult to assess the quality of a sample with a low quantity of RNA. So, the parameters that affects RNA quality may interfere with the quantification process. The expression of mRNA for specific chondrogenic-related genes, was measured by real-time PCR technique in **Chapter V**.

For mRNA extraction, the cell seeded scaffolds were washed with PBS, digested with 50 μL of collagenase at 0.05 % (w/v) to ensure cell removal from the interior of the scaffolds and immersed in 800 μL of TRI reagent® (Laborspirit, Portugal), being then stored at -80 °C until further use. After that, samples were thawed at RT, completed with 160 μL of Chloroform (VWR, Portugal), mixed and kept in ice for 15 min. Then, all samples were centrifuged at 13000 rpm, for 15 min, at 4 °C and the resultant supernatant was completed with an equivalent volume of isopropanol (overnight at -20 °C) to

precipitate the RNA. After a new step of centrifugation, a pellet was obtained that was solubilized in 70% of ethanol, centrifuged again and resuspended in RNase-free water. The RNA concentration was evaluated using micro-spectrophotometry (NanoDrop1000, Thermo Scientific; USA).

Prior to quantification of a target transcript, it is necessary to convert RNA to cDNA for that, RNA was reversed-transcribed into cDNA according to the protocol from qScript cDNA Synthesis Kit (Quanta BioSciences; VWR, USA).

II-5.5.6.4 Gene expression - Real-time polymerase chain reaction (Real-time PCR)

Real time polymerase chain reaction (PCR) was used in **Chapters V**, as technique for detecting and measuring PCR products of interest [73].

The obtained cDNA was used as a template for the amplification of the target genes shown in **Table 1**, according to manufacturer's instructions of the PerfeCtaTM SYBR® Green system (Quanta Biosciences, VWR, USA) in a Mastercycler® ep Gradient S Realplex® thermocycler (Eppendorf; Hamburg, Germany). The following cycler conditions were used: 2 min at 95 °C and 45 cycles of 15 s at 95 °C, 30 s at Tm (°C) (melting temperature depending on the gene; Table II-1) and 30 s at 72 °C. Fluorescence was measured at the end of each amplification cycle. β2-microglobulin (hB2M) was used as reference gene and normalization was performed according to the Livak method, with the day 1 of the experiment (negative control) serving as a calibrator.

Table II-1 - *SOX-9 - SRY-box transcription factor 9; ACAN- Aggrecan; Col2A1- Collagen type II; COMP - Cartilage oligomeric matrix protein; hB2M - β2-microglobulin.

Genes	Primer	Sequence (5'-3')	Tm (°C)	
SOX9	Forward	TTC ATG AAG ATG ACC GAC GC	55,2	NM_000346.4
	Reverse	GTC CAG TCG TAG CCC TTG AG	57,3	
ACAN	Forward	TGA GTC CTC AAG CCT CCT GT	57,9	XM_011521314.1
	Reverse	TGG TCT GCA GCA GTT GAT TC	55,5	
Col2A1	Forward	GAGCAGGAATTCGGTGTGGA	55,2	NM_001844.5
	Reverse	GCCATTCAGTGCAGAGTCCT	58,0	
COMP	Forward	TCT GCA TCA AAG TCG TCC TG	54,9	NM_000095.3
	Reverse	AGG GAT GGA GAC GGA CAT CAG	58,4	
hB2MM	Forward	TGG AGG CTA TCC AGC GTA CT	57,7	NM_004048.3
	Reverse	CGG ATG GAT GAA ACC CAG ACA	57,1	

II-5.5.7. Biological activity - qualitative assessment

II-5.5.7.1 Live/dead cell viability assay

Calcein-AM (AM)/Propidium iodide (PI) staining is a qualitative live/dead assay for the visualization of live and death cells. Live cells have intracellular esterase activity, responsible by the enzymatic conversion of the non-fluorescent calcein acetoxymethyl to the intensely fluorescent calcein through the removal of the acetomethoxy group. PI shows enhanced fluorescence when binding with high affinity to DNA. Contrary to calcein-AM, PI does not permeant the cellular membrane, it binds to the cytoplasmic DNA when the cellular membrane of dead cells is disrupted.

Live/Dead assay was performed in **Chapter III** to study Saos-2 cell line distribution and viability in the different materials formulations. Composite scaffolds were incubated with AM (1:300) and PI (1:1200) solution in culture medium for 30 min in the dark at 37 °C and 5 % CO_2.

In **Chapter V**, AM (1:500) and PI (1:1000) were incubated 10 min in the dark (37°C, 5% CO_2) to study L929 cells adhesion and distribution.

In **Chapter VI** and **Chapter VII**, to qualitatively assess L929 cells and hASC viability during and after printing, respectively, live/dead assay was carried out. Live cells were stained with AM (1:500) and PI (1:1000). The reagents concentration and exposure time was dependent on the sample.

Fluorescence microscopy is a imaging technique that provides high resolution 2D or 3D images by projecting light at a specific wavelength into a desired sample that is absorbed by the fluorophore and again reflected at different wavelengths. Unlike traditional optical microscopy, the application of an array of fluorochromes enables the identification of cells and cellular components with a high degree of specificity. Using multiple fluorescence labeling, different molecules can be simultaneously identified. Due to its attributes, fluorescence microscopy has been considered an important tool in the biomedical field, for cell analysis.

Confocal microscopy has a number of significant advantages over conventional fluorescence microscopy, including increased effective resolution, improved signal-to-noise ratio, depth perception in z-sectioned image, reduced blurring of the image from light scattering and electronic magnification adjustment [75]. However, the sample penetration depth is limited.

For images acquisition, Zeiss Axio Imager Z1m (Germany) fluorescence microscope and Leica SP8 Inverted Confocal Microscope. The equipment used for each specific analysis was selected according to the materials to be analyzed.

II-5.5.7.2 Dapi/Phalloidin for nucleus and cytoskeleton evaluation

Phalloidin is a bicyclic peptide that, when conjugated to fluorescent dyes, binds to actin filament in fixed and permeabilized cells. Cell cytoskeleton has functions in organelle transport, cell division, motility, and signaling, developing thus a crucial role in cell healthy. Cytoskeleton stains provide important information about cytoskeleton dynamics, namely orientation and colonization.

DAPI (4′,6-diamidino-2-phenylindole) is a blue-fluorescent stain (excited at 405 nm) with high affinity for DNA, being frequently used as a nuclear counterstain.

Dapi/phalloidin stanning's were used in **Chapter VI** and **VII** to determine the number of nuclei and to assess the effect of 3D printing onto the cells. Samples were fixed with paraformaldehyde solution and kept at 4 °C. For permeabilization, Triton X-100 (0.2%) was added for 5 min and DAPI

(1:1000)/Ph (1:100) were used for nuclei and cytoplasm staining, respectively, for 20 min. After that, the images were acquired by using a laser scanning confocal microscopy imaging system (TCS SP8, Leica, Wetzlar, Germany) using an excitation wavelength of 405 nm for DAPI, and 561 nm for Ph. Control samples stained with only DAPI and Ph were analyzed. The images were taken using a 20 X immersion objective.

II-5.5.7.3 Histology

Histological analyses is the gold standard for tissue examination, either for research and medical diagnosis [76]. The process of histological staining takes five key stages: fixation, processing, embedding, sectioning and staining. Different staining's are used to identify specific structures, cells and tissues [77].

Samples were collected at the end of each cell culture time-point, washed with PBS and fixed with 10 % (v/v) formalin solution followed by dehydration in a graded series of ethanol baths and embedding in paraffin. After that, the constructs were serially sectioned (4 µm longitudinal sections) using a microtome (Spencer 820, American Optical Company, USA). As last step, sections were washed in distilled water, dehydrated and mounted in Entelan (Millipore, USA), unless otherwise stated. Slides were observed under transmitted microscopy, using the transmitted and reflected light microscope. Images were acquired using the Zen microscope processing software, connected to the digital camera AxioCam MRc5.

Histological tissue sections were evaluated in **Chapter V** with two purposes: for different histological staining's and for immunofluorescence analysis.

II-5.5.7.4 Hematoxylin & Eosin

Hematoxylin & Eosin (H&E) staining is widely employed in the histology field to stain tissues. In medical diagnosis and biomedical research it is a powerful technique to allows the visualization of different cell components [78]. Hematoxylin is a natural basic dye that preferentially stains the acidic components (basophilic cell components), such as nucleic acids in the nucleus. Eosin is a synthetic acidic dye that stains basic components of cells with a pink color, including the cytoplasm or connective tissue.

In this thesis, in **Chapter V**, representative sections of collagen and collagen:hyaluronic acid constructs were stained with Hematoxylin & Eosin from Thermo Scientific (Waltham, USA) following a protocol already stablished.

Since the slices were sectioned longitudinally, this technique provided information about cell distribution inside the constructs, that cannot be achieved with other superficial techniques of analysis.

II-5.5.7.5 Alcian Blue

Alcian Blue staining is primarily used to stain acid mucopolysaccharides. It is a positively charged, very large, molecule that binds to the negatively charged low density mucin found in biological tissues [79].

In this thesis, this staining was used in **Chapter V** to detect the presence of glycosaminoglycans, typically characteristic of cartilage extracellular matrix. For that representative sections of collagen and collagen:hyaluronic acid constructs were stained with Alcian Blue 8GX (1% v/v in 0.5 mol.L^{-1} acetic acid glacial; VWR BDH Prolabo, Briare, France), following a standard protocol.

II-5.5.7.6 Masson's trichrome

Masson's trichrome is generally used as a three-color based staining protocol that selectively colors different molecules.

In this thesis, masson's trichrome was employed in **Chapter V** using a Bio-Optica staining kit (Milan, Italy) according to the manufacturer's instructions. In this kit, weigert's iron hematoxylin stains the nuclei (black), a mixture of Biebrich Scarlet with Acid Fuchsin stains the cytoplasm (red) and aniline blue stains collagenous connective tissues (blue).

Masson's trichrome was used for visualization of collagenous connective tissue. For that, representative sections of the collagen and collagen:hyaluronic acid constructs were stained with Masson's trichome.

II-5.5.7.7 Immunofluorescence

Immunofluorescence (IF), utilize antibodies to obtain qualitative information about protein abundance, distribution and localization [80]. Immunofluorescence is a detection method, during which antibody binding to an antigen and is visualized using a fluorophore.

In **Chapter V**, immunofluorescence was performed to qualitatively assessed the potential of the produced composite to induce chondrogenic differentiation, with and without exogeneous stimulation. For immunodetection, tissue sections were deparaffinized in xylene, re-hydrated and boiled for 4 min in sodium citrate buffer (10 mM sodium citrate (SIGMA, USA), 0.05 % v/v tween 20 (Bio-Rad, Netherlands), pH 6) for antigen retrieval. Sections were maintained for 30 min in 3 % (w/v) of bone serum albumin (BSA, Laborspirit, Lisbon) to block nonspecific antigen binding and incubated with a rabbit anti-SOX 9 antibody (Sigma, Portugal) 1:100 and aggrecan (ACAN) monoclonal antibody (Alfagene, Portugal) 1:50. Alexa Fluor 488 secondary antibody at 1:500 in PBS was added during 1 h at 37 °C. Slices were analyzed using Zeiss Axio Imager Z1m (Germany) fluorescence microscope.

In **Chapter VII**, to evaluate the potential of the 3D printable hydrogels to induce osteogenic differentiation, immunodetection of bone-related proteins was addressed directly in the structures. Cell-laden printed hydrogels were fixed with paraformaldehyde, 16 % (w/v) (VWR, Lisbon Portugal) overnight at 4 °C. After that, cells were permeabilized with 1% (v/v) of Triton X-100/ Tris(hydroxymethyl)aminomethane (TBS) (Sigma-Aldrich, USA). To block unspecific reactions, samples were incubated with 3% (w/v) bovine serum albumin solution (BSA; Sigma-Aldrich, USA). A rabbit anti-human polyclonal antibody against osteopontin (OPN) (Abcam, UK; dilution 1:250) and a mouse anti-RUNX2, clone AS110 (Merck, Germany 1:250) were used as primary antibodies (2 h at RT). Alexa Fluor 488 secondary antibody at 1:500 in TBS was added during 1 h at 37 °C. Samples were analyzed using a Leica SP8 Inverted Confocal Microscope with Incubation.

II-5.5.8. *In vivo* study

II-5.5.8.1 Experimental design

Aiming to evaluate the *in vivo* potential of the collagen:bioapatite produced scaffolds (**Chapter IV**), critical-size bone defects were created in the lateral femoral condyles of New Zealand rabbit models. The materials were implant in both knees, right and left, with a random distribution. An empty group

was used as the control of the experiment. To evaluate the bone defects regeneration, micro-CT analysis of femoral condyles was performed 12 weeks post-implantation (**Figure II-10**).

II-5.5.8.2 Animals

Twelve male New Zealand White rabbits (age between 18 and 21 weeks) weighting 3.7 - 4.0 kg were supplied by a qualified laboratory animal supply center (La Granja cunícola San Bernardo, S.L., Tulebras, Navarra).

The animals were housed in individual enriched cages in the Animal Experimentation Service Facility of the University of Santiago de Compostela (Lugo, Spain) after the ethical approval (procedure code: 03/18/LU-002) as a randomized controlled trial with one inter-subject control.

Animals were maintained under conditions of temperature (15 – 21 ºC), humidity, air renewal and cycle time (12 h alternating cycles of light and dark) controlled according to annex II of directive 86/609/EEC. After a quarantine period of three weeks animals were pre-medicated with Ketamine 25mg/kg/i.m. (Ketamidor® 100 $mg.mL^{-1}$), medetomidine 50µg/kg/i.m. (Sededorm® 1 $mg.mL^{-1}$) and buprenorphine 0.03mg/kg (Bupaq® 0.3 $mg.mL^{-1}$). The anesthesia was maintained by inhalation of an O_2 and 2% isoflurane mixture using a facemask.

II-5.5.8.3 Implants

Cylindrical shape (5 X 5 mm) collagen-based composites were tested. Two different materials and an empty control were randomly assigned to the left or right side according to a computer-generated randomization list until complete a n=8.

In total, 16 biomaterials and 8 empty defects were placed in 12 animals, two per animal. To avoid errors due to the implantation side, half of each biomaterial and half of the empty defects were placed in left femurs and half in rights of each type. The trial period used was 12 weeks.

II-5.5.8.4 Surgical procedure

Critical-size bone defects corresponding to the size of the implanted materials (5 x 5 mm) were created under aseptic conditions in the distal lateral part of femoral condyles by using a trephine connected to a surgical motor (intrasurg 300, Kavo, Biberach, Germany). After that, the wounds were

sutured using a 4-0 vicryl in deep planes and 3-0 nylon for the skin. The animals were monitored throughout the time, the pain was controlled in the first 5 days by using buprenorphine (0.01-0.03 mg/kg/i.m, Buprex, RB Pharmaceuticals) and meloxicam (0.2 mg/kg/ SC, Metacam, Boehringer). As a prophylactic antibiotic it was used enrofloxacin (Syvaquinol® 10% oral) for 3 weeks. The animals were sacrificed with an intravenous overdose of isodium pentobarbital (Dolethal, Vétoquinol) after sedation with Ketamine 25 mg / kg + medetomidine 50µg / kg + buprenorphine 0.03 mg / kg. Subsequently, the distal femurs were recovered by dissection and the use of a bone saw. Specimens were immediately immersed in a 10% buffered formalin solution for a minimum of 2 weeks until the time of processing. For identification we use a code consisting of a number and a letter. The number indicated the animal (from 1 to 12) and the letter the side of the femur (right-R and left-L). All biomaterials were recovered.

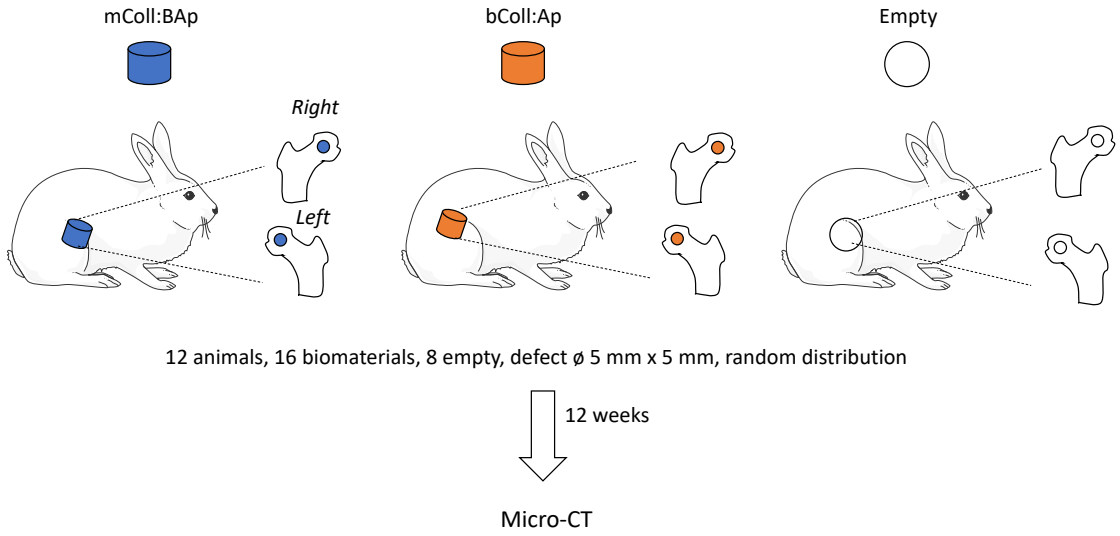

Figure II-10 *In vivo* experimental design.

II-5.6. Statistical analysis

All quantitative data are presented as mean ± standard deviation (SD). Statistical analyses were performed using a GraphPad Prism 5.0 software (GraphPad Software, USA). A Shapiro-Wilk normality test was performed to assess data normality. As data do not followed a normal distribution, the Mann–Whitney U test was used when two groups were compared and the Kruskal-Wallis test followed by Dunn's multiple comparison test when more than two groups were compared.

II-6. REFERENCES

1. Shoulders, M.D. and R.T. Raines, *Collagen structure and stability.* Annual review of biochemistry, 2009. **78**: p. 929-958.
2. Depalle, B., et al., *Influence of cross-link structure, density and mechanical properties in the mesoscale deformation mechanisms of collagen fibrils.* Journal of the mechanical behavior of biomedical materials, 2015. **52**: p. 1-13.
3. Sorushanova, A., et al., *The collagen suprafamily: from biosynthesis to advanced biomaterial development.* Advanced Materials, 2019. **31**(1): p. 1801651.
4. Olatunji, O., *Collagen*, in *Aquatic Biopolymers*. 2020, Springer. p. 261-285.
5. Ashokkumar, M. and P.M. Ajayan, *Materials science perspective of multifunctional materials derived from collagen.* International Materials Reviews, 2020: p. 1-28.
6. Luca, S., et al., *Marine collagen and its derivatives: Versatile and sustainable bio-resources for healthcare.* Materials Science and Engineering: C, 2020. **113**: p. 110963.
7. Coppola, D., et al., *Marine Collagen from Alternative and Sustainable Sources: Extraction, Processing and Applications.* Marine Drugs, 2020. **18**(4): p. 214.
8. Rahman, M.A., *Collagen of extracellular matrix from marine invertebrates and its medical applications.* Marine drugs, 2019. **17**(2): p. 118.
9. Moreira-Silva, J., et al., *Marine collagen isolation and processing envisaging biomedical applications*, ed. N.M.N.R.L. Reis. Vol. 16. 2016, Biomaterials from Nature for Advanced Devices and Therapies: Wiley online library.
10. Lopes, C., et al., *Valorisation of fish by-products against waste management treatments–Comparison of environmental impacts.* Waste management, 2015. **46**: p. 103-112.
11. Al Khawli, F., et al., *Aquaculture and its by-products as a source of nutrients and bioactive compounds.* Advances in Food and Nutrition Research, 2020. **92**: p. 1-33.
12. Coelho, R., et al., *Local indicators for global species: Pelagic sharks in the tropical northeast Atlantic, Cabo Verde islands region.* Ecological Indicators, 2020. **110**: p. 105942.
13. Coulter, A., et al., *Using harmonized historical catch data to infer the expansion of global tuna fisheries.* Fisheries Research, 2020. **221**: p. 105379.

14. Litwiniuk, M., et al., *Hyaluronic acid in inflammation and tissue regeneration.* Wounds, 2016. **28**(3): p. 78-88.

15. Boeriu, C.G., et al., *Production methods for hyaluronan.* International Journal of Carbohydrate Chemistry, 2013. **2013**.

16. Al-Khateeb, R. and J. Prpic, *Hyaluronic Acid: The Reason for Its Variety of Physiological and Biochemical Functional Properties.* Applied Clinical Research, Clinical Trials and Regulatory Affairs, 2019. **6**(2): p. 112-159.

17. Pfeifer, C.G., et al., *Higher ratios of hyaluronic acid enhance chondrogenic differentiation of human MSCs in a hyaluronic acid–gelatin composite scaffold.* Materials, 2016. **9**(5): p. 381.

18. Evans, C.H., V.B. Kraus, and L.A. Setton, *Progress in intra-articular therapy.* Nature Reviews Rheumatology, 2014. **10**(1): p. 11.

19. Gomez, C.G., et al., *Influence of the extraction–purification conditions on final properties of alginates obtained from brown algae (Macrocystis pyrifera).* International Journal of Biological Macromolecules, 2009. **44**(4): p. 365-371.

20. Valente, J., et al., *Alginate based scaffolds for bone tissue engineering.* Materials Science and Engineering: C, 2012. **32**(8): p. 2596-2603.

21. Christensen, B., *Alginates as biomaterials in tissue engineering.* Carbohydrate chemistry: chemical and biological approaches, 2011. **37**: p. 227-258.

22. LeRoux, M.A., F. Guilak, and L.A. Setton, *Compressive and shear properties of alginate gel: effects of sodium ions and alginate concentration.* Journal of Biomedical Materials Research: An Official Journal of The Society for Biomaterials, The Japanese Society for Biomaterials, and The Australian Society for Biomaterials and the Korean Society for Biomaterials, 1999. **47**(1): p. 46-53.

23. Afjoul, H., A. Shamloo, and A. Kamali, *Freeze-gelled alginate/gelatin scaffolds for wound healing applications: An in vitro, in vivo study.* Materials Science and Engineering: C, 2020. **113**: p. 110957.

24. Lee, K.Y. and D.J. Mooney, *Alginate: properties and biomedical applications.* Progress in polymer science, 2012. **37**(1): p. 106-126.

25. Kumta, P.N., et al., *Nanostructured calcium phosphates for biomedical applications: novel synthesis and characterization.* Acta Biomaterialia, 2005. **1**(1): p. 65-83.

26. Bang, L., B. Long, and R. Othman, *Carbonate hydroxyapatite and silicon-substituted carbonate hydroxyapatite: synthesis, mechanical properties, and solubility evaluations.* The Scientific World Journal, 2014. **2014**.

27. Basu, B., *Natural bone and tooth: structure and properties*, in *Biomaterials for musculoskeletal regeneration*. 2017, Springer. p. 45-85.

28. Pina, S.C.A., R.L. Reis, and J.M. Oliveira, *Ceramic biomaterials for tissue engineering.* 2017.

29. Emtiazi, G., F. Shapoorabadi, and M. Mirbagheri, *Chemical and Biological Synthesis of Hydroxy Apatite: Advantage and Application.* International Journa Microbiology Current Research, 2019. **1**: p. 20-22.

30. LeGeros, R.Z. and B. Ben-Nissan, *Introduction to synthetic and biologic apatites*, in *Advances in calcium phosphate biomaterials*. 2014, Springer. p. 1-17.

31. Šupová, M., *Isolation and preparation of nanoscale bioapatites from natural sources: a review.* Journal of nanoscience and nanotechnology, 2014. **14**(1): p. 546-563.

32. Šupová, M., *Substituted hydroxyapatites for biomedical applications: a review.* Ceramics international, 2015. **41**(8): p. 9203-9231.

33. Silva, T.H., et al., *Materials of marine origin: a review on polymers and ceramics of biomedical interest.* International Materials Reviews, 2012. **57**(5): p. 276-306.

34. O'brien, F.J., *Biomaterials & scaffolds for tissue engineering.* Materials today, 2011. **14**(3): p. 88-95.

35. Eltom, A., G. Zhong, and A. Muhammad, *Scaffold techniques and designs in tissue engineering functions and purposes: a review.* Advances in Materials Science and Engineering, 2019. **2019**.

36. Haider, A., et al., *Advances in the scaffolds fabrication techniques using biocompatible polymers and their biomedical application: A technical and statistical review.* Journal of Saudi Chemical Society, 2020. **24**(2): p. 186-215.

37. Ambekar, R.S. and B. Kandasubramanian, *Progress in the advancement of porous biopolymer scaffold: tissue engineering application.* Industrial & Engineering Chemistry Research, 2019. **58**(16): p. 6163-6194.

38. Savina, I.N., et al., *A simple method for the production of large volume 3D macroporous hydrogels for advanced biotechnological, medical and environmental applications.* Scientific reports, 2016. **6**: p. 21154.

39. Deville, S., *Ice-templating, freeze casting: Beyond materials processing.* Journal of Materials Research, 2013. **28**(17): p. 2202-2219.

40. Lin, K., et al., *Advanced Collagen-Based Biomaterials for Regenerative Biomedicine.* Advanced Functional Materials, 2019. **29**(3): p. 1804943.

41. Pieper, J., et al., *Development of tailor-made collagen–glycosaminoglycan matrices: EDC/NHS crosslinking, and ultrastructural aspects.* Biomaterials, 2000. **21**(6): p. 581-593.

42. de Castro Brás, L.E., et al., *Effect of crosslinking on the performance of a collagen-derived biomaterial as an implant for soft tissue repair: A rodent model.* Journal of Biomedical Materials Research Part B: Applied Biomaterials, 2010. **95**(2): p. 239-249.

43. Liu, Q., J. De Wijn, and C. Van Blitterswijk, *A study on the grafting reaction of isocyanates with hydroxyapatite particles.* Journal of biomedical materials research, 1998. **40**(3): p. 358-364.

44. Yeong, W.Y., et al., *Comparison of drying methods in the fabrication of collagen scaffold via indirect rapid prototyping.* Journal of Biomedical Materials Research Part B: Applied Biomaterials, 2007. **82**(1): p. 260-266.

45. García-Carvajal, Z.Y., et al., *Cartilage tissue engineering: the role of extracellular matrix (ECM) and novel strategies*, in *Regenerative medicine and tissue engineering*. 2013, IntechOpen.

46. Poole, A.R., et al., *Composition and structure of articular cartilage: a template for tissue repair.* Clinical Orthopaedics and Related Research®, 2001. **391**: p. S26-S33.

47. Cidonio, G., et al., *The cell in the ink: Improving biofabrication by printing stem cells for skeletal regenerative medicine.* Biomaterials, 2019.

48. Lenchik, L., et al., *Automated segmentation of tissues using CT and MRI: a systematic review.* Academic radiology, 2019. **26**(12): p. 1695-1706.

49. Madrid, A.P.M., et al., *Advances in additive manufacturing for bone tissue engineering scaffolds.* Materials Science and Engineering: C, 2019. **100**: p. 631-644.

50. Landers, R. and R. Mülhaupt, *Desktop manufacturing of complex objects, prototypes and biomedical scaffolds by means of computer-assisted design combined with computer-guided*

3D plotting of polymers and reactive oligomers. Macromolecular Materials and Engineering, 2000. **282**(1): p. 17-21.

51. Lopes, C.d.C.A., et al., *Fourier transform infrared spectroscopy (FTIR) application chemical characterization of enamel, dentin and bone.* Applied Spectroscopy Reviews, 2018. **53**(9): p. 747-769.

52. Schuttlefield, J.D. and V.H. Grassian, *ATR–FTIR spectroscopy in the undergraduate chemistry laboratory. Part I: fundamentals and examples.* Journal of chemical education, 2008. **85**(2): p. 279.

53. He, B.B., *Introduction to two-dimensional X-ray diffraction.* Powder diffraction, 2003. **18**(2): p. 71-85.

54. Olesik, J.W., *Elemental analysis using ICP-OES and ICP/MS.* Analytical Chemistry, 1991. **63**(1): p. 12A-21A.

55. Glassbrook, N. and J. Ryals, *A systematic approach to biochemical profiling.* Current opinion in plant biology, 2001. **4**(3): p. 186-190.

56. Staub, A., et al., *Intact protein analysis in the biopharmaceutical field.* Journal of pharmaceutical and biomedical analysis, 2011. **55**(4): p. 810-822.

57. Juan, H.S., et al., *Micro Computed Tomography in the.* Techniques in Microscopy for Biomedical Applications, 2006. **2**: p. 315.

58. De Graef, M., *Introduction to conventional transmission electron microscopy*. 2003: Cambridge university press.

59. Eshel, G., et al., *Critical evaluation of the use of laser diffraction for particle-size distribution analysis.* Soil Science Society of America Journal, 2004. **68**(3): p. 736-743.

60. Hutmacher, D.W., et al., *State of the art and future directions of scaffold-based bone engineering from a biomaterials perspective.* Journal of tissue engineering and regenerative medicine, 2007. **1**(4): p. 245-260.

61. Armiento, A.R., et al., *Functional Biomaterials for Bone Regeneration: A Lesson in Complex Biology.* Advanced Functional Materials, 2020: p. 1909874.

62. Osswald, T. and N. Rudolph, *Polymer rheology*, ed. T.A.O.N. Rudolph. 2015: Hanser Publishers, Munich • Hanser PublicaΘ ons, CincinnaΘ

63. Marques, C., et al., *Collagen-based bioinks for hard tissue engineering applications: a comprehensive review.* Journal of Materials Science: Materials in Medicine, 2019. **30**(3): p. 32.

64. Whitlow, J., A. Paul, and A. Polini, *Bioactive Materials: Definitions and Application in Tissue Engineering and Regeneration Therapy*, in *Biocompatible Glasses*. 2016, Springer. p. 1-17.

65. Kokubo, T. and H. Takadama, *How useful is SBF in predicting in vivo bone bioactivity?* Biomaterials, 2006. **27**(15): p. 2907-2915.

66. Mozafari, M., et al., *Calcium carbonate: Adored and ignored in bioactivity assessment.* Acta biomaterialia, 2019. **91**: p. 35-47.

67. Assad, M. and N. Jackson, *Biocompatibility evaluation of orthopedic biomaterials and medical devices: A review of safety and efficacy models*. Medical Devices: Biocompatibility Evaluation of Orthopedic Biomaterials. 2019: Elsevier.

68. Cao, T., et al., *Differentiated fibroblastic progenies of human embryonic stem cells for toxicology screening.* Cloning and Stem Cells, 2008. **10**(1): p. 1-10.

69. Rodan, S.B., et al., *Characterization of a human osteosarcoma cell line (Saos-2) with osteoblastic properties.* Cancer research, 1987. **47**(18): p. 4961-4966.

70. Rivera-Izquierdo, M., et al., *An updated review of adipose derived-mesenchymal stem cells and their applications in musculoskeletal disorders.* Expert opinion on biological therapy, 2019. **19**(3): p. 233-248.

71. Freitas-Ribeiro, S., et al., *Strategies for the hypothermic preservation of cell sheets of human adipose stem cells.* PloS one, 2019. **14**(10).

72. Aslantürk, Ö.S., *In vitro cytotoxicity and cell viability assays: principles, advantages, and disadvantages*. Vol. 2. 2018: InTech.

73. Freshney, R., *A Manual of basic technique and specialized applications. 6. Hoboken*, 2010, NJ, USA: John Wiley & Sons, Inc.

74. Fleige, S. and M.W. Pfaffl, *RNA integrity and the effect on the real-time qRT-PCR performance.* Molecular aspects of medicine, 2006. **27**(2-3): p. 126-139.

75. Elliott, A.D., *Confocal Microscopy: Principles and Modern Practices.* Current Protocols in Cytometry, 2020. **92**(1): p. e68.

76. Narayan, R., *Monitoring and evaluation of biomaterials and their performance in vivo*, ed. R.J. Narayan. 2016: Woodhead Publishing.

77. Titford, M., *Progress in the development of microscopical techniques for diagnostic pathology.* Journal of Histotechnology, 2009. **32**(1): p. 9-19.

78. Shirazi, A.Z., E. Fornaciari, and G.A. Gomez, *Deep learning in precision medicine*, in *Artificial Intelligence in Precision Health*. 2020, Elsevier. p. 61-90.

79. Khan, S.A., et al., *Advances in glycosaminoglycan detection.* Molecular Genetics and Metabolism, 2020.

80. Langton, P.D., *Essential guide to reading biomedical papers: recognising and interpreting best practice*. 2012: John Wiley & Sons.

Chapter III

Marine Collagen:Apatite Composite Scaffolds Envisaging Hard Tissue Applications

Chapter III

Marine Collagen:Apatite Composite Scaffolds Envisaging Hard Tissue Applications[1]

III-1. ABSTRACT

The high prevalence of bone defects has become a worldwide problem. Despite the significant amount of research on the subject, the available therapeutic solutions lack efficiency. Autografts, the most common used approaches to treat bone defects have limitations such as donor site morbidity, pain and lack of donor site. Marine resources emerge as an attractive alternative to extract bioactive compounds for further use in bone tissue engineering approaches. On one hand they can be isolated from by-products, at low costs, creating value from products that are considered waste for the fish transformation industry. One the other hand, religious constraints will be avoided. We isolated two marine origin materials, collagen from shark skin (*Prionace glauca*) and calcium phosphates from teeth of two different shark species (*Prionace glauca* and *Isurus oxyrinchus*), and further proposed to mix them to produce 3D composite structures for hard tissue applications. Two crosslinking agents, EDC/NHS and HMDI, were tested to enhance scaffolds' properties, with EDC/NHS resulting in better properties. The characterization of the structures showed that the developed composites could support attachment and proliferation of osteoblast-like cells. A promising scaffold for the engineering of bone tissue is thus proposed, based on a strategy of marine by-products valorization.

[1]This chapter is based on the following publication:

Diogo G. S, Lopez-Senra E., Pirraco R. P, Canadas R. F, Fernandes E. M., Serra J., Pérez-Martín R. I, Sotelo C. G, Marques A. P, González P., Moreira-Silva J., Silva T. H., Reis R. L., *Marine collagen:apatite composite scaffolds envisaging hard tissue applications.* Marine drugs, 2018. 16(8) p:269.

III-2. INTRODUCTION

The regeneration of bone defects represents a growing need and a worldwide concern [1]. Despite the high self-remodeling ability of bone tissue, severe damage can lead to a loss of this innate capacity. Bone grafts, including, autografts, allografts and xenografts are some of the approaches used to treat bone defects [2]. However, limitations such as donor site morbidity, pain and lack of donor site (autografts) and risk of disease transmission or rejection (allografts and xenografts) leave room for alternative approaches [3]. In that sense, tissue engineering and the development of temporary regenerative matrices that provide the 3D environment required for cell proliferation and function promoting tissue growth appears as attractive alternative. While polymers and ceramics have been largely explored to produce such matrices reduced biocompatibility and risk of immunogenicity, respectively, due to synthetic and animal origin components are still observed. Marine resources emerge as an attractive alternative since they are free of mammalian diseases, or, to date, any other transmissible disease, and, at the same time, avoids religious constraints. Moreover, these marine origin materials can be isolated from by-products, at low costs, creating value from products that are considered waste for the fish transformation industry, representing a great opportunity with a huge potential [4-6].

For instance, fish skin and bones have a large amount of bioactive compounds with potential to be applied in health-related applications [5, 7-10], with materials properties depending on the raw material, source and extraction process [11]. Collagen and calcium phosphates represent the most abundant and explored compounds obtained from fish skin and bones, respectively.

Collagen isolated from salmon fish skin was used to produce 3D composites by a biomimetic mineralization process [8]. The high potential of these marine origin structures was demonstrated by the ability of the composites to promote osteogenic differentiation. Moreover, the suitability of marine origin collagen was also proven by others research groups. Fernandes-Silva *et al*, also assessed the excellent properties of marine organisms as a collagen source through the use of shark collagen to produce hydrogels envisioning cartilage tissue regeneration [12].

Considering the excellent properties of calcium phosphates for hard tissue applications, recently it was study the potential of bioapatites obtained from teeth of blue shark specie to promote osteogenic differentiation [14]. The calcium phosphates isolated from shark tooth are not only hydroxyapatite (HAp), the most common used ceramic for hard tissue regeneration, but also HAp enriched with

fluorapatite $Ca_5(PO_4)_3F$, unlike to the mammalian teeth. Moreover, some others elements, such as, magnesium (Mg) and strontium (Sr) are present in their constitution [13, 14]. These ions have been shown to stimulate osteoblastic activity by different mechanisms [15]. Mg ions, for instance, are involved in parathyroid hormone regulation, contributing to the bone homeostasis [16-19] and fluorine has been demonstrated to promote bone formation by the stimulation of osteoblastic activity [20, 21]. Thus, the presence of such ions in the mixture of the marine bioapatite (mBAp) particles and the incorporation of such particles into a type I marine collagen (mColl) matrix (the most abundant protein in hard tissues) can be a perfect combination to ensure a good performance in hard tissues applications using marine origin resources. In that sense, in the present study, collagen extracted from the skin of blue shark (*Prionace glauca*) combined with bioceramic particles obtained from tooth of *Iurus oxyrinchus* and *Prionace glauca* were used to produce 3D structures aiming at hard tissue regeneration.

The physical combination of marine bioapatite particles with marine collagen used to develop the bone-like constructs was tested with two different crosslinking agents, 1-[3-(dimethylamino)propyl]-3-ethylcarbodiimide hydrochloride/N-Hydroxysuccinimide (EDC/NHS) or hexamethylene diisocyanate (HMDI), at different concentrations, to reinforce constructs stability. The crosslinking approaches are illustrated in **Figure III-1**. The resulting scaffolds were characterized, addressing their morphological and mechanical properties, bioactivity upon immersion in simulated body fluid, cytotoxicity and performance towards bone tissue engineering after culture osteoblast-like cells.

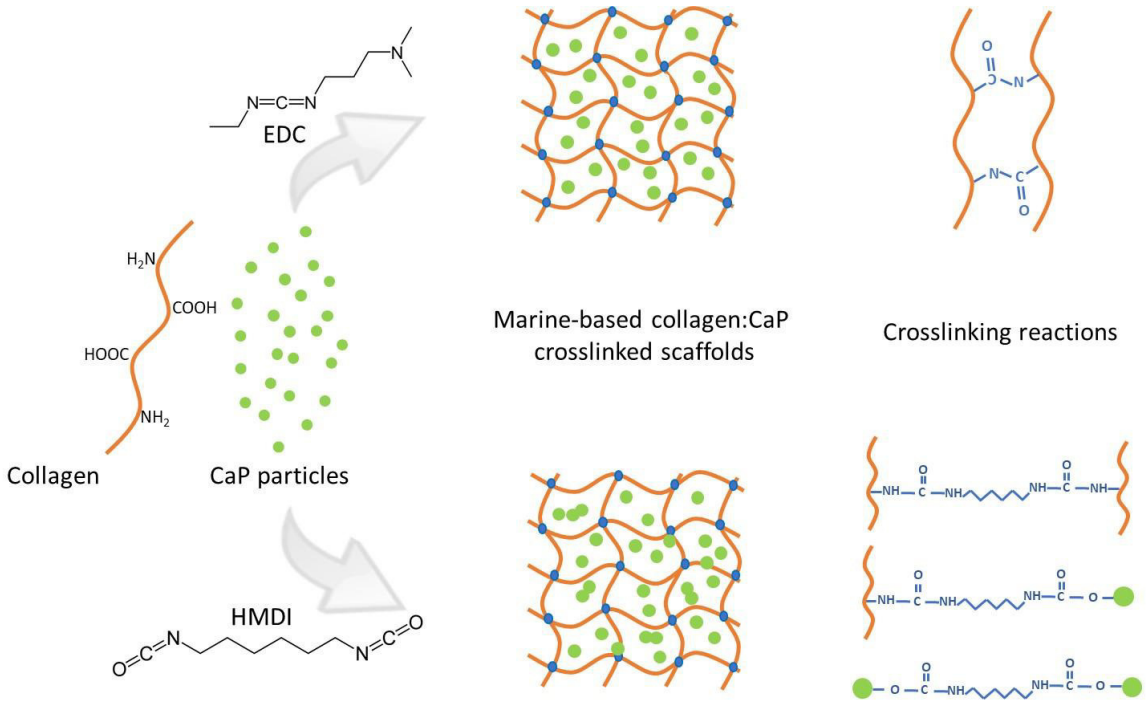

Figure III-1 – Schematic representation of crosslinking reactions for, EDC and HMDI, crosslinking agents.

III-3. MATERIALS AND METHODS

III-3.1. Marine collagen extraction

Marine collagen (mColl) was extracted from shark skin (*Prionace glauca*) by Instituto de Investigaciones Marinas (CSIC, Vigo, Spain). About 10 g of skin pieces were first treated with 0.1 N NaOH (1:10 w/v) by continuous stirring for 24 hours at 4 °C for removing any non-collagenous protein present in the skin. Then, liquid was discarded, and the remaining part was washed several times to stabilize the pH to 7. The resulting treated skin pieces were further stirred overnight with 10 volumes of 0.5 M acetic acid for the extraction of collagen. The extract was centrifuged at 10.000 g for 20 min at 10 °C. Supernatant was dialyzed with D9402-100FT dialysis membranes from Sigma with molecular weight cut-off of 14000 Da, using cold distilled water with several changes for 24 - 72 hand freeze-dried. This mColl was characterized as type I collagen by SDS-PAGE electrophoresis as previously described by Sotelo *et al.* [22].

III-3.2. Marine bioapatite isolation

Marine bioapatite (mBAp) was obtained from shark teeth of *Isurus oxyrinchus* and *Prionace glauca*, provided by Centro Tecnológico del Mar (CETMAR) and by the fishing company COPEMAR SA (Porto de Vigo, Spain), respectively. Teeth were cleaned and washed and further dried at 60 °C for 24 h. After this, teeth were grinded in a ball mill (Retsch MM2000) for 5 minutes with an oscillation frequency between 90 to 100 Hz for powder of 100 to 0.1 μm. This powder of teeth was then pyrolyzed at 950 °C for 12 hours with a heating ramp of 2 °C/min and a cooling ramp of 20 °C/min to remove the organic material of the tooth. The resulting granules of apatite were separated by sieves into a particle size between 20 to 63 μm.

III-3.3. Physicochemical characterization

To evaluate the elementary composition of marine BAp particles, inductively coupled plasma optical emission spectrometry (ICP-OES) and ion chromatography (only measure Fluorine) was carried out (**Table III-1**). Four measurements per condition were taken and data are represented as mean value in weight percentage (wt.%) and with standard deviation.

III-3.4. Scaffolds production

The 3D composites were produced by an optimized method of freeze-dry. Marine collagen was combined with marine bioapatite granules using different formulations: mColl:mBAp ratios of 100:0, 70:30, 50:50, 30:70. The freeze-dried collagen was solubilized at a final concentration of 1.5% in 0.5 M acetic acid followed by dialysis to ensure complete removal of impurities. After that, the isolated mBAp granules were added in the desired proportion to produce the above-mentioned formulations. EDC/NHS or HMDI, the crosslinking agents selected for the present study, were added to the mColl:mBAp mixture at 12.5% or 25% for EDC/NHS and 1% or 5% for HMDI. After allowing the crosslinker to react (24 h), solutions with a viscous appearance were then poured into a mold and freeze-dried for at least 5 days. To wash out any harmful residual compound all scaffolds were thoroughly rinsed with distilled water immediately before using in cell culture experiments.

III-3.5. Stability assay of 3D structures

All the characterization studies were performed after sterilization with γ-irradiation (15 kGγ) [23]. The study of scaffolds stability was carried out by incubation in culture medium during 14 days at 37 °C. During this period, samples were monitored and photographed to classify them according to their degree of stability. Samples that degraded 24 h after contact with culture medium at 37 °C were classify as unstable (-). Samples that degrades 7 days after incubation were reported as averagely stable structures (+) and the ones that maintains their integrity 14 days after culture medium contact were classify as high stable structures, signal (++).

III-3.6. Micro-Computed tomography of 3D structures

Marine bioapatite particles distribution through the collagen matrix was assessed by micro-CT in terms of porosity (%), pore size (μm), trabecular thickness (μm) and pore interconnectivity (%, considering a minimum pore size of 58 μm). For scanning scaffolds (n=3) a high-resolution micro-CT Skyscan 1072 scanner (Skyscan, Kontich, Belgium) with a voltage range and current source between 32 - 40 kV and 220 - 248 uA, respectively, was used. Quantitative parameters were measured by CT-Analyzer software (version 1.12.0.0) from 3D model reconstruction of a representative selection of slices and a designed region of interest. A threshold between 30 - 60 and 120 - 255 was applied for the differentiation of soft (mColl) and hard (BAp particles) materials, respectively. 3D images were finally obtained by CTvox software resulting in a colour scale directly related to the chosen threshold according to the material density/hardness.

III-3.7. Incubation in simulated body fluid

To understand the bioactive nature of the composites, SBF with a ion concentration of Na^+ 142.0, K^+ 5.0, Mg^{2+} 1.5, Ca^{2+} 2.5, Cl^- 147.8, HCO_3^- 4.2, HPO_4^{3-} 1.0 and SO_4^{2-} 0.5 mM, similar to the concentration of the human blood plasma (Na^+ 142.0, K^+ 5.0, Mg^{2+} 1.5, Ca^{2+} 2.5, Cl^- 103.0, HCO_3^- 27, HPO_4^{2-} 1.0 and SO_4^{2-} 0.5 mM), was prepared according to Kokubo *et al*, 2006 [24]. Firstly, the dimensions of the previously produced composites were taken and the volume of SBF needed to submerse and characterize the bioactivity of those composites was determined through the following equation:

$$Vs = \frac{Sa}{10}$$

where Vs is the volume of SBF and Sa correspond to the apparent surface area of each specimen. For the produced scaffolds, the added volume of SBF was greater than the calculated (Vs), since they are porous structures. Three replicates of each condition were immersed in the SBF solution at 37 °C and pH 7.4 (mimicking the physiological conditions) for 1, 3, 7 and 14 days. After that, the samples were removed from the solution and washed with distilled water to avoid the formation of salts during the drying process. To evaluate the apatite formation, samples before and after soaking in SBF were coated with gold and analysed by scanning electron microscopy (SEM) (JSM-6010LV, JEOL, Japan) with an acceleration voltage of 15 kV at different magnifications.

III-3.8. Mechanical tests of 3D structures

In order to study the mechanical behaviour of the mColl:mBAp structures, mechanical assays were carried out under compression mode using an (INSTRON 5540). Five replicates of each condition were tested with a crosshead speed of 2 mm /min and a load cell of 1 kN. The compressive modulus, a measure of material stiffness was determined from the slope of the linear region of the stress-strain curve. However, for the formulations crosslinked with 25% of EDC/NHS this assay was not determined since they did not present an uniform shape.

III-3.9. Evaluation of cell viability

Aiming at evaluating a potential cytotoxicity effect of the composites, Saos-2 cells were cultured in the 3D structures. Saos-2 cells were expanded in Dulbecco's Modified Eagle's Medium (DMEM) supplemented with 10% foetal bovine serum (ALFAGENE, Portugal) and a 1% antibiotic–antimycotic (ALFAGENE, Portugal) mixture. Cells were seeded on top of the different mColl:mBAp combinations in 48-well plates at a density of $2.5x10^4$ cells per scaffold. Metabolic activity at 1 and 3 days after seeding was determined using a 3-(4,5-dimethylthiazol-2-yl)-5-(3 carboxymethoxyphenyl) 2-(4-sulphofenyl)-2*H*-tetrazolium, inner salt (MTS) (VWR, Portugal) assay. This assay quantifies the metabolic activity of the cells by the reduction of tetrazolium salt reagent to formazan after 3 h of incubation at 37 °C. Absorbance intensity, which is directly proportional to the metabolic activity, was measured at 492 nm

using a microplate reader (SYNERGY HT, BIO-TEK). The results are the mean of three independent experiments (n=3) with three replicates for each condition and per experiment [25].

Cell viability in the 12.5% EDC/NHS crosslinked scaffolds, which showed higher values of metabolic activity, was also confirmed staining live/dead cells with calcein-AM (AM)/propidium iodide (PI) (ALFAGENE, Portugal), respectively. Briefly, Saos-2 cells were seeded in mColl:mBAp scaffolds, and 1 and 3 days after seeding, the culture medium was removed and replaced by a AM (1:300) and PI (1:1200) solution in culture medium. After 30 minutes of incubation in the darksamples were washed twice with PBS and immediately visualized by confocal laser scanning microscopy (CLSM) (TCS SP8, Leica). The acquired confocal images are scaffolds mid-section. The scaffolds were cut in half and analysed according to the chosen parameters: slice thickness of 3.66 μm, depth of scanning of approximately 120 μm, no sequential scanning. Regarding the latter parameter, before each experiment, acquisition conditions were tested with samples stained with only PI or only AM to ensure no crosstalk would be detected in the wrong channels.

III-3.10. Statistical analysis

Statistical analysis of the obtained results for the different groups of scaffolds at varied conditions was performed by using Graph Prism Software. Data are presented as the mean ± standard deviation of a least three independent assays. First, a Shapiro-Wilk test was used to establish the assumption of data normality. Since data did not follow a normal distribution, a non-parametric test was used (Kruskal-Wallis test, with Dunn's Multiple Comparison Test. A p value less than 0.05 ($*p<0.05$) was considered statistically significant.

III-4. Results and Discussion

III-4.1. Physicochemical properties of marine bioapatite

The evaluation of marine bioapatite morphology derived from shark teeth was assessed in a previous study performed by López-Álvarez *et al* [13, 26].

By x-ray diffraction it was possible to observe a combination of 65 - 70% apatitic phases (hydroxyapatite and fluorapatite) and 25 - 30% non-apatitic phases (tricalcium Bis (orthophosphate) and

whitlockite) [27, 28]. Morphological characterization by scanning electron microscopy did show particles with a mean pore size around 50 μm. By inductively coupled plasma optical emission spectrometry and ion chromatography (ICP-OES) (**Table III-1**) it was possible to observe that the main elements present in the marine bioapatite were calcium (Ca) and phosphates (P), followed by fluorine (F), sodium (Na) and magnesium (Mg). Others element like strontium (Sr), aluminium (Al), and iron (Fe) were found in a lower concentration. Comparing this elemental composition with the human bone content we can see higher concentrations of Ca, P, F and Na ions for marine origin apatites [30]. These results are in accordance with some other previous studies performed with other marine organisms like cod fish [29].

Table III-1 – Elemental composition (% of weight) of bioapatite determined by ICP-OES and ion chromatography analysis.

Element	Weight (%)
Ca	44.364±5
P	22.8±2.3
F	1.0±0.5
Na	0.9±0.2
Mg	0.65±0.04
Sr	0.25±0.02
K	0.018±0.002
Al	0.007±0.005
Fe	0.006±0.003

III-4.2. Composite scaffolds' and stability

Different composite scaffolds were produced by freeze-dry and crosslinking mixtures of shark skin collagen and shark teeth bioceramics. **Figure III-2** illustrates the structures obtained upon crosslinking with EDC/NHS or HMDI resulting in porous whitish sponges.

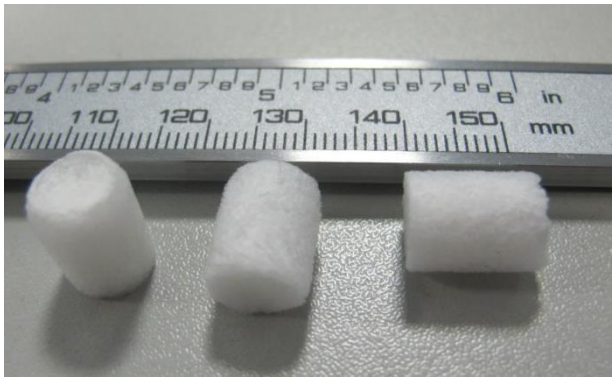

Figure III-2 – Representative composite scaffolds of mColl:mBAp.

The structural stability of the scaffolds, as a measure of the effectiveness of crosslinking reaction and consecutively the success of the processing methodology, was assessed macroscopically after incubation in culture medium for 14 days. The results were summarized in **Table III-2**. From the results it was clear an increase in scaffolds stability in the presence of marine BAp particles as expected. This result is in agreement with other reports that showed scaffolds with improved mechanical properties and slower degradation rate when compared with collagen alone, due to the incorporation of CaP [30]. In terms of crosslinker agents we could observe similar stability for both 12.5%, 25% of EDC/NHS and 5% HMDI crosslinked scaffolds. Structures crosslinked with 1% HMDI were completely degraded 1 day after immersion in culture medium at 37 °C. This result suggests that 1% of HMDI may not be enough to efficiently crosslink the collagen in the scaffolds.

In general, pore size and porosity decrease as the crosslink concentration increases. In the case of EDC/NHS, despite the stability results being similar for both concentrations it was macroscopically observed a loss of the structural integrity for the 25% EDC/NHS formulation. These results were corroborated by SEM images (see **Figure III-3**) which reveal shrinkage of collagen mesh for 25% EDC/NHS crosslinked scaffolds, with a consequent loss of porosity.

Table III-2 – Stability of the produced scaffolds after 14 days in culture medium at 37 °C. (-) represent the structures that were completely degraded 1 day after culture medium, (+) structures that were completely degraded 7 days after incubation (++) structures that maintained integrity 14 days after culture incubation.

mColl:mBAp	25% EDC/NHS	12.5% EDC/NHS	1% HMDI	5% HMDI
100:0	+	-	-	-
70:30	++	++	-	++
50:50	++	++	-	++
30:70	++	++	-	++

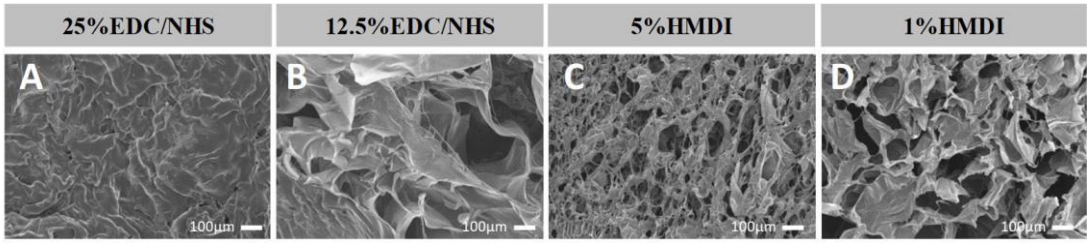

Figure III-3 – Representative SEM images of different mColl crosslinked scaffolds showing the crosslink effect over the microstructure.

III-4.3. Composite scaffolds' morphology

To address the morphological features of the composite scaffolds micro-computed tomography (micro-CT) analysis was performed. A representative example of the 3D composite scaffolds was selected and shown in **Figure III-4** according to a colour scale, which was a result of a threshold applied for the different material densities (considering soft and hard densities for collagen and ceramic, respectively). A homogenous distribution of marine BAp (brown colour) was observed within the collagen matrix (blue colour) (**Figure III-4**), which suggests an optimized method of scaffolds production, characterized by a controlled freezing process. Quantitative information of porosity, pore size and interconnectivity was also obtained from micro-CT analysis, by modelling the structure with CTAn software, as depicted in the results outlined in **Table III-3**. In general, for higher concentration of EDC/NHS and HMDI, 25% and 5%, respectively, a decrease of pore size, porosity and interconnectivity of pores was observed (**Table III-3**). These results are in accordance with the SEM observation (**Figure III-3**), which revealed a collagen mesh shrinkage for the higher EDC/NHS and HMDI crosslinker concentrations. This can be explained by a decrease in the number of free amino groups when the crosslinkers concentration increases as a result of a more extended crosslinking reaction [31, 32].

Trabecular thickness for EDC/NHS conditions is larger as the crosslinker concentration increased, which was determined by modelling a filling of spheres in the structure by CtAn software. The same modelling system was used to calculate the interconnectivity, which decreases with the increase of the crosslinking agent concentration, as described.

Comparing the internal structure of EDC/NHS and HMDI crosslinked scaffolds, in general micro-CT results revealed higher pore size, porosity and interconnectivity for the latter ones. This result suggests a higher efficiency of EDC/NHS to crosslink collagen solutions, leading to the formation of a more compact structure. The reduced crosslinking effect of HMDI may be due to the unspecific reaction of isocyanates, which react not only with amine groups but also with hydroxyl groups (OH), when combined in liquid solutions. This result reveals the importance of using HMDI crosslink reaction under anhydrous conditions in order to reduce the reactivity of isocyanate with unspecific hydroxyl groups [33, 34]. Taking into account the micro-CT and stability results, the efficacy of the scaffolds crosslinked with EDC/NHS at 25% and HMDI at 1% seems to be compromised.

In this way, the formulations of 5% HMDI and 12.5% EDC/NHS were chosen to carry on the study. Assuming a minimum pore size close to 100 μm to promote bone cell adhesion, migration and proliferation, the range of values obtained for both crosslinking conditions seems to be promising for cellular studies [35]. Moreover, obtained porosity (around 80%) comprises bone range porosity.

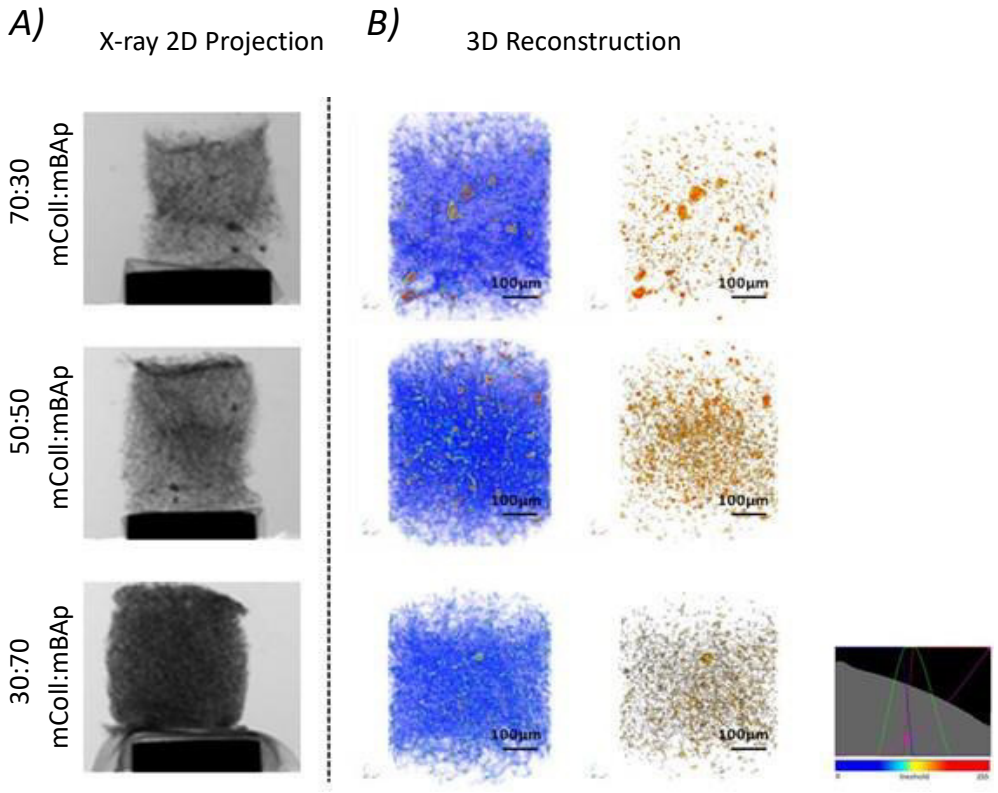

Figure III-4 – Representative images of 12.5% EDC/NHS crosslinked scaffolds obtained by micro-CT. A) X-ray 2D projection and respective B) 3D reconstruction of acquired structures in which the first column shows a reconstruction of both polymeric and ceramic phases, and the second column shows the reconstruction of the ceramic phase. A homogeneous distribution of the materials is observed, according to a colour scale: blue – soft material (mColl); brown – hard material (mBAp).

Table III-3 – Microarchitecture features of the different mColl:mBAp composite scaffolds determined by micro-CT analysis.

mColl:mBAp	Crosslinker	Mean Pore size (µm)	Porosity (%)	Trabecular Thickness (µm)	Inter-connectivity (%)
100:0	25% EDC/NHS	45.5±11.7	48.8±14.8	45.1±8.7	46.4±15.9
100:0	12.5% EDC/NHS	64.1±5.7	72.7±1.8	35.4±5.4	69.3±7.7
100:0	5% HMDI	52.7±11.0	76.3±4.2	27.9±5.5	81.5±8.5
100:0	1% HMDI	115.1±35.6	87.2±1.3	33.2±2.9	69.4±15.1
70:30	25% EDC/NHS	56.5±10.7	48.9±3.4	51.9±4.6	54.3±1.9
70:30	12.5% EDC/NHS	83.4±11.8	78.3±5.7	39.4±1.6	92.1±3.0

70:30	5% HMDI	147.0±38.4	90.4±3.2	41.6±2.7	97.3±1.8
70:30	1% HMDI	161.4±13.7	91.8±2.0	44.4±3.2	97.4±2.1
50:50	25% EDC/NHS	50.5±1.6	49.0±3.1	47.9±2.3	49.8±4.8
50:50	12.5% EDC/NHS	126.3±22.5	85.4±3.2	43.3±0.67	96.8±1.8
50:50	5% HMDI	142.6+24.1	89.4±3.0	43.2±2.2	97.4±1.6
50:50	1% HMDI	155.1±31.3	87.8±5.3	46.1±4.6	87.0±11.8
30:70	25% EDC/NHS	113.8±16.0	69.3±1.3	52.8±2.1	65.7±7.9
30:70	12.5% EDC/NHS	104.4±15.7	73.9±1.9	47.0±1.2	85.4±2.4
30:70	5% HMDI	62.6±6.8	67.5±4.2	40.8±1.7	68.8±9.8
30:70	1% HMDI	172.0±43.3	86.8±8.2	46.8±6.0	89.5±9.5

III-4.4. Composite scaffolds' bioactivity

The SEM images of the composite scaffolds 14 days after incubation in simulated body fluid (SBF) reveal the bioactive nature, i.e., the capacity to induce the mineralization process of the mColl:mBAp formulations structures. Comparing the images before and after SBF (**Figure III-5**) it was possible to see that there was no mineralization in the collagen structures. In opposition, apatite deposition occurs in the mColl:mBAp structures and preferentially over the BAp granules with the characteristic cauliflower structure. This is in agreement with other studies reporting the difficulty of bone-like apatite formation through collagen matrix due to the absence of nucleation sites for apatite grow and highlight the relevance of anionic groups as nucleating agents to promote apatite formation [36] [37]. Indeed it is well known that the presence of calcium phosphates plays an important function in the mineralization process [33, 38] and phosphate groups can attract calcium ions by electrostatic forces contributing for apatite formation [36]. In that sense, we can suggest the particular interest of using the combination of mColl with mBAp to induce the mineralization process.

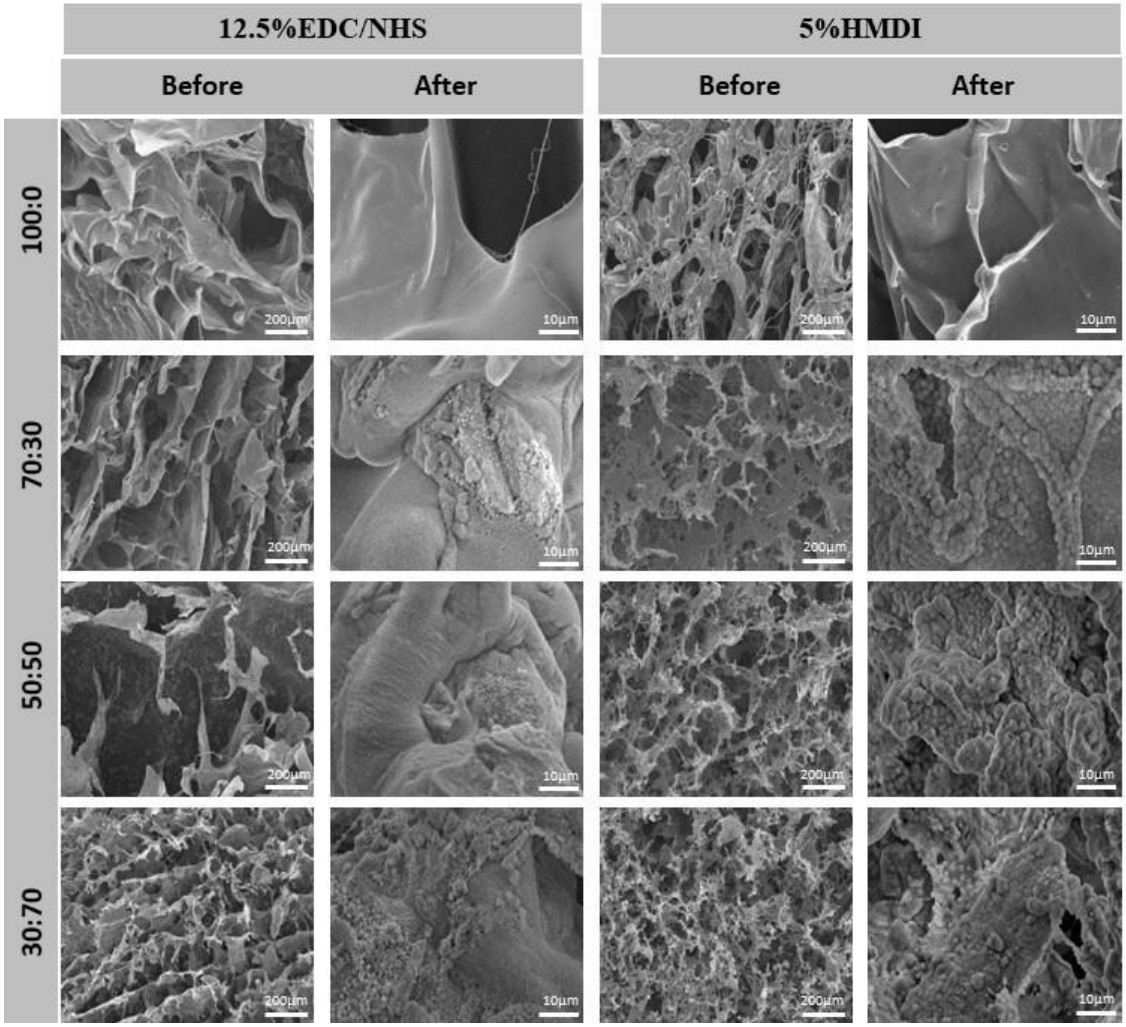

Figure III-5 – Representative SEM images of the mColl:mBAp composites scaffolds before and 14 days after the SBF test confirming the bioactive nature of the formulations as shown by the presence of mineralized deposits.

III-4.5. Mechanical properties of composite scaffolds

The mechanical properties of the developed composite scaffolds were characterized under uniaxial compression load by evaluating the compressive elastic modulus. In general, the compressive modulus results (**Figure III-7**) showed that the presence of mBAp significantly ($p<0.05$) and successively improves scaffolds' mechanical properties. Interestingly, the effect of bioapatite reinforcement was more pronounced in the scaffolds crosslinked with HMDI but independently of the improvements the compressive modulus results are considerably lower than those of the trabecular human bone (100 - 1000 MPa) [39]. Despite the poor mechanical properties of the scaffolds when compared with the native human bone, all scaffolds present stress-strain curves characteristic of highly ductile materials. In **Figure III-6**, it is possible to see a representative example of the scaffolds' mechanical behaviour,

characteristic of flexible foams. This result suggests a high potential of such composites for surgical handling and fixation to the site of the defect.

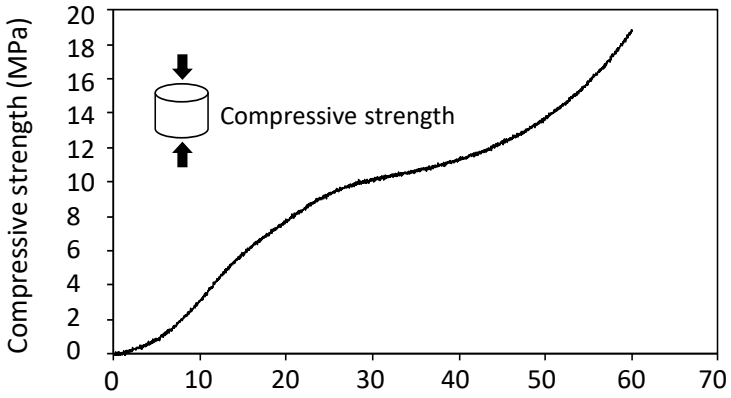

Figure III-6 – Representative example of a stress–strain curve for the mColl:mBAp composite scaffolds.

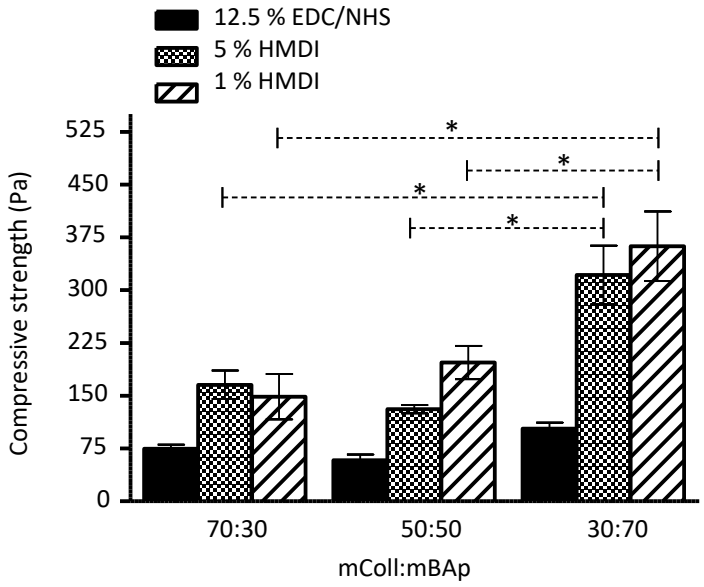

Figure III-7 – Compressive modulus of mColl:mBAp scaffolds crosslinked under different conditions. Kuskal-wallis test with Dunn's Multiple comparison test with a p value lower than 0.05 (*p<0.05) was considered statistically significant.

III-4.6. Cell viability in the composite scaffolds

In order to guarantee that the processing method did not result in any harmful residual compound, the metabolic activity of the osteoblast-like cell line (Saos-2) cultured in the scaffolds for 3 days was assessed.

Comparing the two graphs of the *in vitro* metabolic activity analysis (**Figure III-8**), we can observe better results for the 12.5% EDC/NHS crosslinked scaffolds suggesting a higher cytotoxic effect of HMDI crosslinker. Similar results were achieved within the different mColl:mBAp EDC/NHS formulations, while for the HMDI crosslinked structures higher variability among the different formulations was observed.

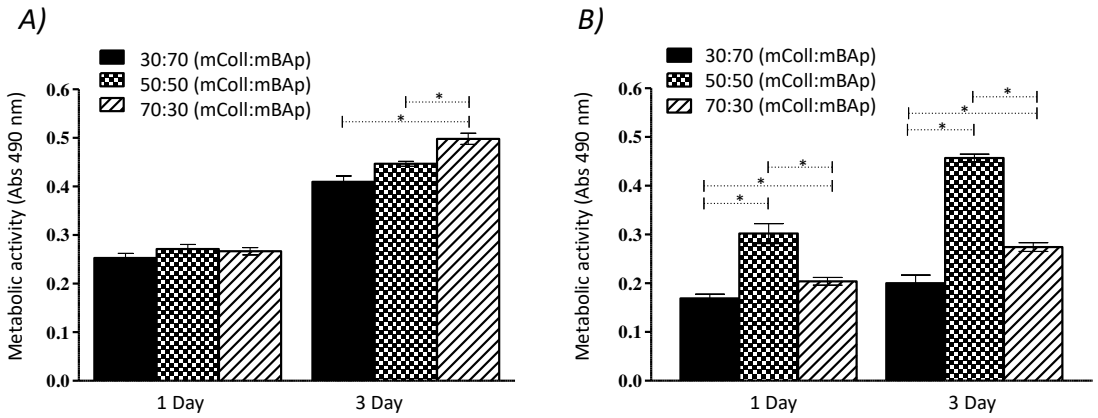

Figure III-8 – Metabolic activity of Saos-2 cells cultured in contact with mColl:mBAp scaffolds crosslinked with A) 12.5% EDC/NHS and B) 5 % HMDI. Results are the mean ± standard error of three independent experiments. Statistical analysis was performed using Kuskal-wallis test with Dunns Multiple comparison Test (* $p < 0.05$).

Considering both the structural stability and the metabolic activity results, the composite scaffolds crosslinked with 12.5% EDC/NHS were selected to further proceed with the biological performance assessment. Live/dead assay was then carried out to complement the MTS assay aiming to confirm the viability of the cells within the 3D structures and along culture. CLSM analysis showed the ability of the scaffolds to support osteoblasts-like cell culture as demonstrated by the viability of the majority of the cells that are within the structures up to 3 days of culture (**Figure III-9**).

Such results confirm the positive effects of the bioapatite presence on cell biological activity already demonstrated in previous works [40-42]. In that sense, fish species can be used as a cheap source to obtain natural calcium phosphates with excellent biological properties.

From this, the selected composite scaffolds exhibited appropriated properties to be further considered for bone regeneration strategies, namely to consider its combination with stem cells promoting its differentiation towards the osteogenic lineage.

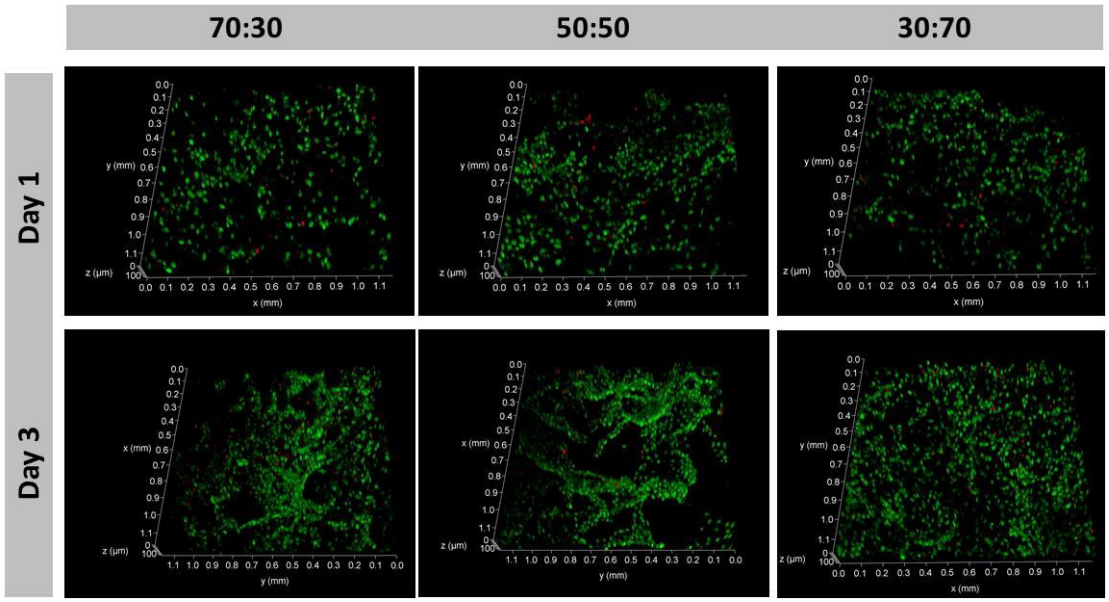

Figure III-9 – Saos-2 cell line adhered on 12.5% EDC/NHS composites 24h hours after seeding and remains viable after 72h. The majority of the cells are viable (green) as demonstrated by the abundant AM stained cells in relation to the PI stained dead cells (red).

III-5. CONCLUSION

Marine organisms emerge as an attractive alternative to mammalian ones as raw-materials for the production of biomaterials despite the challenge to process high-quality and low cost bioactive compounds from fish waste.

The feasibility to fabricate collagen:apatite scaffolds from by-products of marine resources, with a homogeneous distribution of apatite particles throughout the collagen matrix was successfully accomplished in this work. Despite scaffolds properties being affected by different parameters, such as the mColl:mBAp ratio and the crosslinker agent, bioactive stable composite structures were developed. Marine origin Coll:mBAp scaffolds crosslinked with 12.5% EDC/NHS appear to be suitable as potential structures for bone regeneration therapeutic approaches. Their potential to promote osteogenic differentiation is now ongoing work in our lab.

III-6. ACKNOWLEDGMENTS

This work was supported by POCTEP Project 0687_NOVOMAR_1_P, Atlantic Area Transnational Cooperation Programme, Project MARMED (2011-1/164) and FP7 project POLARIS (REGPOT-CT2012-316331). The authors acknowledge also the Centro Tecnológico del Mar (CETMAR, Vigo, Spain) and COPEMAR SA (fishing company, Spain) for the fish by-products. JMS and RP thank FCT respectively for the Post-Doctoral fellowship financed by POPH/FSE (SFRH/BPD/70230/2010) and for the contract IF/00347/2015 and GSD thanks the Doctoral Programme NORTE-08-5369-FSE-000044, supported by Norte Portugal Regional Operational Programme (NORTE 2020).

III-7. REFERENCES

1. Calori, G., et al., *The use of bone-graft substitutes in large bone defects: any specific needs?* Injury, 2011. 42: p. S56-S63.
2. Murugan, R. and S. Ramakrishna, *Development of nanocomposites for bone grafting.* Composites Science and Technology, 2005. 65(15): p. 2385-2406.
3. Lichte, P., et al., *Scaffolds for bone healing: concepts, materials and evidence.* Injury, 2011. 42(6): p. 569-573.
4. Pallela, R., et al., *Biophysicochemical evaluation of chitosan-hydroxyapatite-marine sponge collagen composite for bone tissue engineering.* Journal of Biomedical Materials Research Part A, 2012. 100(2): p. 486-495.
5. Silva, T.H., et al., *Materials of marine origin: a review on polymers and ceramics of biomedical interest.* International Materials Reviews, 2012. 57(5): p. 276-306.
6. Kim, S.-K. and E. Mendis, *Bioactive compounds from marine processing byproducts–a review.* Food Research International, 2006. 39(4): p. 383-393.
7. Boutinguiza, M., et al., *Biological hydroxyapatite obtained from fish bones.* Materials Science and Engineering: C, 2012. 32(3): p. 478-486.
8. Hoyer, B., et al., *Biomimetically mineralized salmon collagen scaffolds for application in bone tissue engineering.* Biomacromolecules, 2012. 13(4): p. 1059-1066.
9. Pallela, R., et al., *Applications of marine collagen-based scaffolds in bone tissue engineering*, 2013, CRC Press: Boca Raton, FL, USA. p. 519-528.

10. Silva, T.H., et al., *Marine origin collagens and its potential applications.* Marine Drugs, 2014. 12(12): p. 5881-5901.
11. Gómez-Guillén, M., et al., *Functional and bioactive properties of collagen and gelatin from alternative sources: A review.* Food Hydrocolloids, 2011. 25(8): p. 1813-1827.
12. Fernandes-Silva, S., et al., *Porous hydrogels from shark skin collagen crosslinked under dense carbon dioxide atmosphere.* Macromolecular Bioscience, 2013. 13(11): p. 1621-1631.
13. López-Álvarez, M., et al., *The improved biological response of shark tooth bioapatites in a comparative in vitro study with synthetic and bovine bone grafts.* Biomedical Materials, 2016. 11(3): p. 035011.
14. Enax, J., et al., *Structure, composition, and mechanical properties of shark teeth.* Journal of Structural Biology, 2012. 178(3): p. 290-299.
15. Tian, M., et al., *In vivo study of porous strontium-doped calcium polyphosphate scaffolds for bone substitute applications.* Journal of Materials Science: Materials in Medicine, 2009. 20(7): p. 1505-1512.
16. Rodríguez-Ortiz, M.E., et al., *Magnesium modulates parathyroid hormone secretion and upregulates parathyroid receptor expression at moderately low calcium concentration.* Nephrology Dialysis Transplantation, 2014. 29(2): p. 282-289.
17. Miki, H., P.B. Maercklein, and L.A. Fitzpatrick, *Effect of magnesium on parathyroid cells: evidence for two sensing receptors or two intracellular pathways?* American Journal of Physiology-Endocrinology and Metabolism, 1997. 272(1): p. E1-E6.
18. Staiger, M.P., et al., *Magnesium and its alloys as orthopedic biomaterials: a review.* Biomaterials, 2006. 27(9): p. 1728-1734.
19. Yamasaki, Y., et al., *Synthesis of functionally graded MgCO3 apatite accelerating osteoblast adhesion.* Journal of Biomedical Materials Research, 2002. 62(1): p. 99-105.
20. Wiegand, A., W. Buchalla, and T. Attin, *Review on fluoride-releasing restorative materials—fluoride release and uptake characteristics, antibacterial activity and influence on caries formation.* Dental Materials, 2007. 23(3): p. 343-362.
21. LeGeros, R., *Chemical and crystallographic events in the caries process.* Journal of Dental Research, 1990. 69(2 suppl): p. 567-574.
22. Sotelo, C.G., et al., *Characterization of collagen from different discarded fish species of the West coast of the Iberian Peninsula.* Journal of Aquatic Food Product Technology, 2015(just-accepted).

23. Delgado, L.M., A. Pandit, and D.I. Zeugolis, *Influence of sterilisation methods on collagen-based devices stability and properties.* Expert Review of Medical Devices, 2014. 11(3): p. 305-314.
24. Kokubo, T. and H. Takadama, *How useful is SBF in predicting in vivo bone bioactivity?* Biomaterials, 2006. 27(15): p. 2907-2915.
25. Diogo, G., et al., *Manufacture of β-TCP/alginate scaffolds through a Fab@ home model for application in bone tissue engineering.* Biofabrication, 2014. 6(2): p. 025001.
26. López-Álvarez, M., et al., *In vivo evaluation of shark teeth-derived bioapatites.* Clinical Oral Implants Research, 2017. 28(9).
27. Hucrrns, J.M., M. ClvrnnoN, and A.N. MInuNo, *Rare-earth-element ordering and structural variations in natural rare-earth'bearing apatites.* American Mineralogist, 1991. 76: p. I165-1173.
28. Hughes, J.M., B.L. Jolliff, and J. Rakovan, *The crystal chemistry of whitlockite and merrillite and the dehydrogenation of whitlockite to merrillite.* American Mineralogist, 2008. 93(8-9): p. 1300-1305.
29. Piccirillo, C., et al., *Extraction and characterisation of apatite-and tricalcium phosphate-based materials from cod fish bones.* Materials Science and Engineering: C, 2013. 33(1): p. 103-110.
30. Johnson, A.J.W. and B.A. Herschler, *A review of the mechanical behavior of CaP and CaP/polymer composites for applications in bone replacement and repair.* Acta Biomaterialia, 2011. 7(1): p. 16-30.
31. Angele, P., et al., *Influence of different collagen species on physico-chemical properties of crosslinked collagen matrices.* Biomaterials, 2004. 25(14): p. 2831-2841.
32. Bax, D.V., et al., *Fundamental insight into the effect of carbodiimide crosslinking on cellular recognition of collagen-based scaffolds.* Acta Biomaterialia, 2017. 49: p. 218-234.
33. Kokubo, T., H.-M. Kim, and M. Kawashita, *Novel bioactive materials with different mechanical properties.* Biomaterials, 2003. 24(13): p. 2161-2175.
34. Liu, Q., J. De Wijn, and C. Van Blitterswijk, *A Study on the Grafting Reaction of Isocyanates with Hydoxyapatite Particles.* HYDROXYAPATITE/POLYMER COMPOSITES FOR BONE REPLACEMENT, 1998: p. 97.
35. Jones, A.C., et al., *The correlation of pore morphology, interconnectivity and physical properties of 3D ceramic scaffolds with bone ingrowth.* Biomaterials, 2009. 30(7): p. 1440-1451.

36. Li, X. and J. Chang, *Preparation of bone-like apatite–collagen nanocomposites by a biomimetic process with phosphorylated collagen.* Journal of Biomedical Materials Research Part A, 2008. 85(2): p. 293-300.

37. Liu, Y., J. Lim, and S.-H. Teoh, *Review: development of clinically relevant scaffolds for vascularised bone tissue engineering.* Biotechnology Advances, 2013. 31(5): p. 688-705.

38. Chai, Y.C., et al., *Current views on calcium phosphate osteogenicity and the translation into effective bone regeneration strategies.* Acta biomaterialia, 2012. 8(11): p. 3876-3887.

39. Kane, R.J., et al., *Hydroxyapatite reinforced collagen scaffolds with improved architecture and mechanical properties.* Acta Biomaterialia, 2015. 17: p. 16-25.

40. Nam, S., et al., *Odontogenic differentiation of human dental pulp stem cells stimulated by the calcium phosphate porous granules.* Journal of tissue engineering, 2011: p. 812547.

41. Gentleman, E., et al., *Surface properties and ion release from fluoride-containing bioactive glasses promote osteoblast differentiation and mineralization in vitro.* Acta Biomaterialia, 2013. 9(3): p. 5771-5779.

42. Niu, Y., et al., *Development of a bioactive composite of nano fluorapatite and poly (butylene succinate) for bone tissue regeneration.* Journal of Materials Chemistry B, 2014. 2(9): p. 1174-1181.

Chapter IV

In vivo Assessment of Marine vs Bovine Origin Collagen-based Composite Scaffolds Promoting Bone Regeneration in a New Zealand Rabbit Model

Chapter IV

In vivo Assessment of Marine vs Bovine Origin Collagen-based Composite Scaffolds Promoting Bone Regeneration in a New Zealand Rabbit Model[1]

IV-1. ABSTRACT

The ability of human tissues for self-repair is limited, which motivates the scientific community to explore new and better therapeutic approaches for tissue regeneration. Collagen and calcium phosphates-based materials, including marine origin materials, are of special interest for Tissue Engineering (TE) applications, particularly in the orthopedic field, due to their close resemblance with the native tissue constitution. Due to the small amount of *in vivo* works performed with marine origin materials, its full potential is yet to be explored. The present manuscript provides a comparative study between a marine-based composite biomaterial and another composed by well-established counterparts (bovine-based composite biomaterial). Blue shark collagen was combined with bioapatite obtained from blue shark's teeth, while bovine collagen was combined with synthetic hydroxyapatite to produce 3D composite scaffolds by freeze-drying. Collagens' characterization showed similar profiles, while apatite particles differed in their composition, being the marine bioapatite a fluoride-enriched ceramic. The 3D microarchitecture was similar for both produced composite scaffolds; however, better mechanical properties were observed for the blue shark collagen:bioapatite composite. To assess their clinical potential, the *in vivo* performance regarding bone tissue regeneration was evaluated in critical-size femoral condyle defects created in New Zealand rabbits. The results (percentage of bone volume (%), trabecular thickness (μm), trabecular separation (μm), and bone mineral density ($g.cm^{-3}$)) did not show significant differences between both scaffolds formulations. However, the degradation and reabsorption rate seemed to be faster for the bovine-origin composite, which highlights a better mechanical support for the marine-origin one.

[1]This chapter is based on the following publication:

Diogo G. S, Permury M., Marques C.F., Sotelo C. G., Pérez-Martín R. I., Serra J., González P., Munõz F., Pirraco R. P., Reis R.L., Silva T. H., *In vivo assessment of marine vs bovine origin composite scaffolds in a New Zealand rabbit model. (Submitted).*

IV-2. INTRODUCTION

In the orthopedic field, allografts, artificial bone grafts and, particularly, autografts, are still the golden standard treatments for critical-size bone defects [1]. However, the limited availability of donor tissue, the morbidity and ultimately, the poor efficiency of these treatments have been driving the scientific community to investigate alternative routes [1, 2]. Thus, many different tissue engineering (TE) approaches have been proposed to improve bone regeneration, being the 3-dimensional (3D) structures the first option since they can recapitulate in a more realistic way the spatial microarchitecture of the native bone [3]. For that, customization by applying different materials composition and processing technologies have been explored to design 3D structures with appropriated mechanical, degradation, and biological properties.

Collagen-based solutions still stand out as particularly promising biomaterials since they offer attractive biological cues that encourage cell and tissue integration *in vivo* with a reduced inflammatory response and, additionally, represent biodegradation and bioresorbability capabilities. Within the "collagen world", mammalian origin collagens still occupy the leaders' position. However, the risk of disease transmission to humans, such as bovine spongiform encephalopathy (BSE), and the associated religious constraints together with ethical perspectives refraining the use of materials from mammal origin, have been limiting its use [4]. In this perspective and considering the growing need for collagen-based therapeutic approaches and the limited sources for safer collagen, the exploration of marine organisms has been increasing, from different fish species to other marine organisms like jellyfish, sponges and mollusks [5].

In vitro, the cytocompatibility of marine-derived biomaterials has been assessed with different cell lines but also with stem cells and the results are promising [6, 7]. Human mesenchymal stem cells cultured on tilapia collagen coated dishes revealed similar cytocompatible results to porcine collagen coated dishes [8]. Collagen from blue shark *Prionace glauca* was used to produce 3D composite scaffolds and the results exhibited better cytocompatibility when compared with bovine collagen scaffolds [7]. Despite the exponential increase of marine origin studies reported in the last years, only a few *in vivo* studies have been described [9-11]. In general, fish derived collagens have lower denaturation temperatures, which may have a negative impact when tested *in vivo* due to its fast biodegradation, eventually contributing to the small amount of *in vivo* works arising from the application of marine origin-materials. In this regard, many different techniques of structures manufacturing are

commonly used to increase collagen stability. Hassanbhai *et al.* did show an higher denaturation temperature of electrospun tilapia collagen membranes when crosslinked with glutaraldehyde, in comparison with a commercial available porcine collagen membrane, Bio-Gide® [12]. The membranes were not cytotoxic and even with their faster *in vivo* degradation, the immune response was similar with that of porcine. Also, Nagai *et al.* revealed outstanding results with scaffolds made of salmon collagen. The crosslinked scaffolds showed a similar microarchitecture and cell proliferation rate comparatively to bovine collagen scaffolds [13].

Bone grafts of natural origin obtained from non-human species, including marine origin by-products, has received much attention in last decades, particularly shark tooth from 2 commercial species, *Isurus oxyrinchus* and *Prionace glauca* [14, 15]. Shark tooth is gaining increasing recognition as a promising, eco-friendly source of bioapatites, since it is an abundant by-product of fishing and environmentally sustainable. The incorporation of the marine bioapatite particles into a marine collagen matrix can be a perfect combination to ensure good performance in hard tissue applications.

Based on our previous outcomes [16], the present work was designed with two purposes: firstly, to validate the *in vivo* potential of using blue shark origin collagen:bioapatite composites scaffolds for regeneration of bone defects; secondly, to compare an entire marine-based biomaterial with one composed by bovine collagen and synthesized hydroxyapatite when implanted *in vivo*. The motivation for selecting bovine collagen and synthetic apatite, as comparison materials, is based on a market assessment, where it was found that most of the collagen and apatite products already in commercialization have bovine and synthetic origin, respectively. Bovine collagen is highly available being mostly obtained from bovine discards, such as hides, tendons and bones, by-products of meat production [17, 18]. Synthetic hydroxyapatite is often used for biomedical applications, mostly because of the non-risk of disease transmission, its predictable homogeneous composition and its low sourcing costs. Critical-size bone defects were created in rabbit models and the biomaterials were implanted, evaluating new bone tissue formation twelve weeks post-implantation, namely addressing the percentage of bone volume, trabecular thickness, trabecular separation, and bone mineral density by micro computed tomography.

IV-3. MATERIALS AND METHODS

IV-3.1. Materials origin

Skin and teeth of blue sharks were obtained from Centro Tecnológico del Mar (CETMAR, Vigo, Spain) and COPEMAR SA (fishing company, Spain).

Collagen was isolated from blue shark (*Prionace glauca* (PG)) and bovine skin. Biological apatite (BAp) was obtained from the teeth of *Prionace glauca* and *Isurus oxyrinchus* and commercial apatite (Ap) was obtained from Plasma Biotal Ltd (Derbyshire, UK).

IV-3.2. Collagen extraction procedure

Marine collagen (mColl) and bovine (bColl) origin collagen were extracted through a very well established acid solubilization method [19]. The process was divided in three main steps: processing of raw materials, that includes size reduction and cleaning followed by pre-treatment with an alkaline solution (0.1 M NaOH, 24 h at 4 °C) to remove non-collagenous proteins; the second step was the extraction of collagen with 1 M acetic acid solution ((1:10 (w:v)) for 72 h at 4 °C. The extracted collagen was precipitated overnight with 2 M NaCl and separated by centrifugation. For purification, the separated collagen was once again solubilized in acetic acid and subjected to a dialysis process with successive decreasing concentrations of acetic acid, for 8 days, to remove any residual contaminations. The final collagen was then freeze-dried.

IV-3.2.1. Amino acid profile

To characterize the extracted marine collagen (mColl) and bovine collagen (bColl), the amino acid composition was quantitatively assessed by using a Biochrom 30 (Biochrom Ltd, Cambridge, U.K) at Centro de Investigaciones Biológicas of the Spanish National Research Council (CSIC), in Madrid (Spain). After extraction, both origin collagens were hydrolyzed and separated through a cation-exchange resin column accordingly to a procedure developed by Spackman, More and Stein in 1958 [20]. The column eluent was mixed with ninhydrin reagent to react with the aminoacids. The colored compounds resulting from the reaction were analyzed at two different wavelengths, 440 and 570 nm.

The quantitative analysis was carried out using Norleucine as an internal standard. The represented results correspond to a mean of three independent measurements.

IV-3.2.2. Fourier transform infrared spectroscopy

To study and compare the chemical composition of both collagens, Fourier transform infrared spectroscopy (FTIR) under an attenuated total reflectance (ATR) (IR Prestige 21, Shimadzu) was carried out. Marine and bovine lyophilized collagen was mixed with potassium bromide (KBr) (1:100, wt.%) and then uniaxially pressed to obtain a transparent disk. Each infrared spectrum was the average of 32 scans collected at 2 cm^{-1} resolution in the wavenumber region of 3500-500 cm^{-1} at room temperature (RT).

IV-3.2.3. Sodium dodecyl sulfate-polyacrylamide gel electrophoresis (SDS-PAGE)

The protein molecular mass was studied by using a 7% polyacrylamide SDS-PAGE characterization gel. SDS-PAGE was prepared by using reagents from sigma and casted on a Biorad Mini Protean II System. Solubilized collagen was mixed with a buffer and heated at 95 °C for 5 min into a digital thermoblock TD150P3 (FALC) until proteins denaturation. After, 8 µL sample loading volume (10 µg per lane) was used. Also, 3 µL of protein marker was loaded with the samples. Electrophoresis was carried out at 75 V for 15 min followed by 150 V until the frontline reached the lower part of the gel. After running, the gel was stained with Coomassie blue R-250 in methanol (50%) and acetic acid (10%) for 30 min followed by destaining with methanol (5%) and acetic acid (7%). Commercial bovine type I collagen (Sigma, Portugal) was used as control.

IV-3.3. Preparation of marine bioapatite particles extracted from blue shark teeth

The biopatite (BAp) particles were extracted from the teeth of *Isurus oxyrinchus* and *Prionace glauca*, provided by Centro Tecnológico del Mar (CETMAR, Vigo, Spain) and by the fishing company COPEMAR S.A. (Porto de Vigo, Spain) [14]. For teeth isolation, the heads of mako shark *Isurus oxyrinchus* and blue shark *Prionace glauca* were boiled in water for 3 h for teeth removal. After, teeth were cleaned and washed, followed by drying at 60 °C for 24 h. For particle size homogeneity, the teeth were ground in a ball mill (Retsch MM2000) for 5 min, with an oscillation frequency between 90 to 100

Hz for powder size of 100 to 0.1 μm. The ground teeth were pyrolyzed at 950 °C for 12 h, to remove the organic material, with a heating ramp of 2 °C/min and a cooling ramp of 20 °C/min. The resulting particles of apatite were separated by sieves below 63 μm of particle size.

IV-3.4. Apatite particles characterization

IV-3.4.1. X-ray diffraction pattern

The crystallinity of the marine BAp particles was studied and compared with the synthetic origin Ap particles by using an x-ray diffractometer. The diffraction measurements were performed using a conventional Bragg–Brentano diffractometer (Bruker D8 Advance DaVinci, Germany) equipped with CuKα radiation. Data sets were collected in the 2θ range of 10 – 60° with a step size of 0.02° and 1 s for each step.

IV-3.4.2. Coulter analysis

The physical characteristics (particle size and particles size distribution) of both the bioapatite (obtained from mako and blue shark teeth) and synthetic apatite powders were evaluated using a particle size analyzer (COULTER LS230, UK), with Fraunhofer optical model. This technique uses electrical impedance to measure the volume of particles as they individually pass through an aperture of defined size.

IV-3.4.3. Scanning electron microscopy (SEM)

SEM analysis was used for two purposes: to study the morphology of the apatite powders and to study the produced scaffolds' surface properties. Dried samples were coated with gold to increase conductivity and were analyzed in a scanning electron microscope (JSM-6010 LV, JEOL, Japan) at 20 kV using different magnifications.

IV-3.5. Preparation of scaffolds

For scaffolds production, a freeze-drying technique was employed, as described before [16]. The isolated freeze-dried collagens were solubilized at 1.5% (w/v) in a 0.5 M acetic acid solution. After, marine BAp or synthetic hydroxyapatite (Plasma Biotal Ltd, UK) were added to the mColl and bColl solutions, respectively. The final mixtures had in their constitution 30% of collagen and 70% of apatite particles (w/w), resulting in 2 different scaffolds formulations: mColl:BAp and bColl:Ap. To increase scaffolds' stability, 1-ethyl-3-(3-dimethylaminopropyl) carbodiimide (EDC) at 12.5% (w/w) was added to promote collagen crosslinking. The reaction was carried at low temperatures (6 °C) for 4 h, being the mixture then poured into a mold and freeze-dried. To wash out any harmful residual compound, all scaffolds were thoroughly rinsed with distilled water immediately before using in cell culture experiments. Scaffold matrices with cylindrical shape (5x5 mm) were used for structural characterization and *in vivo* assessment.

IV-3.5.1. Characterization of scaffolds microarchitecture

The microstructure of the collagen-based composite scaffolds was analyzed using a high-resolution X-ray micro-computed tomography system (Skyscan 1272, Bruker, USA). Dried samples were scanned using a pixel size of 10 μm over a rotation angle of 360º. Porosity, mean pore size, and interconnectivity were assessed after reconstruction of images stacks in a CT-analyzer program by defining a threshold from 30 - 255, to distinguish the composite structure from the pore voids. To understand if the apatite particles were homogenously distributed through the constructs, it was applied a threshold from 65 - 255.

IV-3.5.2. Mechanical assays

The mechanical behavior of both marine and bovine collagen-based 3D constructs was assessed under compression mode using an INSTRON 5540 universal testing machine. Six replicates of each condition were tested with a crosshead speed of 2mm/min and a load cell of 1 kN. The compressive modulus, a measure of material stiffness, was determined from the slope of the linear region of the stress-strain curve.

IV-3.6. *In vivo* evaluation of collagen-based composite scaffolds

IV-3.6.1. Animals

Twelve male New Zealand White rabbits (age between 18 and 21 weeks) weighting 3.7 - 4.0 kg were supplied by a qualified laboratory animal supply center (La Granja cunícola San Bernardo, S.L., Tulebras, Navarra).

The animals were housed in individual enriched cages in the Animal Experimentation Service Facility of the University of Santiago de Compostela (Lugo, Spain) after the ethical approval (procedure code: 03/18/LU-002) as a randomized controlled trial with one inter-subject control.

Animals were maintained under conditions of temperature (15 - 21 °C), humidity, air renewal and cycle time (12 h alternating cycles of light and dark) controlled according to annex II of directive 86/609/EEC. After a quarantine period of three weeks animals were pre-medicated with Ketamine 25mg/kg/i.m. (Ketamidor® 100 $mg.mL^{-1}$), medetomidine 50µg/kg/i.m. (Sededorm® 1 $mg.mL^{-1}$) and buprenorphine 0.03 $mg.kg^{-1}$ (Bupaq® 0.3$mg.mL^{-1}$). The anesthesia was maintained by inhalation of an O_2 and 2% isoflurane mixture using a facemask.

IV-3.6.2. Implants

Cylindrical shape (5 X 5 mm) collagen-based composites were tested. Two different materials and an empty control were randomly assigned to the left or right side according to a computer-generated randomization list until achieving an n=8.

In total, 16 biomaterials and 8 empty defects were placed in 12 animals, two per animal. To avoid errors due to the implantation side, half of each of the biomaterials and half of the empty defects were placed in left femurs and half in rights of each type. The trial period used was 12 weeks

IV-3.6.3. Surgical procedure

Critical-size bone defects with cylindrical shape (5 X 5 mm), were created under aseptic conditions in the distal lateral part of femoral condyles by using a trephine connected to a surgical motor (intrasurg 300, Kavo, Biberach, Germany). After that, the wounds were sutured using a 4-0 vicryl in deep planes

and 3-0 nylon for the skin. The animals were monitored throughout time, the pain was controlled in the first 5 days by using buprenorphine (0.01-0.03 mg/kg/i.m, Buprex, RB Pharmaceuticals) and meloxicam (0.2 mg/kg/ SC, Metacam, Boehringer). As a prophylactic antibiotic enrofloxacin (Syvaquinol® 10% oral) was used for 3 weeks. The animals were sacrificed with an intravenous overdose of isodium pentobarbital (Dolethal, Vétoquinol) after sedation with Ketamine 25mg / kg + medetomidine 50µg / kg + buprenorphine 0.03mg / kg. Subsequently, the distal femurs were recovered by dissection and the use of a bone saw. Specimens were immediately immersed in a 10% buffered formalin solution for a minimum of 2 weeks until the time of processing. For identification we use a code consisting of a number and a letter. The number indicated the animal (from 1 to 12) and the letter the side of the femur (right-R and left-L). All biomaterials were recovered.

IV-3.6.4. Micro-CT of the defects filled with the biomaterials

To evaluate the *in vivo* regeneration of the bone defects created in the rabbit femoral condyles, all samples were micro-CT scanned using the Skyscan x-ray micro-computed tomography 1272 (Skyscan, Kontich, Belgium). Fixed samples were scanned with an aluminum/copper filter at 13 µm pixel size resolution with an X-ray source voltage of 90 kV and current source of 111 µA, 0.4 rotation steps and 2 averaging frames during 0h:56m:36s of scanning. The micro-CT images were reconstructed with NRecon software version 1.1.3 (Skyscan) and the reconstructed images were reoriented with a Dataviewer software version 1.17.0.0 (Skyscan) for subsequent analysis. To qualitatively assess the percentage of bone volume inside of the defect) a cylindrical region of interest (ROI) corresponding to the bone defect size filled with the different structures was applied. Phantoms of 0.25 and 0.75 $g.cm^{-3}$ were scanned and reconstructed with the same parameters for bone mineral density (BMD) calibration. All analyses were performed by trained staff who did not know what material was being analyzed.

IV-4. RESULTS AND DISCUSSION

IV-4.1. Protein profile

Collagen has been extracted from different animals, with three main methods being reported, resulting in salt-soluble collagen (SSC), acid-soluble collagen (ASC), and pepsin-soluble collagen (PSC).

The properties of the produced biopolymer are, thus, directly affected by the species of origin and by the selected method for its extraction. Based on that, blue shark collagen was compared with bovine collagen, golden standard material in biomedical applications, with both being extracted with an acid-based method, to finally prepare collagen-based composites for TE (**Figure IV A**). The high amino acid content, typically characteristic of collagen protein, was demonstrated by quantitative analysis of the amino acid profile (**Figure IV B**). The extracted collagens had a similar profile, being rich in glycine (Gly), proline (Pro) and hydroxyproline (OHPro). Glycine was the highest prevalent amino acid in both collagens, representing around 30% of the total protein. This finding is in good agreement with other studies, since glycine appears regularly at every third residue throughout the collagen molecules [21, 22]. Pro (11.2% of bovine collagen and 10.1% of marine collagen) and OHPro (8.2% and 6.5% of bovine collagen and marine collagen, respectively) were found within the range already described in the literature [20, 23]. Blue shark collagen had a lower Pro and OHPro content in comparison with bovine collagen, following the same tendency generally observed between collagens from marine organisms and from mammals. Animal species living in aquatic environment have lower body temperatures comparatively to terrestrial mammals because of their evolutionary adaptation (in general, marine environment is colder than terrestrial ecosystems and the marine organisms lack the physiological mechanism to maintain a certain body temperature) and the contents of these amino acids are known to be related with the thermal stability of collagens. In fact, these amino acids hold a critical role in the maintenance of the triple-helix structure integrity, which has a high influence on collagen denaturation temperature [24].

FTIR was performed to chemically characterize the extracted collagens (**Figure IV -1C**). The spectra showed very similar profiles for both tested collagens, with the presence of the characteristic peaks of amide A, amide B, amide I, amide II and amide III, assigned to the collagen protein. Amide A peak, typically observed between 3000-3500 cm^{-1}, was seen at 3320 cm^{-1}, as a result of the N-H stretching vibration associated with the intermolecular hydrogen bonding in the carboxyl groups. The amide B peak, relative to the asymmetric and symmetric stretch of CH_2, was identified at 2918 cm^{-1}, even though being less evident for *Prionace glauca* collagen. Strong peaks around 1660 cm^{-1} and 1543 cm^{-1} associated with C=O stretch (amide I) and N-H deformation (amide II), characteristics of proteins, were found in spectra of both collagens. The C-N stretch of amide III was located at 1243 cm^{-1}. The results are in accordance with the chemical pattern of collagen [21].

Shark and bovine skin collagen, isolated in this work, were identified as being mainly type I collagen given the characteristic electrophoretic profile obtained with SDS-PAGE (**Figure IV-1D**). The characteristic alpha 1, alpha 2 and beta components, with alpha 1 being more intense than alpha 2, typically attributed to type I collagen in mammals, were found in both extracted collagens. This finding matches well with the available bovine type I collagen commercialized by Sigma and used as reference material, which suggests the suitability of using blue shark *Prionace glauca* skins as a promising alternative source of collagen.

A)

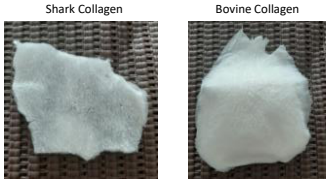

B)

Amino acid (570nm)	*Shark* mol ‰	Bovine
Asp	45	48
Thr	23	18
Ser	44	38
Glu	75	74
Gly	318	323
Ala	118	112
Cys	2	3
Val	21	20
Met	15	12
Ile	17	10
Leu	26	25
Nleu	14	19
Tyr	4	5
Phe	17	17
Ohlys	8	7
His	8	6
Lys	25	25
Arg	52	42
OHpro	**65**	**82**
Pro	**101**	**112**
Total	1000	1000

C)

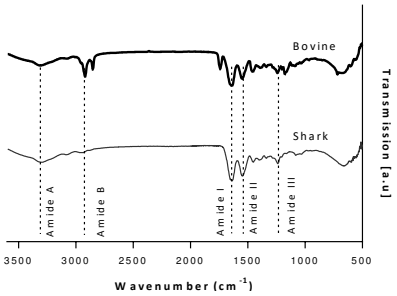

D)

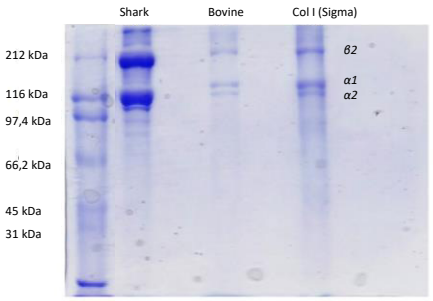

Figure IV-1 - Characterization of blue shark and bovine collagen. A) Lyophilized shark and bovine collagen; B) Amino acid composition. C) FTIR spectra, showing the characteristic profile of collagen protein, namely the several amide peaks. D) SDS-PAGE of shark and bovine extracted collagen exhibiting representative band pattern (α1, α2 and β), together with reference type I collagen.

IV-4.2. Apatite and bioapatite particles characterization

Chemically synthesized apatite particles, like hydroxyapatite (HAp) ($Ca_{10}(PO_4)_6(OH)_2$), are mainly obtained from the reaction of calcium with phosphate solutions. Despite being the first choice within all calcium phosphates sources when considering biomedical use, the distinctive physicochemical properties of synthetic HAp when compared with natural hydroxyapatite, results in a lower biological activity [25, 26] . It has been hypothesised that extracting hydroxyapatite from natural sources, like

bones and teeth, result in apatite particles with preserved chemical and structural properties, which leads to the exploration of new possible sources. In the present work, the potential of using teeth from *Isurus oxyrinchus* and *Prionace glauca* sharks to obtain a biological apatite material was further explored [16]. The thermal conversion of shark teeth, considered a biowaste by the fishing industry, resulted in samples exhibiting an x-ray diffraction pattern characteristic of a crystalline material. The XRD patterns of marine bioapatite particles presented in **Figure IV-2A** confirmed the presence of two phases (one apatite and other non-apatite) with sharp and well defined diffraction peaks, confirming that the pyrolysis was efficient, with no trace of organic material after the heat treatment [16]. The apatite-CaF ($Ca_5(PO_4)_3F$) phase (ICDD 04-016-2909) presented the most intense peaks at 31.87 and 33.04 for the crystal planes (12 1) and (3,0,0), while the non-apatite phase, whitlockite (ICDD 04-079-2186), had the most intense peaks at 31.24 and 34.59 for the crystal planes (0 2 10) and (2 2 0) (**Figure IV-2A**). According to our previous work [16], the marine bioapatite particles extracted from teeth of shark have in their composition, in addition to calcium and phosphorus, other ions such as fluoride, magnesium, sodium, among others, leading to lower Ca/P ratio, justifying the formation of non-apatite phase (whitlockite) [27]. Additionally, the presence of Mg^{2+} promotes the decomposition of apatite phase into whitlockite, because the ionic radius of Mg^{2+} is smaller than that of Ca^{2+} [28]. Commercial synthetic apatite exhibited the characteristic pattern of hydroxyapatite (ICDD 01-089-4405), as expectable, without any other phase.

Particle/agglomerate size distributions (PSD) of marine BAp and commercial Ap powders are presented in **Figure IV-2B**. As depicted in the graph, PSD of Ap resulted in a sharper peak when compared with BAp, suggesting a higher homogeneity of particle size of the former. The measured average particle/agglomerate sizes were 3.511 µm for Ap particles and 17.95 µm for BAp particles (more than 5 times higher), even though, for the BAp the particle size ranged from 1 to 60 µm. SEM micrographs (**Figure IV-2C**) shows the morphological features of BAp and Ap powders. Both powders consisted of small agglomerates with distinctive shaped particles: the BAp particles showing mostly roundish forms, while the Ap had rod-like particle. Comparing the results obtained by coulter analysis with SEM micrographs, it is shown that individual particles of BAp are actually smaller than initially considered, and the high degree of particles agglomeration could be responsible for the higher values of mean particle size obtained from the coulter analysis.

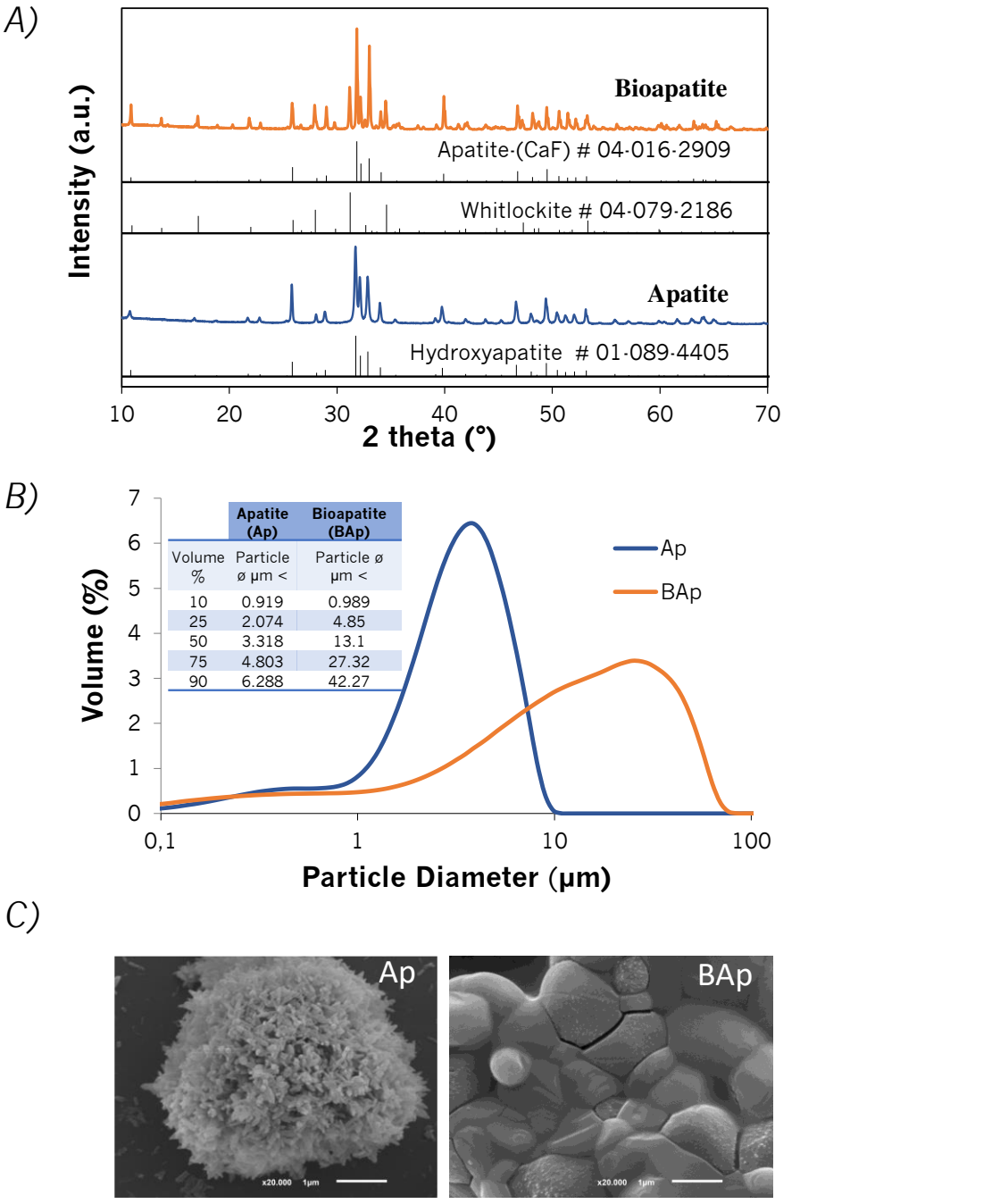

Figure IV-2 - Apatite (Ap) and Bioapatite (BAp) particles characterization. A) X-ray diffraction pattern. B) Coulter analysis illustrating particle size and distribution. C) SEM morphological analysis.

IV-4.3. Microstructure of scaffolds

For the 3D porous structures fabrication, a conventional freeze-drying process was applied. In comparison with other conventional processing methodologies of scaffolds production, like gas foaming and salt leaching, freeze-drying is still considered the most useful technique for fabrication of porous structures with natural polymers [29-31]. It is an advantageous technique for collagen-based scaffolding production because it can almost preserve the native structural form and the biological properties of collagen [32]. The ice crystals growth during the freezing process allows the formation of porous structures and, at same time, the elimination of the solvents during the lyophilization process, without resulting in polymer degradation [29]. SEM microscopy was employed to determine scaffolds' surface morphology. As depicted in **Figure IV-3A**, both collagen-based scaffolds revealed a regular distribution of pores with slight macroscopic differences. It seems that mColl:BAp scaffold formulation resulted in larger pores in comparison with the bovine-based formulation. In contrast, there was an apparently higher tendency for particles agglomeration (see highly magnified SEM images) in the bColl:Ap condition.

Scaffolds microarchitecture features, namely porosity, pore size and interconnectivity, have been described to have a crucial role for the fate of seeded cells, by promoting nutrients and oxygen diffusion into the interior of the structures [33]. Such parameters cannot be rigorously controlled by freeze-drying technique, but can be modulated by varying materials concentration, crosslinking degree and freezing temperature and time. To assess scaffolds internal microarchitecture, quantitative and qualitative micro-CT analysis was performed. To differentiate organic and inorganic components on the sample, a color coding was employed according to materials density, from 0 to 255 (density scale). The green color refers to collagen, while purple represents the densest material, which corresponds to the Ap or BAp particles. The qualitative results (**Figure IV-3B**) showed a better distribution of BAp throughout the marine collagen when compared with Ap distribution within bovine collagen. This is represented by the higher homogeneity of the purple color in the marine-based composite scaffolds, suggesting the feasibility of the method used for the production of these scaffolds.

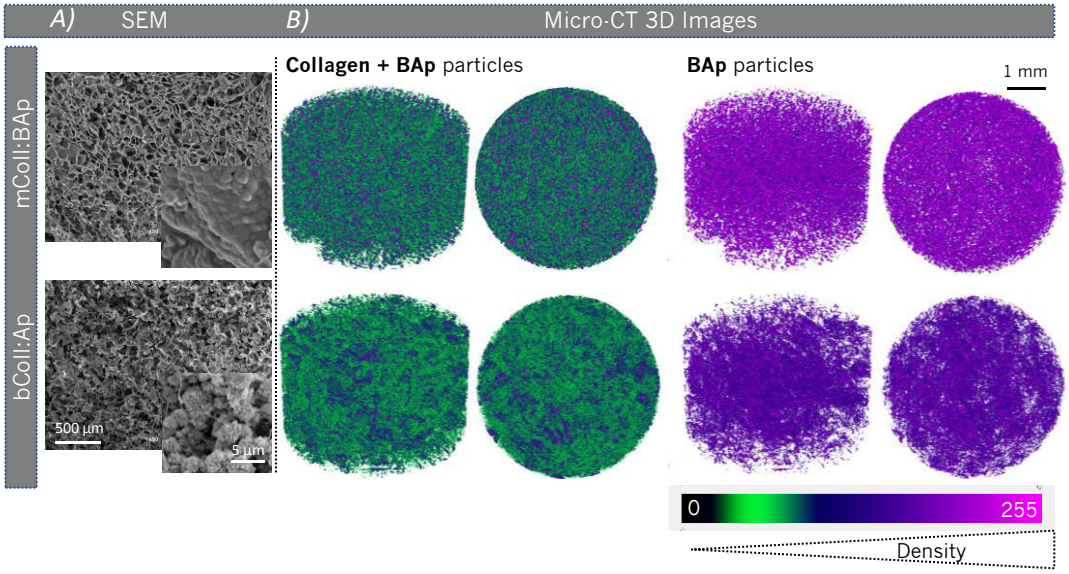

Figure IV-3 - Microarchitecture characterization of the produced composites scaffolds. A) Morphological characterization of scaffolds by SEM analysis. B) Qualitative micro-CT images with green representing less dense material (collagen) and in purple the Ap and BAp particles.

Quantitatively, both groups of scaffolds showed a porous architecture with a pore size distribution from 10 to 600 µm, with more than 50% of pores ranging from 70 to 150 µm (**Figure IV-4A**). Pores with size lower than 100 µm have been found to promote cell adhesion due to their large surface area, while pores larger than 100 µm encourages cell infiltration[34]. In an attempt to explore the potential of using hydroxyapatite particles obtained from fish bones of salmon, Lowe *et al.* prepared 3D composites scaffolds by freeze-dying technique, which exhibited pore size ranging from 23 – 354 µm that revealed to be adequate features to induce periosteum-derived mesenchymal stem cells proliferation and mineralization[35].

Mean pore size calculated in a CT analyzer software after selection of a thresholding from 30 to 255 (to discard void spaces) was higher for mColl:BAp (86.8±3.1) when compared with the bColl:Ap (65.3 ±1.5) formulation (**Figure IV-4B**). Thus, it is expected that cells can colonize faster and more efficiently the marine based composite scaffolds.

In addition, the processing methodology used for scaffolds production resulted in pore interconnectivity (**Figure IV-4C**) varying between 81.9±4.5 and 63.8±4.4 for mColl:mBAp and bColl:Ap, respectively, although no significant statistical differences were observed. High interconnective porous structures are greatly desired for nutrients perfusion and oxygen transport throughout the entire

structure, which ultimately sustain their positive biological performance.

The lowest porosity (58.6±1.5) was found for the bColl:Ap formulation comparatively to mColl:mBAp (73.6±1.5) (**Figure IV-4D**). It is believed that the higher agglomeration of Ap within the bovine collagen matrix, as aforementioned, reduced the nucleation spots for ice crystals formation and growth, resulting in less porous scaffolds.

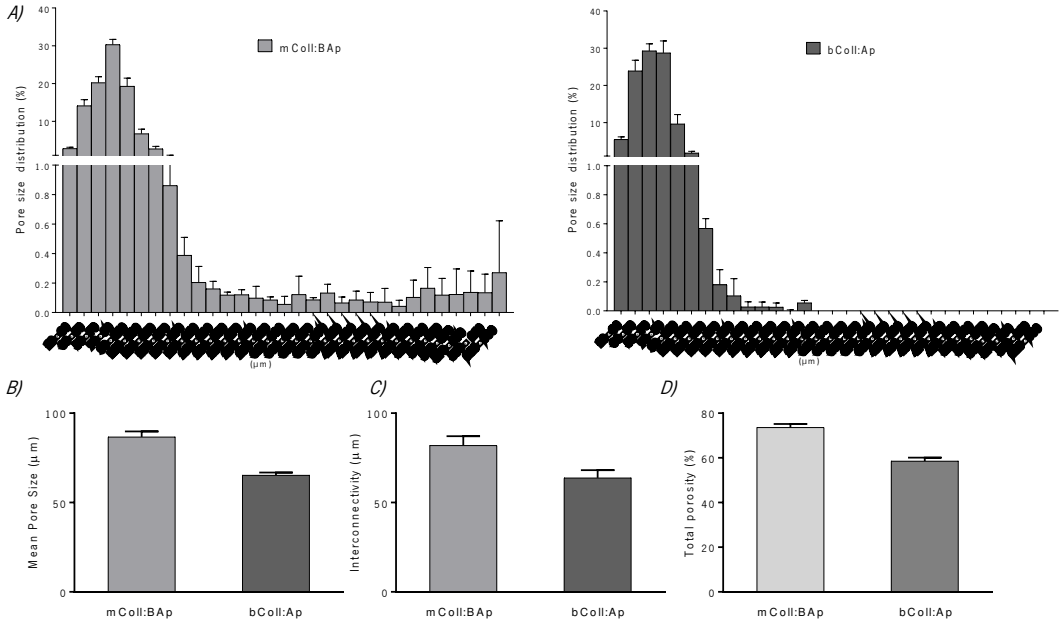

Figure IV-4 - Quantitative micro-CT of the produced collagen-based composite scaffolds. A) Pore size distribution. B) Mean pore size (µm), C) Interconnectivity (%) and D) Total porosity (%). Mann Whitney test was used to compare the two conditions, with a p value lower than 0.05 (*p<0.05) considered statistically significant. No statistical differences were observed between groups.

IV-4.4. Mechanical Properties

Bioengineered scaffolds should provide mechanical structural support and biological cues for cell attachment, while new tissue is formed. Internal scaffolds' microarchitecture, including porosity, pore size and interconnectivity are important features to determine the final mechanical properties. Despite the adequate biochemical features and promised biocompatibility, engineered collagen scaffolds are normally characterized by limited mechanical strength [36]. A popular approach to enhance the collagen mechanical strength is its combination with other robust components, such as ceramics, as it was adopted in this work. The mechanical properties of the developed composite scaffolds were

assessed under uniaxial compression load. The bioapatite reinforced shark collagen scaffolds displayed a higher compression modulus when compared with apatite strengthened bovine collagen scaffolds (**Figure IV-5**). The obtained results can be associated with the higher viscosity of marine collagen due to the selected conditions of processing. The temperature chosen for the crosslinking reaction (4 °C) was advantageous to increase fish collagen viscosity. However, the same was not observed for bovine collagen that is less viscous at lower temperatures. The motivation to select this temperature was based on previous works that reported that marine collagens have inferior viscosity properties and denature at high temperatures, including blue shark collagen [24]. The small differences in terms of biochemical composition can affect collagen behaviour as collagen triple helix structure is highly influenced by the amino acid composition. The lower content of glycine, Pro and OHPro of marine collagen demands a strict control of temperature. In addition, it is described in literature that, generally, unmodified fish origin collagens present lower mechanical strength than the ones extracted from bovine sources, since it is less crosslinked [37]. However, the mechanical properties can be modulated by altering collagen concentration and by applying physical or chemically crosslinking agents. The mechanical properties of the scaffolds herein presented indicate that the chemical reaction with EDC combined with freeze-drying resulted in scaffolds with different properties, being advantageous in improving the mechanical behavior of the blue shark collagen:bioapatite scaffolds comparatively to the bovine collagen:synthetic apatite ones. This result can also be strongly related with the physicochemical properties of fluoride-enriched hydroxyapatite. Previous studies demonstrated that fluoride-enriched apatites increase the mechanical strength of hydroxyapatite. Finally, both scaffolds presented a spongy-like behavior with stress-strain curves characteristic of highly ductile materials. This feature is of great interest to pursue the regeneration of several tissues, including bone defects, due to its easy surgical handling and proper fixation to the site of implantation.

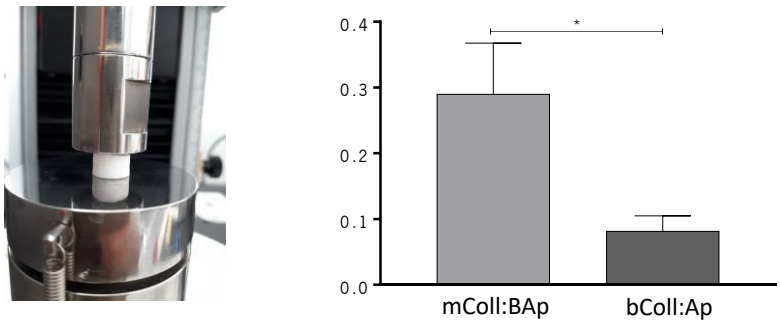

Figure IV-5 - Uniaxial compression tests revealed better mechanical properties for mColl:BAp formulation. Mann Whitney test was used to compare conditions, with a p value lower than 0.05 considered statistically significant (*p<0.05).

IV-5. *IN VIVO* ASSESSMENT – DEFECTS REGENERATION CAPABILITIES

In vivo assessment – Defects regeneration capabilities

Aiming to evaluate the *in vivo* potential of the collagen:apatite produced scaffolds, critical-size bone defects were created in the lateral femoral condyles of New Zealand rabbit models. The materials were implanted in both knees, right and left, with a random distribution. An empty group was used as the control of the experiment. To evaluate the bone defects regeneration, micro-CT analysis of femoral condyles was performed 12 weeks post-implantation. **Figure IV-6**, represents overall the process from the materials origin to materials implantation and analysis.

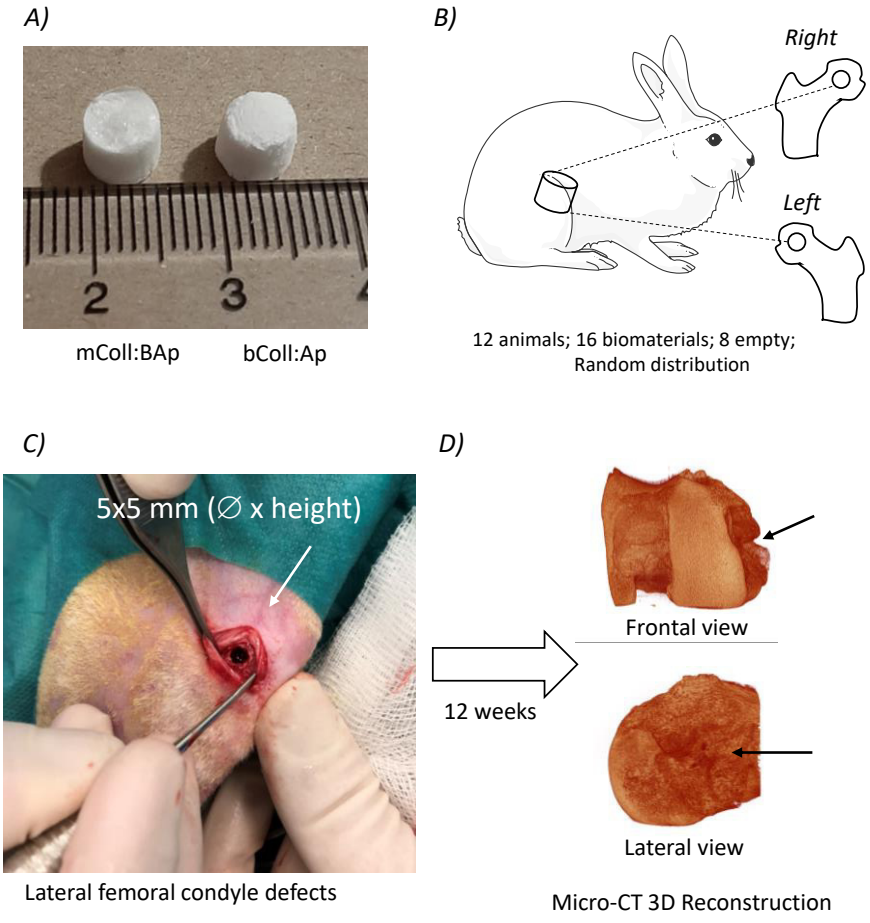

Figure IV-6 - A) Collagen-based composite scaffolds, bColl:Ap and mColl:BAp. B) Schematic representation of the experimental design for materials implantation. C) Surgical procedure. D) Micro-CT evaluation of the regenerated defects.

From qualitative data analysis it was observed that, in general, there was no visible material in the bColl:Ap implanted condyles. In contrast, for the mColl:BAp scaffolds it can still be observed part of the implanted structure in both 2D and 3D images (highlighted by blue arrows) (**Figure IV-7 A,B**). Based on these observations, it is hypothesized that the bColl:Ap structures resorption was faster, with the presence of residual mColl:BAp implanted structures being related with their higher cohesiveness and mechanical properties, as previously discussed. More interestingly, there was bone ingrowth into the middle of the mColl:BAp construct (highlighted by yellow arrows) (**Figure IV-7 A,B**). This result could be greatly influenced by the high pores interconnectivity of the implanted structure that allowed body fluid circulation and cell migration promoting new tissue formation [38], unlike other *in vivo* studies that have been reporting the limited bone tissue penetration due to the poor pores interconnectivity of the implanted constructs. A minimal pore size of 100 μm has been reported to allow bone tissue formation inside the pores of composites, being pores with diameters ranging from 200 to 400 μm considered optimal [39]. In addition, fluoride-enriched apatite has been described as an effective way to decrease apatite solubility. This feature might slow the degradation rate of the construct [40] .

After images stacks reconstruction and repositioning, the 3D micro-CT information was obtained by applying a threshold from 65 to 255, directly proportional to materials density. Nevertheless, in most cases it was difficult to distinguish the implanted material from the new bone formation. Therefore, to make the analysis coherent, the calculated percentage of bone volume refers to new tissue plus scaffold. Percentage of bone volume (new bone formation + scaffold) calculated in a CT analyzer software after a ROI selection resulted in values of 20 ± 7.5% for mCol:BAp and 26 ± 10.0% for bColl:Ap, without significant statistical differences between these values and the observations made in the empty defects (28 ± 6.6 %) (**Figure IV-8**). Twelve weeks after implantation, the percentage of bone volume in the implanted marine collagen-apatite material was as good as other reported ceramic-based materials that demonstrated around 20% of new bone formation [41-43].

The similarities obtained between both collagen-based composites support the use of marine-origin materials as a viable and promising strategy for bone TE scaffolding. The lack of significant statistical differences between the implanted materials with the empty group can be associated with the type of tissue that was formed. The fact of having a similar percentage of bone volume does not mean that the same quality of tissue of produced. Studies have been reporting the incidence of fibrous tissue formation in the absence of bioengineered constructs, since the lack of bioactive cues does not attract the migration of the desired cells into the defect, while promoting the migration of fibroblasts and blood

vessels that fill the empty areas with fibrous tissue [44]. In addition, the preserved mColl:BAp construct 12 weeks post-implantation can be advantageous to provide an adequate long-term mechanical support. It is well-known that a balance between the degradation rate of the structures and the new bone formation is a key factor to determine the success of the implanted materials to regenerate the target tissue [41]. In contrast, the fast resorption rate of the bovine-based structures can compromise an adequate long-term mechanical support.

In terms of trabecular bone thickness, the results did not show significant differences between both composite scaffolds and with the empty group. However, it could be observed that the trabecular separation, corresponding to the void spaces amid the trabeculae (pores), were more homogeneous for the mCol:BAp. Probably, the remaining material together with the newly formed tissue left room for a well-organized matrix distribution, which better guided tissue regeneration. Bone mineral density calculated from calibrated phantoms revealed similar results, 0.32 ± 0.10 $g.cm^{-3}$ for mColl:BAp and 0.37 ± 0.13 $g.cm^{-3}$ for bColl:Ap composite scaffolds' (**Figure IV-7**), which are within the range described in the literature for rabbit models bone density [43, 45].

Taken together, the results of the physical-chemical characterization of collagen-based composite scaffolds and their performance on *in vivo* regeneration of bone tissue in rabbit model suggest the use of marine origin biomaterials as an effective and sustainable alternative to mammals-derived or synthetic materials for the engineering of bone tissue in a regenerative medicine context.

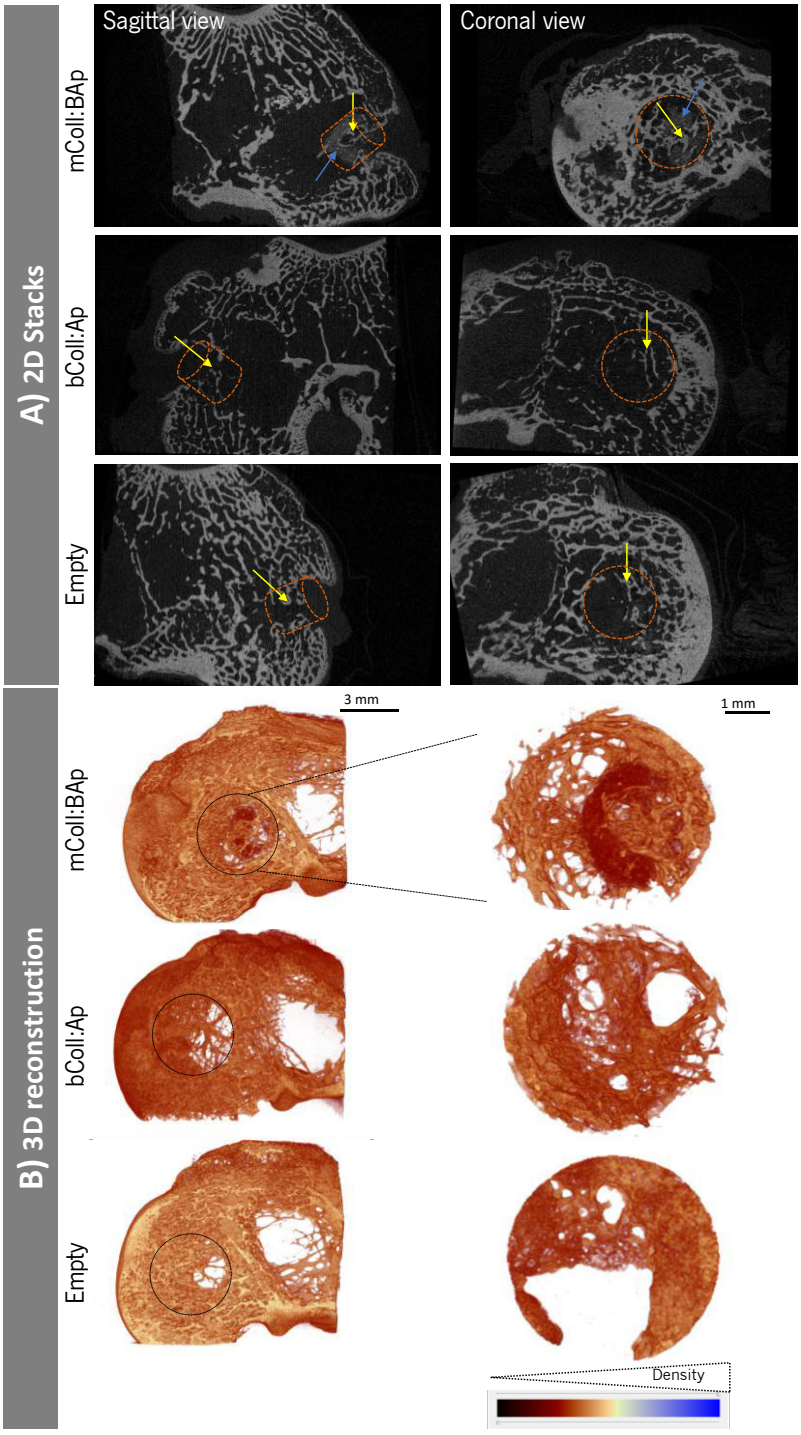

Figure IV-7 - Micro-CT qualitative assessment of the regeneration of bone defects in rabbit femoral condyles treated with mColl:BAp or bColl:Ap composite scaffolds (empty defect used as control). A) 2D micro-CT images from a sagittal and coronal view. Lesioned areas (Region of interest (ROI)) of femoral condyle were highlighted in orange. B) 3D reconstruction of rabbit femoral condyles and the volume of interest (VOI) used for the quantitative analysis, defined as a cylindrical shape of 5 x 5 mm (∅ x height), which coincides with the projected defect filled with the different scaffolds.

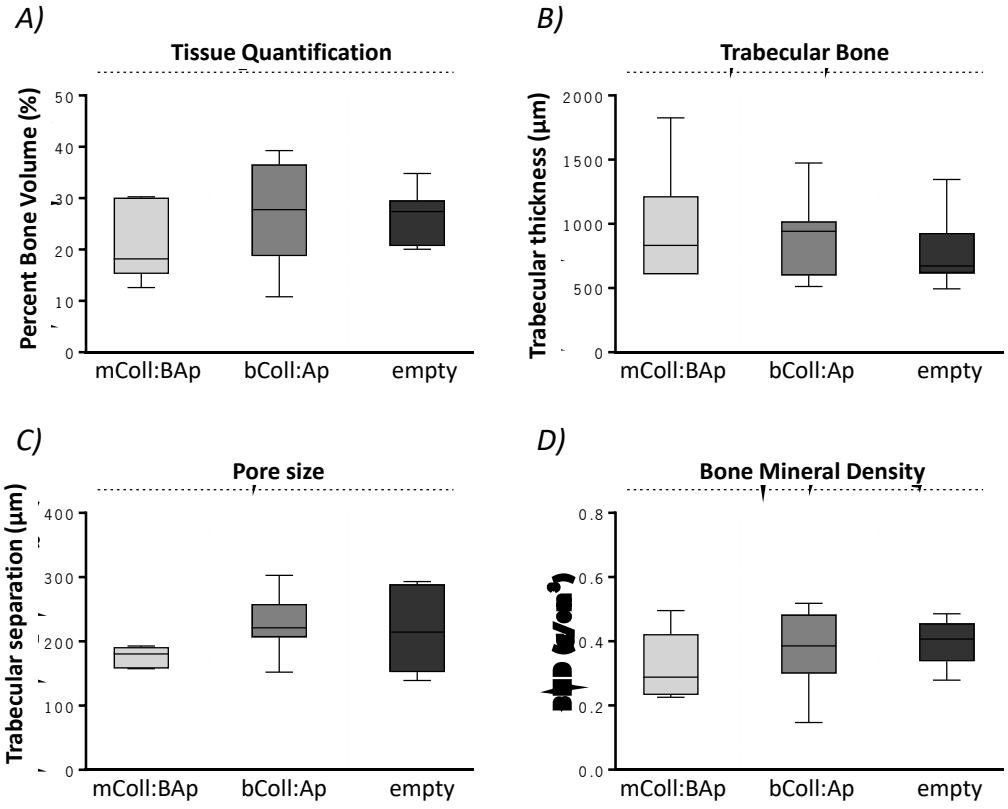

Figure IV-8 - 3D quantitative micro-CT analysis of the new tissue formation in the selected ROIs. A) Tissue quantification (percent bone volume plus scaffold (%)). B) Trabecular thickness (µm). C) Trabecular separation (µm). D) Bone mineral density (g.cm^{-3}). Results are the median (line) ± standard error of 8 samples per structure condition. Statistical analysis was performed using Kuskal-Wallis test with Dunns Multiple comparison Test (* $p < 0.05$). There were no significant differences between groups.

IV-6. CONCLUSIONS

Marine and bovine collagen revealed a similar profile with the presence of α1, α2 and β components, typically characteristics of collagen protein, while the bioapatite and the apatite particles differed in its composition, being bioapatite a fluoride-enriched ceramic. Structures microarchitecture characterization demonstrated that both scaffolds formulations presented high porosities, being the marine origin scaffolds more porous. In addition, bioapatite reinforced fish collagen scaffolds displayed a higher compression modulus when compared with apatite reinforced bovine collagen.

As a first screening to test the produced structures, 8 animals (per condition) were subjected to biomaterials implantation. Tissue quantified inside the defect did not significantly vary between groups treated with each of the scaffolds' formulations. The results suggest that the combination of blue shark collagen and bioapatite particles could result in 3D composites structures with bone regeneration

capabilities, being an attractive choice to regenerate bone defects. However, to make the study more robust, further research is required to confirm their potential and functionality in a long term, perhaps increasing the number of biomaterials to be tested and studying other time points. For instance, the results obtained in this study demonstrated that different origin collagens and apatite particles resulted in different reabsorption rates, suggesting other outcomes is studies using another animal model, namely larger animals and larger bone defects.

The obtained findings can be useful to guide scientists to explore how the different combinations of polymer-ceramic materials can influence bone tissue therapeutic approaches, guiding the physicians to select the right material for each specific treatment, towards a more personalized medicine.

IV-7. Acknowledgments

This study was funded by the Portuguese Foundation for Science and Technology (FCT) under the scope of the BiogenInk project (M-ERA-NET2/0022/2016), by European Regional Development Fund through INTERREG Spain-Portugal Programme, under the scope of 0245_IBEROS_1_E project, through INTERREG Atlantic Area Programme, under the scope of BLUEHUMAN (EAPA_151/2016) project and through Norte de Portugal Regional Operational Program (NORTE 2020), under the scope of Structured project NORTE-01-0145-FEDER-000021. The Doctoral Programme NORTE-08-5369-FSE-000044 supported by NORTE 2020, under the PORTUGAL 2020 Partnership Agreement, through the European Social Fund, is also greatly acknowledge by the PhD fellowship of GSD. RP and CM thank FCT for the contracts IF/00347/2015 and CEECIND/04687/2017, respectively. The authors acknowledge also the Centro Tecnológico del Mar (CETMAR, Vigo, Spain) and COPEMAR SA (fishing company, Spain) for the kind offer of the used by-products for the production of collagen.

IV-8. References

1. Roberts, T.T. and A.J. Rosenbaum, *Bone grafts, bone substitutes and orthobiologics: the bridge between basic science and clinical advancements in fracture healing.* Organogenesis, 2012. **8**(4): p. 114-124.
2. García-Gareta, E., M.J. Coathup, and G.W. Blunn, *Osteoinduction of bone grafting materials for bone repair and regeneration.* Bone, 2015. **81**: p. 112-121.

3. Caddeo, S., M. Boffito, and S. Sartori, *Tissue engineering approaches in the design of healthy and pathological in vitro tissue models.* Frontiers in bioengineering and biotechnology, 2017. **5**: p. 40.
4. Sionkowska, A., et al., *The review of versatile application of collagen.* Polymers for Advanced Technologies, 2017. **28**(1): p. 4-9.
5. Silva, T.H., et al., *Marine origin collagens and its potential applications.* Marine drugs, 2014. **12**(12): p. 5881-5901.
6. Nagai, N., et al., *In vitro growth and differentiated activities of human periodontal ligament fibroblasts cultured on salmon collagen gel.* Journal of Biomedical Materials Research Part A: An Official Journal of The Society for Biomaterials, The Japanese Society for Biomaterials, and The Australian Society for Biomaterials and the Korean Society for Biomaterials, 2007. **82**(2): p. 395-402.
7. Elango, J., et al., *Rheological, biocompatibility and osteogenesis assessment of fish collagen scaffold for bone tissue engineering.* International journal of biological macromolecules, 2016. **91**: p. 51-59.
8. Hsu, H.-H., et al., *Chondrogenic differentiation of human mesenchymal stem cells on fish scale collagen.* Journal of bioscience and bioengineering, 2016. **122**(2): p. 219-225.
9. Mredha, M.T.I., et al., *Anisotropic tough double network hydrogel from fish collagen and its spontaneous in vivo bonding to bone.* Biomaterials, 2017. **132**: p. 85-95.
10. Mori, H., et al., *Development of a salmon-derived crosslinked atelocollagen sponge disc containing osteogenic protein-1 for articular cartilage regeneration: in vivo evaluations with rabbits.* BMC musculoskeletal disorders, 2013. **14**(1): p. 174.
11. Hadzik, J., et al., *A silver carp skin derived collagen in bone defect treatment–A histological study in a rat model.* Annals of Anatomy-Anatomischer Anzeiger, 2016. **208**: p. 123-128.
12. Hassanbhai, A.M., et al., *In vivo immune responses of cross-linked electrospun tilapia collagen membrane.* Tissue Engineering Part A, 2017. **23**(19-20): p. 1110-1119.
13. Nagai, N., et al., *Application of cross-linked salmon atelocollagen to the scaffold of human periodontal ligament cells.* Journal of bioscience and bioengineering, 2004. **97**(6): p. 389-394.
14. López-Álvarez, M., et al., *In vivo evaluation of shark teeth-derived bioapatites.* Clinical Oral Implants Research, 2017. **28**(9): p. e91-e100.

15. López-Álvarez, M., et al., *The improved biological response of shark tooth bioapatites in a comparative in vitro study with synthetic and bovine bone grafts.* Biomedical Materials, 2016. **11**(3): p. 035011.
16. Diogo, G.S., et al., *Marine collagen/apatite composite scaffolds envisaging hard tissue applications.* Marine drugs, 2018. **16**(8): p. 269.
17. Ghodbane, S.A. and M.G. Dunn, *Physical and mechanical properties of cross-linked type I collagen scaffolds derived from bovine, porcine, and ovine tendons.* Journal of Biomedical Materials Research Part A, 2016. **104**(11): p. 2685-2692.
18. Noorzai, S., et al., *Collagen Extraction from Various Waste Bovine Hide Sources.* Waste and Biomass Valorization, 2019: p. 1-12.
19. Sotelo, C.G., et al., *Characterization of collagen from different discarded fish species of the west coast of the Iberian Peninsula.* Journal of aquatic food product technology, 2016. **25**(3): p. 388-399.
20. Alves, A.L., et al., *Cosmetic potential of marine fish skin collagen.* Cosmetics, 2017. **4**(4): p. 39.
21. Sousa, R.O., et al., *Acid and enzymatic extraction of collagen from Atlantic cod (Gadus Morhua) swim bladders envisaging health-related applications.* Journal of Biomaterials Science, Polymer Edition, 2020. **31**(1): p. 20-37.
22. Luca, S., et al., *Marine collagen and its derivatives: Versatile and sustainable bio-resources for healthcare.* Materials Science and Engineering: C, 2020: p. 110963.
23. Tylingo, R., et al., *Isolation and characterization of acid soluble collagen from the skin of african catfish (Clarias gariepinus), salmon (Salmo salar) and baltic cod (Gadus morhua).* J Biotechnol Biomater, 2016. **6**(234): p. 2.
24. Elango, J., et al., *Evaluation of differentiated bone cells proliferation by blue shark skin collagen via biochemical for bone tissue engineering.* Marine drugs, 2018. **16**(10): p. 350.
25. Granito, R.N., et al., *Hydroxyapatite from fish for bone tissue engineering: A promising approach.* International journal of molecular and cellular medicine, 2018. **7**(2): p. 80.
26. Pon-On, W., et al., *Hydroxyapatite from fish scale for potential use as bone scaffold or regenerative material.* Materials Science and Engineering: C, 2016. **62**: p. 183-189.
27. Raynaud, S., et al., *Calcium phosphate apatites with variable Ca/P atomic ratio I. Synthesis, characterisation and thermal stability of powders.* Biomaterials, 2002. **23**(4): p. 1065-1072.

28. Cheng, H., et al., *Synergistic interplay between the two major bone minerals, hydroxyapatite and whitlockite nanoparticles, for osteogenic differentiation of mesenchymal stem cells.* Acta biomaterialia, 2018. **69**: p. 342-351.
29. Perez-Puyana, V., et al., *Influence of the processing variables on the microstructure and properties of gelatin-based scaffolds by freeze-drying.* Journal of Applied Polymer Science, 2019. **136**(25): p. 47671.
30. Chen, L., et al., *Synthesis and cytocompatibility of collagen/hydroxyapatite nanocomposite scaffold for bone tissue engineering.* Polymer Composites, 2016. **37**(1): p. 81-90.
31. Ashokkumar, M. and P.M. Ajayan, *Materials science perspective of multifunctional materials derived from collagen.* International Materials Reviews, 2020: p. 1-28.
32. Lin, K., et al., *Advanced Collagen-Based Biomaterials for Regenerative Biomedicine.* Advanced Functional Materials, 2019. **29**(3): p. 1804943.
33. Marques, C.F., et al., *Novel sintering-free scaffolds obtained by additive manufacturing for concurrent bone regeneration and drug delivery: Proof of concept.* Materials Science and Engineering: C, 2019. **94**: p. 426-436.
34. Zhang, Q., et al., *Pore size effect of collagen scaffolds on cartilage regeneration.* Acta biomaterialia, 2014. **10**(5): p. 2005-2013.
35. Lowe, B., et al., *Preparation and characterization of chitosan-natural nano hydroxyapatite-fucoidan nanocomposites for bone tissue engineering.* International journal of biological macromolecules, 2016. **93**: p. 1479-1487.
36. Khan, F. and M. Tanaka, *Designing smart biomaterials for tissue engineering.* International journal of molecular sciences, 2018. **19**(1): p. 17.
37. Coppola, D., et al., *Marine Collagen from Alternative and Sustainable Sources: Extraction, Processing and Applications.* Marine Drugs, 2020. **18**(4): p. 214.
38. Miño-Fariña, N., et al., *Quantitative analysis of the resorption and osteoconduction of a macroporous calcium phosphate bone cement for the repair of a critical size defect in the femoral condyle.* The Veterinary Journal, 2009. **179**(2): p. 264-272.
39. Flautre, B., et al., *Porous HA ceramic for bone replacement: role of the pores and interconnections–experimental study in the rabbit.* Journal of Materials Science: Materials in Medicine, 2001. **12**(8): p. 679-682.

40. Pajor, K., L. Pajchel, and J. Kolmas, *Hydroxyapatite and Fluorapatite in Conservative Dentistry and Oral Implantology–A Review.* Materials, 2019. **12**(17): p. 2683.

41. Hao, F., et al., *Assessment of calcium sulfate hemihydrate–tricalcium silicate composite for bone healing in a rabbit femoral condyle model.* Materials Science and Engineering: C, 2018. **88**: p. 53-60.

42. Duan, R., et al., *Modulating Bone Regeneration in Rabbit Condyle Defects with Three Surface-Structured Tricalcium Phosphate Ceramics.* ACS biomaterials science & engineering, 2018. **4**(9): p. 3347-3355.

43. Chevrier, A., et al., *Interspecies comparison of subchondral bone properties important for cartilage repair.* Journal of Orthopaedic Research, 2015. **33**(1): p. 63-70.

44. Chen, C.L., et al., *A comparison of the bone regeneration and soft-tissue-formation capabilities of various injectable-grafting materials in a rabbit calvarial defect model.* Journal of Biomedical Materials Research Part B: Applied Biomaterials, 2019. **107**(3): p. 529-544.

45. Chen, H., et al., *Bone marrow stimulation of the medial femoral condyle produces inferior cartilage and bone repair compared to the trochlea in a rabbit surgical model.* Journal of Orthopaedic Research, 2013. **31**(11): p. 1757-1764.

Chapter V

Prionace glauca Skin Collagen Bioengineered Constructs as a Promising Approach to Trigger Cartilage Regeneration

Chapter V

Prionace glauca Skin Collagen Bioengineered Constructs as a Promising Approach to Trigger Cartilage Regeneration[1]

V-1. ABSTRACT

Representing a strategy of marine by-products valorization, based on isolation of biocompounds and assessment of biomedical applicability, the potential of blue shark (*Prionace glauca* (PG)) skin collagen to induce chondrogenic differentiation of human adipose stem cells (hASC) was investigated, with and without exogenous stimulation. For that, a cryogelation method was applied to produce highly interconnected porous 3-dimensional (3D) constructs made of collagen and collagen:hyaluronic acid (20:1). *In vitro* studies reveal that hASC adhere abundantly to the constructs which then promotes the early chondrogenic differentiation of those cells. These findings are supported by the mRNA expression encoding chondrogenic-related markers like Coll II and Sox-9 that are markedly upregulated at an early stage for both conditions, with and without exogenous stimulation. The introduction of hyaluronic acid (Hya) seems to play a crucial role at later time points, as shown by the evident immunodetection of aggrecan (ACAN), even without exogeneous stimulation. It is hypothesized that the PG collagen itself can support chondrogenic differentiation at early time points, but exogenous stimulation is required to ensure phenotype maintenance. The present work highlights the relevance of using blue shark collagen biopolymer as building block to produce highly effective temporary matrices for cartilage applications.

[1]This chapter is based on the following publication:

Diogo G. S., Carneiro F., Freitas-Ribeiro S., Sotelo C. G., Pérez-Martín R. I., Pirraco R. P., Reis R. L., Silva T. H., *Prionace glauca* skin collagen bioengineered constructs as a promising approach to trigger cartilage regeneration. *(Submitted).*

V-2. INTRODUCTION

Considering the avascular nature of the human native cartilage, injuries and degenerative conditions seriously compromise its intrinsic functionalities [1, 2]. Generally, cartilage damages are physiologically irreversible, requiring specific treatments. Many different approaches have been used to treat cartilage lesions including perforations and microfractures; osteochondral autografts, mosaicplasty and allografts transplantation; and autologous chondrocyte implant (ACI) or mesenchymal stem cells (MSCs). ACI approaches can be also used in combination with 3D matrices (matrix-induced autologous chondrocyte implantation, MACI) [3-5].

The standard treatments are inspired in bone marrow stimulation techniques, since they are straightforward, fast and inexpensive. However, in more severe cases wherein the total replacement of the tissue is needed, mesenchymal stem cells stimulation itself is not sufficiently effective [6, 7], with ACI and MACI techniques emerging as promising alternatives to treat larger defects, generally larger than 2.5 cm^2 [3].

Over the past years, bioactive substitutes based on Tissue Engineering (TE) strategies have been thus proposed and developed. Despite the large efforts on the subject, the clinical use of TE 3D structures is still limited to a few commercially available products with the best natural matrix being Chondro-Gide® (Geistlich Pharma AG, Wolhusen, Switzerland) [8]. Chondro-Gide® is a porcine collagen-based matrix established as a first-line treatment when combined with microfracture technique [9]. It is considered a cost-effective one-step technique for the treatment of traumatic cartilage defects offering a helpful environment for mesenchymal stem cells differentiation and new cartilage formation [10]. It can be also used as an MACI approach when cultured with autologous chondrocytes. However, this approach is a time-consuming process since it requires an arthroscopy to isolate the chondrocytes and a culture period before implantation.

Considering the growing life expectancy and the associated rising prevalence of cartilage-related diseases on one side, and the regulatory issues associated with risk of disease transmission when using mammal's origin , on the other side, new collagen sources exploration has been pursued, namely by addressing the marine environment [11-15].

In contrast to humans, pigs, and nearly all other vertebrates, sharks do not undergo endochondral ossification being thus an attractive model for cartilage regeneration especially because their entire skeleton is composed of cartilage [16]. *Prionace glauca* is one of the most caught shark species, most

of it due to bycatch, being its by-products highly available [17]. Collagen isolated from its skin is easily obtained and has shown similar features to that of mammals [18, 19]. In addition, early studies demonstrated that the high orientation of marine collagen can be advantageous to guide cartilage regeneration [20, 21].

In line with this, this work addressed the potential of blue shark *Prionace glauca* (PG) skin collagen-based 3D structures to promote human adipose stem cells (hASC) differentiation into chondrogenic lineage with and without exogeneous stimulation. To enhance the micropore interconnectivity of the constructs, a cryogelation method was applied using blending with hyaluronic acid (Hya) [22]. Interconnective micro-porous structures have shown to promote not only cell adhesion but also cell proliferation and extracellular matrix (ECM) formation and infiltration within the scaffolds, showing great potential for cartilage tissue regeneration, especially when envisioning the use of cell-free strategies.

The obtained results support the biomedical applicability of PG skin collagen, representing a strategy of marine by-products valorization, potentially contributing to Sustainable Development Goal 14 and SDG3.

V-3. MATERIALS AND METHODS

V-3.1. Materials origin

Collagen (mainly type I) was extracted from blue shark (*Prionace glauca*) skin at Instituto de Investigaciones Marinas (CSCI, Vigo, Spain), according to a previously described protocol [19]. After skin cleaning and size reduction, about 10 g of material was subjected to an alkaline treatment (10 volumes of 0.1 M NaOH) under magnetic stirring in a cold room (3 – 5 °C) for 24 h in order to remove the non-collagenous proteins and pigments. By centrifugation, the supernatant was removed, and the residue was washed with distilled water. To start the acid soluble extraction process, 10 volumes of 0.5 M acetic acid was added and maintained in magnetic stirring overnight. The extract was centrifuged at 10°C and the supernatant was dialyzed against distilled water for 2 days in a cold room (3 – 5 °C) and freeze-dried.

Hyaluronic acid sodium salt from Streptococcus equi (Hya) (Molecular weight (Mw):1.5-1.8x10^6) was obtained from Sigma- Aldrich, USA.

V-3.2. Scaffolds' preparation by cryogelation

The cryogelation method was used to produce highly interconnective microporous structures from the use of shark collagen and shark collagen combined with hyaluronic acid [22, 23]. The previously extracted collagen was solubilized in a 10 mM hydrochloric acid (HCl, Sigma-Aldrich, USA) solution at 1% (w/v) of concentration. Hyaluronic acid was solubilized at 0.5% (w/v) in distillated water and added to the collagen solution with a final concentration of 0.05%.

The cryogelation and crosslinking reaction was carried out at low temperatures (-20 °C) for 4 h by the addition of 1-[3-(dimethylamino) propyl]-3-ethylcarbodiimide hydrochloride (EDC) (Mw: 191,70 $g.mol^{-1}$, Sigma-Aldrich, USA) at 60 mM of final concentration. To wash out any harmful residual crosslinker, all cryogels were thoroughly rinsed with distilled water immediately before freeze-drying.

V-3.3. Micro-Computed tomography

The microarchitecture of the dried collagen-based networks was analyzed using a high-resolution x-ray microtomography system skyscan (1272, Bruker, USA). Samples were scanned using a pixel size of 5 µm over a rotation angle of 360°, with a rotation step of 0.4°. Representative data sets of 300 slices were transformed into binary images using a dynamic threshold between 25 - 255 (grey values) to distinguish the polymeric material from pore voids. Such data were used to assess the morphometric analysis, namely structures porosity, pore size, trabecular thickness and pores interconnectivity (CT Analyser, v1.15.4.0, Bruker, USA). 3D virtual models of representative regions in the bulk of the materials were created using an image processing software (CTvox, v 3.0.0, Bruker, USA) [24].

V-3.4. Water uptake capacity

Several testing methods were conducted to demonstrate the main physical and chemical properties of the micelles Water absorption capacity of the different materials was studied by immersion of structures in an aqueous solution [25]. Briefly, the dried samples (n=3) were initially weighted and immersed in PBS during 24 h at 37 °C. After 24 h they were removed from the solutions and quickly blotted on a filter paper. Their weight was measured (wt) and compared to the initial dry weight (w0). The water uptake ratio (wp) was defined according to Eq (1).

$$\text{Eq 1. } wp\ (\%) = (wt - w0) / wt \times 100$$

V-3.5. Rheological properties

The mechanical properties of the structures were evaluated by using a Kinexus pro+rheometer (Malvern Instruments, UK), with a specific acquisition software rSpace (Malvern Instruments, UK). Viscoelastic properties were determined using oscillatory assays that involve the use of two plates (a stationary plate and an oscillatory plate), and a material set between the plates, in which a sinusoidal shear deformation was applied, and the resultant stress response was measured.

The shear strain was achieved through frequency sweep curves, after linear viscoelastic region (LVER) determination. Then, frequency sweep curves were obtained from 0.1 Hz to 10 Hz of frequency, at a shear strain of 0.1% at 37 °C. All these experiments were repeated at least 3 times.

V-3.6. *In vitro* assessment of biocompatibility

V-3.6.1. Cell isolation and expansion

To assess 3D structures potential cytotoxicity, and the suitability to induce and maintain human adipose stem cells (hASC) differentiation, *in vitro* cellular assays were performed. Briefly, hASCs were isolated from the stromal vascular fraction (SVF) of subcutaneous adipose tissue samples of patients submitted to liposuction procedures [26], after informed consent and under a protocol with the department of plastic surgery of Hospital da Prelada (Porto, Portugal) and approved by relevant ethical committees. Cells were expanded in Minimum Essential Medium alpha (α-MEM) (ALFAGENE, Portugal) supplemented with sodium bicarbonate (2.2%) (Sigma-Aldrich, USA), 10% fetal bovine serum (FBS) (ALFAGENE, Portugal), 1% penicillin/streptomycin (ALFAGENE, Portugal) at 37 °C in 5% of CO_2 until passage 3. After 80% of confluence cells were tripsinized with TrypIE™ Express (Life Technologies, USA) and a seeding density of $2x10^6$ cells per scaffold was used based on a top down approach with 50 µL of droplet without additional medium in order to increase seeding efficacy. After 1 h a final volume of 500 µL was completed with culture medium. The culture medium was changed every 2 - 3 days.

V-3.6.2. Cytotoxicity and viability assays

Prior to cell differentiation studies, as a first biological approach and to guarantee that the used materials and the processing methodology did not result in any harmful residual compound, the

metabolic activity of hASC cultured in the structures was evaluated 24 h, 48 h and 72 h after cell seeding. Metabolic activity was determined using a 3-(4,5-dimethylthiazol-2-yl)-5-(3 carboxymethoxyphenyl) 2-(4-sulphofenyl)2*H*-tetrazolium, inner salt (MTS, VWR) assay that quantifies the metabolic activity of the cells by reduction of tetrazolium salt reagent to formazan after a period of incubation (3 h) at 37 °C [24]. Absorbance intensity, which is directly proportional to the metabolic activity, was measured at 492 nm using a microplate reader (Synergy HT, USA). The results are the mean of three independent experiments (n=3) with three replicates for each condition and per experiment.

To qualitatively assess cell viability, calcein-AM (AM)and propidium iodide (PI; Life Technologies, USA) stainings were performed 1 and 7 days after cell culture. Briefly, 1:500 and 1:1000 of AM and PI with a final concentration of 1 $\mu g.mL^{-1}$ and 5 $\mu g.mL^{-1}$ were used. After 10 min in the dark at 37°C in the CO_2 incubator samples were immediately examined using a Zeiss Axio Imager Z1 m fluorescence microscope.

V-3.7. Human adipose stem cells differentiation

The cell-seeded constructs used to study the potential of the structures to promote chondrogenic differentiation were cultured in basal and chondrogenic conditions. The basal conditions were maintained with the same medium used for hASC cells expansion and the chondrogenic conditions were treated with a supplemented medium, namely Minimum Essential Medium alpha (α-MEM) without fetal bovine serum (FBS) supplemented with insulin-transferrin-selenium-G supplement (ITS; Invitrogen), 1 mM dexamethasone (Sigma-Aldrich), 0.1 M sodium pyruvate (Invitrogen), 0.17 mM ascorbic acid-2-phosphate (Wako Pure Chemical Industries, Ltd.), 0.35 mM L-proline (Sigma-Aldrich) and 10 $ng.mL^{-1}$ TGF-3 [27].

V-3.8. Micro-Computed tomography after cell culture

To study the influence of cell culture in the morphological features of the different constructs, the microarchitecture of the dried collagen-based networks was analyzed 21 days after cell culture by using a high-resolution x-ray micro-computed tomography system Skyscan (1272, Bruker, USA), according to the parameters mentioned above. Control scaffolds (scaffolds without seeded cells) were used.

V-3.9. DNA quantification assay

Cell proliferation capacity was evaluated by dsDNA quantification using the Quant-iTPicoGreen dsDNA assay (Alfagene), in which the amount of dsDNA is directly proportional to the cell number. After each culture, samples cultured with hASC under basal and chondrogenic conditions were washed with a PBS solution and digested with collagenase (Sigma-Aldrich, USA) at 0.05% (w/v) concentration to ensure the complete removal of DNA from the collagen matrix. After that, 1 mL of ultrapure water was added to each well material and maintained at 37 °C per 1h and further kept at –80 °C. For analysis, the samples were thawed at RT and to complete the lysis of cell membrane all samples were sonicated for 15 min in a cold-water bath to avoid DNA degradation. Fluorescence was measured using an excitation/emission wavelength of 485/528 nm, respectively, in a microplate reader (Synergy HT, BioTek, USA). The quantification of DNA was calculated based on a standard curve for DNA prepared by using DNA standards between 0 and 2 $\mu g.mL^{-1}$. The results are the mean of three independent experiments (n=3) with three replicates for each condition and per experiment.

V-3.10. RNA isolation and real-time quantitative polymerase chain reaction

To evaluate the expression of the chondrogenic related genes, real-time PCR was carried out 7, 14 and 21 days after cell seeding in both scaffolds' formulations maintained under basal and chondrogenic conditions. Briefly, after each culture period all scaffolds were washed with PBS, digested with 50 µL of collagenase at 0.05% (w/v) to ensure cell removal from the interior of the scaffolds and immersed in 800 µL of TRI reagent® (Laborspirit, Portugal), being then stored at -80 °C until further use. For the RNA extraction, samples were thawed at RT, completed with 160 µL of Chloroform (VWR, Portugal), mixed and kept in ice for 15 min. After that, all samples were centrifuged at 13000 rpm, for 15 min, at 4 °C and the resultant supernatant was completed with an equivalent volume of isopropanol (overnight at -20 °C) to precipitate the RNA. After a new step of centrifugation, a pellet was obtained that was solubilized in 70% of ethanol, centrifuged again and resuspended in RNase-free water. The RNA concentration was evaluated using micro-spectrophotometry (NanoDrop1000, Thermo Scientific; USA). RNA was reversed-transcribed into cDNA according to the protocol from qScript cDNA Synthesis Kit (Quanta BioSciences; VWR, USA). The obtained cDNA was used as a template for the amplification of the target genes shown in **Table V-1**, according to manufacturer's instructions of the PerfeCtaTM SYBR® Green system (Quanta Biosciences, VWR, USA) in a Mastercycler® ep Gradient S Realplex®

thermocycler (Eppendorf; Germany). The following cycler conditions were used: 2 min at 95 °C and 45 cycles of 15 s at 95 °C, 30 s at Tm (°C) (melting temperature depending on the gene; **Table V-1**) and 30 s at 72 °C. Fluorescence was measured at the end of each amplification cycle. β2-microglobulin (hB2M) was used as reference gene and normalization was performed according to the Livak method (2 -ΔΔCT method), with the Day 1 of the experiment (negative control) serving as a calibrator [27].

Table V-1 - Primer sequences used for RT-PCR procedures.*

Gene	Primer	Sequence (5'-3')	Tm (°C)	
SOX9	Forward	TTC ATG AAG ATG ACC GAC GC	55.2	NM_000346.4
	Reverse	GTC CAG TCG TAG CCC TTG AG	57.3	
ACAN	Forward	TGA GTC CTC AAG CCT CCT GT	57.9	XM_011521314.1
	Reverse	TGG TCT GCA GCA GTT GAT TC	55.5	
COL II	Forward	GAGCAGGAATTCGGTGTGGA	55.2	NM_001844.5
	Reverse	GCCATTCAGTGCAGAGTCCT	58.0	
COMP	Forward	TCT GCA TCA AAG TCG TCC TG	54.9	NM_000095.3
	Reverse	AGG GAT GGA GAC GGA CAT CAG	58.4	
hB2MM	Forward	TGG AGG CTA TCC AGC GTA CT	57.7	NM_004048.3
	Reverse	CGG ATG GAT GAA ACC CAG ACA	57.1	

*SOX-9 - SRY-box transcription factor 9; ACAN- Aggrecan; Col2A1- Collagen type II; COMP - Cartilage oligomeric matrix protein; hB2M - β2-microglobulin.

V-3.11. Histological analysis

To understand if the cells could migrate and spread within the polymeric network of the structures created by cryogelation, histological analysis was performed. Samples were collected at the end of each cell culture time-point, washed with PBS and fixed with 10% (v/v) formalin solution followed by dehydration and embedding in paraffin. After that, the constructs were serially sectioned (4 μm longitudinal sections) using a microtome (Spencer 820, American Optical Company, USA). Hematoxylin & Eosin (Thermo Scientific, USA) staining, following standard protocols, was performed to evaluate cell

distribution through the different longitudinal sections and ECM formation within the constructs. For immunohistochemistry, paraffin tissue sections were deparaffinized in xylene, re-hydrated and boiled for 4 min in sodium citrate buffer (10 mM sodium citrate (Sigma-Aldrich, USA), 0.05% v/v tween 20 (Bio-Rad, Netherlands), pH 6) for antigen retrieval. Afterwards, sections were maintained for 30 min in 3% (w/v) of bone serum albumin (BSA, Laborspirit, Portugal) to block nonspecific antigen binding. Sections were incubated with a rabbit anti-SOX 9 antibody (Sigma-Adrich,USA) 1:100 and aggrecan (ACAN) monoclonal antibody (Alfagene, Portugal) 1:50. Alexa Fluor 488 secondary antibody at 1:500 in PBS was added during 1 h at 37 °C. Slices were analyzed using a Zeiss Axio Imager Z1m (Germany) fluorescence microscope.

V-4. RESULTS AND DISCUSSION

V-4.1. Scaffolds' properties

V-4.1.1. Microarchitecture and water uptake

To assess the effect of the cryogelation in the structural properties of both collagen-based constructs, 3-D reconstructions obtained after x-ray micro-computed tomography acquisitions were performed and the quantitative results were analyzed in a specific CT analyzer program (**Figure V-1**). From the qualitative 2D (**Figure V-1A**) and 3D (**Figure V-1B**) images reconstruction it was possible to observe a homogenous distribution of the pores.

Quantitative results showed a pore size distribution between 5 and 615 μm with a mean pore size and interconnectivity ranging from 258.3± 29.2 to 293.1±50.7 and 70.7±4.9 to 87.2±2.8 μm for Collagen (Coll) and Collagen:Hyaluronic (Coll:Hya) structures, respectively. The total porosity was around 91% for both conditions. The introduction of Hya in the system resulted in larger pores with a higher interconnectivity between them, without affecting the total porosity. These results were not significantly different between the two produced formulations. The ice crystals created by the cryogelation technique were efficient to generate large pores with interconnective microporosities in both formulations, which might be appropriated for cell culture and migration. Pore wall thickening around 16 μm was observed as a result of the rearrangement of the polymeric network and a physical accumulation of polymer around the crystals during the cryogel formation [28].

When the dried cryogels were soaked in an aqueous solution of PBS, they quickly swollen up to 92% (Coll) and 95% (Coll:Hya) of retention capacity, 15 min after immersion. This fast water uptake was enabled by the high pore size and interconnectivity of both cryogels formulations [29]. To confirm if the maximum absorption capacity was achieved the study was monitored until 24 h after immersion in PBS and the result did not changed. From a clinical point of view, such property is of extreme importance. When implanted in a defect, the constructs will quickly absorb the fluids around the tissue and fill the defect properly [29].

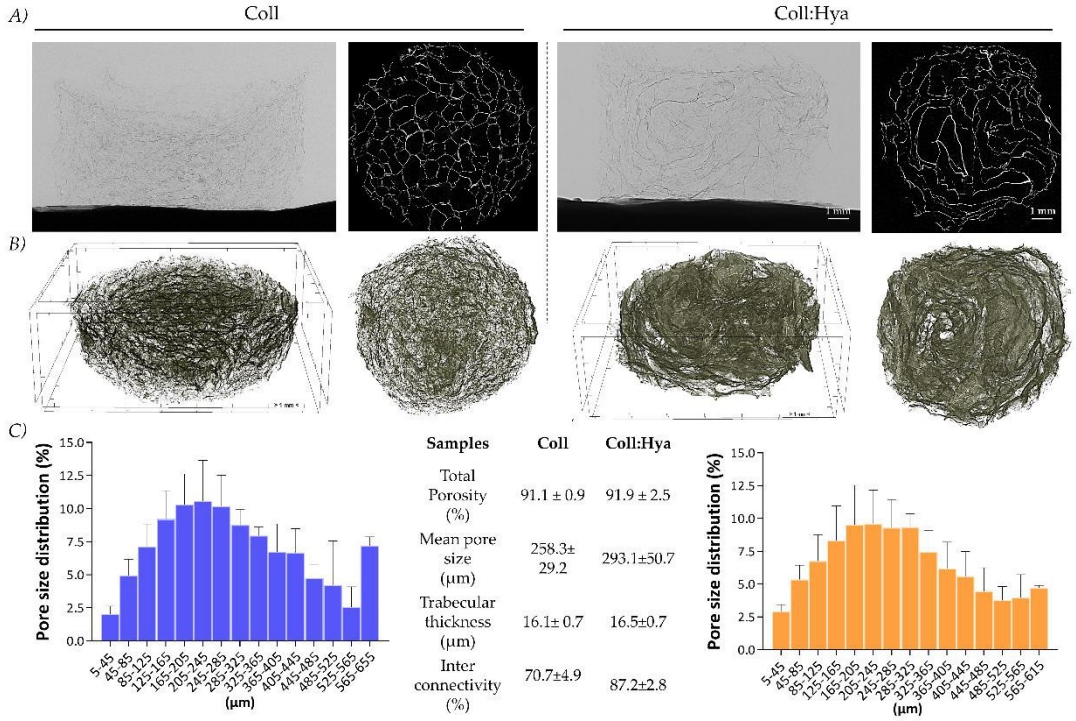

Figure V-1 – 3-D porous structures characterization. (A) X-ray micro-CT acquisitions of the Coll and Coll:Hya structures (scale bar = 1000 µm). Cross-sections were reproduced showing the pore size and shape for each formulation (scale bar = 1000 µm). (B) 3D reconstruction of 3D structures (C) pore size distribution (%), total porosity (%), mean pore size (µm), mean wall thickness (µm) and interconnectivity (%).

V-4.2. Rheological properties

To evaluate the mechanical stability of cryogels, the storage and loss modulus were studied in function of frequency through oscillatory shear rheometry assays. In a frequency sweep assay, the measurements were made over a range of oscillation frequencies between 0.1 - 10 Hz at a constant temperature of 37 °C. The elastic modulus G' was nearly independent of frequency for both cryogels

conditions, characteristic of a solid-like material, indicating that the materials are highly structured. Such findings confirm the high stability of the cryogels as a result of an efficient crosslinking reaction.

Measurements of storage modulus at 1 Hz showed higher values for pure collagen (1010 Pa) in comparison with Coll:Hya (493 Pa), being the collagen cryogels stiffer (**Figure V-2**). From 2 Hz of frequency, G' starts to decrease with a significant decrease from 6 and 4 Hz for Coll and Coll:Hya hydrogels, respectively. The point wherein the storage modulus declined, and the G'' exceeded G', was considered the point where the hydrogels became more fluid-like, losing their structure. The ratio between the storage and loss modulus was higher for the Coll:Hya cryogels formulation, indicating a greater elasticity and shape recovery ability.

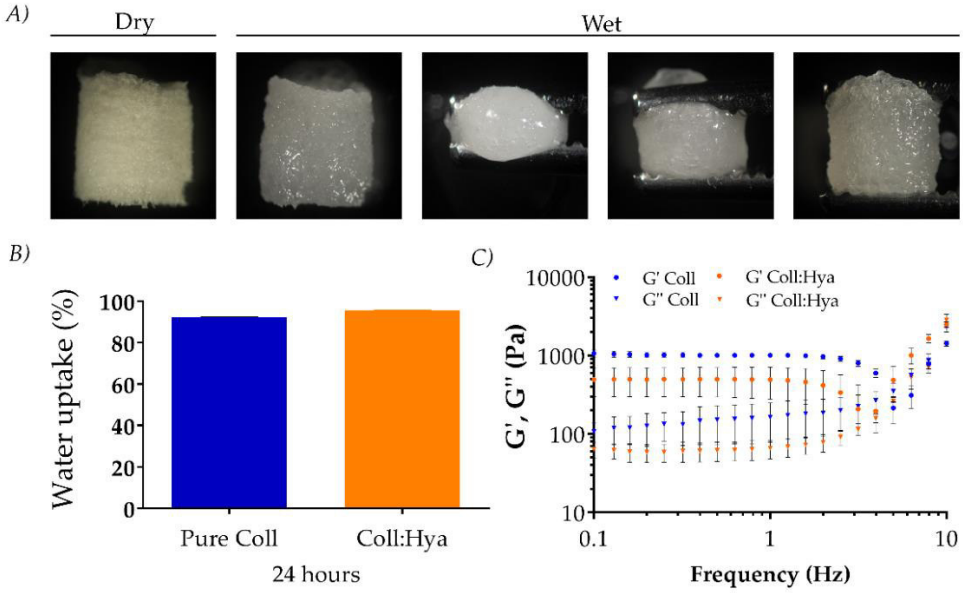

Figure V - V-2 – A) Sequential macroscopic demonstration of the Coll cryogel. Spongy-like behavior was observed after compression - Representative example. B) Water uptake for Coll and Coll:Hya hydrogels, 24 h after immersion in PBS. C) rheological properties, G' and G'' of hydrogels determined in a frequency sweep assay. Measurements were performed using a shear strain of 0.1%, at 37 °C.

V-4.3. *In vitro* biological performance with hASC

V-4.3.1. Quantitative metabolic activity and qualitative live/dead assay

As a first approach to evaluate the biologic performance of the developed scaffolds, the metabolic activity of hASC was assessed 24, 48 and 72 h after cell seeding. As disclosed by the obtained results (**Figure V-3**), there was an increase in the metabolic activity from day 1 to day 2 and 3, without

significant statistical differences to cells cultured in the bottom of the well. Moreover, no differences were observed between the two types of the prepared structures.

To qualitatively assess cells viability, live (green) and dead (red) cells were stained with calcein and propidium iodide after 1 and 7 days in culture. This assay revealed that hASC initially seeded at the same density in both conditions were homogeneously distributed throughout the scaffolds. It was clear that most of the cells were viable (green) after 1 day of culture. The cells covered the surface 7 days after seeding on all samples which suggests cells proliferation throughout the scaffolds.

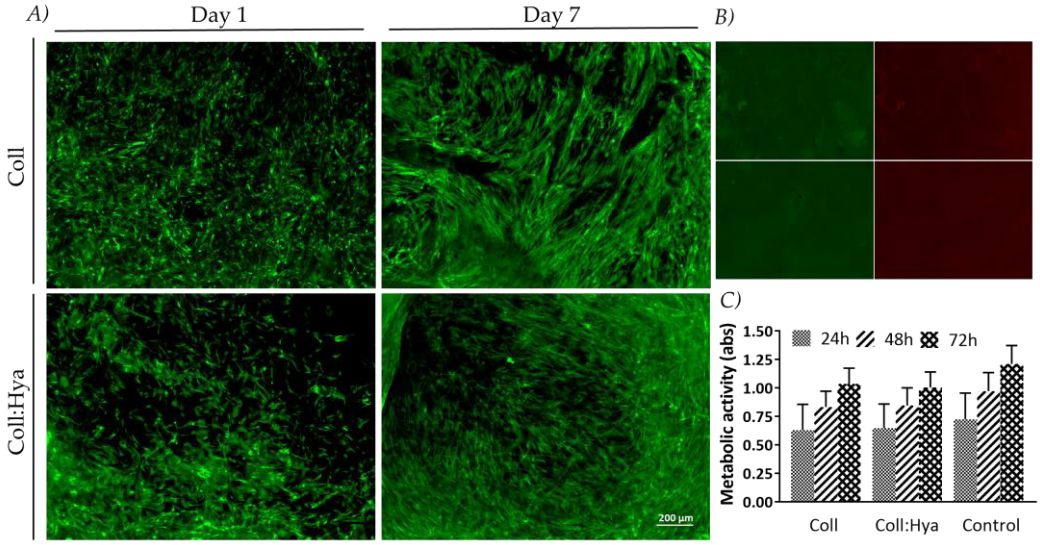

Figure V-3 – (A) Live (green) / dead (red) staining (scale bar: 200 µm) of the hASCs cultured on the Coll and Coll:Hya cryogels 1 and 7 after cultured in basal conditions, B) Control scaffolds – scaffolds without seeded cells stained with calcein-AM (green) and propidium iodide (red) demonstrating the background given by the material itself. C) Metabolic activity of hASC cultured in contact with scaffolds. Results are the mean ± standard error of three independent experiments. Statistical analysis was performed using Kruskal-wallis test with Dunns Multiple comparison Test (* $p < 0.05$).

V-4.3.2. Histological analysis - hematoxylin and eosin staining's

To confirm if the green signal increase corresponded to the proliferative state of the cells, tissue sections with 20 µm thick, sectioned longitudinally (to cover the interior of the scaffold), were stained with hematoxylin and eosin (H&E), 1 and 7 days after cell seeding. As depicted in the different H&E stained micrographs images (**Figure V-4**), there was a significant increase in the cell density from day 1 to day 7 as can be observed by the increase in nucleus amounts stained with hematoxylin. These findings suggest the proliferative state of the cells.

Cell migration and infiltration into the interior of a 3D structure is crucial for new tissue formation. Previous works have shown that the rate of cell attachment, migration and infiltration is largely influenced by the scaffolds' pore size. In general, scaffolds with small pores, ø < 100 μm, have been characterized by high surface area for cell attachment but very challenging for cell penetration. Larger pores, ø > 100 μm are often required to enable an higher cell seeding efficiency and migration to the central regions of the construct, but if they are too large the cells cannot bridge the pores and fail to completely populate the scaffold [30].

Different cell types prefer different pore size. In general, mesenchymal stem cells are morphologically bigger and can bridge the pores easily [31, 32]. In our study, cell attachment and proliferation were positively favored by the size of the pores (averaging 250 - 300) created by the cryogelation process. The hASC spread out to the scaffolds' core as was possible to observe from the longitudinal histologic images (**Figure V-4**) demonstrating the ability of the cells to infiltrate and migrate within the different group conditions.

In addition, the cell-seeded cryogels showed severe macroscopic contraction from day 1 to day 7, which was probably a cell-mediated process resulting from the increase of cell density. It was evident that 7 days after cell culture, both scaffolds were completely colonized by the hASC. Regarding these results, it was possible to conclude that both conditions exhibited a good cytocompatibility and could support cells proliferation without any cytotoxic effect.

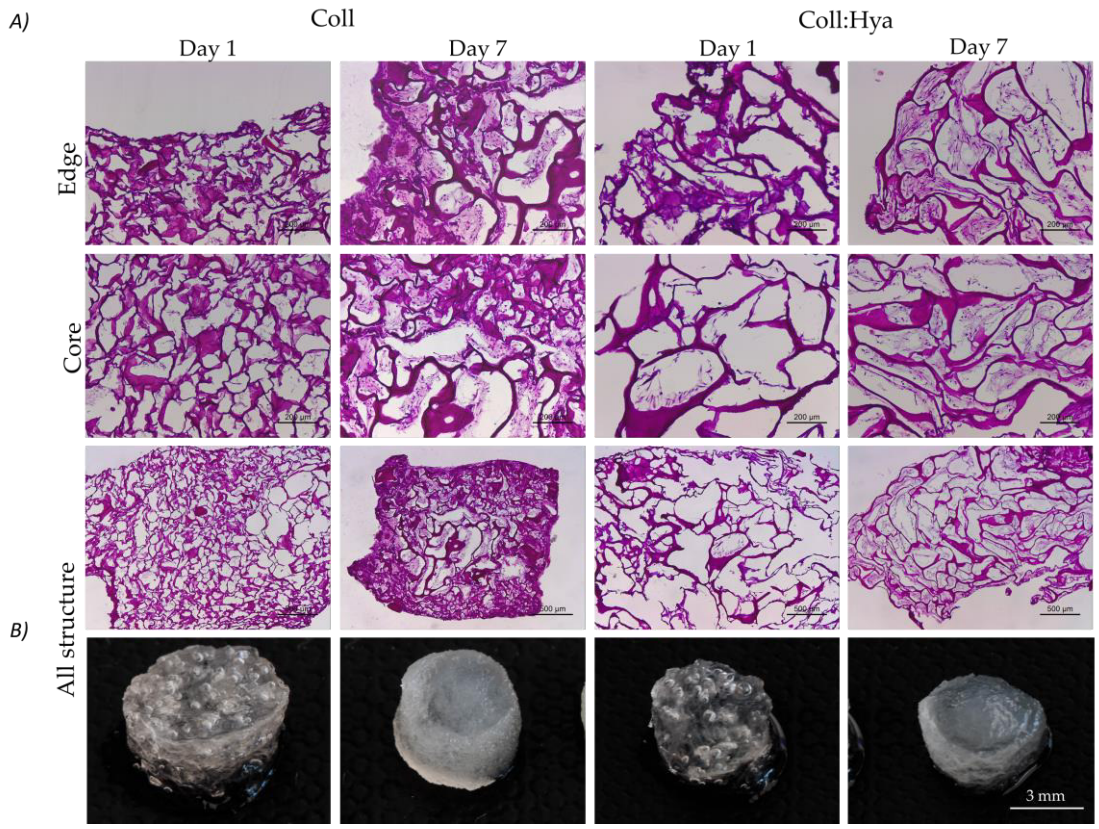

Figure V-4 – Representative histological images after 1 and 7 days of hASC cultured in Coll and Coll:Hya constructs under basal conditions. Tissue sections with 20 µm were stained with Hematoxylin and Eosin for the nucleus and extracellular matrix, respectively (scale bar: 200 µm (core and edge) and 500 µm for the entire scaffold). B) Macroscopic demonstration of scaffolds contraction after 7 days of cell culture (scale bar: 3 mm).

V-4.4. Human adipose stem cells differentiation

After assessing the non-cytotoxicity of the cryogels, their potential to promote stem cells chondrogenic differentiation was investigated. Some scaffolds were maintained in basal medium without FBS that contains extra nutrients and cytokines that may potentiate a chondrogenic effect. Such approach was used to better mimic the limited nutrient microenvironment exhibited in the natural articular cartilage. The other half of samples was treated with basal medium supplemented with FBS and transforming growth factor β-3 that is commonly used in culture medium as an inductor of stem cells chondrogenic differentiation [33]. Considering the previously observed contraction in the cell-seeded scaffolds and to better evaluate the effect of cells on scaffolds' structure, both scaffold formulations were analyzed by micro-CT 21 days after cell culture in basal and chondrogenic conditions. Scaffolds without cells maintained in basal culture medium were used as the control of the experiment to exclude the influence of the culture time and medium composition.

Micro-CT quantitative results showed a pore size reduction after 21 days of culture for the scaffolds cultivated in culture medium itself (comparison of **Figure V-1** (**Table V-1**) and **Figure V-5B**). It means that there was a slight influence of the culture conditions on the structures. Even without cells the pore size decreased, probably due to the natural degradation of the material. However, scaffolds pore size reduction was more robust when cultured with cells, it can be associated with the effect of cell-mediated contraction. For Coll-seeded structures maintained in basal and chondrogenic conditions, it was observed, a pore size decrease of 23% and 43% (**Figure V-5**) in comparison with cell-free scaffolds cultivated 21 days. Coll:Hya constructs showed an higher decrease, 58% for basal and 69% for chondrogenic conditions. In general, pore size decline was accompanied by a reduction of pore interconnectivity and scaffolds' total porosity (**Figure V-5**).

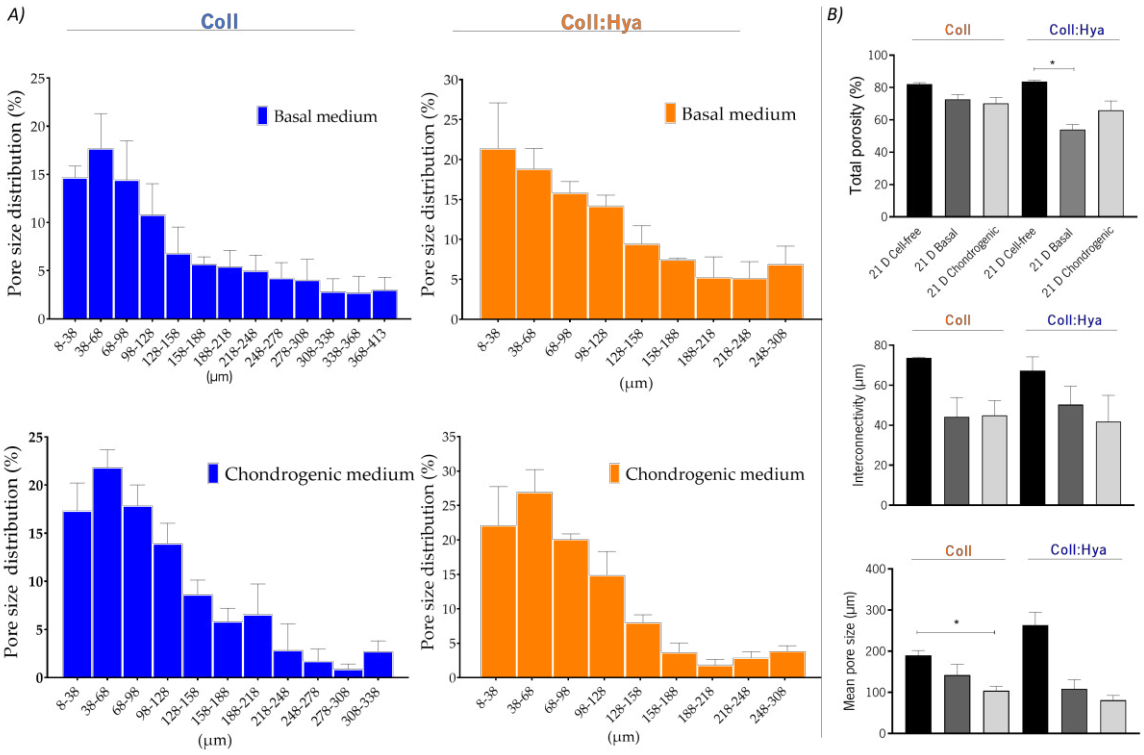

Figure V-5 – Micro-CT analysis. 3-D porous structures characterization after 21 days of cell culture. (A) Pore size distribution(%) of scaffolds maintained in basal and chondrogenic medium. B) Total porosity (%), mean pore size (µm) and interconnectivity (%). Statistical analysis was performed using Kruskal-wallis test with Dunns Multiple comparison Test (* p <0.05).

The effect of scaffolds' cell-mediated contraction in chondrogenesis is still poorly understood and controversial [34]. Cell-mediated contraction has been demonstrated to have a crucial role in obtaining and retaining newly synthesized matrix as a result of the increase in cell density [35, 36]. At same time,

other works have been reporting that scaffolds' contraction reduces the size of pores, leading to a lack of cell migration into the interior [32, 37]. In our study, cell-mediated contraction resulted in new synthesized matrix (**Figure V-8**).

V-4.4.1. DNA quantification of hASC

After an initial increase in cell density, qualitatively assessed by live/dead and H&E staining's, the DNA amount was quantified from day 7 to day 21. The DNA content decreased gradually from day 7 to day 21 (**Figure V-6**) as a result of a cell number decrease (significant differences were only observed in chondrogenic conditions), probably due to the chondrogenic differentiation of the hASC. In fact, previous works have reported that DNA content declines during the first weeks of *in vitro* chondrogenesis [38]. After the initial mesenchymal stem cells condensation, the 3D cell culture density increases reaching a confluent state and consequently leading to a cell-mediated contraction. In this case, the oxygen and nutrients can be scarce in the core causing cell-death unlike what is happening in the more peripheric regions. This is a time-dependent situation that is restored after cells are adapted to the conditions and start matrix production [39].

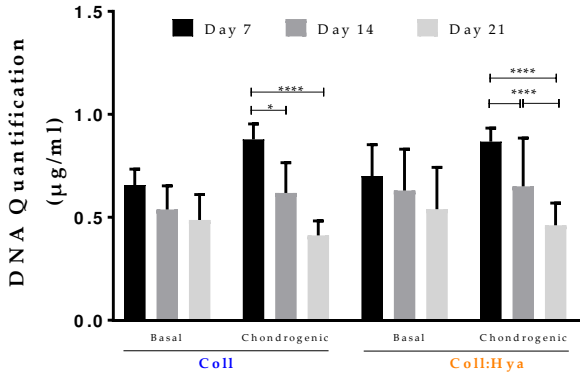

Figure V-6 – DNA quantification for Coll and Coll:Hya formulations maintained in basal and chondrogenic conditions. Results are the mean ± standard error of three independent experiments. Statistical analysis was performed using Kuskal-wallis test with Dunns Multiple comparison Test (* $p < 0.05$).

V-4.4.2. Real time PCR and Immunodetection

The differentiation of hASCs seeded onto the scaffolds created by cryogelation was evaluated by quantifying the mRNA expression (**Figure V-7**) of chondrogenesis-related markers. The mRNA expression of chondrogenesis-related markers, such as SOX-9, Col II, ACAN and COMP was evaluated after 7, 14

and 21 days of cell culture by RT-PCR. SOX-9 and Col II, known as transcription factors expressed at relatively early stages, were quantified 7 days after culture under basal and chondrogenic conditions, being observed a slight decrease of SOX-9 expression from day 14 to 21, except for the Coll:Hya formulation maintained in chondrogenic medium. The expression of COMP was also upregulated for all formulations under all medium conditions, except for Coll:Hya structures maintained in basal conditions. The expression of ACAN, a cartilage ECM proteoglycan produced relatively at later stages was dowregulated for all formulations except for Coll:Hya cultured under chondrogenic conditions [40].

Complementary, the immunodetection of SOX-9 and ACAN in the 3D constructs was also assessed 21 days after cell seeding (**Figure V-7**). The immunofluorescence images (**Figure V-7B**) showed the protein expression of both chondrogenic-related markers after 21 days of culture in chondrogenic differentiation medium. In basal culture conditions, the expression of ACAN was only observed for the Col/Hya condition. It seems that the addition of Hya into the collagen network accelerated the expression of cartilage-related genes. Hya is commonly found in native articular cartilage tissues and apparently promoted the cellular infiltration and favored expression of chondrogenic markers [25]. Kawasaki *et al*, incorporated Hya at different concentrations (0, 0.01, 0.1, 1.0 $mg.mL^{-1}$) in type I collagen gel, and they found that Hya at 0.1 $mg.mL^{-1}$ was optimal for enhancing chondrocyte proliferation [41]. In our study, it was demonstrated that 0.05 $mg.mL^{-1}$ was enough to successfully induce chondrogenic differentiation. In an early culture period, it can be observed that the use of blue shark collagen itself gives the boost needed to start chondrogenic differentiation, through the expression of early chondrogenic markers, even in basal conditions.

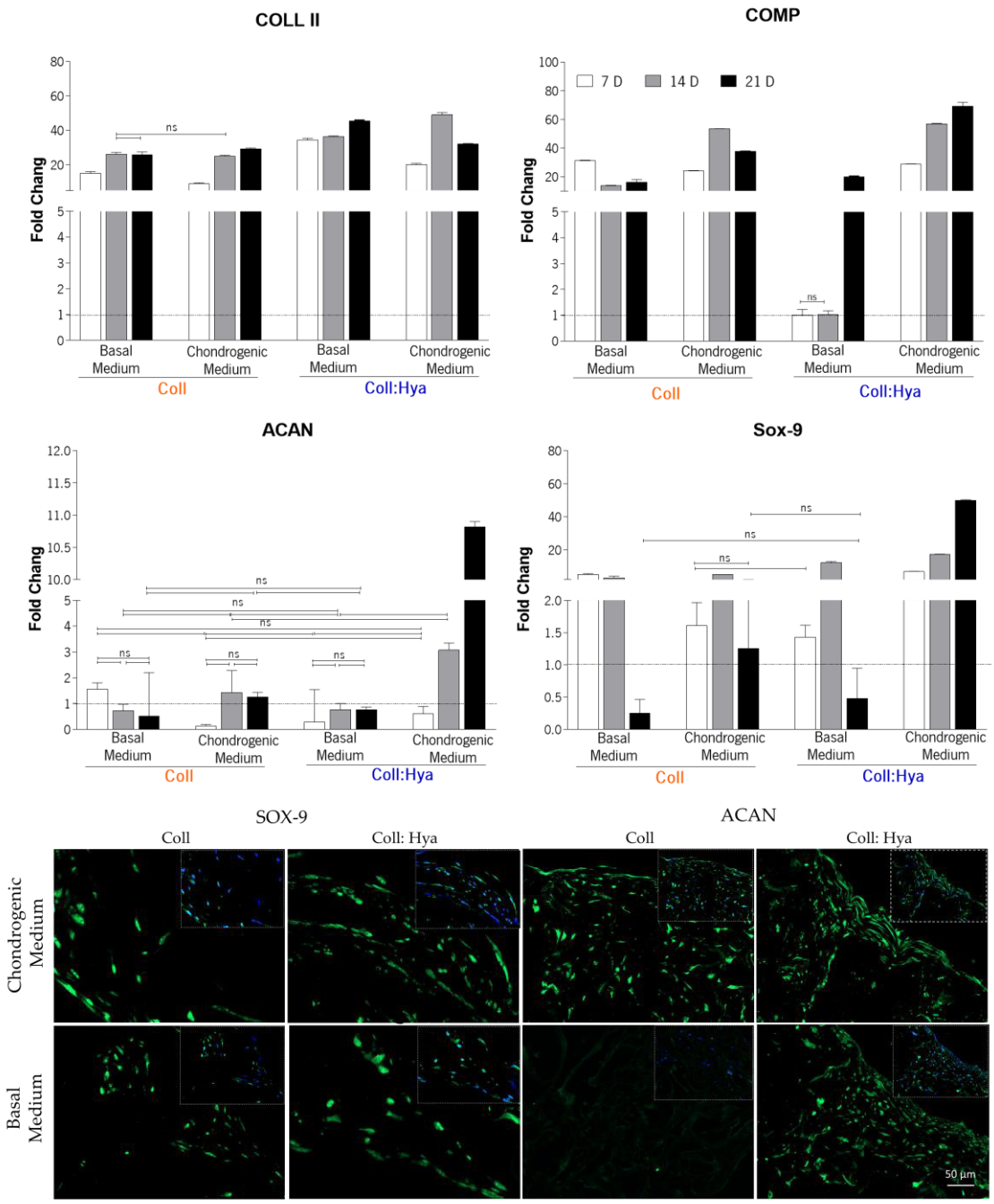

Figure V-7 - Quantitative and qualitative expression of chondrogenic-related markers by hASCs after 21 days of culture on the Coll and Coll:Hya structures. (A) mRNA expression encoding Coll II, SOX-9, COMP and ACAN (B) Immunofluorescence detection of representative chondrogenic-related markers, SOX-9 and ACAN under basal and chondrogenic conditions (Scale bar: 50 µm).

V-4.4.3. Masson's trichrome and alcian blue detection

For the detection of ECM sulfated proteoglycans (**Figure V-8**) and to confirm the presence of cartilaginous ECM, all culture conditions at 21 days were stained with alcian blue and masson's trichrome (MT). In all conditions structures was confirmed the expression of alcian (Glicosaminoglycans)

and MT (Collagen). Naturally, as would be expected, the alcian and MT stainings were more pronounced in the structures cultured in chondrogenic medium.

These observations were consistent with the previously obtained results for the expression of chondrogenic-related genes and immunodetection. Moreover, these results are comparable with the results revealed by other *in vitro* studies performed with collagen-based matrices, even the ones obtained for the best natural matrix (Chondro-Gide®) made of porcine collagen [42]. In contrast to synthetic polymers (Alpha Chondro Shield), higher cell adhesion and chondrogenic differentiation of stem cells from different origins was demonstrated for Chondro-Gide®.

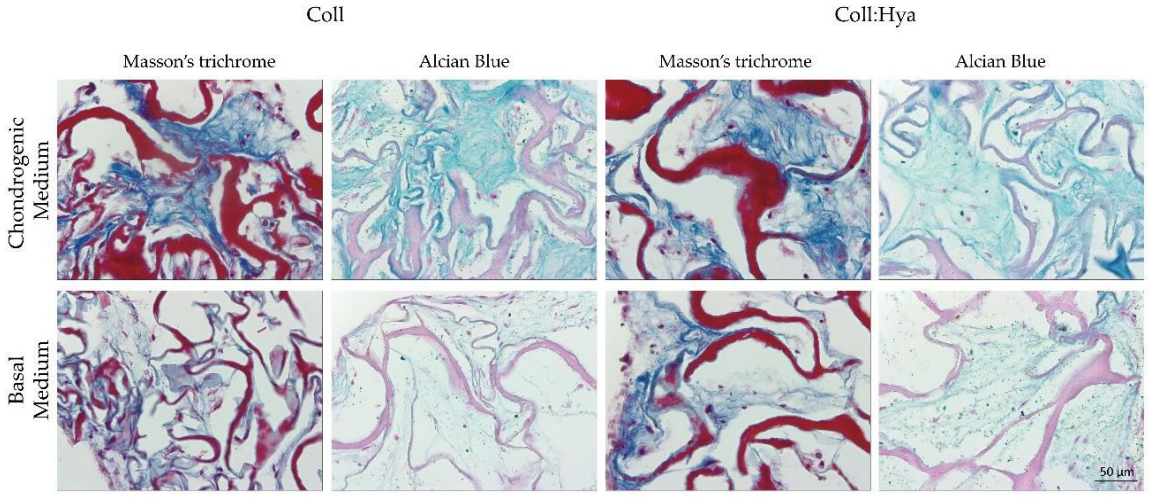

Figure V-8 – Masson's trichrome (dark blue) and Alcian blue (light blue) were used as histological stainings for collagen and GAGs detection in the ECM (scale bar: 50 µm).

V-5. CONCLUSION

The *in vitro* differentiation of hASC into the chondrogenic lineage without any additional exogeneous induction component was successfully achieved based on a strategy of marine by-products valorization combined with a Tissue Engineering approach. The current findings suggest the use of blue shark skin collagen, in a cryogel form, as potential inductor of early hASC chondrogenic differentiation, supported by the expression of markers such as Coll II and SOX-9, even when cultured in basal conditions. However, the introduction of Hya seems to play a crucial role to maintain a chondrocytic phenotype at later stages. The successfully developed cryogels can be explored as a promising alternative of natural commercially available matrices for cartilage repair based on porcine collagen.

V-6. ACKNOWLEDGMENTS

This study was funded by the Portuguese Foundation for Science and Technology (FCT) under the scope of the BiogenInk project (M-ERA-NET2/0022/2016), by European Union through INTERREG Atlantic Programme, under the scope of BLUEHUMAN (EAPA_151/2016) project. The Doctoral Programme NORTE-08-5369-FSE-000044, supported by Norte Portugal Regional Operational Programme (NORTE 2020), under the PORTUGAL 2020 Partnership Agreement, through the European Social Fund, is also greatly acknowledge by the PhD fellowship of GSD. RP thanks FCT for the contract IF/00347/2015. The authors acknowledge also the Centro Tecnológico del Mar (CETMAR, Vigo, Spain) and COPEMAR SA (fishing company, Spain) for the kind offer of the used by-products for the production of collagen.

V-7. REFERENCES

1. Makris, E.A., et al., *Repair and tissue engineering techniques for articular cartilage.* Nature Reviews Rheumatology, 2015. 11(1): p. 21.
2. Correa, D. and S.A. Lietman. *Articular cartilage repair: current needs, methods and research directions*. in *Seminars in Cell & Developmental Biology*. 2017. Elsevier.
3. Huang, B.J., J.C. Hu, and K.A. Athanasiou, *Cell-based tissue engineering strategies used in the clinical repair of articular cartilage.* Biomaterials, 2016. 98: p. 1-22.
4. Armiento, A., et al., *Biomaterials for articular cartilage tissue engineering: Learning from biology.* Acta biomaterialia, 2018. 65: p. 1-20.
5. Simon, T.M. and D.W. Jackson, *Articular cartilage: injury pathways and treatment options.* Sports medicine and arthroscopy review, 2018. 26(1): p. 31-39.
6. Demange, M.K., et al., *Intralesional osteophyte regrowth following autologous chondrocyte implantation after previous treatment with marrow stimulation technique.* Cartilage, 2017. 8(2): p. 131-138.
7. von Keudell, A., et al., *Autologous chondrocyte implantation to isolated patella cartilage defects: two-to 15-year follow-up.* Cartilage, 2017. 8(2): p. 146-154.
8. McCarthy, H. and S. Roberts, *A histological comparison of the repair tissue formed when using either Chondrogide® or periosteum during autologous chondrocyte implantation.* Osteoarthritis and cartilage, 2013. 21(12): p. 2048-2057.

9. Fontana, A., *A novel technique for treating cartilage defects in the hip: a fully arthroscopic approach to using autologous matrix-induced chondrogenesis.* Arthroscopy techniques, 2012. 1(1): p. e63-e68.
10. Gille, J., et al., *Matrix-associated autologous chondrocyte implantation: a clinical follow-up at 15 years.* Cartilage, 2016. 7(4): p. 309-315.
11. Silva, T.H., et al., *Marine origin collagens and its potential applications.* Marine drugs, 2014. 12(12): p. 5881-5901.
12. Felician, F.F., et al., *Collagen from marine biological sources and medical applications.* Chemistry & biodiversity, 2018. 15(5): p. e1700557.
13. Berillis, P., *Marine collagen: Extraction and applications.* Research Trends in Biochemistry, Molecular Biology and Microbiology; Madhukar, S., Ed, 2015: p. 1-13.
14. Lim, Y.-S., et al., *Marine Collagen as A Promising Biomaterial for Biomedical Applications.* Marine drugs, 2019. 17(8): p. 467.
15. Alves, A., et al., *Cosmetic potential of marine fish skin collagen.* Cosmetics, 2017. 4(4): p. 39.
16. Burnsed, O.A., et al., *Hydrogels derived from cartilage matrices promote induction of human mesenchymal stem cell chondrogenic differentiation.* Acta biomaterialia, 2016. 43: p. 139-149.
17. *The IUCN Red List of Threatened Species.*; Available from: http://www.iucnredlist.org.
18. Fernandes-Silva, S., et al., *Porous hydrogels from shark skin collagen crosslinked under dense carbon dioxide atmosphere.* Macromolecular bioscience, 2013. 13(11): p. 1621-1631.
19. Sotelo, C.G., et al., *Characterization of collagen from different discarded fish species of the West coast of the Iberian Peninsula.* Journal of aquatic food product technology, 2016. 25(3): p. 388-399.
20. Matsumoto, R., et al., *Rapid oriented fibril formation of fish scale collagen facilitates early osteoblastic differentiation of human mesenchymal stem cells.* Journal of Biomedical Materials Research Part A, 2015. 103(8): p. 2531-2539.
21. Hsu, H.-H., et al., *Chondrogenic differentiation of human mesenchymal stem cells on fish scale collagen.* Journal of bioscience and bioengineering, 2016. 122(2): p. 219-225.
22. Rodrigues, S.C., et al., *Preparation and characterization of collagen-nanohydroxyapatite biocomposite scaffolds by cryogelation method for bone tissue engineering applications.* Journal of biomedical materials research Part A, 2013. 101(4): p. 1080-1094.

23. Salgado, C.L., et al., *Biodegradation, biocompatibility, and osteoconduction evaluation of collagen-nanohydroxyapatite cryogels for bone tissue regeneration.* Journal of Biomedical Materials Research Part A, 2016. 104(1): p. 57-70.
24. Diogo, G., et al., *Marine collagen/apatite composite scaffolds envisaging hard tissue applications.* Marine drugs, 2018. 16(8): p. 269.
25. Davidenko, N., et al., *Collagen–hyaluronic acid scaffolds for adipose tissue engineering.* Acta biomaterialia, 2010. 6(10): p. 3957-3968.
26. Freitas-Ribeiro, S., et al., *Strategies for the hypothermic preservation of cell sheets of human adipose stem cells.* PloS one, 2019. 14(10).
27. Casanova, M.R., et al., *Chondrogenesis-inductive nanofibrous substrate using both biological fluids and mesenchymal stem cells from an autologous source.* Materials Science and Engineering: C, 2019. 98: p. 1169-1178.
28. da Silva, L.P., et al., *Engineering cell-adhesive gellan gum spongy-like hydrogels for regenerative medicine purposes.* Acta biomaterialia, 2014. 10(11): p. 4787-4797.
29. Gürer, B., et al., *A novel strategy for cartilage tissue engineering: Collagenase-loaded cryogel scaffolds in a sheep model.* International Journal of Polymeric Materials and Polymeric Biomaterials, 2018. 67(5): p. 313-321.
30. Zhang, Q., et al., *Pore size effect of collagen scaffolds on cartilage regeneration.* Acta biomaterialia, 2014. 10(5): p. 2005-2013.
31. Irawan, V., et al., *Collagen scaffolds in cartilage tissue engineering and relevant approaches for future development.* Tissue engineering and regenerative medicine, 2018. 15(6): p. 673-697.
32. Schindeler, A., et al., *Effect of Collagen-Glycosaminoglycan Scaffold Pore Size on Matrix Mineralisation and Cellular Behaviour in Different Cell Types.* 2016.
33. Yi, S.W., et al., *Gene expression profiling of chondrogenic differentiation by dexamethasone-conjugated polyethyleneimine with SOX trio genes in stem cells.* Stem cell research & therapy, 2018. 9(1): p. 341.
34. Visscher, D.O., et al., *Cartilage tissue engineering: preventing tissue scaffold contraction using a 3D-printed polymeric cage.* Tissue Engineering Part C: Methods, 2016. 22(6): p. 573-584.
35. Vickers, S.M., L.S. Squitieri, and M. Spector, *Effects of cross-linking type II collagen-GAG scaffolds on chondrogenesis in vitro: dynamic pore reduction promotes cartilage formation.* Tissue Engineering, 2006. 12(5): p. 1345-1355.

36. Tang, S. and M. Spector, *Incorporation of hyaluronic acid into collagen scaffolds for the control of chondrocyte-mediated contraction and chondrogenesis.* Biomedical Materials, 2007. 2(3): p. S135.

37. Haugh, M.G., et al., *Crosslinking and mechanical properties significantly influence cell attachment, proliferation, and migration within collagen glycosaminoglycan scaffolds.* Tissue Engineering Part A, 2011. 17(9-10): p. 1201-1208.

38. Liu, J., et al., *Bionic cartilage acellular matrix microspheres as a scaffold for engineering cartilage.* Journal of Materials Chemistry B, 2019. 7(4): p. 640-650.

39. Fischer, J., et al., *Time-dependent contribution of BMP, FGF, IGF, and HH signaling to the proliferation of mesenchymal stroma cells during chondrogenesis.* Journal of cellular physiology, 2018. 233(11): p. 8962-8970.

40. Mahapatra, C., et al., *Differential chondro-and osteo-stimulation in three-dimensional porous scaffolds with different topological surfaces provides a design strategy for biphasic osteochondral engineering.* Journal of tissue engineering, 2019. 10: p. 2041731419826433.

41. Kawasaki, K., et al., *Hyaluronic acid enhances proliferation and chondroitin sulfate synthesis in cultured chondrocytes embedded in collagen gels.* Journal of cellular physiology, 1999. 179(2): p. 142-148.

42. Kohli, N., et al., *An in vitro comparison of the incorporation, growth, and chondrogenic potential of human bone marrow versus adipose tissue mesenchymal stem cells in clinically relevant cell scaffolds used for cartilage repair.* Cartilage, 2015. 6(4): p. 252-263.

Chapter VI

Cell-Laden Biomimetially Mineralized Shark-Skin-Collagen-Based 3D Printed Hydrogels for the Engineering of Hard Tissues

Chapter VI

Cell-Laden Biomimetically Mineralized Shark-Skin-Collagen-Based 3D Printed Hydrogels for the Engineering of Hard Tissues[1]

VI-1. ABSTRACT

Mineralization processes based on co-precipitation methods have been applied as a promising alternative to the most commonly used methods of polymer–ceramic combination, direct mixing, and incubation in simulated body fluid (SBF) or modified SBF. In the present study, for the first time, the *in situ* mineralization (ideally hydroxyapatite formation) of blue shark (*Prionace glauca* (PG)) collagen to fabricate 3D printable cell-laden hydrogels is proposed. In the first part, several parameters for collagen mineralization were tested until optimization. The hydroxyapatite formation was confirmed by FTIR, XRD, and TEM techniques. In the second part, stable bioinks combining the biomimetically mineralized collagen with alginate (AG) (1:1, 1:2, 1:3, and AG) solution were used for 3D printing of hydrogels. The addition of Ca^{2+} ions into the system did present a synergistic effect: by one side, the *in situ* mineralization of the collagen occurred, and at same time, they were also useful to ionically crosslink the blends with alginate, avoiding the addition of any cytotoxic chemical crosslinking agent. Mouse fibroblast cell line survival during and after printing was favored by the presence of PG collagen as exhibited by the biological performance of the hydrogels. Inspired in a concept of marine byproduct valorization, 3D bioprinting of *in situ* mineralized blue shark collagen is thus proposed as a promising approach, envisioning the engineering of mineralized tissues.

[1]This chapter is based on the following publication:

Diogo G.S, Marques C. F., Sotelo C. G., Pérez-Martín R. I., Pirraco R. P, Reis R. L., Silva T. H., *Cell-Laden Biomimetically Mineralized Shark-Skin-Collagen-Based 3D Printed Hydrogels for the Engineering of Hard Tissues*. ACS Biomaterilas Science and Engineering. 2020, 6: p: 3664–3672.

VI-2. INTRODUCTION

Composite 3D structures based on collagen-apatite materials have been widely employed in the Tissue Engineering (TE) field, with the vision of mineralized tissues' regeneration [1]. Collagen has been receiving increasing attention as a biomaterial for use in regeneration of several tissues, since it is a key protein sustaining extracellular matrix (ECM) structure and comprises RGD (Arginine-Glycine-Aspartic acid) domains which positively affect cell attachment, migration and growth by its specific interactions with cell integrin receptors [2, 3]. Apatite-based materials have been used due to their intrinsic excellent biocompatibility and bioactivity, encouraging cell adhesion, proliferation and osteogenic differentiation [1]. Hydroxyapatite (HAp), the major inorganic component of bone tissue is usually the first option in scaffold production for bone regeneration [1]. Considering the excellent properties of calcium phosphates for hard tissue applications, various methods of polymer-ceramic combination have been explored and applied. Direct mixing of calcium phosphate powder with polymer solution or scaffold immersion in simulated body fluid (SBF) or modified SBF are the most used techniques. However, both methods bring disadvantages. Direct mixing is an uncontrolled method and can result in lack of particle distribution homogeneity through the polymer matrix, which limits scaffolds bioactivity. Soaking scaffolds in simulated body fluid requires long time of incubation, which can alter the release characteristics of any encapsulated therapeutic agents or biological factors [4]. In that sense, co-precipitation methods emerge as a good alternative. When compared to scaffolds prepared by physically mixing of collagen and apatite particles, co-precipitation can be used to better control particles distribution and improve the effectiveness in mimicking of the native tissue by the scaffold nano-structure [5]. Such method involves the reaction of calcium-rich substrates with aqueous solutions of phosphate sources, providing the PO_4^{3-} ions needed for HAp formation [6]. Considering the advantages of the technique, different authors have been studying the potential of producing three-dimensional scaffolds made of mineralized collagen. Gelinsky *el al.* studied the potential of producing porous scaffolds by inducing *in situ* mineralization of type I collagen from bovine [7]. In a more recent work, they also study the potential of the *in situ* mineralization method using a marine collagen source [8, 9].

However, most of the conventional scaffolding methodologies, like gas foaming, salt leaching and freeze drying, are considered uncontrolled methods resulting in lack of biofunctionality, especially due to deficient cell homogeneity, lack of vascularization networks and consequent necrotic core in the case of thick constructs. Therefore, the possibility to better control scaffolds' architecture accuracy, including

pore size, porosity and reproducibility, makes printing techniques a hopeful and alternative approach [10-12]. We proposed for the first time the fabrication of cell-laden 3D printable hydrogels by using a biomimetic approach of *in situ* mineralization of *Prionace glauca* (PG) collagen combined with alginate. Alginate is a biocompatible and degradable natural polymer characterized by its fast gelation in the presence of di- or trivalent cations like calcium (Ca^{2+}), making it a useful material for 3D printing [13], while collagen provides cell activating sites to promote cell adhesion, migration and proliferation [2, 14]. Using a marine by-product for the production of collagen, we are adding value to a product that is considered waste for the fishing transformation industry, materializing its huge potential [15, 16]. PG has become a promising collagen source due to the intrinsic characteristics of this biopolymer, namely regarding applications in biomedicine [17, 18]. The resulting 3D printed cell-laden scaffolds were characterized, and its biological performance was addressed by encapsulating a fibroblast cell-line.

VI-3. MATERIALS AND METHODS

VI-3.1. *In situ* mineralization of PG skin collagen

Collagen was extracted from blue shark (*Prionace glauca*) skin through an acidic method previously established [19]. Hydrochloric acid (HCl, Sigma-Aldrich, Lisbon, Portugal) at 10 mM was used as a solubilizing agent of collagen. To induce collagen mineralization, calcium chloride ($CaCl_2$, VWR, Lisbon, Portugal) and ammonium hydrogenphosphate ($(NH4)_2HPO_4$), Sigma-Aldrich, Lisboa, Portugal) were used as calcium and phosphorous precursors, respectively. Briefly, PG collagen (20 $mg.mL^{-1}$) was mixed with $CaCl_2$ followed by neutralization with sodium hydroxide (NaOH, Enzimatic, SA, Lisbon, Portugal) at 15 mM. After that, $(NH_4)_2HPO_4$ was added as a phosphate supplier of the reaction considering a 1.67 calcium-to-phosphorous ratio. To promote hydroxyapatite formation, the process was carried out for 2 h at low temperature (6 °C) under magnetic stirrer at controlled pH (8). The entire process was maintained under sterile conditions.

VI-3.2. Fourier transform infrared (FTIR) spectroscopy

The chemical composition of mineralized and pure collagen was analyzed by Fourier transform infrared spectroscopy (FTIR) under attenuated total reflectance (ATR) (IRPrestige 21, Shimadzu). To perform IR spectroscopy, the previously *in situ* mineralized PG collagen was frozen at -80 °C and

lyophilized. After that, the sample was mixed with potassium bromide (KBr) (1:100, wt.%) and then uniaxially pressed to obtain a transparent disk. Each infrared spectrum was the average of 32 scans collected at 2 cm^{-1} resolution in the wavenumber region of 3600-500 cm^{-1} at room temperature (RT) [20].

VI-3.3. X-ray diffraction (XRD)

The crystallinity of the *in situ* mineralized PG collagen was investigated using an x-ray diffractometer. The sample preparation was similar to that for FTIR. The diffraction measurements were performed using a conventional Bragg–Brentano diffractometer (Bruker D8 Advance DaVinci, Germany) equipped with Cu Kα radiation. Data sets were collected in the 2θ range of 10 – 60° with a step size of 0.02° and 1 s for each step [20].

VI-3.4. Transmission electron microscopy (TEM) analysis

To corroborate the results obtained by x-ray diffraction, TEM analysis was performed. The mineralized collagen solution was diluted 100 times and deposited on TEM grids, ultrathin carbon film on lacey carbon support film, 400 mesh, copper (IESMAT). For the images, was used a transmission electron microscope (TEM) (JEOL 2200F), operated at an acceleration voltage of 200 kV. Micrographs were recorded with a 1k×1k CCD camera (multi scan, Gatan, USA), and fed to a computer for on line image processing (Digital Micrograph 3.3.1., Gatan).

VI-3.5. Thermogravimetric analysis (TGA)

The inorganic content (corresponding to the CaP particles) in the *in situ* mineralized collagen was determined by thermogravimetric analysis. Three samples of lyophilized mineralized collagen weighing around 7 mg were analyzed by using a Simultaneous Thermal Analyzer (STA7200, Hitachi) and the measurements were recorded from 40 to 105 °C and 105 to 600 °C with a heating rate of 10 °C min^{-1} in nitrogen and oxygen, respectively. Derivative thermogravimetry (DTG) provides the decomposition rate of the samples, and it is useful for the evaluation of the different steps of mass loss. The amount of sample at the end (600 °C) corresponds to the inorganic part. The results are the mean of three independent experiments [21].

VI-3.6. Cell-laden bioinks' preparation

To prepare the cell-laden bioinks, different blends of PG mineralized collagen and alginate were tested. Mineralized collagen solution was prepared as previously mentioned. Alginate (Sigma-Aldrich) was solubilized in 0.9% (w/v) sodium chloride (NaCl, Laborspirit, Lisbon, Portugal) solution under mild stirring at room temperature (overnight) and was used to increase solution viscosity. Mineralized collagen and alginate concentrations were fixed at 2% and 12% (w/v), respectively, and combined accordingly to the following ratios: collagen:alginate (v/v) 1:1, 1:2, 1:3 and AG (pure alginate). The different combinations resulted in four different final concentrations of collagen and alginate. Mouse fibroblast cell line (L929 from THERMO FISHER, Lisbon, Portugal) were expanded in DMEM low glucose, supplemented with 10% fetal bovine serum (ALFAGENE, Carcavelos, Lisbon) and 1% penicillin/streptomycin (ALFAGENE, Lisbon) and cultured until 80% of confluence. After that, the cell-laden bioinks were prepared by encapsulating $1.2x10^6$ cells.mL^{-1}. Briefly, 250 μL of culture medium containing the respective number of cells, were transferred by pipetting into the middle of each bioink blend, and manually carefully stirred to create an homogenous distribution of the cells.

VI-3.7. Printing process

Each cartridge was filled with 2.5 mL of biomaterial being followed by the 3D printing with the respective encapsulated cells. The printing process was carried out at room temperature (25 °C) using sterile material. Cell-laden bioinks were printed using a bioprinter V1 (REGEMAT 3D, Granada, Spain) with a printing nozzle of 410 μm of inner diameter, at a printing speed of 10 $mm.s^{-1}$. A standard 3D printing software was used to design the 3D mesh structures: 12 x 12 x 2.8 mm (width x length x height), in a total of 6 layers with 1000 μm of pore size. After the printing, the 3D structures were ionically crosslinked during 3 minutes with a 10% (w/v) $CaCl_2$ solution dissolved in DMEM. **Figure VI-1** illustrates the overall bioprinting process for 3D cell-laden constructs fabrication, resulting from the combination of mineralized PG collagen and alginate.

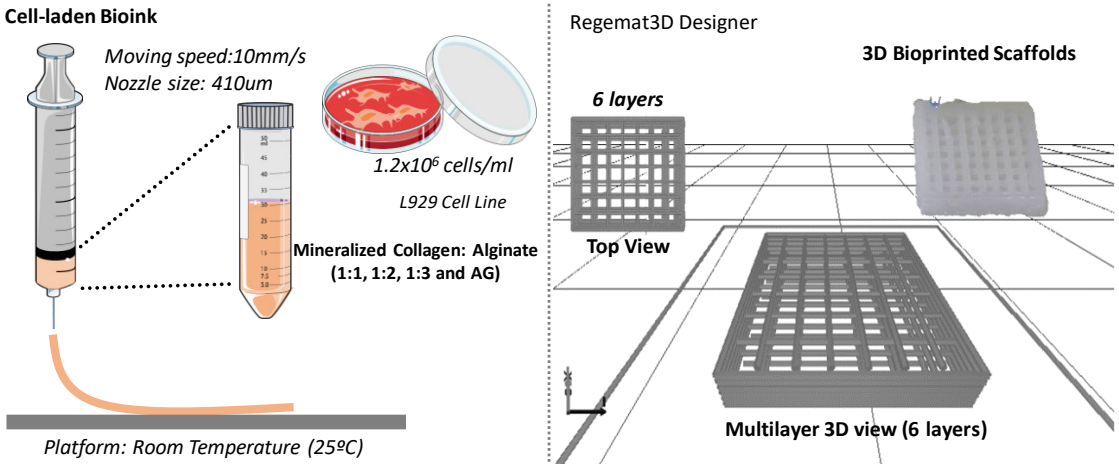

Figure VI-1- Schematic representation of the process to fabricate cell-laden mineralized collagen:alginate hydrogels by using a Regemat3D V1 bioprinter dispensing system.

VI-3.8. Rheological properties

To assess the printability of the different blends' composition, and to study the influence of rheological properties on cell survival, oscillatory and viscosity studies using a rheometer (Kinexus Prot, Malvern) were carried out. The apparent viscosity was measured in viscometry mode using a cone and plate sensor system (4° / 40 mm). The visco-elastic properties were assessed using the same rheometer equipped with plate and plate sensor, with a 1 mm gap size. In the oscillatory mode a solvent trap was used to prevent water evaporation from the samples during the tests and the temperature was maintained at 37 °C throughout the measurement period [22].

The shear rate was swept from 0.01 to 10 and 0.01 to 100 s^{-2} to determine the elastic modulus (G´) and viscosity, respectively, with records taken every 10 points per frequency sweep range.

VI-3.9. Biological characterization of cell-laden PG printable gels

VI-3.9.1. Live/dead assay of the constructs

Cell viability of the constructs, 1 and 7 days after printing, was conducted using a live/dead viability assay. After each culture period, cell-laden constructs were incubated in dark conditions for 30 min at 37 °C in culture medium containing calcei-AM (AM) (1:500) and propidium iodide (PI) (1:1000) to stain the live and dead cells, respectively. After incubation, samples were observed in a transmitted

and reflected light microscope (Zeiss, Germany) with the green staining representing the live cells and red staining comprising dead cells. To control for non-specific staining, acquisitions of scaffolds without cells were stained with PI or AM.

VI-3.9.2. DAPI and phalloidin analysis

To study cell morphology in the different cell-laden printed hydrogels, diamidino-2-phenylindole (DAPI) (1:100) and phalloidin (Ph) (1:500) staining were used. Briefly, cell membranes were permeabilized with Triton X-100 (0.2%) for 5 min and further stained with DAPI:Ph in the nuclei and cytoplasm, respectively, for 20 min. After that, the images were acquired by using a laser scanning confocal microscopy imaging system (TCS SP8, Leica, Wetzlar, Germany) using an excitation wavelength of 405 nm for DAPI, and 561 nm for Ph. Control samples stained with only DAPI and Ph were analyzed. The images were taken using a 20 x immersion objective.

VI-3.9.3. DNA quantification

To assess cell number within the hydrogels throughout time, dsDNA content was measured after each culture period, 1 and 7 days, respectively. For this, all the constructs were washed with PBS and 1 mL of distillated water was added to each well material and maintained at 37 °C, followed by a thermal shock (-80 °C). The DNA content was determined using a Quant-IT PicoGreen dsDNA Assay Kit using excitation/emission wavelengths of 485/528 nm, respectively, in a microplate reader (Synergie HT, Bio-Tek). The standard curve for DNA was generated from the fluorescence of different DNA solutions with standard concentrations. The results are the mean of three independent experiments (n=3) with three replicates for each condition and per experiment.

VI-3.9.4. Metabolic activity

To study the metabolic activity of cells in the different bioink blends, 3-(4,5-dimethylthiazol-2-yl)-5-(3 carboxymethoxyphenyl) 2-(4-sulphofenyl)-2*H*-tetrazolium, inner salt (MTS) (VWR) assay was used and normalized with the DNA quantification results. Cell-laden structures were maintained in culture conditions, 37°C and 5% CO_2 for 7 days. This assay quantifies the metabolic activity of the cells by the reduction of tetrazolium salt reagent to formazan after 3 h of incubation at 37 °C. Absorbance intensity,

which is directly proportional to the metabolic activity, was measured at 492 nm using a microplate reader (SYNERGY HT, BIO-TEK). The results are the mean of three independent experiments (n=3) with three replicates for each condition and per experiment.

VI-3.10. Statistical analysis

Statistical analysis of the obtained results for the different groups of scaffolds at varied conditions was performed by using GraphPad Prism software (GraphPad Software Inc., USA). Data are presented as the mean ± standard deviation of a least three independent assays. First, a Shapiro-Wilk test was used to establish the assumption of data normality. Since data did not follow a normal distribution, a non-parametric test was used (Kruskal-Wallis test, with Dunn's Multiple Comparison Test and a p value less than 0.05 (*$p<0.05$) was considered statistically significant).

VI-4. RESULTS AND DISCUSSION

VI-4.1. Physical-chemical characterization of mineralized PG collagen.

In the present study, the intention was to develop an ionic method to address a collagen apatite composite material, instead of using a direct mixture [18]. The idea was the creation of a biomimetic approach to closer mimic the structural organization of the human native bone taking advantage of the method to fabricate stable inks. For that, the *in situ* mineralization (preferentially hydroxyapatite formation) of PG collagen by using a co-precipitation method was proposed. The apatite formation throughout the collagen is an ionic process that starts with the nucleation of calcium ions onto carboxyl groups that is a key factor to promote the hydroxyapatite formation onto collagen fibrils. This process is only completed when these calcium ions bind to the added phosphate ions and it only occurs under determined conditions. [23]. To study the efficiency of the method, FTIR was used as a first physico-chemical characterization, that was useful to identify the chemical composition of the previously mineralized collagen. **Figure VI-2** shows the FTIR spectra of the pure (black) and mineralized (grey) collagen. The broad band around 3500 cm^{-1} present in both spectra resulted from different units' vibration with hydrogen associated with the presence of water in the sample or N-H stretching (amide A) [5, 8]. The strong peaks around 1660 cm^{-1} cm can be assigned to C=O stretch of amide I. The given peaks at 1540 and 1200 cm^{-1} arise from N-H deformation of amide II and C-N stretch of amide III,

respectively. The presence of the bands between 500-600 and 1200-965 cm^{-1} in the FTIR spectrum of mineralized PG collagen (grey line) corresponds to the anti-symmetric and symmetric blending vibration of the PO_4^{3-} groups [2, 15], which confirmed the efficiency of the mineralization process. Additionally, from the absorption ratio (close to 1) between amide III (1235 cm^{-1}) and the peak at 1450 cm^{-1} for the mineralized collagen spectrum, the preservation of the collagen triplex helix could be confirmed, which is a strong indication that no denaturation occurs during the whole preparation process [20, 24].

To verify if the reaction conditions (pH 8, 6 °C, calcium-to-phosphate-ratio = 1.67) were suitable for the formation of hydroxyapatite, XRD (**Figure VI-3**) was carried out. From data analysis, the patterns of the mineralized collagen (**Figure VI-3**) confirmed the formation of the HAp phase (ICDD 00-055-0592) with the most intense XRD peaks at 2θ = 31.7 and 32.9 corresponding to the diffraction planes (3 0 0) and (1 1 2). These results are in good agreement with the FTIR results, confirming that the P-O bonds detected in the mineralized collagen FTIR spectrum correspond to the formation of hydroxyapatite, suggesting the efficacy of collagen *in situ* mineralization to produce HAp. Comparing these results with the ones obtained by Xia *et al.*, wherein the biomimetic mineralization of type I rat tail collagen was induced by immersion in mSBF, similar peaks were observed [5]. However, in that study, the diffraction peak was broad, indicating the poor crystallinity of the mineralized scaffolds. From our method the resulting peaks are sharp and well defined suggesting the high degree of crystallinity of the biomimetically produced HAp. Our results are in accordance with the results obtained by Gelinsky *et al.* and Hoyer *et al.* performed with bovine and salmon collagen, respectively [7, 8].

As complementary information and to corroborate the X-ray diffraction results, the mineralized collagen solution was investigated by transmission electron microcopy (TEM). In **Figure VI-4**, the co-precipitation of apatite crystals onto the collagen fibrils was demonstrated. The apatite crystals are represented by the dark and dense phases, with a plate-like appearance in a random orientation, as indicated by arrows. The results are well correlated and comparable with what was observed in other studies [25, 26]. Moreover, at high magnifications, the crystalline profile of the co-precipitated apatite could be observed. The apatite crystals are represented by a well-defined pattern (indicated by arrows, right image) unlike the amorphous phase of collagen.

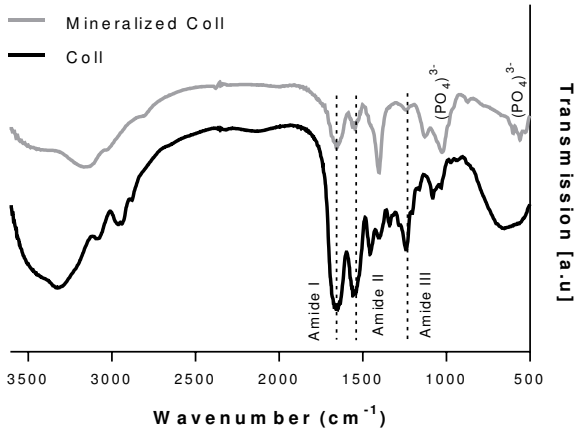

Figure VI-2 - FT-IR spectra of pure (black) and mineralized (grey) PG collagen

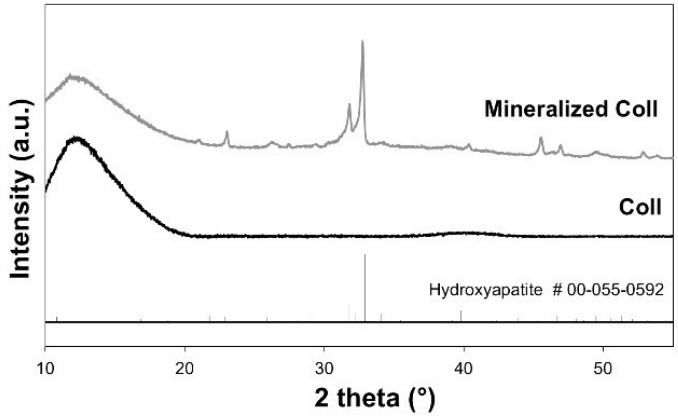

Figure VI-3 - X-ray diffraction spectra of pure (black) and mineralized (grey) PG collagen.

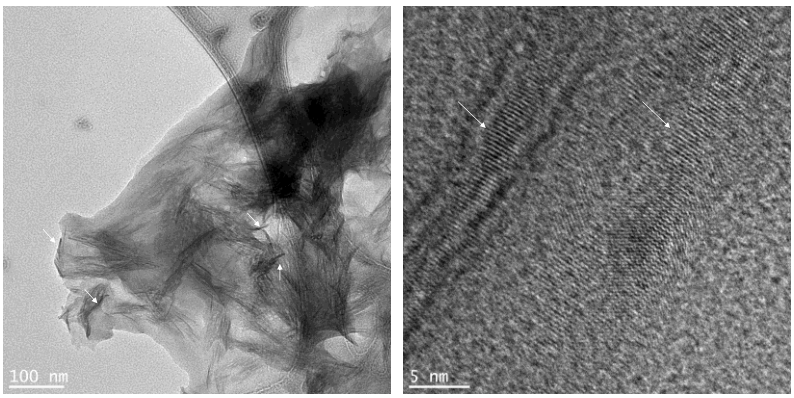

Figure VI-4 - TEM image of mineralized collagen demonstrating plate-like apatite (some crystals indicated by arrows) throughout the collagen fibrils (left image), and high magnifications showing the crystalline profile of the co-precipitated apatite (right image).

To investigate the ratio between the organic and inorganic components of the mineralized PG collagen, thermogravimetry of the freeze-dried sample was performed, assessing the mass decrement throughout the heating process. The characteristic DTG curve for mineralized collagen, measured in nitrogen, showed a characteristic peak between room temperature to 105 °C, resulting from sample dehydration, corresponding to 6.7% ± 3,0 of mass loss. In the characteristic oxygen DTG curve, three peaks (between 200 and 500 °C) corresponding to collagen degradation (59.8% ± 2.4) were observed (**Figure VI-5**). The organic part was completely burned at 500 °C and the final mass, corresponding to the inorganic part produced during the *in situ* mineralization process, was 33.43% ± 0.70. These ratio is quite different from the composition of natural human bone which is mainly composed by carbonate-rich hydroxyapatite (approximately 70%) [27].

Based on this collagen-to-mineral ratio, we propose in the future to approximate this value with the composition of ECM of the human native bone by increasing both Ca and P concentrations.

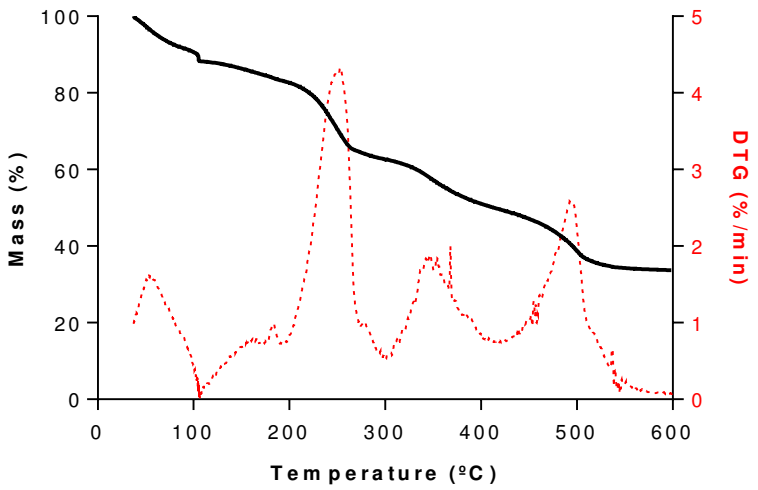

Figure VI-5 - TG and DTG curves of mineralized PG collagen.

VI-4.2. Bioinks characterization of mineralized PG collagen:alginate blends

Generally, an ideal bioink material for 3D cell-laden printing should gather a combination of desirable physical and biological properties [28]. The physical properties should enable a shear-thinning behavior, to guarantee not only the correct flow through the nozzle but also the filament shape during the printing process, ensuring 3D model fidelity and scaffolds' reproducibility. The biological properties (cell signalling) should ensure the scaffolds' biofunctionality [29]. Nevertheless, each bioprinting

technique requires specific bioink properties in order to reproduce 3D geometries with high accuracy and viability of the embedded cells or even bioactive molecules [28]. To assess the feasibility of our proposal, four different bioink formulations were studied to find the most suitable ratios of mineralized PG collagen:alginate (1:1, 1:2, 1:3 and AG) regarding the rheological properties, shape faithfulness, and biological performance. To do that, a step-by-step optimization process of the printing parameters based on a macroscopic observation of the printed scaffolds was used as a quick way to establish a starting point to achieve hydrogels with a relative shape accuracy. In that sense, alginate concentrations were adjusted accordingly to the features of the used printer in order to accomplish accurate hydrogels and to further combine with PG mineralized collagen.

From the rheological results, the viscosity and storage modulus (G′), of the 1:1, 1:2 and 1:3 bioink blends were found to be different than those of the alginate bioink (**Figure VI-6** and **Table VI-1**), nearly twice higher. These results can be related to the high concentration (12%) of the alginate bioink [30]. As previously described, for extrusion-based dispensing systems, printing accuracy is directly proportional to the viscosity [31, 32]. Shear-thinning behavior could be observed in **Figure VI-6** (left) for all tested condition, where viscosity decreases as the shear rates increases. Within the collagen-based bioinks, oscillatory frequency measurements, **Figure VI-6** (right), showed that storage modulus (G′) is higher for the 1:1 formulation (mineralized collagen:alginate), which can be related to the presence of higher amounts of Ca^{2+} ions, since this is the formulation with more mineralized collagen and less alginate concentration. As previously described, Hap formation throughout the collagen is an ionic process based on the addition of calcium ions. This process was proposed to have a synergistic effect on the designed system. In fact, the added ions were important to induce HAp formation (as could be confirmed by XRD and TEM images) but, at same time, they were also useful to ionically crosslink the alginate solution, making stable and stiff inks [33]. A decrease in the collagen concentration is directly associated with a decrease of the Ca^{2+} ions, and thus, the 1:2 and 1:3 formulations are represented by a lower storage modulus, due to a minor effect of the ionic crosslinking. As a consequence of the lower storage modulus the filaments start to merge and pore closure occurred, leading to a loss of the structure (**Figure VI-6**) [34]. Such effect was pronounced for the formulation 1:3 that exhibited the lower storage modulus. In fact, this last-mentioned formulation has more alginate in its constitution, however it means that has small amounts of mineralized collagen, being the Ca^{2+} scarcer and consequently a poor effect of ionic crosslinking. (**Figure VI-7**).

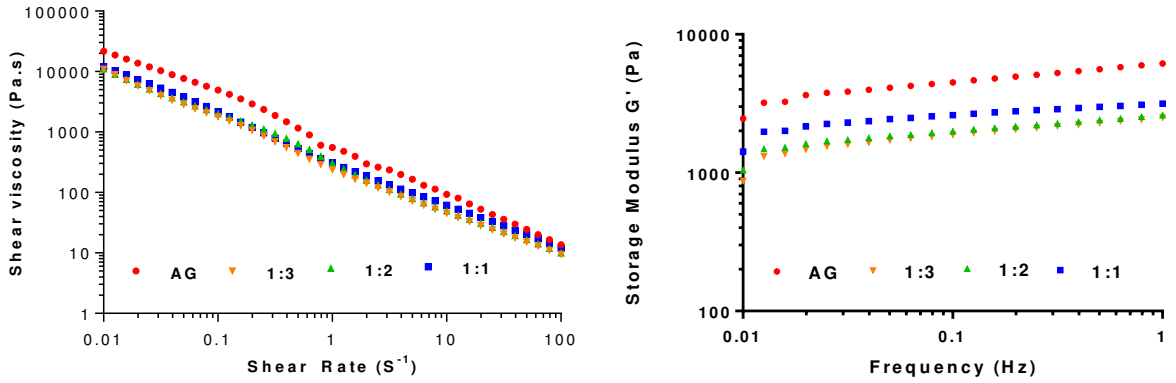

Figure VI-6 - Influence of mineralized PG collagen: alginate concentration on rheological properties measured at 37◦C. At left the different bioinks viscosities depending on shear rate is represented, and at right, the storage Modulus (G') at each applied oscillatory frequency is represented.

Tabela VI-1 - Viscosity (Pa.s) and stiffness (Pa) for the different bioink conditions.

Samples	1:1	1:2	1:3	AG
Viscosity (Pa.s) at 0.01 s^{-1}	12000	11100	11000	21700
Storage Modulus (Pa) at 1 Hz	3160	2610	2500	6160

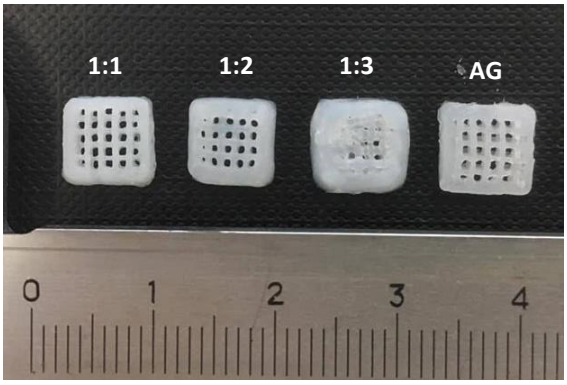

Figure VI-7 - Photograph of the printed hydrogels: from left to right, decreased concentrations of mineralized collagen.

VI-4.3. Cell response in cell-laden mineralized *Prionace glauca* collagen hydrogels

As a first biological approach of each biomaterial blend, *in vitro* assays using a fibroblast cell-line were maintained for 7 days. To qualitatively assess cell viability, live (green) and dead (red) cells were stained with calcein and propidium iodide in the cytoplasm and nucleus, respectively. **Figure VI-8** shows the fluorescence images of the constructs 1 and 7 days after printing. As it is possible to observe 1 day after printing, the incorporated cells in the different bioink blends were homogeneously distributed through all constructs, which indicates a successful mixing of the cells in the different ink blends. Nevertheless, significant differences in terms of green signal intensity (viable cells) were detected for the collagen-based bioinks when compared with alginate alone. This result can be related with the high viscosity and stiffness of the alginate bioink, 21700 Pa.s and 6160 Pa, respectively (**Figure VI-6**): high viscous bioinks are associated with an increased shear stress during the printing process, leading to cell damage [35]. To successfully obtain a mechanically stable and cell-viable construct, the bioink material should comprise an adequate range of rheological properties [22].

Since the physical properties (viscosity and stiffness) of the bioink materials have a great influence on cell survival during the printing, bioinks with similar mechanical properties should be compared. The three conditions with similar viscoelastic properties (1:1, 1:2, and 1:3) showed equivalent results 1 day after printing, with the green signal being identical between the different mineralized PG collagen:alginate bioink formulations. However, 7 days after cell culture the green signal was only significantly higher for the more concentrated collagen-based bioinks, 1:1 and 1:2. In the control condition (AG), as expected, the intensity of the red signal was evidenced. Since most of the cells died during printing, only the cells near to the pores survived. In the 1:3 formulation, a weaker green signal intensity was observed when compared with 1:1 and 1:2. Such a result indicated that the alginate-based materials do not provide adequate cues to guide cell survival and proliferation [36]. The qualitative assessment of cells morphological behavior 7 days after cell culture was performed acquiring DAPI and phalloidin fluorescence images (**Figure VI-8**, DAPI:Ph column). Cells spreading was significantly pronounced for the 1:1 and 1.2 bioink blends when compared to the pure alginate hydrogels.

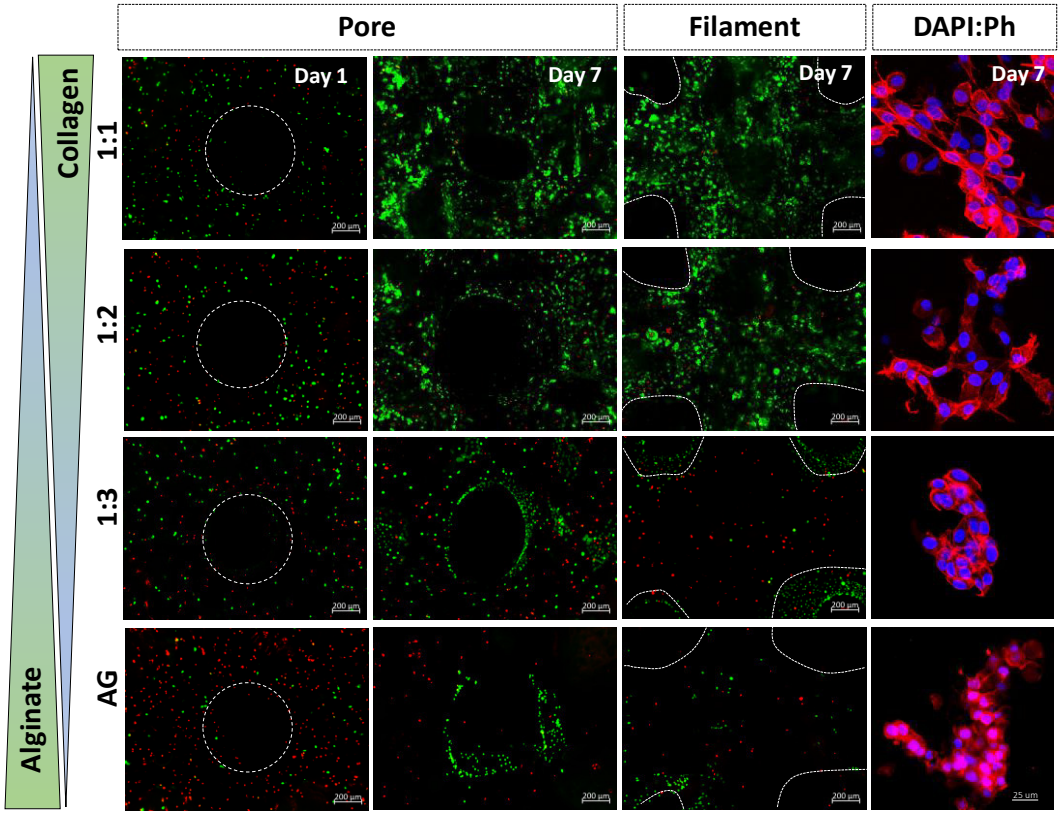

Figure VI-8- Live/dead images of fibroblast cell-line encapsulated in the different bioink blends, 1 and 7 days after printing. Viable cells stained in green color are more pronounced in the 1:1 and 1:2 blends. Dead cells (red) were abundant in the alginate conditions. Right column shows fluorescence microscopy images after DAPI and phalloidin staining to assess cell morphology.

The qualitative results were corroborated by quantitative assays (DNA and normalized MTS). The increased green signal in 1:1 and 1:2 conditions from day 1 to day 7 correlated well with the higher amount of double strained DNA (that is directly proportional to the cell number) assessed 7 days after cell-laden printing, confirming the ability of cells to proliferate in mineralized collagen hydrogels. In the remaining two conditions this increase was not so evident as cell number was affected by the higher alginate concentration. Moreover, to understand the influence of the produced hydrogels in the cell-line metabolic activity, MTS assay was performed, and the presented values resulted from normalization with DNA values (**Figure VI-9** left), 1 and 7 days after cell culture. In general, the metabolic activity was higher for the more concentrated collagen conditions (1:1 and 1:2) and there were no significant differences from day 1 to day 7. This suggests that these two conditions are highly cytocompatible. For the 1:3 condition, the metabolic activity per µg of DNA reduced drastically from day 1 to day 7

(****p<0.0001). The alginate concentration did compromise cell viability, with a low metabolic activity being observed already at day 1.

As the main conclusions, the 1:1 and 1:2 bioink blends were found to be highly efficient for obtaining biologically significant cell-laden 3D hydrogels when compared with 1:3 and AG. The survival of cells was favored by the presence of mineralized PG collagen, as indicated by the increase in cell density 7 days after cell culture. Marine derived collagen could guide cellular activities by inducing a good cellular response. As previously reported by other studies, this was possible due to the bioactive cues present in marine collagens [18, 37-39].

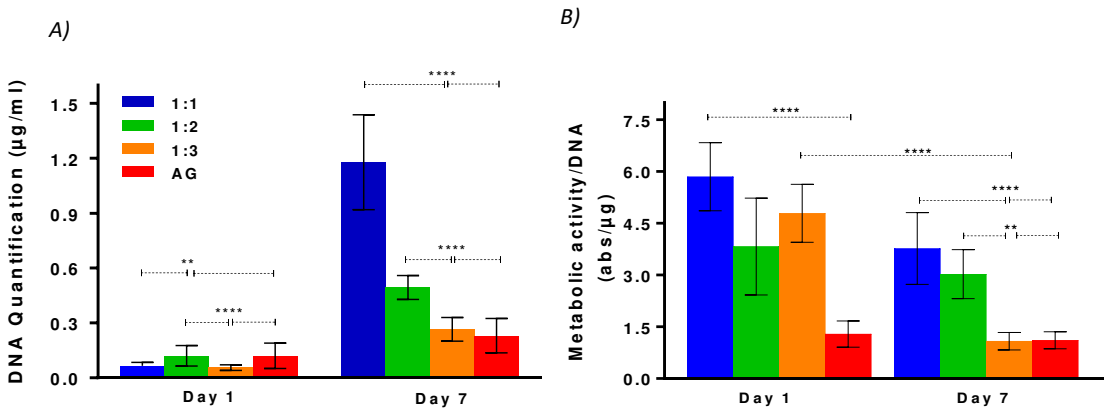

Figure VI-9 - DNA and MTS quantification of the different 3D printed hydrogels with the correspondent statistical analysis (p< 0.0035, *** p< 0.0008 and **** p<0.0001).**

VI-5. CONCLUSIONS

Successfully designed and printed cell-laden hydrogels made of in situ mineralized PG collagen through a tissue engineering biomimetic approach were achieved. In total 30% (w/w) of all mineralized collagen was confirmed as the hydroxyapatite phase. Different bioink blends resulting from the combination of this mineralized collagen with alginate were developed, being tested and optimized to obtain suitable mechanical and biological properties. From the evaluation of the different cell laden bioinks taking in consideration material properties, printability and cellular performance, the inks with more collagen revealed better results in a short-term 3D culture. Marine origin materials emerged as a safe and attractive alternative to mammalian materials for processing with advanced fabrication techniques, confirming the growing relevance of marine biomaterials in biomedical scientific

community. A promising marine-based hydrogel for the engineering of mineralized tissues is thus proposed based on a 3D printing manufacture strategy.

VI-6. ACKNOWLEDGMENTS

This study was funded by the Portuguese Foundation for Science and Technology (FCT) under the scope of the BiogenInk project (M-ERA-NET2/0022/2016), by the European Union Seventh Framework Programme (FP7/2007-2013) through grant agreement n. ERC-2012-ADG 20120216-321266 (ERC Advanced Grant ComplexiTE) and by INTERREG Atlantic Area Programme under project BlueHuman (EAPA_151/2016). The Doctoral Programme NORTE-08-5369-FSE-000044 and Structured Projects NORTE-01-0145-FEDER-000021 and NORTE-01-0145-FEDER-000023, supported by Norte Portugal Regional Operational Programme (NORTE 2020), under the PORTUGAL 2020 Partnership Agreement, through the European Social Fund, are also greatly acknowledge. RP thanks FCT for the contract IF/00347/2015. The authors acknowledge also the Centro Tecnológico del Mar - Fundación CETMAR (Vigo, Spain) and COPEMAR SA (fishing company, Spain) for the kind offer of fish by-products.

VI-7. REFERENCES

1. Turnbull, G., et al., *3D bioactive composite scaffolds for bone tissue engineering.* Bioactive materials, 2018. **3**(3): p. 278-314.
2. Schlie-Wolter, S., A. Ngezahayo, and B.N. Chichkov, *The selective role of ECM components on cell adhesion, morphology, proliferation and communication in vitro.* Experimental cell research, 2013. **319**(10): p. 1553-1561.
3. Zhang, D., et al., *The development of collagen based composite scaffolds for bone regeneration.* Bioactive materials, 2018. **3**(1): p. 129-138.
4. Luo, Y., et al., *Alginate/nanohydroxyapatite scaffolds with designed core/shell structures fabricated by 3D plotting and in situ mineralization for bone tissue engineering.* ACS applied materials & interfaces, 2015. **7**(12): p. 6541-6549.
5. Xia, Z., M. Villa, and M. Wei, *A biomimetic collagen–apatite scaffold with a multi-level lamellar structure for bone tissue engineering.* Journal of Materials Chemistry B, 2014. **2**(14): p. 1998-2007.

6. Sassoni, E., *Hydroxyapatite and other calcium phosphates for the conservation of cultural heritage: A review.* Materials, 2018. **11**(4): p. 557.
7. Gelinsky, M., et al., *Porous three-dimensional scaffolds made of mineralised collagen: preparation and properties of a biomimetic nanocomposite material for tissue engineering of bone.* Chemical Engineering Journal, 2008. **137**(1): p. 84-96.
8. Hoyer, B., et al., *Biomimetically mineralized salmon collagen scaffolds for application in bone tissue engineering.* Biomacromolecules, 2012. **13**(4): p. 1059-1066.
9. Bernhardt, A., B. Paul, and M. Gelinsky, *Biphasic scaffolds from marine collagens for regeneration of osteochondral defects.* Marine drugs, 2018. **16**(3): p. 91.
10. Wang, X., et al., *3D bioprinting technologies for hard tissue and organ engineering.* Materials, 2016. **9**(10): p. 802.
11. Duarte Campos, D.F., et al., *Bioprinting organotypic hydrogels with improved mesenchymal stem cell remodeling and mineralization properties for bone tissue engineering.* Advanced healthcare materials, 2016. **5**(11): p. 1336-1345.
12. Marques, C.F., et al., *Collagen-based bioinks for hard tissue engineering applications: a comprehensive review.* J Mater Sci Mater Med, 2019. **30**(3): p. 32.
13. Yang, X., et al., *Collagen-alginate as bioink for three-dimensional (3D) cell printing based cartilage tissue engineering.* Materials Science and Engineering: C, 2018. **83**: p. 195-201.
14. Lee, H.J., et al., *A New Approach for Fabricating Collagen/ECM-Based Bioinks Using Preosteoblasts and Human Adipose Stem Cells.* Advanced healthcare materials, 2015. **4**(9): p. 1359-1368.
15. Kim, S.-K. and E. Mendis, *Bioactive compounds from marine processing byproducts–a review.* Food Research International, 2006. **39**(4): p. 383-393.
16. Fernandes-Silva, S., et al., *Porous hydrogels from shark skin collagen crosslinked under dense carbon dioxide atmosphere.* Macromolecular bioscience, 2013. **13**(11): p. 1621-1631.
17. Elango, J., et al., *Evaluation of differentiated bone cells proliferation by blue shark skin collagen via biochemical for bone tissue engineering.* Marine drugs, 2018. **16**(10): p. 350.
18. Diogo, G., et al., *Marine collagen/apatite composite scaffolds envisaging hard tissue applications.* Marine drugs, 2018. **16**(8): p. 269.
19. Sotelo, C.G., et al., *Characterization of Collagen from Different Discarded Fish Species of the West Coast of the Iberian Peninsula.* Journal of Aquatic Food Product Technology, 2016. **25**(3): p. 388-399.

20. Alves, A.L., et al., *Cosmetic potential of marine fish skin collagen.* Cosmetics, 2017. **4**(4): p. 39.
21. Sionkowska, A. and J. Kozłowska, *Characterization of collagen/hydroxyapatite composite sponges as a potential bone substitute.* International Journal of Biological Macromolecules, 2010. **47**(4): p. 483-487.
22. Ribeiro, A., et al., *Assessing bioink shape fidelity to aid material development in 3D bioprinting.* Biofabrication, 2017. **10**(1): p. 014102.
23. Kikuchi, M., et al., *Self-organization mechanism in a bone-like hydroxyapatite/collagen nanocomposite synthesized in vitro and its biological reaction in vivo.* Biomaterials, 2001. **22**(13): p. 1705-1711.
24. Silva, T., et al., *Marine origin collagens and its potential applications.* Marine drugs, 2014. **12**(12): p. 5881-5901.
25. Hong, S.I., S.K. Hong, and D.H. Kohn, *Nanostructural analysis of trabecular bone.* Journal of Materials Science: Materials in Medicine, 2009. **20**(7): p. 1419-1426.
26. Reznikov, N., R. Shahar, and S. Weiner, *Bone hierarchical structure in three dimensions.* Acta biomaterialia, 2014. **10**(9): p. 3815-3826.
27. Ma, P.X., *Biomimetic materials for tissue engineering.* Advanced drug delivery reviews, 2008. **60**(2): p. 184-198.
28. Hölzl, K., et al., *Bioink properties before, during and after 3D bioprinting.* Biofabrication, 2016. **8**(3): p. 032002.
29. Ouyang, L., et al., *Effect of bioink properties on printability and cell viability for 3D bioplotting of embryonic stem cells.* Biofabrication, 2016. **8**(3): p. 035020.
30. Markstedt, K., et al., *3D bioprinting human chondrocytes with nanocellulose–alginate bioink for cartilage tissue engineering applications.* Biomacromolecules, 2015. **16**(5): p. 1489-1496.
31. Das, S., et al., *Bioprintable, cell-laden silk fibroin–gelatin hydrogel supporting multilineage differentiation of stem cells for fabrication of three-dimensional tissue constructs.* Acta biomaterialia, 2015. **11**: p. 233-246.
32. Di Giuseppe, M., et al., *Mechanical behaviour of alginate-gelatin hydrogels for 3D bioprinting.* Journal of the mechanical behavior of biomedical materials, 2018. **79**: p. 150-157.
33. Tampieri, A., et al., *HA/alginate hybrid composites prepared through bio-inspired nucleation.* Acta biomaterialia, 2005. **1**(3): p. 343-351.

34. Chung, J.H., et al., *Bio-ink properties and printability for extrusion printing living cells.* Biomaterials Science, 2013. **1**(7): p. 763-773.

35. Kim, Y.B., H. Lee, and G.H. Kim, *Strategy to achieve highly porous/biocompatible macroscale cell blocks, using a collagen/genipin-bioink and an optimal 3D printing process.* ACS applied materials & interfaces, 2016. **8**(47): p. 32230-32240.

36. Rowley, J.A., G. Madlambayan, and D.J. Mooney, *Alginate hydrogels as synthetic extracellular matrix materials.* Biomaterials, 1999. **20**(1): p. 45-53.

37. Liu, C. and J. Sun, *Potential application of hydrolyzed fish collagen for inducing the multidirectional differentiation of rat bone marrow mesenchymal stem cells.* Biomacromolecules, 2014. **15**(1): p. 436-443.

38. Elango, J., et al., *Rheological, biocompatibility and osteogenesis assessment of fish collagen scaffold for bone tissue engineering.* International journal of biological macromolecules, 2016. **91**: p. 51-59.

39. Yamada, S., et al., *Potency of fish collagen as a scaffold for regenerative medicine.* BioMed research international, 2014. **2014**.

Chapter VII

Next Generation Bioink based on Mineralized Shark Collagen with Intrinsic Osteogenic Properties: a Step Towards the Future of Bone Regeneration

Chapter VII

Next Generation Bioink Based on Mineralized Shark Collagen with Intrinsic Osteogenic Properties: a Step Towards the Future of Bone Regeneration[1]

VII-1. ABSTRACT

3D printing with incorporated living cells – bioprinting – has gained special attention on tissue engineering approaches, aiming to closer recapitulate the target tissue microenvironment. However, it raises additional complexity related with the need to use cell-friendly printing conditions that still comply with material printing fidelity. Inspired on the composite nano structural organization of mineralized tissues, this work reports the efficiency of the chemical approach followed to in situ mineralize blue shark skin collagen, at a nano scale level, to ultimately produce stable inks. The impact of initial cellular density was evaluated by testing three different concentrations (2.5, 5 and 7.5 $x10^6$ cell.mL^{-1}) of human adipose stem cells (hASC), where biological results demonstrated improved cell viability with the higher density of encapsulated cells. Immunodetection of RUNX2 and Osteopontin 21 days after cell culture confirmed the potential of the ink to induce osteogenic differentiation without any exogenous stimulation, which may be due to successful cell-to-ink interaction and the Ca^{2+} ions released from the co-precipitated hydroxyapatite. A combination of mineralized shark collagen, alginate and hASC is thus proposed as bioink with intrinsic osteogenic properties for the regeneration of bone tissue.

[1]This chapter is based on the following publication:

Diogo G. S, Marques C.F., Freitas-Ribeiro S., Sotelo C. G., Pérez-Martín R. I., Pirraco R. P., Reis R.L., Silva T. H., *Next generation bioinks based on mineralized shark collagen with intrinsic osteogenic properties: a step towards the future of bone regeneration. (submitted).*

VII-2. INTRODUCTION

An ideal 3-dimensional (3D) Tissue Engineering (TE) scaffold should mimic the extracellular matrix (ECM) of the targeted tissue, or at least stimulate its production, to provide an helpful microenvironment for cell growth and tissue regeneration [1]. Vascularization and appropriated angiogenic properties of bioengineered scaffolds are found to play a key role for nutrients and oxygen transport, which strongly determines the success or failure of scaffolds. Conventional techniques of scaffolding production like freeze-dry, gas foaming and salt-leaching are commonly deprived of desired network vasculatures due to inadequate 3D microarchitecture, which often results in cell death and scaffolds failure. 3D printing strategies have been used to address such challenges by providing more sophisticated structures [2-6]. Combining 3D printing strategies with conventional techniques can be a step forward to develop more complex 3D structures [7]. It was recently demonstrated that the combination of 3D printing technology with solvent casting and particle leaching resulted in sophisticated scalable vasculatures with biomimetic architectures. In fact, the interconnected microchannels and the micro porosities created in the walls efficiently increased cell infiltration into the scaffold core and vessels formation [7].

More recent and promising, 3D bioprinting (printing with living cells) techniques have been adopted for TE to better mimic and recreate the target tissue. However, 3D bioprinting requires a specific set of conditions, particularly an aqueous environment (hydrogels are preferred), an adequate oxygen and nutrient diffusion, as well as a suitable pH and osmolarity, which gives a favourable microenvironment to enable new ECM formation [3]. Cells interaction with inks is highly dependent on the rheological, structural and chemical signalling properties, which increases complexity and raises particular challenges [8, 9]. Although there's a large variety of materials employed to prepare bioinks (inks with living cells), bioactive inks to support the incorporated living cells are still lacking [9].

The marine ecosystem is populated by a significant variety of species representing a huge potential for new resources exploration, being bioactive molecules the most requested [10]. Within the different bioactive molecules, collagen has been getting special attention due to its intrinsic bioactivity (as the presence of RGD (arginine-glycine-aspartic acid) domains) [11, 12]. A large amount of wasted or underutilised by-products (skins, scales, bones and others) resulting from the fish processing industry have been explored to extract high quality collagen, without any risk of disease transmission to humans (like bovine spongiform encephalopathy (BES) mammals), free of religious constraints, with fewer regulatory and control problems than collagen from terrestrial mammals and its derivates (that have been restricted on countries reporting cases of BSE) [13-16] .

In the present work three main objectives were proposed, 1) the preparation of a bioactive and biomimetic ink with incorporated human adipose stem cells (hASC); 2) the optimization of cell density; and 3) the assessment of the osteogenic potential of the prepared bioink without any exogenous osteogenic stimulation, in a long term culture. Past studies have demonstrated the feasibility of the inks during the printing process, but few studies have been demonstrating its potential in a long term [9]. In our previous work, we demonstrated the successful functionalization of collagen carboxylic groups (COOH) with calcium ions (Ca^{2+}) used to mineralize collagen with nano Hap (hydroxyapatite), being also shown how this mineralized collagen could improve the inks stability. Here, we focused the work on understanding how cells density affect cell viability and how the release of the Ca^{2+} ions from the mineralized collagen could favour the osteogenic differentiation of hASC through the activation of specific cellular signalling pathways. Previous studies have demonstrated that a microenvironment sustained with Ca^{2+} ions could modulate *in vitro* and *in vivo* cell signalling, being thus ceramics-based materials preferentially used for bone regeneration [17-19]. In an attempt to provide a next generation bioink with intrinsic osteogenic properties, the viability of the encapsulated hASC was evaluated until day 14 and their differentiation was evaluated after 21 days of culture by appraising the expression of osteogenic related markers by immunocytochemistry.

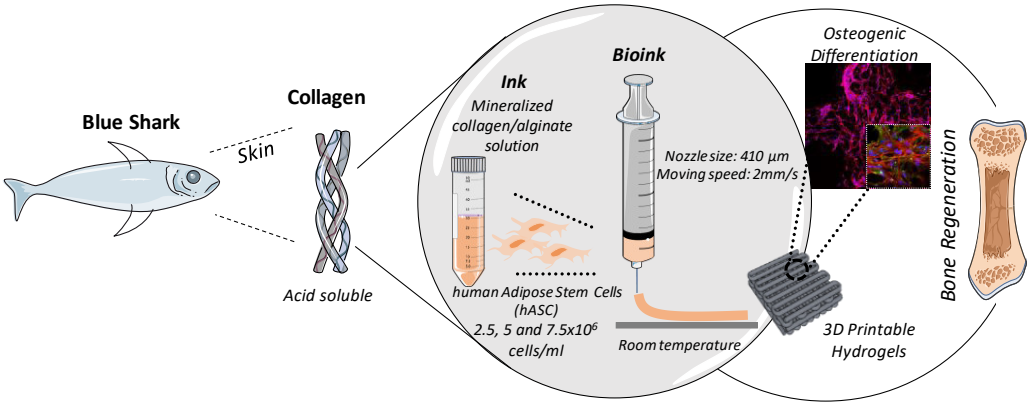

Figure VII-1 - Schematic representation of blue shark collagen processing into 3D cell-laden printable inks and its osteogenic potential.

VII-3. MATERIALS AND METHODS

VII-3.1. Collagen extraction procedure

Collagen (mainly type I) was extracted from blue shark (*Prionace glauca*) skin, according to the methodology used by Hwang *et al* [20, 21]. Firstly, the raw material was submitted to a preparation

process, including cleaning and size reduction. After that, about 10 g of material was weighed and subjected to an alkaline treatment (10 volumes of 0.1 M NaOH) under magnetic stirring in a cold room (3–5 °C) for 24 h in order to remove the non-collagenous proteins and pigments. After centrifugation, the supernatant was removed, and the remaining pellet was washed with distilled water (three times). The acid soluble extraction process was started with the washed pellet by stirring overnight with 10 volumes of 0.5 M acetic acid. The extract was centrifuged at 10,000 × g for 20 min at 10 °C and the supernatant was dialyzed against distilled water for 2 days in a cold room, at 3–5 °C. Volume of dialyzed collagen extract was measured and freeze-dried. The dried material corresponded to the amount of the extracted acid soluble collagen (ASC).

VII-3.2. Aminoacidic content analysis

To characterize the extracted *Prionace glauca* collagen, the amino acid pattern was studied through a quantitative amino acid analysis using a Biochrom 30 (Biochrom Ltd, Cambridge, U.K) at Centro de Investigaciones Biológicas of the Spanish National Research Council (CSIC), in Madrid (Spain). After all extraction and purification processes, the collagen was hydrolyzed and separated through a cation-exchange resin column accordingly to a procedure developed by Spackman, More and Stein in 1958 [22]. The column eluent was mixed with ninhydrin reagent to react with the aminoacids. The reaction formed colored compounds that were analyzed at two different wavelengths, 440 and 570 nm. Norleucine was used as an internal standard for the quantitative analysis. The results are the mean of three independent measurements.

VII-3.3. Sodium dodecyl sulfate-polyacrylamide gel electrophoresis (SDS-PAGE)

The protein molecular mass analysis was studied by using SDS-PAGE through a 10% running gel and 4% of stacking gel. SDS-PAGE was prepared by using reagents from Sigma and casted on a Biorad Mini Protean II System. Solubilized collagen was mixed with a buffer heated at 95 °C for 5 min into a digital thermoblock TD150P3 (FALC) until proteins denaturation. After that, a 15 µL sample loading volume (10 µg per lane) was used. Also, 4 µL of protein marker was loaded with the samples. Electrophoresis was carried out at 75 V for 15 min followed by 150 V until the frontline reached the lower part of the gel. After running, gel was stained with coomassie blue R-250 in methanol (50%) and acetic acid (10%) for 30 min followed by destaining with methanol (5%) and acetic acid (7%). ´

VII-3.4. Fourier transform-infrared (FT-IR) spectroscopy

As a complementary information of collagen characterization, the chemical composition of pure collagen was analyzed by Fourier transform infrared spectroscopy (FTIR) under attenuated total reflectance (ATR) (IRPrestige 21, Shimadzu). After extraction, the collagen solution was frozen at -80°C, lyophilized and the resulting material (collagen) was mixed with potassium bromide (KBr) (1:100, wt.%) and then uniaxially pressed to obtain a transparent disk. Each infrared spectrum was the average of 32 scans collected at 2 cm^{-1} resolution in the wavenumber region of 3500-500 cm^{-1} at room temperature (RT).

VII-3.5. Collagen mineralization

For collagen mineralization, a 2% (20 mg. mL^{-1}) collagen solution was prepared in 10 mM hydrochloric acid (HCl, Sigma-Aldrich, Lisbon, Portugal). The mineralization started with the addition of a calcium source ($CaCl_2$, VWR, Lisbon, Portugal) to nucleate the carboxylic (COOH) groups of collagen. To induce the formation of hydroxyapatite phase, the solution was neutralized with sodium hydroxide (NaOH, Enzimatic, SA, Lisbon, Portugal) at 15 mM. After that, $(NH_4)_2HPO_4$ was added as a phosphate supplier of the reaction considering a 1.67 calcium-to-phosphorous ratio. The process was maintained under magnetic stirring for 2 h at low temperature (6 °C). All the process was maintained under sterile conditions.

VII-3.6. X-Ray diffraction analysis

X-ray diffraction was performed to study the suitability of the method to induce collagen mineralization by assessing the crystal patterns of formed calcium phosphate ceramics. The diffraction measurements were performed using a conventional Bragg–Brentano diffractometer (Bruker D8 Advance DaVinci, Germany) equipped with Cu Kα radiation. The XRD patterns were collected from 10 to 60° on a 2θ scale in steps of 0.02° with a counting time of 1 s for each step. Different samples were carried out to confirm the reproducibility of the method.

VII-3.7. Transmission electron microscopy (TEM) analysis

To evaluate the mineralized collagen crystalline structure at the nanoscale level, HR-TEM analysis was carried out. The mineralized collagen solution was deposited on TEM grids, ultrathin 6 carbon film on lacey carbon support film, 400 mesh, copper (IESMAT). For the images, a transmission electron microscope (TEM) (JEOL 2200F) was used, operated at an acceleration voltage of 200 kV. For data analysis, Digital Micrograph 3.3.1. software (Gatan Inc., USA) was used. The lattice spacing was measured based on the histogram analysis obtained from the Inverse fast fourier transform (IFFT) of the HR-TEM micrographs.

VII-3.8. Collagen-based ink preparation

For the ink preparation, we used the methodology established in our previous work [23]. Briefly, mineralized collagen solubilized at 2 mg. mL^{-1} and sodium alginate (Sigma-Aldrich, Lisbon, Portugal), solubilized at 12 mg. ml^{-1} in 0.9% (w/v) sodium chloride (NaCl, Mw:58,44, Laborspirit, Lisbon, Portugal) solution, were combined in different proportions (1:1, 1:2 and 1:3 of mineralized collagen:alginate (v/v). Here, an intermediate condition between 1:1 and 1:2 (earlier confirmed as the best conditions) was prepared. So, the final ink had in its constitution (8.75:67.5 mg. mL^{-1} of mineralized collagen/alginate).

VII-3.9. Inks rheological properties

To study how temperature affects collagen rheological properties, oscillatory temperature sweep experiments were carried out using a Kinexus Prot, Malvern rheometer. The complex viscosity (n*), storage (G'), and tangent delta (tan δ = G''/G') were obtained by using a measuring system composed by an upper stainless steel parallel plate of 8 mm diameter (PU20 SR1740SS), with 1 mm gap size. A temperature sweep ranging between 4 °C and 45 °C with a ramping rate of 2 °C min^{-1} (1% strain and frequency = 1 Hz) was conducted within the range of the Linear Viscoelastic Region (LVER) previously determined. The shear rate was swept from 0.01 to 10 and 0.01 to 100 s^{-2} to determine the elastic modulus (G´) and viscosity, respectively, with the recordings taken every 10 points per frequency sweep range.

VII-3.10. 3D printing methodology

For bioprinting a REGEMAT (Granada, Spain) 3D PRINTER dispensing system was used. Squares with 8 mm in length and 2 mm in height with 750 μm of pore size (considered as the distance between the parallel struts) were printed with 90° orientation between adjacent layers, at 10 mm. s^{-1} with a printing nozzle of 410 μm of inner diameter. The final printed hydrogels were constituted by 6 layers. Each cartridge was filled with 2.5 mL of ink solution with incorporated living cells at different concentrations (2.5, 5 or 7.5 x 10^6 cells. mL^{-1}). The printing was carried out at 20 °C and the resulting 3D structures were characterized.

VII-3.11. Scanning electron microscopy (SEM)

To evaluate the microarchitecture of the 3D printed structures, printed hydrogels were lyophilized and coated with gold to be analyzed in a scanning electron microscope (JSM-6010 LV, JEOL, Japan). High-Resolution Field Emission Scanning Electron Microscope with Focused Ion Beam (FIB – SEM) (AURIGA COMPACT, ZEISS) was used to observe the newly formed hydroxyapatite.

VII-3.12. Micro-Computed tomography (micro-CT)

The microstructure and architecture of the 3D printed hydrogels were studied through a microcomputed tomography (micro-CT) technique. The samples were lyophilized and scanned using a high-resolution micro-CT (SkyScan 1272, Bruker, USA) with a pixel size of 8 μm, voltage range of 50 Kv and current source of 200 μA (version 1.1.3). Approximately 250 projections were acquired over a rotation angle of 360°, with a rotation step of 0.3°. Data sets were reconstructed using a standardized cone-beam reconstruction software (NRecon 1.6.10.2, Bruker). Representative data set of the slices was segmented into binary images with a dynamic threshold between 30–255. After that, the binary images were used for morphometric analysis (CT Analyser, v1.15.4.0, Bruker) and to build the 3-D models (CTvox, v 3.0.0, Bruker). Quantitative information of total porosity (%), pore size (μm), pore distribution (%) and interconnectivity (%) was assessed for the hydrogels' filaments. The results are presented as the mean of the measurements on three hydrogel samples.

VII-3.13. Preparation of Bioinks

For cell culture, human adipose stem cells (hASC) were used. The multipotent potential of stem cells makes them an attractive choice for use in different tissues regeneration. Here, they were isolated from the human subcutaneous adipose tissue from liposuction procedures performed at Hospital da Prelada (Porto), after patient's informed consent and under a collaboration protocol approved by the ethical committees of both institutions following a previously reported protocol. Cells were isolated as described before [24]. Before encapsulation, cells were expanded in Minimum Essential Medium alpha (α-MEM) (ALFAGENE, Portugal) supplemented with sodium bicarbonate (2.2%) (Sigma-Aldrich, MO, USA), 10% fetal bovine serum (FBS) (ALFAGENE, Carcavelos, Lisbon), 1% penicillin/streptomycin (ALFAGENE, Portugal) until passage 3.

After reaching 80% of confluence, cells were tripsinized and encapsulated in the collagen-based ink at different densities: $2.5x10^6$, $5x10^6$ and $7.5x10^6$ cells.mL^{-1}. Briefly, 150 µL of culture medium containing the respective number of cells were transferred by pipetting into the middle of each syringe, and carefully stirred to create a homogenous distribution of the cells. The resulting 3D printed hydrogels were maintained in basal α-MEM conditions for a maximum of 21 days with changes of medium at every three days. Scaffolds without cells were kept under the same culture conditions and used as controls.

VII-3.14. Live/Dead assay

As a first biological approach, cell viability during printing was tested for the three different cell densities. Live cells were stained with calcein-AM (AM) (1:500) in the cytoplasm and generated green fluorescence, whereas dead cells were labeled with propidium iodide (PI) (1:1000) which binds to DNA and fluoresces red. For analysis, leica SP8 inverted confocal microscope with Incubation was used for images acquisition. The processing was done in the ImageJ software. For quantification, the channels were treated separately by selecting an appropriated threshold. The results are the mean of 6 measurements, 2 images per sample and 2 samples per replicate.

VII-3.15. Metabolic Activity

To study the metabolic activity for the different encapsulated cells density, 3-(4,5-dimethylthiazol-2-yl)-5-(3 carboxymethoxyphenyl) 2-(4-sulphofenyl)-2*H*-tetrazolium, inner salt (MTS) (VWR, Lisbon, Portugal) assay was used. Cell-laden structures were maintained in culture conditions, 37 °C and 5 % CO_2, and the MTS assay was performed 1, 7 and 14 days after cell culture. This assay quantifies the metabolic activity of the cells by tetrazolium salt reduction to formazan after 3 hours of incubation at 37 °C. Absorbance intensity, which is directly proportional to metabolic activity, was measured at 492 nm using a microplate reader (SYNERGY HT, BIO-TEK). The results are the mean of three independent experiments (n=3) with three replicates for each condition and per experiment.

VII-3.16. Immunodetection of bone-related proteins

To evaluate the potential of the 3D printable hydrogels to induce osteogenic differentiation, immunodetection of bone-related proteins was performed. Human ASCs incorporated in the collagen-based ink were fixed with paraformaldehyde 16% (w/v) (VWR, Lisbon Portugal) overnight at 4 °C. After that, cells were permeabilized with 1% (v/v) of Triton X-100/Tris(hydroxymethyl)aminomethane (TBS) (Sigma-Aldrich, USA). To block unspecific reactions, samples were incubated with 3 % (w/v) bovine serum albumin (BSA; Sigma-Aldrich, USA). A rabbit anti-human polyclonal antibody against osteopontin (OPN; Abcam, Cambridge, UK; dilution 1:250) and a mouse anti-human RUNX2, clone AS110 (Merck, Germany 1:250) were used as primary antibodies (2 hat room temperature). Alexa Fluor 488 secondary antibodies at 1:500 with reactivity for rabbit and mouse, respectively, were added in a TBS solution for 1 h at 37 °C. Samples were analyzed using a leica SP8 inverted confocal microscope.

VII-3.17. Statistical analysis

All quantitative data are presented as mean ± standard deviation (SD). Statistical analyses were performed using a GraphPad Prism 5.0 software (GraphPad Software, USA) and the Kruskal-Wallis test followed by Dunn's multiple comparison test.

VII-4. RESULTS AND DISCUSSION

VII-4.1. Collagen characterization

The high biodiversity offered by marine ecosystem makes it an amazing inspiration for different biomolecules exploration [25]. Collagen is one of the most attractive proteins within the marine world, thanks to its intrinsic biological properties. Among the different marine organisms, fish skins have been widely preferred to extract type I collagen. Fish skins, including shark skin, are largely available being thus a promising source to scale up industrially. Moreover, past studies have been reporting the similarity of type I fish skin collagen from that of mammals. Type I collagen is recognized in mammals by the presence of two or more different chains (heterotrimers): typically alpha 1 and alpha 2 chains, and a beta component structure [26-28]. The Prionace glauca collagen, isolated through an acid soluble method, was identified as type I collagen. From the SDS-PAGE, the characteristic alpha 1 and alpha 2 bands appear around 100 kDa and a beta component about 250 kDa (**Figure VII-2A**). This result is consistent with our previous findings [29] and well correlated with the results recently reported by Jeevithan Elango [30]. Moreover, collagen protein has a unique aminoacidic content. Firstly, glycine (Gly) is present in every sequence of three aminoacids (Gly-X-Y) in each chain of the collagen triple helix, commonly followed by proline (Pro) occupying the X or Y position and the post-translationally modified hydroxyproline (OHPro) in the Y position. Such aminoacids have a key role for the stability of the polyproline II conformation of the individual chains, increasing the collagen triple-helix stabilization. In general, collagen from fish skin has a similar amino acid composition to that of mammals, with major differences associated to the lower Pro and OHpro contents, which directly influences the triple helix stability and consequently the denaturation temperature. The obtained amino acid profile (**Figure VII-2B**) is compatible with this, showing glycine representing around 1/3 (31.8%) of the whole *Prionace glauca* collagen amino acids, 10% corresponding to the Pro content (101/1000) and 6.5% to OHPro (65/1000). Comparing with acid soluble collagen obtained from other fish species like salmon (Pro 7.3% and OPpro 4.8%) and codfish (Pro 9.1% and OHPro 5.5%), Prionace glauca skin collagen revealed a higher content of Pro and OHpro [22, 31]. Usually, collagens from cold sea fishes have lower degrees of hydroxyproline than those from warm or tropical seas like Prionace glauca that prefers temperatures between 12 - 20 °C. The presence of high hydroxyproline content increases the denaturation temperature (28 - 30 °C) of Prionace glauca collagen when compared with collagens from cold water

fishes, as previously demonstrated [30]. Such information is a useful tool to better understand the ideal conditions wherein the collagen should be processed.

To complement the information on the chemical composition of the extracted collagen, FTIR spectroscopy was performed. The reference peaks of amide A and B and amide I, II and III, characteristic of collagen protein, are present in the obtained spectra, as illustrated in **Figure VII-2D**). Generally, amide A is observed between 3000-3500 cm^{-1} as a result of the N-H stretching vibration typically associated with the intermolecular hydrogen bonding in the carboxyl groups. It appears in *Prionace glauca* collagen sample in the same area (3320 cm^{-1}). The amide B, relative to the asymmetric and symmetric stretch of CH2 was identified at 2949 cm^{-1}. The strong peaks around 1660 cm^{-1} can be assigned to C=O stretch characteristic of proteins amide I band. The given peaks at 1540 and 1200 cm^{-1} arise from N-H deformation of amide II and C-N stretch of amide III, respectively.

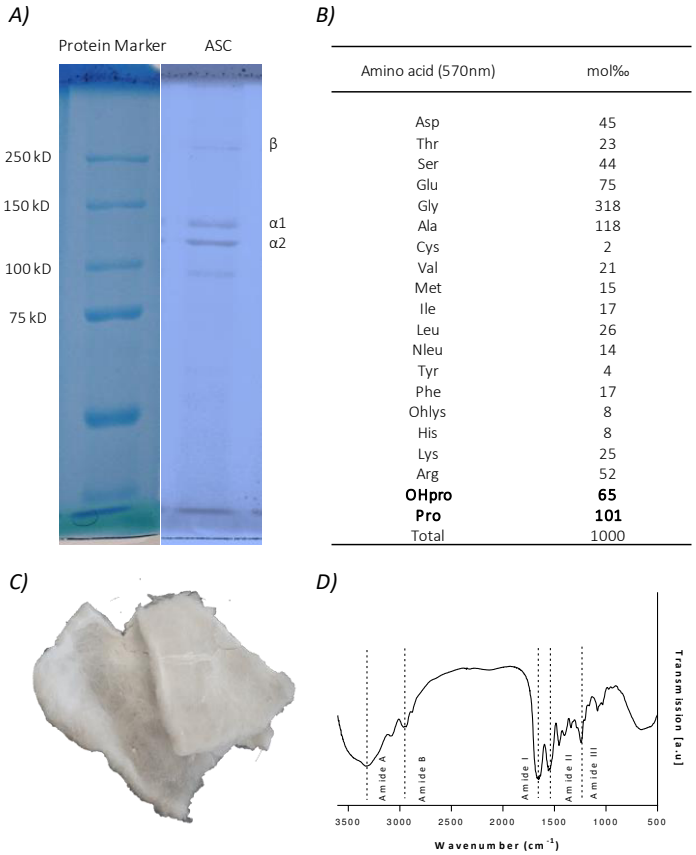

Amino acid (570nm)	mol‰
Asp	45
Thr	23
Ser	44
Glu	75
Gly	318
Ala	118
Cys	2
Val	21
Met	15
Ile	17
Leu	26
Nleu	14
Tyr	4
Phe	17
Ohlys	8
His	8
Lys	25
Arg	52
OHpro	**65**
Pro	**101**
Total	1000

Figure VII-2 - Characterization of Prionace glauca collagen extracted by an acidic method, compatible with type I collagen. A) SDS-PAGE band pattern of Prionace glauca collagen with α1, α2 and β components; B) Amino acid content, with a suggestive hydroxyproline (OHPro) contents; C) Lyophilized collagen and D) FTIR spectrum illustrating the characteristic amide peaks.

VII-4.2. Collagen mineralization

Natural bone has in its constitution mineralized collagen [32], being the biomineralization process the initial stage of the bone formation and a continuous process to reach mature bone. Thus, biomineralization is important not only to start but also to maintain the biological mechanism and stable routes of bone formation. In vivo, bone tissue is in a constant and stable homeostasis, wherein old bone tissue is replaced by newly formed bone. In vitro, the biomineralization and self-assembly of collagen is under study and different investigations have been carried out to recapitulate the in vivo process. Different approaches have been employed to biomimetically mineralize collagen [33, 34].

Here, we proposed the mineralization of collagen under controlled pH (7 - 8), temperature (6 - 8 °C) and ion concentration (calcium-to-phosphate ratio =1.67). The provided conditions were used to recapitulate the pH and temperature environment of the human body [32]. As a first chemical approach, to assess the suitability of the used method to mineralize collagen, x-ray diffraction (XRD) was carried out. This technique is a useful tool to distinguish a crystalline material from an amorphous one. As depicted in **Figure VII-3B**, the XRD spectrum is dominated by strong peaks at 31.7° and 32.9°, corresponding to the planes 300 and 111, respectively, identified as the most intense in the ICDD 00-055-0592 of HAp phase. The appearance of less intense peaks was also detected at 25.95°, corresponding to plane 002. Such findings match well with the IFFT diffractogram micrographs obtained from the HR-TEM images (**Figure VII-3A**). The presence of a crystalline zone was observed (**Figure VII-3A1**) throughout an amorphous matrix (**Figure VII-3A2**). The lattice spacing (d=0.34 nm, Figure 3 A3) of the oriented apatite crystals involved in an amorphous matrix were identified as the plan 002 (**Figure VII-3B**). According to the literature, the biomineralization process can result in crystals with different structures, shapes, size, orientation and alignment, which results in a complex hierarchical structure. The mechanical and physiological properties of human native bone are highly dependent on these parameters.

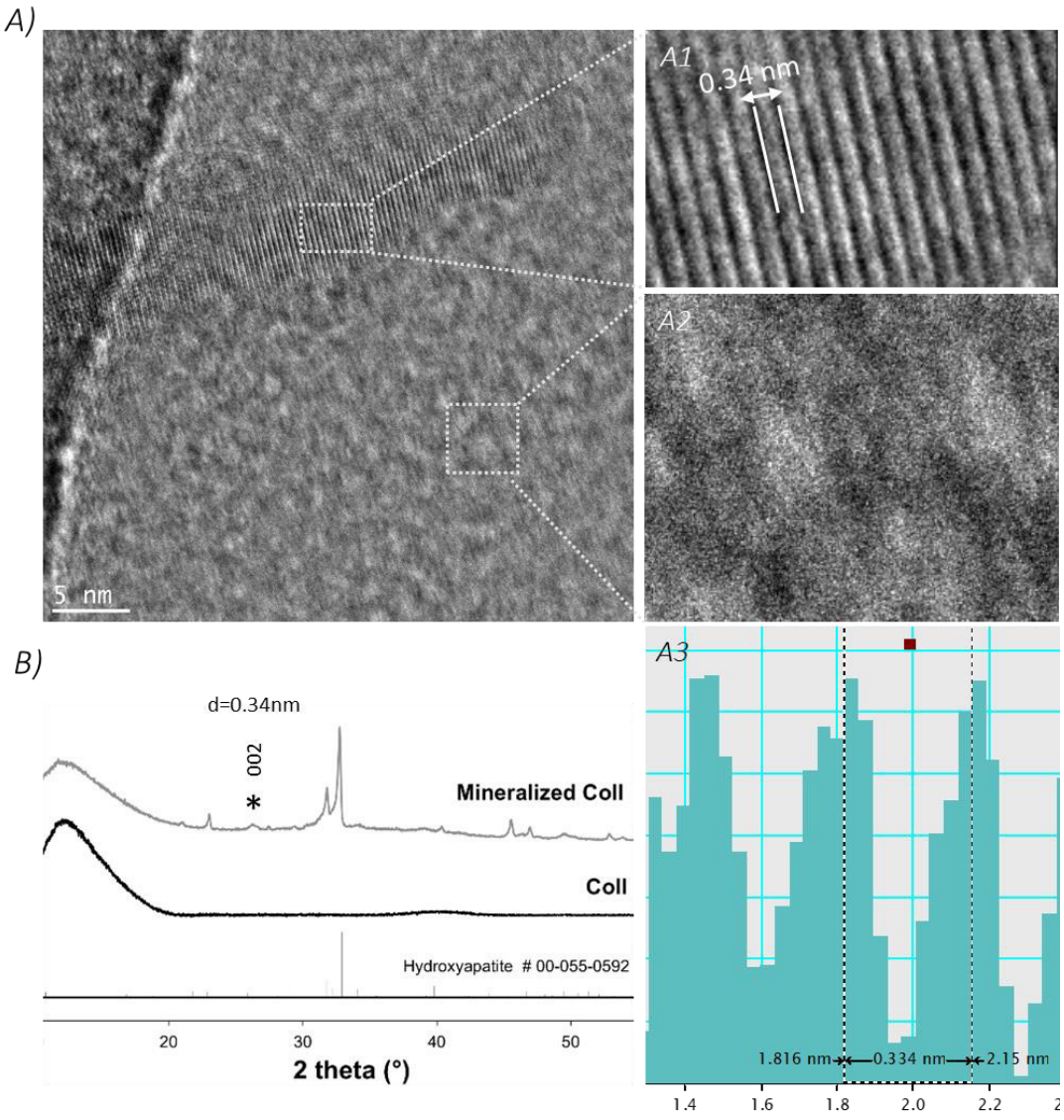

Figure VII-3 - A) HR-TEM micrographs of mineralized collagen; A1) IFFT obtained from a crystalline zone, A2) IFFT obtained from an amorphous zone and A3) Interplanar measurements (d=0.34nm) of the crystalline zone. B) X-ray diffraction of pure and mineralized collagen. Identification of the plane 002 corresponding to an interplanar distance of 0.34 nm.

VII-4.3. Inks characterization

To meet tissue specific functionalities, biofabrication with incorporated living cells has been developed [35]. In contrast to the cell seeding approaches, 3D printing cell-laden technologies provides improved biological and mechanical cues that better mimic the tissue environment [35, 36].

To successfully achieve a 3D printed cell-laden construct, several challenges should be considered including *i)* the physic-chemical properties to induce cell signaling, *ii)* the viscoelastic properties that

allow inks printing without affecting cell viability during and after printing and *iii)* adequate mechanical properties to accompany tissue remodeling and regeneration. Focusing on these crucial parameters, collagen-based approaches have been explored in the printing field. Nevertheless, the use of collagen for 3D printing is very challenging since collagen is a temperature dependent protein [37]. In general, marine collagen stiffness significantly declines over increasing temperatures due to the collapse of the triple-helix arrangement, in contrast to mammalian origin collagens. Lee et al, in a recent work, showed that porcine type I collagen presented the maximum stiffness at 36.2 °C (gelation temperature) [38]. Also, Kim *et al* demonstrated the influence of the temperature over the storage modulus. They observed that the maximum storage modulus of porcine collagen (solubilized at 7%) was achieved at 41.5 °C, but due to the constraints in terms of cell viability (high shear stress), they performed the experiments with 5% of collagen concentration [39].

Thus, to study *Prionace glauca* collagen (2% (w/v)) stability, the storage modulus and tan δ of Prionace glauca were evaluated across a temperature sweep from 4 to 40 °C. In fact, an increase in the temperature resulted in a lower storage modulus and a higher tan δ (**Figure VII-4A**) [40]. The maximum storage modulus (between 5 - 10 °C) corresponds to the gelation temperature of Prionace glauca collagen. Above 20 °C, a slight decrease in collagen stiffness was observed, reaching a completely liquid phase at 32 °C. In contrary to porcine type I collagen, Prionace glauca collagen is stiffer at low temperatures and it is more sensitive to a higher temperature. Thus, in general, the printing of marine collagen requires stabilizing agents (as glutaraldehyde, EDC or genipin, among others) or combination with other materials to increase its performance. However, most of the crosslinking agents cannot be directly used in cell-laden approaches since they may cause cellular toxicity [39]. Here, collagen from blue shark was functionalized into the carboxyl groups (COOH) with Ca2+ ions to increase its bioactivity and stability. Remarkably, the induction of hydroxyapatite formation within the collagen matrix increased both the stiffness (from 174.4 to 668.7 Pa) and the thermal stability (from 20 to 27 °C) (**Figure VII-4A** and B). The final ink (mineralized collagen/alginate) also presented a significant increase in stiffness (6690 Pa) with stable properties throughout the tested temperature range (**Figure VII-4C**). In addition, a shear thinning behavior was observed (Figure 4D), which indicates a proper flow of the ink through the nozzle. The use of Ca^{2+} to promote mineralization could also act as a "safe" crosslinker to bind collagen to the alginate by acting as ion gelation agent on alginate. This synergistic chemical approach on the use of Ca^{2+} ions thus enabled the production of a stiff and stable ink.

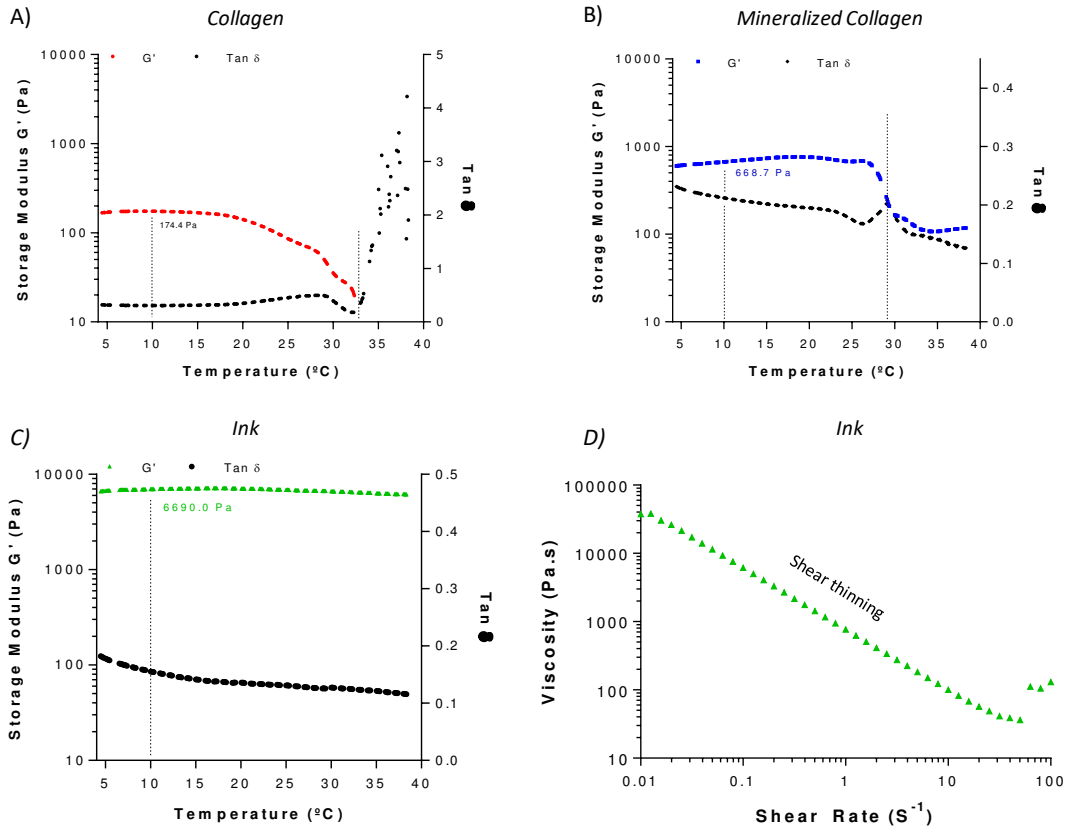

Figure VII-4 – Influence of temperature in the rheological properties of collagen. A) collagen B) mineralized collagen C) mineralized collagen/alginate ink. D) Variability of ink viscosity with shear rate, at 20 °C, evidencing a shear thinning behavior.

VII-4.4. Microarchitecture analysis of the 3D printed hydrogels

Square hydrogels measuring 8 mm in length with 2 mm in height were printed through a layer by layer process, with 90° orientation between adjacent layers. Scanning electron microscopy (SEM) and microcomputed tomography (micro-CT) analysis was carried out to finely investigate the microarchitecture of the 3D printed hydrogels. Printing accuracy resulting from the manufacturing process was firstly studied by SEM through the analysis of pore and filaments fidelity. **Figure VII-5** (A1 and A2) shows a top view of the produced structures and the results displayed a homogeneous distribution of the pores with a well-defined shape. The printing accuracy is well comparable with other works where mammalian origin collagen was printed. Lee et al demonstrated that employing a low temperature (-40 °C) platform enhanced collagen/alginate-based inks printability. More recently, they also showed the printability of collagen/ECM/silk-fibroin hydrogels in the same conditions [41, 42]. In fact, they obtained an outstanding printing fidelity, but the used technique is not adequate when considering cell-laden approaches due to the too low temperature. Other studies have been reporting

the use of chemical crosslinking agents to increase collagen stability [43]. With our printing conditions (20 °C) and, without any chemical crosslinking agent, we could conjugate printing fidelity with incorporated living cells, which leaves room for the use of marine collagen as a promising material for 3D printing. At higher SEM resolution, it was observed that the material deposition creates an aligned pattern (**Figure VII-5 A3** and **A4**) that may be a useful way to guide cells distribution and orientation. In addition, hydroxyapatite formation was also observed at high magnifications with its characteristic appearance (**Figure VII-5 A5**).

Most studies present micrographs to demonstrate printing fidelity, but to the best of our knowledge few studies have been investigating the internal microarchitecture of the filaments, which is considered a crucial parameter to ensure cells survival and enable full scaffold population. Thus, the internal structure of the filaments was studied through micro-CT (**Figure VII-5B**). A filament with 64.37±7.2% of total porosity was measured for the printed hydrogels with a correspondent pore size distribution ranging between 16 to 240 µm (average 98.35±7.5 µm). The filament microporosities are well interconnected (63.22±12.7 %). The presence of smaller porosities has been demonstrated to enhance the surface area and the permeability of the constructs, which provides more protein adsorption sites. In the case of approaches for bone, they can also serve as nucleation spots for precipitation of bone-like apatite contributing for the expression of osteogenic-related markers [44].

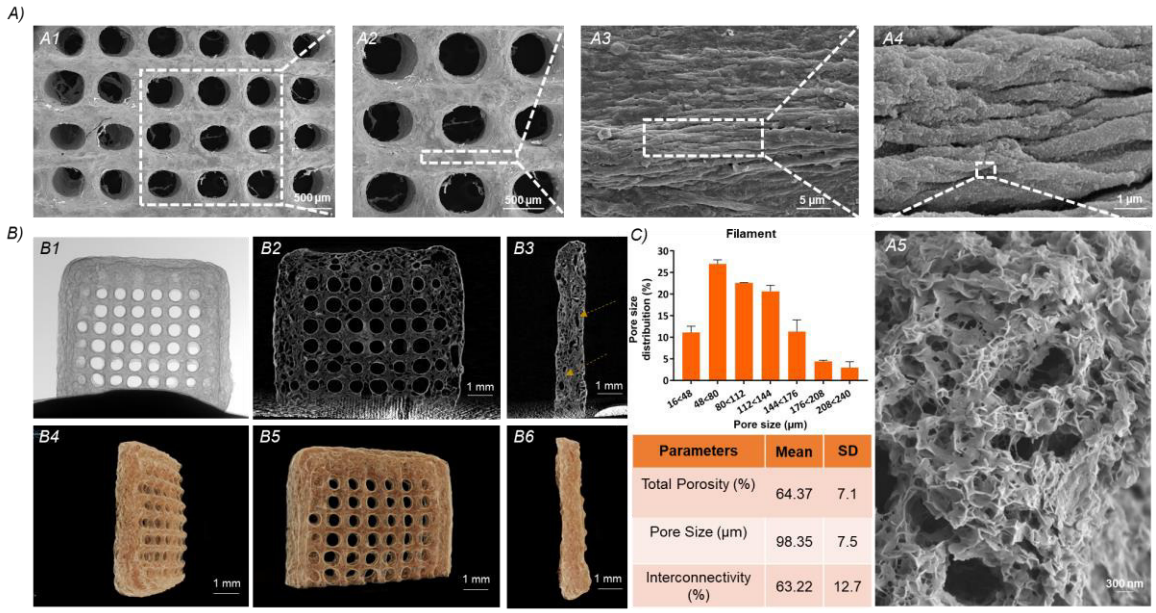

Figure VII-5 - Hydrogels microarchitecture characterization. A) SEM images showed the printing accuracy at different magnification (A1, A2, A3, A4) and high resolution SEM micrographs showed the hydroxyapatite that was formed throughout the collagen matrix (A5). B) Micro-CT 2D (B1, B2, B3) and 3D (B4, B5, B6) reconstructions. C) Micro-CT quantitative results showed interconnected microporosities within the printed filaments.

VII-4.5. *In vitro* performance of cell-laden inks

As previously described, an ideal bioink should consider not only the rheological properties that promote printing accuracy but also the cell microenvironment. Bioactive inks that retain the capacity to be extruded with minimal forces are thus preferred. The 3D bioprinting designed system was biologically tested by incorporating hASC, cells harvested from the human adipose tissue, with multipotent capabilities able to initiate and stimulate new tissue ingrowth [45]. According to the literature, cell density should be tuned according to the intrinsic properties of the ink (biological cues and rheological behavior) and the tissue of interest, in such a way that an adequate cell distribution within the printed filaments can be achieved resulting in required cell-to-cell interactions. Cidonio *et al* reported in a very recent review work that 5–10×10^6 cells.mL^{-1} has been considered the ideal range concentration for cell encapsulation for bone tissue [46]. Therefore, as a first screening, the *in vitro* studies were carried out by encapsulating 3 different cell densities, 2.5x×10^6, 5 x 10^6 and 7.5 x 10^6 cells.mL^{-1}. To qualitatively assess cell death during printing, a live (green) / dead (red) assay was carried out. For quantification, the confocal images were processed using the imageJ software. Figure 6 showed that the lowest cell density (2.5x×10^6 cells.mL^{-1}) resulted in a poor cell distribution but in a higher cell survival during printing. The intermediate composition revealed a good cell distribution and a

good cell survival. In contrast, encapsulating a higher cell number (7.5×10^6 cells.mL^{-1}) resulted in a lower cell survival during printing. In fact, these results are well correlated with what could be expected, since increasing cell density leads to an increase in cell-wall contact, resulting in cell death after passing the aperture of the nozzle. Moreover, high cell densities have been associated with high cell-to-cell interaction resulting in cell overload and hypoxia. Nevertheless, the results are included in a normal range of cell survival, with most studies reported in literature describing a typical cell viability of between 70-90% when incorporated in optimized inks. Only few studies reported cell viability in suboptimal conditions [9].

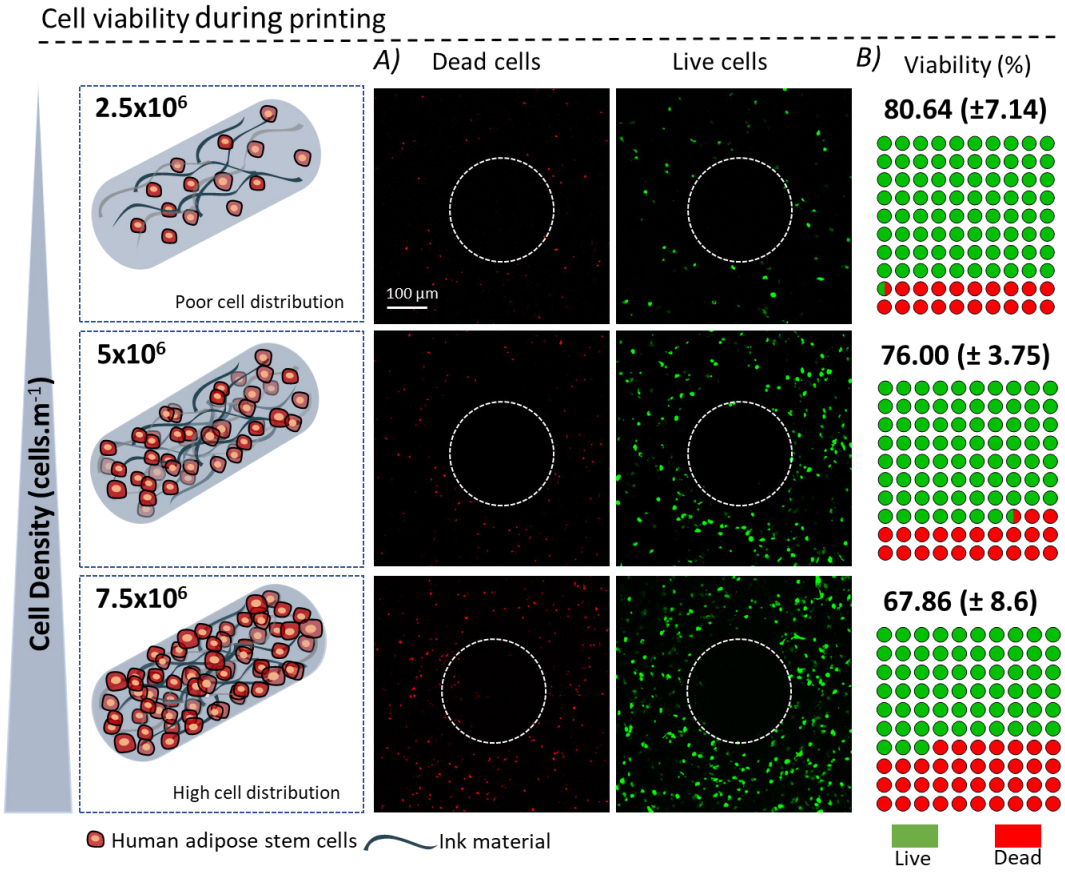

Figure VII-6 – hASC viability during printing. A) Confocal images of live (green) / dead (red) assay for the hASC incorporated at different densities (with the pores highlighted with a circle). B) Quantitative results were calculated in imageJ software from the images obtained in confocal. The results are the mean of 2 samples per experiment with two analysis per sample (for each condition). Cell death increases as cell density increases.

VII-4.6. Cell functionality in the long-term

While past studies have been typically reporting cell viability during printing, since the act of extrusion and the printing process causes stress for cells, few studies have been done to determine cell

behavior in the long-term. Thus, the present study was thought to investigate cell viability and function in a long-term towards bone tissue regeneration. Earlier studies reported that the rheological properties, inks composition and cells density affected both short and long-term cell signaling and functionality [45].

Here, the main goal was to study the influence of cell density in an optimized ink in a long period of culture. 3D printable hydrogels with incorporated hASC were maintained for 21 days in basal culture conditions without any exogenous stimulation to better mimic the microenvironment of the native tissue. After 7 days in culture media, hASC incorporated at $2.5x10^{6}$ cell.mL^{-1} showed a round shape appearance, as could be observed by fluorescence microscopy (**Figure VII-7B**). In contrast, elevated numbers of encapsulated hASC (≥ $5\times10x^{6}$ cell.mL^{-1}) showed a slight cell spreading (indicated by arrows in **Figure VII-7A**) as a result of the enhanced cell-to-cell interaction. After 14 days of culture, the cells stained at green increased for the formulations with more cells, particularly for the formulation with 7.5 x 10^{6} cells.mL^{-1}.

Moreover, the qualitative assessment of cells morphological behavior after 14 days in culture was performed by confocal microscopy in samples stained with DAPI (nucleus) and phalloidin (cytoskeleton) (**Figure VII-7B**). While cells encapsulated at $2.5x10^{6}$ cells.mL^{-1} were scarce and presented a round shape morphology, cells spreading was more pronounced for the formulation encapsulated with a density of 7.5 $x10^{6}$ cells.mL^{-1} (**Figure VII-7B**). Uniform cell distribution was observed throughout the entire scaffold, with cells displaying a preferred straight orientation over the filament (Figure 8, DAPI:ph 21 days). In addition, to be able to identify the specific position of cells, a color coding was employed to identify a range from 0 to 350 μm of depth. The blue color indicates more superficial cells, while red represents cells that colonized the scaffolds' interior (**Figure VII-8A**). Results suggest that the printed hydrogels could support cell survival and spread inside of the filaments.

The bioactive nature of the ink in combination with the selected cell density ($7.5x10^{6}$ cells.mL^{-1}) seemed to promote a strong mitogenic effect over the cells as suggested by MTS assay (**Figure VII-7C**) and DAPI staining (**Figure VII-8A**).

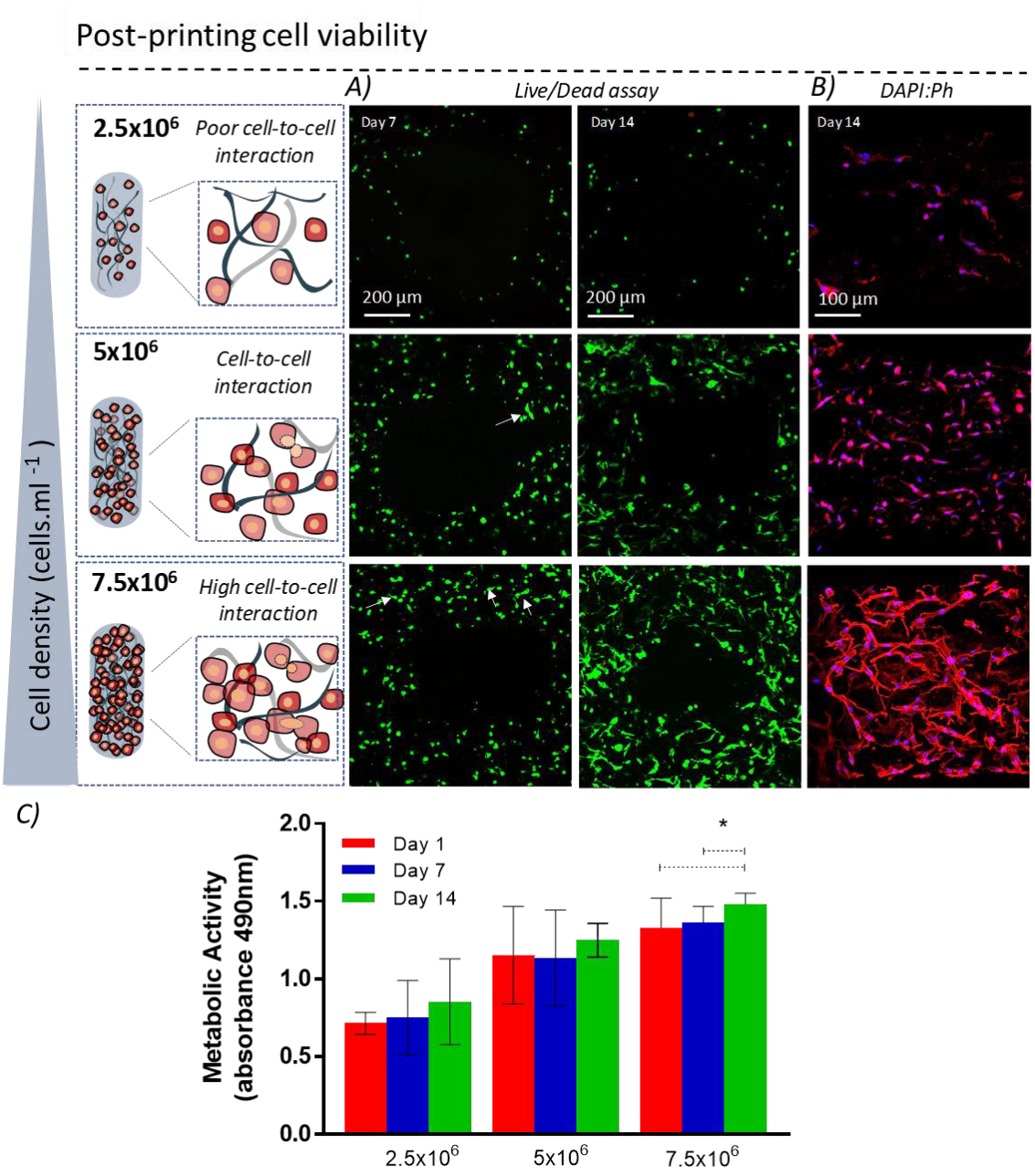

Figure VII-7 - Fluorescence microscopy images of the 3D printed hydrogels. A) Cell viability live (green) / dead (red) assay after 7 and 14 days of cell culture. B) DAPI (nuclei) /phalloidin (cytoskeleton) images of hASC incorporated at 2, 5 and 7.5 x 10 6 cell-ml-1 14 after culture. C) hASCs metabolic activity 1, 7 and 14 days after printing (with *p<0.05) as determined by MTS assay.

Furthermore, the obtained findings suggest that the ink composition itself could provide osteogenic cues to start differentiation of hASC without any additional exogeneous stimulation. This conclusion is based on the immune detection for RUNX2 and osteopontin 21 days after printing (**Figure VII-8B**). In fact, it is well known that RUNX2 expression drives the mesenchymal stem cells differentiation into osteoblastic lineage and induces expression of other bone-related genes. This result was corroborated

with the intense expression of osteopontin, an extracellular structural protein of bone, 21 days printing. It is thus hypothesized that the activation of osteogenic differentiation of mesenchymal stem cells can be potentially explained by the successfully cell-to-ink interaction and in a second instance by the release of Ca^{2+} ions from the co-precipitated nano HAp [47]. According to the literature, the extracellular release of calcium can modulate the cell response with benefits for bone tissue applications [48].

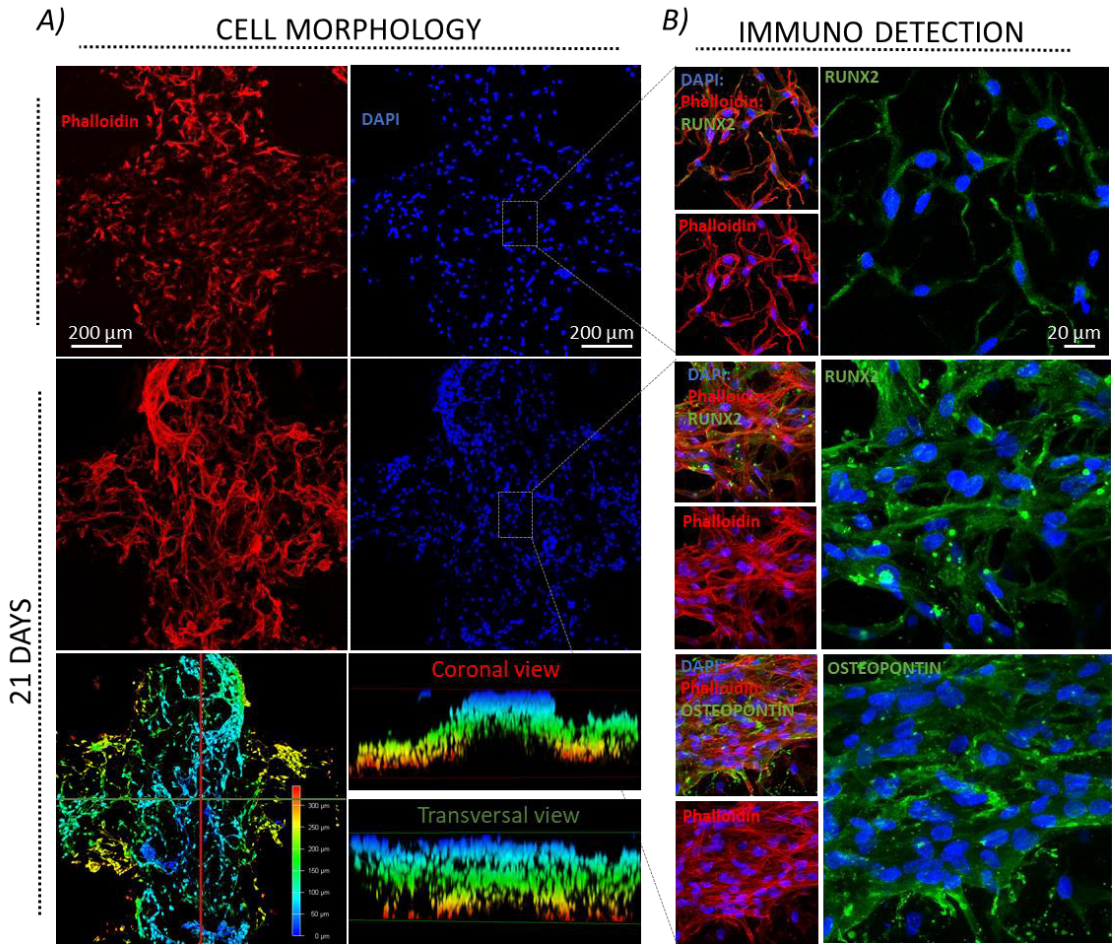

Figure VII-8 - Fluorescence microscopy images after proper staining illustrative of long term cell culture of brioprinted mineralized collagen:alginate:hASC scaffolds. A) DAPI (nuclei) /phalloidin (cytoskeleton) images of hASC incorporated at 7.5 x 10 6 cell.ml-1, 14 and 21 days after cell culture. Cell distribution throughout the 3D printed hydrogels, 2D and 3D view. B) Immunodetection of osteogenic-related markers, RUNX2 and Osteopontin.

VII-5. CONCLUSIONS

In the present manuscript, a stable mineralized blue shark collagen:alginate bioink supporting high cell viability was obtained, enabling the printing of hydrogels that, after 21 days of cell culture, maintained their structural properties while preserving cells morphology and osteogenic phenotype.

Collagen mineralization increased its stiffness, with Ca^{2+} ions used for hydroxyapatite formation promoted as well the ion gelation of alginate as a non-toxic crosslinking process increasing ink stability. Nevertheless, the rheological properties of the inks established to enable its printability and stability did not compromise cell viability through tested culture time. In an early stage, during printing, cell viability was favored by the lowest tested density (2.5 x 10^6 cells.mL^{-1}), due to the protective effect that the ink could have on cells, shielding these from the contact with the nozzles' walls. At later stages, the high cell density (7.5 x 10^6 cells.mL^{-1}) could be advantageous, due to the higher cell-to-cell contact that contributes to enhance cell viability in a long term. However, care should be taken as very high cell density can result in cell saturation and hypoxia, which conveys that bioink performance is highly dependent on initial cell density. From the immunodetection of RUNX2 and osteopontin, osteogenic-related markers, it is hypothesized that Ca^{2+}, used to *in situ* mineralize the blue shark collagen, could stimulate the hASCs differentiation into osteogenic lineage without any exogeneous stimulation.

Inspired on a concept of marine by-products valorization, this work has shown a bioactive and biomimetic ink with chemical cues capable to activate signaling pathways of encapsulated stem cells, highly promising for bone tissue regeneration.

VII-6. ACKNOWLEDGMENTS

This study was funded by the Portuguese Foundation for Science and Technology (FCT) under the scope of the BiogenInk project (M-ERA-NET2/0022/2016), by European Regional Development Fund through INTERREG Atlantic Area Programme, under the scope of BLUEHUMAN (EAPA_151/2016) project and through Norte de Portugal Regional Operational Program (NORTE 2020), under the scope of Structured project NORTE-01-0145-FEDER-000021. The Doctoral Programme NORTE-08-5369-FSE-000044 supported by NORTE 2020, under the PORTUGAL 2020 Partnership Agreement, through the European Social Fund, is also greatly acknowledge by the PhD fellowship of GSD. RP and SF-R thank FCT for the investigator contract IF/00347/2015 and PhD grant PD/BD/135252/2017, respectively. The authors acknowledge also the Centro Tecnológico del Mar (CETMAR, Vigo, Spain) and COPEMAR SA (fishing company, Spain) for the kind offer of the used by-products for the production of collagen.

VII-7. REFERENCES

1. Dzobo, K., et al., *Advances in regenerative medicine and tissue engineering: Innovation and transformation of medicine.* Stem cells international, 2018. **2018**: p. 2495848.
2. Zhang, L., et al., *Three-dimensional (3D) printed scaffold and material selection for bone repair.* Acta biomaterialia, 2019. **84**: p. 16-33.
3. Chimene, D., R. Kaunas, and A.K. Gaharwar, *Hydrogel Bioink Reinforcement for Additive Manufacturing: A Focused Review of Emerging Strategies.* Advanced Materials, 2020. **32**(1): p. 1902026.
4. Ashammakhi, N., et al., *Advancing frontiers in bone bioprinting.* Advanced healthcare materials, 2019. **8**(7): p. 1801048.
5. Fedorovich, N.E., et al., *Scaffold porosity and oxygenation of printed hydrogel constructs affect functionality of embedded osteogenic progenitors.* Tissue Engineering Part A, 2011. **17**(19-20): p. 2473-2486.
6. Derakhshanfar, S., et al., *3D bioprinting for biomedical devices and tissue engineering: A review of recent trends and advances.* Bioactive materials, 2018. **3**(2): p. 144-156.
7. Lei, D., et al., *3D printing of biomimetic vasculature for tissue regeneration.* Materials Horizons, 2019. **6**(6): p. 1197-1206.
8. Kumar, A., et al., *Low temperature additive manufacturing of three dimensional scaffolds for bone-tissue engineering applications: Processing related challenges and property assessment.* Materials Science and Engineering: R: Reports, 2016. **103**: p. 1-39.
9. Rutz, A.L., P.L. Lewis, and R.N. Shah, *Toward next-generation bioinks: tuning material properties pre-and post-printing to optimize cell viability.* MRS Bulletin, 2017. **42**(8): p. 563-570.
10. Felician, F.F., et al., *Collagen from marine biological sources and medical applications.* Chemistry & biodiversity, 2018. **15**(5): p. e1700557.
11. David, G., *Collagen-based 3D structures—versatile, efficient materials for biomedical applications*, in *Biopolymer-Based Formulations*. 2020, Elsevier. p. 881-906.
12. Sorushanova, A., et al., *The collagen suprafamily: from biosynthesis to advanced biomaterial development.* Advanced Materials, 2019. **31**(1): p. 1801651.

13. Pal, G.K. and P. Suresh, *Sustainable valorisation of seafood by-products: recovery of collagen and development of collagen-based novel functional food ingredients.* Innovative Food Science & Emerging Technologies, 2016. **37**: p. 201-215.
14. Suresh, P., T.G. Kudre, and L.C. Johny, *Sustainable valorization of seafood processing by-product/discard*, in *Waste to Wealth*. 2018, Springer. p. 111-139.
15. Berillis, P., *Marine collagen: Extraction and applications.* Research Trends in Biochemistry, Molecular Biology and Microbiology; Madhukar, S., Ed, 2015: p. 1-13.
16. Diogo, G.S., et al., *Marine collagen/apatite composite scaffolds envisaging hard tissue applications.* Marine drugs, 2018. **16**(8): p. 269.
17. Gabusi, E., et al., *Extracellular calcium chronically induced human osteoblasts effects: specific modulation of osteocalcin and collagen type XV.* Journal of cellular physiology, 2012. **227**(8): p. 3151-3161.
18. Dvorak, M.M., et al., *Physiological changes in extracellular calcium concentration directly control osteoblast function in the absence of calciotropic hormones.* Proceedings of the National Academy of Sciences, 2004. **101**(14): p. 5140-5145.
19. Barradas, A.M., et al., *A calcium-induced signaling cascade leading to osteogenic differentiation of human bone marrow-derived mesenchymal stromal cells.* Biomaterials, 2012. **33**(11): p. 3205-3215.
20. Hwang, J.-H., et al., *Purification and characterization of molecular species of collagen in the skin of skate (Raja kenojei).* Food Chemistry, 2007. **100**(3): p. 921-925.
21. Sotelo, C.G., et al., *Characterization of collagen from different discarded fish species of the west coast of the Iberian Peninsula.* Journal of aquatic food product technology, 2016. **25**(3): p. 388-399.
22. Alves, A.L., et al., *Cosmetic potential of marine fish skin collagen.* Cosmetics, 2017. **4**(4): p. 39.
23. Diogo, G.S., et al., *Cell-laden Biomimetically Mineralized Shark Skin Collagen-based 3D Printed hydrogels for the Engineering of Hard Tissues.* ACS Biomaterials Science & Engineering, 2020.
24. Freitas-Ribeiro, S., et al., *Strategies for the hypothermic preservation of cell sheets of human adipose stem cells.* PloS one, 2019. **14**(10).
25. Silva, T.H., et al., *Marine origin collagens and its potential applications.* Marine drugs, 2014. **12**(12): p. 5881-5901.

26. Gelse, K., E. Pöschl, and T. Aigner, *Collagens—structure, function, and biosynthesis.* Advanced drug delivery reviews, 2003. **55**(12): p. 1531-1546.
27. Bae, I., et al., *Biochemical properties of acid-soluble collagens extracted from the skins of underutilised fishes.* Food chemistry, 2008. **108**(1): p. 49-54.
28. Singh, P., et al., *Isolation and characterisation of collagen extracted from the skin of striped catfish (Pangasianodon hypophthalmus).* Food chemistry, 2011. **124**(1): p. 97-105.
29. Blanco, M., et al., *Hydrolysates of fish skin collagen: An opportunity for valorizing fish industry byproducts.* Marine drugs, 2017. **15**(5): p. 131.
30. Elango, J., et al., *Evaluation of differentiated bone cells proliferation by blue shark skin collagen via biochemical for bone tissue engineering.* Marine drugs, 2018. **16**(10): p. 350.
31. Tylingo, R., et al., *Isolation and characterization of acid soluble collagen from the skin of african catfish (Clarias gariepinus), salmon (Salmo salar) and baltic cod (Gadus morhua).* J Biotechnol Biomater, 2016. **6**(234): p. 2.
32. Cui, Y., H. Cui, and X.-M. Wang, *Preparation and Characterization of Biomimetic Mineralized Collagen*, in *Mineralized Collagen Bone Graft Substitutes*. 2019, Elsevier. p. 23-60.
33. Takallu, S., et al., *Plate-shape carbonated hydroxyapatite/collagen nanocomposite hydrogel via in situ mineralization of hydroxyapatite concurrent with gelation of collagen at pH= 7.4 and 37° C.* Journal of Biomedical Materials Research Part B: Applied Biomaterials, 2019. **107**(6): p. 1920-1929.
34. Hoyer, B., et al., *Biomimetically mineralized salmon collagen scaffolds for application in bone tissue engineering.* Biomacromolecules, 2012. **13**(4): p. 1059-1066.
35. Wang, X., et al., *3D printing of polymer matrix composites: A review and prospective.* Composites Part B: Engineering, 2017. **110**: p. 442-458.
36. He, Y., et al., *Research on the printability of hydrogels in 3D bioprinting.* Scientific reports, 2016. **6**: p. 29977.
37. Marques, C., et al., *Collagen-based bioinks for hard tissue engineering applications: a comprehensive review.* Journal of Materials Science: Materials in Medicine, 2019. **30**(3): p. 32.
38. Lee, J., et al., *Development of a tannic acid cross-linking process for obtaining 3D porous cell-laden collagen structure.* International journal of biological macromolecules, 2018. **110**: p. 497-503.

39. Kim, Y.B., H. Lee, and G.H. Kim, *Strategy to achieve highly porous/biocompatible macroscale cell blocks, using a collagen/genipin-bioink and an optimal 3D printing process.* ACS applied materials & interfaces, 2016. **8**(47): p. 32230-32240.
40. Wu, Z., et al., *Bioprinting three-dimensional cell-laden tissue constructs with controllable degradation.* Scientific reports, 2016. **6**(1): p. 1-10.
41. Lee, H., et al., *Mineralized biomimetic collagen/alginate/silica composite scaffolds fabricated by a low-temperature bio-plotting process for hard tissue regeneration: fabrication, characterisation and in vitro cellular activities.* Journal of Materials Chemistry B, 2014. **2**(35): p. 5785-5798.
42. Lee, H., et al., *Fabrication of micro/nanoporous collagen/dECM/silk-fibroin biocomposite scaffolds using a low temperature 3D printing process for bone tissue regeneration.* Materials Science and Engineering: C, 2018. **84**: p. 140-147.
43. Bell, A., M. Kofron, and V. Nistor, *Multiphoton crosslinking for biocompatible 3D printing of type I collagen.* Biofabrication, 2015. **7**(3): p. 035007.
44. Zhang, K., et al., *Effect of microporosity on scaffolds for bone tissue engineering.* Regenerative biomaterials, 2018. **5**(2): p. 115-124.
45. Mendes, B.B., et al., *Human platelet lysate-based nanocomposite bioink for bioprinting hierarchical fibrillar structures.* Biofabrication, 2019. **12**(1): p. 015012.
46. Cidonio, G., et al., *The cell in the ink: Improving biofabrication by printing stem cells for skeletal regenerative medicine.* Biomaterials, 2019. **209**: p. 10-24.
47. Li, Q., et al., *Hydroxyapatite/collagen three-dimensional printed scaffolds and their osteogenic effects on human bone marrow-derived mesenchymal stem cells.* Tissue Engineering Part A, 2019. **25**(17-18): p. 1261-1271.
48. Sharma, A., et al., *Investigating the Role of Sustained Calcium Release in Silk-Gelatin-Based Three-Dimensional Bioprinted Constructs for Enhancing the Osteogenic Differentiation of Human Bone Marrow Derived Mesenchymal Stromal Cells.* ACS Biomaterials Science & Engineering, 2019. **5**(3): p. 1518-1533.

SECTION 4

GENERAL CONCLUSIONS

Chapter VIII

General conclusions and future perspectives

Chapter VIII

General conclusions and future perspectives

VIII-1. GENERAL CONCLUSIONS

Collagen is by far the oldest protein found to date, being ubiquitous in the Animal kingdom. One fourth of the human total body protein is represented by collagen and it is widespread by most of tissues, like skin, bone, cartilage, tendons, ligaments, blood vessels and cornea, as the main component of the extracellular matrix. The use of collagen for biomedical applications have been largely explored, being, nowadays, the protein with the highest commercial value. Currently, primary sources of collagen have bovine and porcine origin, which may have the risk of zoonotic diseases transmission to humans, by one side, and religious constraints, by other side. At the same time, the exploitation of terrestrial mammals bioresources is not hand in hand with the life growing expectancy and the crescent demand for collagen. For all this reasons, the contemporary society across the world, and particularly the scientific community, are facing an urgent need for sustainable, eco-friendly and safety bioresources.

The Ocean, specifically the marine ecosystem, is populated by an enormous variety of species with a huge potential for extraction of different bioactive molecules. Fishes and the by-products resulting from the fishing transformation industry are undervalued, but they can be processed for the production of different materials with industrial relevance, including health and well-being sectors, representing potential advances in the biomedical field, while creating added market value. This was the framework of this thesis, studying the interaction of collagen obtained from blue shark (*Prionace glauca*) skin with cells and living tissues, to address its potential for the engineering of bone and cartilage, successfully demonstrated in different works.

It could be concluded that blue shark collagen can be processed by employing the same methodologies already in use for mammals collagen, particularly freeze-dry and 3D bioprinting. In the first three Chapters of the experimental section, this thesis highlights the versatility of the freeze-dry technique to process the blue shark collagen into different porous structures for different end-uses, like cartilage and bone regeneration. The results proved that collagen from blue shark can be crosslinked by

applying the same crosslinking agents of mammals collagen, with the use of ECD/NHS revealing more effective with the present conditions. *In vitro*, the produced structures supported different cell line (fibroblast-, osteoblast- and chondrocyte-like cells) survival, as well as human adipose stem cells viability and differentiation, which indicates the suitability of blue shark collagen to be used in cell culture, namely as building block for the development of 3D matrices or scaffolds. *In vivo*, the validation of blue shark collagen to be used as component of implantable biomaterials was tested in critical-size defects created in femoral condyle of New Zealand rabbit models. The results exhibited by composites scaffolds, resulting from the freeze-drying of mixtures of blue shark collagen and bioapatite, 12-weeks post implantation, illustrate well their regeneration capabilities, which were similar to the performance observed with bovine collagen-based composite scaffolds.

Having in mind more complex structures and aiming to better mimic the human native tissues, in the last two Chapters of the experimental section it was proposed the use of blue shark collagen as major component of bioinks used for 3D bioprinting of tissue engineering constructs envisaging bone tissue regeneration. The efficiency of a materials chemistry approach (co-precipitation) followed in these Chapters' work to prepare blue shark mineralized inks, particularly with the appearance of hydroxyapatite phase, was successfully achieved. As far as we know, this approach was for the first time attempted for the development of inks for bioprinting. The ionic crosslinking of alginate mixed with the mineralized blue shark collagen dismissed the addition of any chemical crosslinking agent (which often represents cytotoxicity), enabling the manufacturing of 3D structures that supported the printing of cells (L929 fibroblast-like cell line and stem cells) and, moreover, were capable to trigger the osteogenic differentiation of hASC without any exogenous stimulus. Together, these two works can have important implications on the design of printable mineralized materials with incorporated living cells – bioinks – for the engineering of hard tissues, by highlighting the potential of collagen as building block, presenting the in-situ mineralization approach and emphasizing the relevance of cell density on the performance of bioinks.

As final remark, the work developed under the scope of this thesis has contributed to further unveil the great potential of the marine ecosystem for production of sustainable, eco-friendly, and safe materials with promising usage in the biomedical field. The developed work gives the opportunity to better understand the use of marine biomass for collagen extraction and processing with its possible applicability in the biomedical field. The results herein presented evidence the potential that is still hidden in the ocean depths, hopefully being an inspiration to deeply explore marine resources as a viable and promising source of biomolecules with interesting features for tissue engineering

applications. On the other hand, the thesis shed light on the processing of marine origin collagens, particularly blue shark collagen, which is really challenging, demanding a strict control of temperature, concentration, and stabilization procedures. Having this in mind, the use of blue shark collagen can result in highly promising structures for tissue engineering, offering not only similarity with a major component of human ECM, but also versatility regarding chemical, mechanical and biological properties.

From the simplest to more complex, from Nature to tissue engineering, this thesis gives an innovative way to look to the sea improving the future of materials science and humans' health well-being.

VIII-2. FUTURE PERSPECTIVES

From an experimental point of view, a significantly amount of work was done, revealing very attractive results for the engineering of mineralized tissues. However, there is still space for improvements and to explore other approaches and strategies that were not attempted in this thesis. Focusing on the developed works, different issues can be pinpointed to better discuss and understand the obtained results. For instance, the work developed in **Chapter IV** that was focused on the *in vivo* evaluation of the potential of marine composite scaffolds, leaves open a set of questions that can be potentially answered by increasing the number of materials to be tested. In fact, the lack of statistical differences, either between the two origin composite formulations and the empty control, can be highly related with the limited number of samples. In addition, robust results can be achieved with a histomorphometry analysis, namely regarding the quality and features of the new tissues formed. Regarding **Chapter VII**, the feasibility of using collagen from blue shark for 3D bioprinting was successfully achieved. However, to better confirm the osteogenic potential of the prepared ink, other osteogenic-related markers could be tested, and longer periods of culture could be explored, namely to address the new tissue formation. The applicability of marine collagen for preparation of inks for 3D bioprinting was proved, but their usage to developed more complex structures, based on the hierarchical structure of native tissues, still needs more exploration. It is, yet, highly dependent on the use of alginate, and alternative ways to increase the required viscosity could be pursued, namely by the use of new – cell-friendly – crosslinking factors and the interaction with other biopolymers to mimic more closely the composition of the native ECM. Despite the promising results achieved so far, there is still a long way to go until clinical applications can be proposed.

The increasing demand for collagen for the healthcare related field, including medical devices, is currently driving the market of collagens, particularly marine collagens, which is expected to grow fast in the next few years. To date, the use of marine origin collagens in the biomedical field is poorly explored since most of the studies have been focusing on fundamental research to a better understanding of marine collagens activity. Most studies have been using marine collagen in its native form, but the predictions indicate that the number of works performed with marine origin collagens in the biomaterials field aiming the regeneration of hard tissues will increase in years to come, due to the urgency for new and alternative therapeutic approaches to treat this kind of tissue injuries that are highly associated with the aging population. For that, it is expected in a near future the development of more advanced processing techniques to create more complex structures and more *in vivo* works to deepen understand the potential of such structures.